Deposit & Copying of Dissertation Declaration

UNIVERSITY OF CAMBRIDGE

Board of Graduate Studies

Please note that you will also need to bind a copy of this Declaration into your final, hardbound copy of thesis - this has to be the very first page of the hardbound thesis.

1 Surname (Family Name)	Forenames(s)	Title
Lago Cooke	Santiago Guillermo	Dr.

2 Title of Dissertation as approved by the Degree Committee

A NOVEL PIPELINE FOR DRUG DISCOVERY IN NEUROPSYCHIATRIC DISORDERS USING HIGH-CONTENT SINGLE-CELL SCREENING OF SIGNALLING NETWORK RESPONSES EX VIVO

In accordance with the University Regulations in *Statutes and Ordinances* for the PhD, MSc and MLitt Degrees, I agree to deposit one print copy of my dissertation entitled above and one print copy of the summary with the Secretary of the Board of Graduate Studies who shall deposit the dissertation and summary in the University Library under the following terms and conditions:

1. Dissertation Author Declaration

I am the author of this dissertation and hereby give the University the right to make my dissertation available in print form as described in 2. below.

My dissertation is my original work and a product of my own research endeavours and includes nothing which is the outcome of work done in collaboration with others except as declared in the Preface and specified in the text. I hereby assert my moral right to be identified as the author of the dissertation.

The deposit and dissemination of my dissertation by the University does not constitute a breach of any other agreement, publishing or otherwise, including any confidentiality or publication restriction provisions in sponsorship or collaboration agreements governing my research or work at the University or elsewhere.

2. Access to Dissertation

I understand that one print copy of my dissertation will be deposited in the University Library for archival and preservation purposes, and that, unless upon my application restricted access to my dissertation for a specified period of time has been granted by the Board of Graduate Studies prior to this deposit, the dissertation will be made available by the University Library for consultation by readers in accordance with University Library Regulations and copies of my dissertation may be provided to readers in accordance with applicable legislation.

3 Signature	Date

Corresponding Regulation

Before being admitted to a degree, a student shall deposit with the Secretary of the Board one copy of his or her hard-bound dissertation and one copy of the summary (bearing student's name and thesis title), both the dissertation and the summary in a form approved by the Board. The Secretary shall deposit the copy of the dissertation together with the copy of the summary in the University Library where, subject to restricted access to the dissertation for a specified period of time having been granted by the Board of Graduate Studies, they shall be made available for consultation by readers in accordance with University Library Regulations and copies of the dissertation provided to readers in accordance with applicable legislation.

A NOVEL PIPELINE FOR DRUG DISCOVERY IN NEUROPSYCHIATRIC DISORDERS USING HIGH-CONTENT SINGLE-CELL SCREENING OF SIGNALLING NETWORK RESPONSES *EX VIVO*

SANTIAGO GUILLERMO LAGO COOKE

DEPARTMENT OF CHEMICAL ENGINEERING AND BIOTECHNOLOGY

DARWIN COLLEGE

UNIVERSITY OF CAMBRIDGE

THIS DISSERTATION IS SUBMITTED FOR THE DEGREE OF DOCTOR OF PHILOSOPHY

29 JANUARY 2016

A NOVEL PIPELINE FOR DRUG DISCOVERY IN NEUROPSYCHIATRIC DISORDERS USING HIGH-CONTENT SINGLE-CELL SCREENING OF SIGNALLING NETWORK RESPONSES *EX VIVO*

SANTIAGO GUILLERMO LAGO COOKE

ABSTRACT

The current work entails the development of a novel high content platform for the measurement of kinetic ligand responses across cell signalling networks at the single-cell level in distinct PBMC subtypes *ex vivo.* Using automated sample preparation, fluorescent cellular barcoding and flow cytometry the platform is capable of detecting 21, 840 parallel cell signalling responses in each PBMC sample. We apply this platform to characterize the effects of neuropsychiatric treatments and CNS ligands on the T cell signalling repertoire. We apply it to define cell signalling network abnormalities in PBMCs from drug-naïve first-onset schizophrenia patients (n=12) relative to healthy controls (n=12) which are subsequently normalized in PBMCs from the same patients (n=10) after a six week course of clinical treatment with the atypical antipsychotic olanzapine. We then validate the abnormal cell signalling responses in PBMCs from an independent cohort of drug-naïve first-onset schizophrenia patients (n=25) relative to controls (n=25) and investigate the specificity of the abnormal PBMC responses in schizophrenia as compared to major depression (n=25), bipolar disorder (n=25) and autism spectrum disorder (n=25). Subsequently we conduct a phenotypic drug screen using the US Food and Drug Administration (FDA) approved compound library, in addition to experimental neuropsychiatric drug candidates and nutraceuticals, to identify compounds which selectively normalize the schizophrenia-associated cell signalling response. Finally these candidate compounds are characterized using structure-activity relationships to reveal specific chemical moieties implicated in the putative therapeutic effect.

PREFACE

This dissertation is the result of my own work and includes nothing which is the outcome of work done in collaboration except as declared in the Preface and Acknowledgements and specified in the text.

It is not substantially the same as any that I have submitted, or, is being concurrently submitted for a degree or diploma or other qualification at the University of Cambridge or any other University or similar institution except as declared in the Preface and specified in the text. I further state that no substantial part of my dissertation has already been submitted, or, is being concurrently submitted for any such degree, diploma or other qualification at the University of Cambridge or any other University of similar institution except as declared in the Preface and specified in the text

It does not exceed the prescribed word limit for the relevant Degree Committee.

TABLE OF CONTENTS

CHAPTER 1

INTRODUCTION

1.1 BACKGROUND AND SIGNIFICANCE

The current work entails the development of a novel neuropsychiatric drug discovery pipeline based on *ex vivo* functional cytomics, for drug target discovery, and FDA approved compound library screening for the identification of novel drug candidates. Below we review the challenges in the current field of neuropsychiatric drug discovery relative to the increasing unmet medical need. Subsequently we present the novel *ex vivo* functional cytomics pipeline and suggest ways in which it seeks to address these challenges. Finally we will describe the application of this platform to neuropsychiatric drug discovery in schizophrenia.

1.1.1 NEUROPSYCHIATRIC DISORDERS A PERSISTENT UNMET MEDICAL NEED

In few areas of post-genomic drug discovery is the disconnect between improved scientific resources and a lack of novel drug entities as devastatingly apparent as in the case of neuropsychiatric disorders[1–4]. Modern biomedical methods allow genomic sequencing, determination of three-dimensional protein structure and synthesis of drug-like compound at rates that exceed the capacity available four decades ago by several orders of magnitude[5]. Nevertheless the number of novel drugs approved by the US Food and Drug Administration (FDA) per billion dollars of US research and development (R&D) spending (adjusted for inflation) has decreased steadily by half every nine years since the 1950s, a phenomenon recognized by 'Eroom's Law'[5]. This trend in decreased R&D efficiency is even more striking for neuropsychiatric disorders where no drugs with fundamentally different mechanisms of action have emerged for over two decades [3,6–9]. This lack of innovation has contributed to the fact that several of the main pharmaceutical companies have abandoned their CNS R&D initiatives[5].

Neuropsychiatric disorders represent an enormous burden on worldwide health, accounting for 31% of years lived with disability (YLD) and a lifetime prevalence of up to 20% of the global population (17% for major depression and 0.5-1% each for schizophrenia, bipolar disorder and autism respectively)[10,11]. They are associated with significant comorbidities including cardiovascular disease, suicide , substance abuse , immune disorders, obesity and diabetes[10,12,13]. Current treatments are effective in only 40-60% of individuals, dependent on the disease in question[14–17]. They provide partial symptomatic relief and not reversal of disease aetiology[14–17]. Adverse side effects and delayed onset of therapeutic action, from weeks to months, are persistent problems[3,8]. The fact that the global market for treatment of neuropsychiatric disorders is vast while the discovery of novel drug treatments so scarce, highlights the immense difficulties encountered to date and the urgent requirement to develop novel strategies capable of addressing this unmet medical need.

1.1.2 CURRENT BOTTLENECK IN NEUROPSYCHIATRIC DRUG DISCOVERY

There is a fundamental lack of understanding in the pathophysiology of neuropsychiatric disease which has compromised the identification of novel drug targets[9]. All of the major neuropsychiatric medications share mechanisms of action with compounds that were discovered serendipitously during clinical administration in other disease indications in the 1950s and 1960s. For example antipsychotic medications were discovered through use of chlorpromazine as a pre-anaesthetic, antidepressants stem from use of iproniazid for tuberculosis and mood stabilizers for treatment of bipolar disorder arose through the use of lithium carbonate in urology and sodium valproate for epilepsy[1,3,18].

The elucidation that many of these 'blockbuster' drugs discovered by chance share mechanisms of action involving normalization of monoaminergic (e.g. dopamine, serotonin and noradrenaline) neurotransmission has led to the dominance of the 'monoamine hypothesis' for psychiatric pathophysiology[8,19]. Although these drugs have revolutionized the treatment of mental disorders they have also come to represent a double-edged sword in the long-term. The pharmaceutical industry has focused on producing a vast array of monoaminergic derivatives with improved efficacy, safety or administration profiles. This 'me-too' drug development strategy represents a reduced risk of failure especially in the presence of recently increased regulatory standards[20]. However, because the fundamental mechanisms of efficacy remain similar, subtypes of symptoms and patient cohorts which were refractory to the original drugs in the series have often remained underserved by successive waves of monoaminergic drugs. For example in schizophrenia the

second generation antipsychotic clozapine has provided a substantial increase in efficacy for treatment of positive symptoms, such as hallucinations and disordered thoughts, with the advantage of reduced extrapyramidal side effects compared to the first generation antipsychotics. However it has done less to improve negative symptoms such as anhedonia or avolition or cognitive deficits and is associated with potentially life threatening agranulocytosis and metabolic side effects[14,16,21]. Likewise the tenuous relationship between behavioural traits in preclinical animal models and neuropsychiatric symptoms in humans is often validated using drugs with monoaminergic mechanisms of action[6–8]. Therefore the drugs which are developed using these preclinical models by definition fall within the monoaminergic doctrine. Furthermore the full mechanisms of action of many of the monoaminergic drugs are yet to be characterized[3].

1.1.3 GENOMIC ANALYSES OF NEUROPSYCHIATRIC DISORDERS

In an attempt to better understand the pathophysiology of neuropsychiatric diseases and identify drug targets outside of the monoaminergic doctrine of therapy researchers have implemented multiple 'bottom-up' non-hypothesis driven molecular profiling strategies such as genomics, proteomics and metabolomics. Measures of genetic influence, including recurrence risk and heritability index, suggest psychiatric disorders such as schizophrenia, bipolar disorder and autism are among the most heritable common diseases[11,22,23]. Therefore the identification of intrinsic physiological drug targets is, in theory, feasible with these methodologies. However the genomic complexity and interaction with environmental factors has made causative genetic elements difficult to isolate. This is demonstrated by lack of Mendelian inheritance ratios between twins and unpredictable segregation patterns in families[23].

Only very recently with the advent of genome wide association studies (GWAS), whole exome sequencing and copy number variation (CNV) studies, which are sufficiently powered (tens of thousands of cases and controls), is the genetic landscape of neuropsychiatric disorders beginning to be resolved[23]. For example the largest GWAS study in schizophrenia to date (36,989 cases vs. 113,075 controls) revealed significant associations to 108 genomic loci encompassing approximately 600 genes[24]. These include the dopamine 2 receptor gene (DRD2), widely considered the primary target of efficacious antipsychotic medications, and genes such as GRM3 (metabotropic glutamate receptor), GRIN2A (NMDA receptor subunit 2A), GRIA1 (AMPA receptor subunit GluA1) and SRR (serine racemase), which are involved in putative alterations in glutamatergic neurotransmission and synaptic plasticity in schizophrenia[24,25].

Despite the profound contribution these studies have made towards a better understanding of the genetic basis of neuropsychiatric pathogenesis, there remain several limitations in terms of translating these findings into novel treatments. First in the case of the schizophrenia GWAS data there are often multiple genes implicated at a given locus. Therefore it is not clear which genes actually contribute to pathogenesis and which are simply in linkage disequilibrium with true causative variants[26]. Second very few associated SNPs correspond to non-synonymous exonic polymorphisms which alter protein function. Instead the majority represent synonymous polymorphisms or are present within introns or intergenic regions[26,27]. Third each associated locus only accounts for a very marginal increase in disease risk with odds ratios (ORs) typically under 1.1 and differences in allele frequency between cases and controls less than 2%[10,26]. While whole exon sequencing and CNV studies have to some extent overcome these limitations, by identifying genetic variants with higher penetrance and protein coding mutations, these abnormalities are relatively rare[28,29]. These results suggest that genetic risk for neuropsychiatric disorders results from the combination of multiple common risk alleles each with a small incremental contribution and occasionally rare alleles with a more profound contribution. Even so polygenic risk profile scores (RPSs) currently account for only 7% of the liability to develop schizophrenia[24]. While extrapolations based on potential larger sample sizes in the future suggest that up to 33% of genetic liability might be indexed by RPS, this still falls considerably short of the 65-80% heritability derived from family and monozygotic twin studies[10,26]. This feature has similarly been reported for other major neuropsychiatric disorders including bipolar disorder, major depression, autism spectrum disorder and attention–deficit/ hyperactivity disorder (ADHD)[30].

Finally, leaving these considerations aside, the most poignant obstacle is understanding the functional implications of these putative risk genes and more importantly how they interact to elicit the altered cellular and organismal phenotypes associated with disease. For example the current best practice for validating the significance of neuropsychiatric GWAS risk loci is to demonstrate a differential expression of the risk alleles in the brain, using expression quantitative trait loci (eQTL) mapping, and subsequently predict their mutual interaction *in silico*[31]. This is confounded by the fact that currently both eQTL catalogues and pathway analysis databases are insufficiently curated to provide meaningful functional analyses relative to the complexity of the biological system[24,32]. In many cases these resources implicate non-specific pathophysiological alterations such as cell motility, glycolysis, synaptic plasticity or differentiation[32]. While these results serve to generate hypotheses they are too general to represent 'druggable' targets. In some cases potent risk alleles, for example in catechol-O-methyltransferase (COMT), neuregulin 1 (NRG1) and disrupted in schizophrenia (DISC1) genes, have been linked to phenotypic differences in brain functional magnetic resonance imaging (fMRI) and cognitive function indicative of schizophrenia. However

even when single genetic variants can be linked to relevant pathology at the highest order of complexity it is still unclear how these phenotypes arise at the cellular level. Finally even if the pathways in which multiple genetic risk factors interact could be accurately predicted, we still lack a viable cellular model in which to test them[33]. The methodology in the current project seeks to address these challenges by using live peripheral blood mononuclear cells (PBMCs) from neuropsychiatric patients and controls as a viable model, and *ex vivo* functional cytomics as a means to empirically measure functional alterations in cell signalling pathways associated with disease.

1.1.4 DIFFERENTIAL DIAGNOSIS AND THE NEUROPSYCHIATRIC SPECTRUM

The recent explosion of genetic association data has also confirmed the long suspected overlap of risk alleles between related neuropsychiatric disorders. For example voltage-gated calcium channel subunits CACNA1C and CACNB2, which were highly significant in the largest schizophrenia GWAS to date, were also among the four top loci implicated in a combined cohort of five different neuropsychiatric diseases (schizophrenia (SCZ), bipolar disorder (BD), major depression (MDD), autism spectrum disorders (ASD) and attention deficit hyperactivity disorder (ADHD)), relative to controls, in the largest cross-disorder GWAS[24,34]. Similarly DISC 1 and DISC 2 genes are two of the most widely reported risk factors for schizophrenia[26,35,36]. However even in the original pedigree in which these genes were discovered, carriers of the pathogenic translocation received varying diagnoses including schizophrenia, schizoaffective disorder, and major depression[36,37]. DISC1 mutations have also subsequently been linked to bipolar disorder and different forms of autism[36,38]. The current understanding of the relative strengths of genetic association between neuropsychiatric disorders is summarized in a recent comparison by the Cross-Disorder Group of the Psychiatric Genomics Consortium (CDG-PGC)[30]. Genetic pleiotropy is not confined to neuropsychiatric disorders and some studies suggest that up to 17% of disease-associated genes in humans contribute to multiple disorders[39]. Thus whilst also being related to each other, neuropsychiatric disorders are linked to a range of other medical conditions in the emerging concept of disease networks[40,41]. This is exemplified by the coincidence of schizophrenia with metabolic and cardiovascular disorders[13,42]. While this was long thought to be an effect of antipsychotic therapy, recent evidence suggests that there might be a common genetic predisposition between these disorders, with the direction of causality being the subject of lively debate[43,44].

Concurrent with the recently defined genetic overlap between neuropsychiatric disorders is the persistent and formidable clinical challenge of defining neuropsychiatric phenotypes. Psychiatric

diagnoses do not fall into discrete clinical groups. They represent a wide spectrum of disorders with a gradation of overlapping symptoms shared across different conditions[22,45]. The difficulties in neuropsychiatric nosology are evident throughout its inception with distinctions between bipolar and unipolar depression or autism and childhood schizophrenia being formally recognized only in the 1950s and 1970s respectively[46,47]. Even today 20% of individuals who meet the criteria for one disorder in the Diagnostic and Statistical Manual of Mental Disorders IV (DSM-IV) also fulfil the criteria for at least two more[45]. This results in a lack of diagnostic stability, with up to 50% of patients with a major psychiatric disorder switching diagnosis over a 10 year period[48]. An alternative approach suggests that these classifications should be reframed in terms of multiple dimensions of symptoms, for example compulsivity, which can be expressed in varying degrees across different diagnostic categories[45]. Nevertheless the decision to class a patient in a given diagnostic group remains a subjective observation of behavioural symptoms at the hands of medical practitioners and not an objective measure of biological aetiology[49]. While significant progress has been made in recent years using blood based biomarkers to improve the accuracy of neuropsychiatric diagnoses these methods are yet to be widely implemented in clinical practice[49–54]. For example the first blood-based test for diagnosis of schizophrenia was released to the market in 2010[50]. The test was highly sensitive for detecting schizophrenia relative to controls. However it lacked specificity for distinguishing between schizophrenia and bipolar disorder. This highlights the fact that differential diagnosis is a more persistent bottleneck in clinical psychiatry relative to case-control definition.

In many cases the diagnosis is ultimately defined by relative response to treatment following successive rounds of pharmacological titration across different drug classes[14]. This process can have a devastating effect on patient quality of life and can even exacerbate the initial symptoms[48]. Thus in many ways the critical issue facing medical practitioners is treatment choice more so than specific disease nosology[15,46,55]. In this respect it has been suggested that within each of the major neuropsychiatric disorders there are subgroups of patients with distinct disease aetiologies which influence treatment response[10]. For example in schizophrenia activation of brain microglia and proinflammatory cytokines have been proposed to characterize subgroups of patients with deleterious negative symptoms and cognitive deficits which are refractory to most antipsychotic treatments[16,56,57]. Taken together these findings suggest that there is an urgent need to identify predictive biomarkers of treatment response. Moreover in terms of drug target discovery it is necessary to transcend the usual case-control design confined to a single neuropsychiatric disease. Instead it is potentially more informative to include multiple related neuropsychiatric disorders within the initial discovery design and also to correlate the biological changes to changes in symptom subscales over the course of clinical treatment. The present study aims to address these challenges by using a longitudinal cohort of schizophrenia patients before and after antipsychotic

treatment, for the purpose of drug target discovery, and subsequently a combined cohort of different neuropsychiatric diseases to validate the specificity of the drug target in schizophrenia.

1.1.5 SYSTEMS LEVEL FUNCTIONAL EXPLORATION AND THE CONCEPT OF 'COPING'

The patient profiling strategies applied to date in the form of genomics, transcriptomics and proteomics represent a significant advance towards systems biology in the sense that they quantify a large proportion of the elements within the biological system. However they lack the dimensionality of a true systems biology approach in that they do not measure the strength of interactions between these elements and how they change over time to impact the integrated phenotype. The dynamic nature of disease processes and loss of homeostatic mechanisms can only be assessed empirically if the same samples are subjected to multiple system perturbations or functional challenges with kinetic resolution. The Overt Glucose Tolerance Test (OGTT) for insulin resistance is a physiological example of this principle. A diabetic and metabolically healthy individual might have similar resting blood glucose and insulin levels. However it is only upon administration of a high dose of glucose and subsequent tracking of blood glucose levels over time that the in-ability of the diabetic individual to maintain glucose homeostasis is revealed. Likewise in psychiatry life stress is an important predisposing factor. For some individuals a relatively small amount of stress is enough to precipitate psychiatric pathology, whereas others do not develop pathology despite elevated stress exposure. It is not the stress itself, but the variable capacity of each individual to cope with stress, that dictates whether pathology will develop. This concept of 'coping' is well recognized at the psychological level however it is equally important across all levels of organism complexity. There are two fundamental prerequisites to exploit the potential of this concept within the framework of molecular neuropsychiatric drug discovery: firstly a methodology which provides a systems understanding of the composite molecular disease process and secondly a physiologically relevant model in which to implement it.

1.1.6 PERIPHERAL BLOOD MONONUCLEAR CELLS AS A SURROGATE MODEL FOR CNS PATHOLOGY

It is becoming increasingly apparent that neuropsychiatric diseases are systemic disorders with parallel manifestations in the brain and peripheral tissues. In the case of the blood this is exemplified in several studies by our group and others which have used multiplex immunoassays and mass spectrometry to identify serum proteins and peptides which constitute biomarkers of

neuropsychiatric illnesses including schizophrenia, bipolar disorder, major depression and autism spectrum disorders[50,52,53,58–61]. Importantly these serum biomarkers have been used to predict the onset of schizophrenia or major depressive disorder before manifestation of overt clinical symptoms[54,62,63]. While this is vital for early intervention strategies it also suggests that there is a profound intrinsic representation of neuropsychiatric disorders in the blood. Similar studies have also correlated serum proteins to different mood states within bipolar disorder or different putative disease aetiologies, for example immune dysregulation or abnormal hormone and growth factor secretion in the case of schizophrenia[43,44,64–66]. Finally they have addressed the critical challenges of treatment response and side effect prediction[67,68].

With respect to peripheral blood mononuclear cells (PBMCs) the majority of published work in neuropsychiatry has focused on alterations in relative proportions of different PBMC subsets, their activation status or their cytokine secretion profile. Subsets commonly assessed include monocytes, T helper (Th1, Th2, Th17), T cytotoxic, T regulatory, B cells and natural killer (NK) cells[69–72]. While these studies have been vital in elucidating immunological dysfunction in these disorders, and have even been linked to pathogenic mechanisms in the brain such as microglial activation and brain T cell infiltration, there is also substantial evidence that PBMCs might provide valuable models for the systemic alteration of CNS targets. For example PBMCs express a range of neurotransmitter receptors (e.g. D1-5, CB1/2, 5HT1A/2/5A, GABA, mACh, nACh, β-2A, MR, GR, NMDA), neurotrophin receptors (BDNF, NGF) and monoamine transporters (DAT, 5-HTT) which are reported to mediate neuropsychiatric pathogenesis[73–76]. They also share many of the intracellular signalling cascades which have been implicated in neuropsychiatric disorders, downstream of the aforementioned receptors in neurons, including Akt-GSK-3β, PLC-PKC, cAMP-PKA and MAPK-ERK[77–81]. Furthermore many of these receptors or their cell signalling substrates have been shown to be altered in neuropsychiatric patient PBMCs and correlated to therapeutic efficacy or disease severity[81–86].

The Akt-GSK-3β pathway provides an example of how PBMCs can serve as valuable sentinel tissue for aetiological neuropsychiatric mechanisms in the brain. First, in neurons Akt1 and GSK-3β serve to integrate intracellular signal transduction following the activation of cell surface receptors intimately linked to neuropsychiatric pathology. These include G protein-coupled receptors (GPCRs) and receptor tyrosine kinases (RTKs) activated by neurotransmitters (e.g. dopamine and 5-HT) and neurotrophic ligands (e.g. BDNF and NGF) respectively[80,87]. Second, polymorphisms in Akt1 and GSK-3β have been associated with risk for schizophrenia and bipolar disorder respectively and, in the case of GSK-3β, response to mood stabilizing or antidepressant medication[88–94]. Third, the expression of Akt1 and phosphorylated GSK-3β (pS9) is reported to be altered in both *post mortem* brain and PBMCs from schizophrenia and bipolar disorder patients respectively[88–95]. Fourth

behavioural symptoms in mice are reminiscent of schizophrenia, following Akt1$^{-/-}$ knockdown, and of both depressive and manic mood states in bipolar disorder following alanine mutation of the GSK-3β (pS9) regulatory site[88–94]. Finally, and most importantly, changes in total Akt1 and GSK-3β (pS9) phosphorylation have been linked to clinical treatment response and symptom severity in bipolar disorder and schizophrenia patient PBMCs respectively[88–94,96]. Taken together these findings suggest that Akt1 and GSK-3β represent an aetiological genetic predisposition to neuropsychiatric disorders with systemic representation in both the brain and PBMCs. Crucially their function is modified by efficacious clinical neuropsychiatric treatments suggesting that previously unexplored drugs which modulate their activity in PBMCs might constitute novel treatments for these diseases.

While the Akt1- GSK-3β pathway is presented as an example, there are multiple studies which have shown alterations in other CNS targets in PBMCs. For example 5HT-2A receptor clustering in lymphocytes is reversed by eight weeks of antidepressant therapy and associated to treatment response[86]. In schizophrenia diagnostic subscale scores (including BPRS, PANSS and AIMS) were correlated to D2 receptor expression on CD8+ T cells and D4 receptor expression on CD4+ T cells[85]. The finding is also concurrent with reports that D4 receptor polymorphisms are related to age of onset and disease severity in schizophrenia[97]. CB2 receptor expression has been shown to be increased in PBMCs from children with autism spectrum disorders[98].

Despite the potential validity of PBMCs as live cellular models for neuropsychiatric disorders, especially considering the impracticalities of obtaining live human brain tissue, this resource has remained largely unexploited by previous studies for several reasons. Firstly almost all studies which have accessed these CNS targets in PBMCs have solely examined basal expression of mRNA or proteins without functional testing. For example while D2/4 receptor expression is reported to be altered in T cells from schizophrenia patients, it is not known whether these receptors are functionally affected in terms of active coupling to different intracellular signalling cascades, ligand induced internalization and desensitization, isoenergetic conformational change or receptor ensemble formation in the disease state[99]. Likewise in the example provided of Akt1-GSK-3β it is not known whether these signalling proteins have the same up- or down-stream regulatory partners, or indeed a complete rewiring of the cell signalling network, in neuropsychiatric disease. Secondly, many pathological alterations in cell signalling may not be immediately apparent unless assessed in the presence of a cellular stressor. In other words it is not the relative levels of cell signalling proteins which determine the disease but instead how they react as a network to functional challenge[100].

Thirdly the few studies which have conducted functional testing in PBMCs of neuropsychiatric patients have done so using a reduced set of stimulants and readouts to provide validation of a pre-existing hypotheses related to immune function, for example glucocorticoid suppression of IL-6 secretion in MDD or mitogen-induced cytokine secretion (IL-2, IL-6, IL10 and IFN-γ) in schizophrenia[101,102]. While these studies provide valuable insight into disease mechanisms they do not constitute a systems level interrogation of cellular pathology capable of generating novel hypotheses. In contrast one study which assessed whole proteome changes in schizophrenia PBMCs relative to controls, following stimulation of the T cell receptor complex using staphylococcal enterotoxin B and anti-CD28, identified abnormalities across glycolytic pathway proteins which were not detected in the unstimulated state[103]. Albeit limited to a single stimulant cocktail, this highlights the potential for the generation of novel hypotheses when a functional challenge is combined with high content measurements. Finally most of the functional studies in PBMCs in neuropsychiatry to date have focused on PBMCs as a whole and not on specific cell subtypes, such as T or B cells, which are known to have significantly different functional repertoires[104]. Taken together there is a need for high content functional analysis of specific PBMC subsets in neuropsychiatric disorders to accurately determine their utility for drug target discovery.

1.1.7 *EX VIVO* FUNCTIONAL CYTOMICS AS A NOVEL PLATFORM FOR NEUROPSYCHIATRIC DRUG DISCOVERY

To address this need we have developed a platform capable of high-content single –cell screening of functional ligand-receptor interactions and downstream signalling mechanisms in PBMCs *ex vivo* **(Fig. 1.1)**. The platform uses flow cytometry, fluorescent cell barcoding and automated sample preparation to enable the parallel detection of multiple functional ligand responses across multiple cell signalling epitopes and cell subtypes in heterogeneous primary cell populations. Briefly, PBMCs from neuropsychiatric patients and controls are incubated with small ligand libraries for up to 30 min. These libraries are designed to include a mechanistically diverse set of ligands such as CNS receptor agonists, neuropsychiatric medications, cytokines, hormones/ growth factors, antigens and intracellular signalling modulators. The cells are then fixed, permeabilized and multiplexed using fluorescent cell barcoding[105]. Subsequently the responses to each of the ligands are detected by measuring the expression and phosphorylation status of intracellular signalling epitopes which span a wide variety of pathways, for example Akt/GSK-3β, PKA, PKC, MAPK, JAK/STAT, IL1R/TLR and TCR/BCR. Finally different PBMC subtypes are resolved using immunophenotyping.

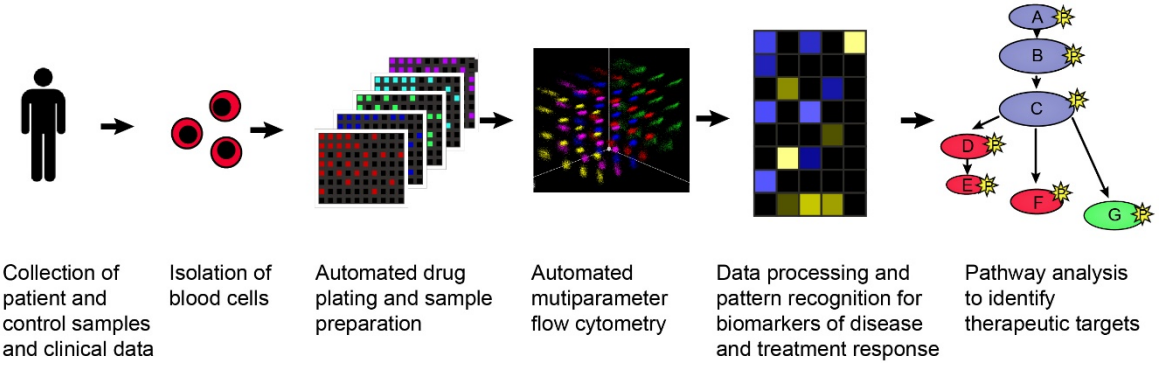

Figure 1.1 *Ex vivo* functional cytomics as a novel platform for neuropsychiatric drug discovery

This creates a combinatorial expansion of the number of functional assays performed in each PBMC sample. For example under the current dimensions of each parameter that will be presented in this work it is possible to measure the response of up to 80 ligands across 80 cell signalling epitopes in three PBMC subtypes *ex vivo*. This creates a three dimensional matrix of up to 19,200 parallel functional assays measurable in each PBMC sample at a given time point **(Fig. 1.2)**. Thus each data point derived from this technology can be indexed as a function of the ligand used for stimulation, the cell signalling epitope used for detection and the PBMC subtype in which it was measured. Each combination of these parameters is referred to as a cell signalling response 'node'. All the nodes together form a unique profile which is indicative of the functional repertoire of the PBMCs from each donor. Additionally the same matrix can be repeated at different time points to provide kinetic resolution of cell signalling responses.

Comparison of these profiles between donors in different clinical groups, for example schizophrenia vs. control, allows the identification of cell signalling responses which are altered in the disease state. It can alternatively be used to compare patients before and after clinical treatment, for example antipsychotic therapy in schizophrenia, and determine which cell signalling responses are associated to clinical drug efficacy. Finally it can be used to differentiate cell signalling responses between related neuropsychiatric disorders for example schizophrenia (SCZ), bipolar disorder (BD), major depression (MDD) and autism spectrum disorders (ASD). The ultimate objective of these comparisons is to identify an aberrant functional cell signalling response which is specific to a particular neuropsychiatric disorder and is normalized by efficacious clinical treatment. This response then constitutes a drug target against which compound libraries, for example the FDA library, can be screened to derive novel drug candidates.

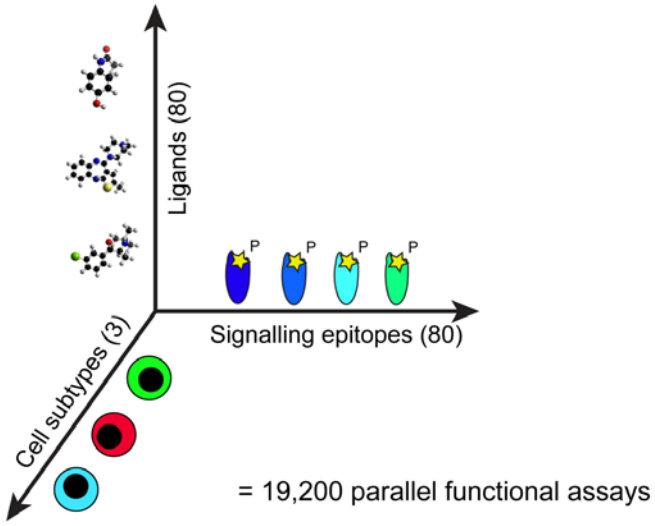

Figure 1.2 Combinatorial expansion of the number of functional assays conducted in each PBMC sample using *ex vivo* functional cytomics. Figure shows the maximum number of conditions assessed for each of the parameters in the current study. Each data point or 'cell signalling node' is a function of the ligand used for stimulation, the cell signalling epitope used for detection and the PBMC subtype in which it was measured. All possible combinations of these variables, defined as ligands (n=80) x signalling epitopes (n=80) x cell subtypes (n=3), creates a total of 19,200 parallel functional assays or 'cell signalling nodes' measurable in each PBMC samples. Comparison of these high content response profiles between clinical groups allows the identification of biomarkers of disease and treatment response.

1.1.8 COMPARISON OF *EX VIVO* FUNCTIONAL CYTOMICS TO THE STATE OF THE ART

While the methodological details of *ex vivo* functional cytomics are described in more detail in **Chapter 2** and at the beginning of **Chapter 3**, it is important to highlight the potential advantages of this technology relative to the state of the art. First, with many drug discovery efforts still based on isolated biochemical assays or recombinant cell lines the use of live primary cells from patients affected by neuropsychiatric disease is paramount to the physiological relevance of the assay. Although limited by the number of cells available the use of primary human tissue at the early stages of the drug development pipeline is associated with a higher potential success rate for the targets and compounds discovered[99]. Second the use of functional testing in live cells allows the elucidation of relevant disease specific alterations in cell signalling networks which are not observable simply by quantification of the protein levels in their basal state. This includes alterations in homeostatic and regulatory mechanisms consistent with the concept of 'cellular coping'. Third cell signalling

pathway alterations are a common conclusion in many genomic and proteomic screens in neuropsychiatry. However these assumptions are confounded by incomplete annotation of protein function and moreover network connectivity as described earlier. Using the current technology we can measure the parallel activation status of key hubs in these cell signalling networks directly in live patient cells and furthermore assess their connectivity through correlated responses to ligand stimulation. Thus it is possible to empirically test leading theories in neuropsychiatric pathway dysfunction, in addition to potentially revealing new ones, as opposed to relying on *in silico* imputation.

Fourth, as described earlier the majority of genetic risk for neuropsychiatric disorders has yet to be indexed and, from what is known so far, each patient is likely to have a different combination of common but weak, or rare but penetrate risk alleles[24,106,107]. The current technology provides the potential to summarize these complex genetic risk factors with heterogeneous manifestations as integrated cellular phenotypes. Thus while we may not know the full catalogue and annotation of genes and proteins involved in the pathogenesis of each patient we can still potentially derive points of mechanistic convergence in terms of cell signalling which represent common drug targets. These points of mechanistic convergence can be thought of as functional endophenotypes. In other words they are biological traits which are more tractable and amenable to drug screening than the disparate and complex molecular pathways from which they arise. By extension the cellular responses altered in the disease state can form the basis of phenotypic drug screening for potential novel therapeutic compounds capable of normalizing these responses. Thus, in contrast to target based drug discovery, potential treatments can be identified even before the molecular mechanisms are fully understood.

Fifth, the technology allows us to interrogate, using a series of specific and potent ligands, many of the CNS receptors and downstream signalling cascades described earlier for which function in PBMCs is unknown. Furthermore the majority of the ligands used in the present functional cytomic platform target GPCRs, RTKs or ion channels while the cell signalling epitopes are predominantly located on protein kinases and phosphatases. Collectively GPCRs, RTKs, ion channels and protein kinases and phosphatases represent the targets for the vast majority of currently approved medications consistent with their role as key cellular functional executioners[108–110]. Thus targeting these proteins in the drug target discovery phase represents heuristic screening of the most 'druggable' part of the genome. Importantly, many of these highly functional molecules, for example GPCRs, have a relatively low level of expression. Therefore, in the case of proteomics, they often remain undetected relative to more abundant housekeeping proteins. In contrast an

amplified signalling event downstream of these low abundance receptors can be accurately measured using fluorescence flow cytometry[111].

Sixth, the ability to measure the effects of a ligand across multiple signalling pathways in parallel allows the identification of compounds with multi-target efficacies, a feature common to existing neuropsychiatric drugs[112]. Conversely it also allows the identification of potentially toxic off target signalling interactions. Identification of toxic side effects in primary cells at the drug discovery phase can reduce the costly risk of failure at later stages in the drug development pipeline[113,114]. Finally the ability to measure responses at the single-cell level affords the statistical power necessary to identify clinically relevant functional phenotypes in minority cell populations within a heterogeneous primary sample[100].

1.1.9 CLINICAL RELEVANCE OF *EX VIVO* FUNCTIONAL CYTOMICS

The development of the *ex vivo* functional cytomics platform draws heavily on previous work by Nolan *et al*. This includes the pioneering detection of phosphorylation events in single-cell signalling networks in response to ligand stimulation using flow cytometry ('phospho-flow cytometry') and the high content multiplexing of different stimulation conditions using fluorescent cell barcoding (FCB)[105,115,116]. One particular study by this group serves to illustrate the potential clinical impact of this methodology with respect to several of the features described above[117]. The authors assessed the phosphorylation status of several cell signalling proteins (STAT1, 3, 5, 6, p38 and Erk1/2) under basal conditions or in response to ligand stimulation (IFN-γ, IL-3, G-CSF, GM-CSF and FLT3) in CD33+ blast cells from patients with acute myeloid leukaemia (AML) relative to CD33+ cells in healthy controls. First, differences in the phosphorylation status of these signalling epitopes in normal vs. malignant cells was only distinguishable following stimulation with cytokines and growth factors and not in the basal state. Second, the cell signalling profiles allowed the definition of a subgroup of patients with poor response to chemotherapy and corresponding genetic abnormalities (including Flt3 mutation) associated to poor prognosis. Taken together these results highlight how a functional cytomic response can summarize the genetic differences between patients into a phenotype which is more relevant to holistic disease physiology, in this case myeloid proliferation mediated by G-CSF, and treatment response prediction. By extension this functional cellular phenotype also provides the mechanistic basis for a readily implementable cellular screening assay for the discovery of novel drugs. Finally the functional screening also revealed specific subsets of blasts with altered response profiles within each patient. This highlights the potential of phospho-flow cytometry to identify clinically relevant pathogenic subtypes at the single-cell level within

heterogeneous primary cell populations. Similar applications of this technology have also yielded clinically relevant results in terms of characterizing immune cell signalling responses in other forms of haematological cancer, viral and bacterial infections and autoimmune disorders[118–122].

The current application of *ex vivo* functional cytomics seeks to extend the clinical relevance of these technological applications whilst distinguishing itself in two important features. First, all the aforementioned studies involve diseases where the primary pathology is recognized in immune cells. In contrast in neuropsychiatric disorders, despite the increasingly accepted role of the immune system, the primary manifestation of pathology is still attributed to the brain. Thus we seek to provide a novel application of this methodology in which immune cell signalling responses are used as a surrogate model for aberrant function of brain cell lineages including neurons, astrocytes and microglia. Second, to achieve this objective we have expanded the repertoire of functional ligands and cell signalling epitopes measured beyond the dimensions of previous *ex vivo* studies and included many ligands and readouts specific to CNS pathology. To our knowledge this represents the most extensive functional characterization of live cells from neuropsychiatric patients and controls to date.

1.1.10 DRUG REPURPOSING IN NEUROPSYCHIATRIC DISORDERS

Drug repurposing (also referred to as 'repositioning' or 'reprofiling') involves the screening of approved drugs for use in novel indications. A frequently cited example is sildenafil (Viagra; Pfizer) which was originally developed as an anti-angina medication[110]. The advantage of screening approved medications is that the resulting drug candidates already have well documented toxicology, pharmacokinetic, dosing and medicinal chemistry profiles obtained during the original clinical trials and history of public use[110]. This expedites clinical trials in the new indication and reduces the risk of failure due to adverse side effects or poor pharmacokinetics in humans, features which are responsible for the high attrition rate (over 90%) of the majority of novel drug entities[110]. By extension this means that repurposed drugs can potentially reach the clinic in less time and that this strategy is within the reach of small-medium enterprises and academic collaborations with limited resources relative to large pharmaceutical companies[110]. This is a formidable advantage considering the average ten year development pipeline and over € 2 billion cost of bringing a new drug to market[110,123]. Drug repurposing is also directly relevant to the current project in neuropsychiatry in several ways. Firstly, the majority of compounds used currently for the treatment of neuropsychiatric disorders derive from lead compounds which were repurposed following the discovery of beneficial neuropsychiatric side-effects during application to other

indications. Thus it is a strategy which has served the field well in the past. Secondly in the FDA drug screening stage of the current project we seek to normalize an aberrant cell signalling response observed in PBMCs from schizophrenia patients relative to controls. This drug discovery initiative therefore represents a phenotypic screen in the sense that the full mechanism of altered cellular signalling in the disease state is not characterized. As the majority of the FDA approved drugs have well documented targets and mechanisms of action, their relative interactions with the targeted response can be used to dissect the mechanism of aberrant cell signalling in patients. An elegant example of this differential pharmacology strategy is the elucidation of the role of 5-HT2A receptor antagonists, such as atypical antipsychotics, in preventing human polyomavirus JC (JCV) from infecting astrocytes and oligodendrocytes leading to progressive multifocal leukoencephalopathy (PML)[110,124]. Finally the extensive annotation of bio-distribution for FDA approved compounds allows drug candidates to be readily prioritized in terms of brain penetrance at the initial stages of the neuropsychiatric drug discovery pipeline.

1.2 AIMS OF THE CURRENT STUDY

1. Establish a robust high content screening platform for the quantification of cell signalling responses relevant to neuropsychiatric disease mechanisms in PBMCs *ex vivo* **(Chapter 3).**

2. Identify abnormal alterations in the cell signalling repertoire of PBMCs from individuals with schizophrenia, relative to healthy controls, and track how these alterations are normalized by *in vivo* antipsychotic therapy **(Chapter 4).**

3. Assess the relative specificity of the potential drug targets in schizophrenia relative to other major neuropsychiatric diseases including bipolar disorder, autism spectrum disorder and major depressive disorder **(Chapter 4).**

4. Discover novel classes of FDA approved compounds which are capable of normalizing the cell signalling responses associated with schizophrenia pathology **(Chapter 5).**

1.3 STUDY DESIGN

This project is conducted in four stages, consistent with each of the aims above, which sequentially form a novel *ex vivo* drug discovery pipeline for neuropsychiatric disorders **(Fig. 1.3)**. The experimental conditions at each stage in terms of PBMC samples usage, the dimensions of each step within the high content assay and principal outcomes are further detailed in **Fig. 1.4**.

The first stage ('time course', **Fig. 1.3b and 1.4a; Chapter 3**) involves establishing a robust high-content functional cytomics platform for the quantification of cell signalling responses relevant to neuropsychiatric disease mechanisms in PBMCs *ex vivo.* This stage uses PBMCs from healthy control donors and focuses on T cells as the most abundant PBMC cell type. The first step is to establish a robust fluorescent cell barcoding (FCB) protocol which enables 80 populations of PBMCs, each treated with different ligands or vehicle conditions, to be multiplexed and therefore combined in the same antibody staining reaction for detection of cell signalling changes. This allows reproducible staining across the ligand conditions, increased dimensionality for high content analysis and also efficient use of the limited PBMC samples. The second step involves testing a diverse set of ligands

(n=70) and cell signalling epitopes (n=78) across four different time points (1, 5, 15 and 30 min) to provide a total of 21,840 parallel assays in each PBMC sample. This allows the selection of a subset of the most active ligand-epitope combinations and the single most active time point for application in the subsequent stage using limited clinical samples. We also use the kinetic response profiles of each ligand to validate the sensitivity and specificity of the platform, with respect to characteristic T cell cytokine signalling networks, and explore its potential for identifying surrogate models of CNS drug efficacy including neuropsychiatric medications and experimental drug candidates.

The second stage ('antipsychotic intervention', **Fig. 1.3c and 1.4b; Chapter 4**) involves applying the refined set of ligand-epitope combinations (56 ligands vs. 66 epitopes) at a single time point (30 min) to PBMCs (specifically T cells) derived from a longitudinal cohort of drug-naive male schizophrenia patients before (n=12) and after (n=10) six weeks of treatment with the antipsychotic olanzapine in addition to matched healthy control donors (n=12). Comparison of schizophrenia patients before treatment to controls allows the identification of putative signalling mechanisms altered in the disease state. Comparison of schizophrenia patients before and after treatment allows the determination of surrogate markers of drug efficacy *in vivo*. Specifically we focus on which cell signalling responses are altered in the disease state and normalized by antipsychotic intervention *in vivo*. These normalized responses are then prioritized in terms of their validity as putative drug targets for the subsequent drug screening stage using the FDA approved compound library. We also correlate the changes in specific cell signalling responses to changes in positive and negative syndrome scale (PANSS) scores over the course of olanzapine treatment to assess the potential of the platform to derive biomarkers of clinical efficacy which are specific to symptom subscales. Finally we explore the relationship between PBMC cell signalling responses to acute olanzapine administration *ex vivo* and chronic clinical olanzapine treatment *in vivo* in terms of the potential for treatment response prediction.

The third stage ('differential diagnosis', **Fig. 1.3d and 1.4c; Chapter 4**) involves the replication of the putative schizophrenia drug targets, from the antipsychotic intervention study, in an independent cohort of drug-naive schizophrenia patients (n=25) and controls (n=25) and assessment of their relative specificity for schizophrenia as compared to other major neuropsychiatric disorders including bipolar disorder (n=25), autism spectrum disorder (n=25) and major depressive disorder (n=25). Furthermore the relative specificity of the putative drug targets across different PBMC subsets (CD4+ T cells, CD4- T cells and B cells) is resolved.

In the fourth stage ('FDA library screening', **Fig. 1.3e and 1.4d; Chapter 5**) the most significantly altered cell signalling response specific to schizophrenia, identified in the proceeding clinical studies (antipsychotic intervention and differential diagnosis), is subjected to compound screening using the FDA library and selected experimental drugs (946 compounds in total) in control PBMCs (n=6-12). This allows the identification of compounds with the potential to normalize the altered response observed in schizophrenia.

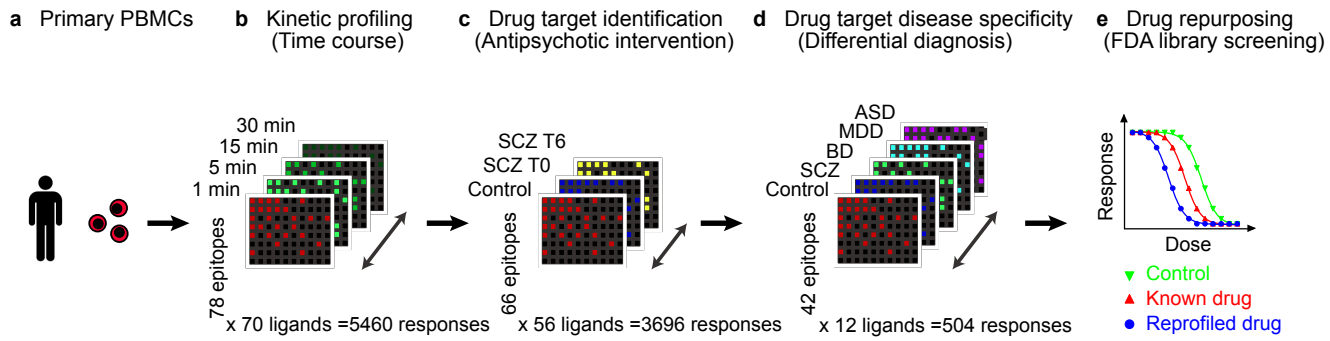

Figure 1.3 ***Ex vivo*** **CNS drug discovery pipeline. (a)** Human primary peripheral blood mononuclear cells (PBMCs) provide an accessible *ex vivo* model of physiological single-cell phenotypes in health and disease. **(b)** Time course exploration of responses to 70 ligands (including CNS ligands and neuropsychiatric treatments) across 78 diverse cell signalling epitopes (5460 responses in total) in T cells from healthy control donors (n=8) at 1, 5, 15 and 30 min ligand incubation times. **(c)** Identification of functional drug targets by comparing T cell signalling response profiles of 56 ligands across 66 cell signalling epitopes (3696 responses) in PBMC samples from three clinical groups: healthy controls (n=12), antipsychotic drug-naïve schizophrenia patients (SCZ T0; n=12) and the same patients following six weeks of clinical treatment with the atypical antipsychotic olanzapine (SCZ T6; n=10). **(d)** Evaluation of the disease specificity of the functional drug targets for schizophrenia relative to other major neuropsychiatric disorders by comparing cell signalling response profiles to 12 ligands across 42 cell signalling epitopes (504 responses) in different PBMC subtypes (CD4+ T cells, CD4- T cells and B cells) from five clinical groups: healthy controls (n=100), antipsychotic drug-naïve schizophrenia (SCZ; n=25), bipolar disorder (BD; n=25), major depressive disorder (MDD; n=25), autism spectrum disorder (ASD; n=25). **(e)** Modelling of schizophrenia disease-associated cellular responses and screening of FDA approved drugs (repurposing) and experimental neuropsychiatric compounds (n=946 in total) in T cells from healthy control PBMC donors (n=6-12).

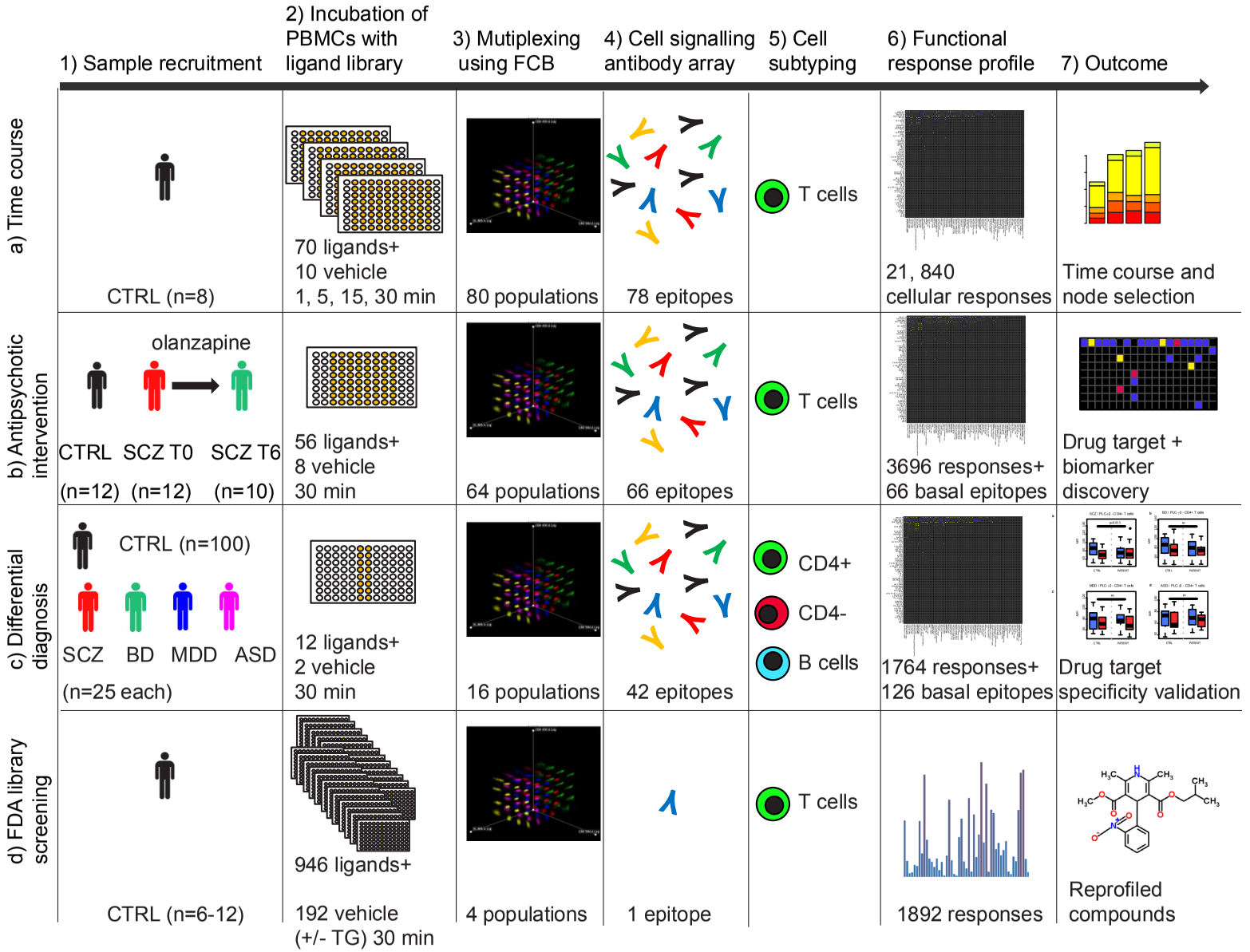

Figure 1.4 Experimental design for each stage of the project including clinical recruitment of PBMC samples, experimental dimensions of the functional cytomics assay and principal outcomes.

CHAPTER 2

MATERIALS AND METHODS

The Materials and Methods relevant to all studies are described below. Methods relevant to specific substudies are indicated by the following abbreviations where necessary: time course (TC), antipsychotic intervention (AI), differential diagnosis (DD) and FDA compound library screening (FDA).

2.1 CLINICAL SAMPLE RECRUITMENT

For the TC and FDA studies, healthy control PBMC donors were recruited at the Cambridge Centre for Neuropsychiatric Research, Cambridge University, UK. For the AI study, first-onset antipsychotic drug-naive schizophrenia patients before (n=12) and the same patients after (n=10) six weeks of treatment with the atypical antipsychotic medication olanzapine (10-20mg/day), in addition to matched controls (n=12), were recruited from the Erasmus Medical Centre, Rotterdam, the Netherlands. For the DD study, patients in each disease group (n=25) and matched controls (n=25/ group) were recruited from clinical centres as follows: schizophrenia (University Hospital Marqués de Valdecilla, Santander, Spain), major depressive disorder (Westfälische Wilhelms University Hospital, Münster, Germany), bipolar disorder (Foundation Biological Psychiatry, Sofia, Bulgaria and Union House, Cambridgeshire and Peterborough Mental Health Foundation Trust, Cambridge, UK) and autism spectrum disorder (Cambridge Autism Research Centre, Cambridge University, Cambridge, UK). The medical faculty ethical committees responsible for the respective sample collection sites approved the study protocols. Informed consent was given in writing by all participants and clinical investigations were conducted according to the Declaration of Helsinki[125] and Standards for Reporting of Diagnostic Accuracy[126]. Please refer to respective AI and DD chapters for demographic information and statistical matching of clinical participants. Participants from different clinical groups, alongside quality control (QC) samples from healthy control donors, were randomized across different plate positions and experimental days for both AI and DD studies.

Diagnoses of neuropsychiatric pathology were conducted by experienced psychiatrists and were based on the Diagnostic and Statistical Manual of Mental Disorders-IV-Text Review (DSM-IV-TR) [3] and International Statistical Classification of Diseases and Related Health Problems- 10th Revision (ICD- 10) [4]. Clinical rating scales used to diagnose patients and quantify symptoms in each clinical study were as follows: Schizophrenia (AI): Positive and Negative Syndrome Scale (PANSS). Schizophrenia (DD): Brief Psychiatric Rating Scale (BPRS), Scale for the Assessment of Positive Symptoms (SAPS) and Scale for the Assessment of Negative Symptoms (SANS). Bipolar disorder (DD): Young Mania Rating Scale (YMRS), Hamilton Rating Scale for Depression (HAM-D) and Inventory of Depressive Symptomatology- Clinician (IDS-C). Major Depressive Disorder (DD): Inventory of Depressive Symptomatology Clinician (IDS-C). Autism (DD): autism-spectrum quotient (AQ), empathy quotient (EQ) and systemizing quotient-revised (SQ-R).

The exclusion criteria for patients and controls included: additional neuropsychiatric diagnoses other than the targeted one, other neurological disorders including epilepsy, mental retardation, multiple sclerosis, immune/ autoimmune disorders, infectious disease, metabolic disorders including diabetes, cardiovascular disease, hepatic and renal insufficiency, gastrointestinal disorders, endocrine disorders including hypo-/ hyperthyroidism and hypo-/ hypercortisolism , respiratory diseases, cancer, severe trauma, pregnancy/ lactation, substance abuse including psychotropic drugs and alcohol, somatic medication with brain side-effects, somatic medication affecting the immune system including glucocorticoids, anti-inflammatory/immunomodulating drugs and antibiotics.

2.2 PBMC ISOLATION AND CULTURE

Peripheral blood mononuclear cells (PBMCs) were prepared from blood collected into 7.5 ml sodium heparin tubes (BD Biosciences,) with the exception of schizophrenia and control samples which were prepared at the University Hospital Marqués de Valdecilla (Santander, Spain) and which were collected into 7.5 ml tubes containing acid citrate dextrose solution A. Whole blood was pelleted, diluted 1: 1 with Dulbecco's phosphate-buffered saline solution (PBS; Sigma–Aldrich) and centrifuged over Ficoll (GE Healthcare) at 750 g for 20 min at 23 ^{o}C. PBMCs were extracted from the interphase, washed three times with PBS at 300 g for 10 min and cryopreserved at 5×10^6 cells/ml in heat-inactivated foetal bovine serum (FBS; Life Technologies) containing 10% dimethyl sulfoxide (DMSO; Sigma–Aldrich) or, in the case of samples collected at the Foundation Biological Psychiatry (Sofia, Bulgaria) in complete Roswell Park Memorial Institute (RPMI) media with 10% DMSO (RPMI-1640 with sodium bicarbonate (Sigma-Aldrich), 10 % FBS (Life Technologies), 50 U/ml penicillin and

50 µg/ml streptomycin (Life Technologies), 2 mM L-alanyl-L-glutamine dipeptide (Life Technologies) and 10% DMSO).PBMCs were thawed at 37^{o}C and resuspended in sterile conditions in complete RPMI media with deoxyribonuclease (DNAse) (RPMI-1640 with sodium bicarbonate (Sigma-Aldrich), 10 % FBS (Life Technologies), 50 U/ml penicillin and 50 µg/ml streptomycin (Life Technologies), 2 mM L-alanyl-L-glutamine dipeptide (Life Technologies) and 20 µg/ml DNAse (Sigma-Aldrich)). The cells were counted using a Coulter Counter (Beckman Coulter), pelleted and resuspended at 1*10^{6} cells/ml (TC, AI and FDA studies) or 2*10^{6} cells/ml (DD study). The cells were rested for 24 hours at 37°C/ 5 % CO_2 either in cell culture flasks (TC and AI studies) or, via a 40µm cell strainer, in 96-well polypropylene plates (Starlab; FDA and DD studies).

2.3 PREPARATION OF FUNCTIONAL LIGANDS AND COMPOUND LIBRARIES

Ligands (including cell signalling activators/ inhibitors and receptor agonists/ antagonists) were purchased from Sigma-Aldrich, Tocris/ Bio-Techne, eBioscience/ Affymetrix, R&D systems, Life Technologies, Abcam, Antibodies-online and Enzo Life Sciences. CHIR 99021 and JB1121 were provided by collaborators Haggarty SJ and Petryshen TL at the Broad Institute, Cambridge, MA, USA. **Table 2.1** lists the ligands used with their primary mechanisms of action and final assay concentrations. Stock solutions of ligands were prepared in sterile conditions. Initial solubilization was achieved using DMSO where possible and alternatively PBS, H_2O or H_2O with equimolar NaOH as per the manufacturer's instructions. Intermediate dilutions were made in PBS and DMSO was added to equivalent amounts for each ligand and vehicle.

The FDA approved compound library (n=786, v. 2.0; Enzo Life Sciences) was extended to incorporate experimental compounds (n=160) either contributed by collaborators (Jones-Brando L, Yolken R, Posner GH, D'Angelo JG, Hencken CP(Johns Hopkins University School of Medicine, Baltimore, MD, USA), McNulty J (McMaster University, Hamilton, Ontario, Canada), Wagner FF, Holson EB, Petryshen TL, Haggarty SJ (Broad Institute, Cambridge, MA, USA) and Williams RS (Royal Holloway University of London, Egham, UK)) or representing positive controls/ nutraceuticals, related to putative drug targets, from the Cambridge Centre for Neuropsychiatric Research (CCNR) compound library **(Table 2.2)**. Initial solubilisation was conducted using DMSO where possible and alternatively PBS, H_2O or H_2O with equimolar NaOH as per the manufacturer's instructions. Intermediate dilutions were prepared using complete RPMI media without penicillin-streptomycin (RPMI-1640 with sodium bicarbonate (Sigma-Aldrich), 10 % FBS (Life Technologies) and 2 mM L-alanyl-L-

glutamine dipeptide (Life Technologies)). DMSO was added to equivalent amounts across all compounds and the vehicle. The final assay concentration of the majority (95%, n=899) of compounds in the extended FDA library was 20 μM with some exceptions in the experimental compounds from collaborators and ligands included from the CCNR library **(Table 2.2)**. The choice of a final assay concentration of 20 μM is consistent with established protocols for high-throughput functional screening of small molecule (<900 daltons) drug libraries in PBMCs and other cell types[127,128]. It also represents the maximum assay concentration of compound obtainable, following dilution of the 10 mM FDA library stock, which does not exceed the threshold toxicity concentration for functional assays of 0.2% DMSO[128–131]. Compounds assayed at concentrations other than 20 μM (5%, n=47) reflected either dilutions of existing 20 μM library compounds or compounds for which *in vitro* EC_{50} data differed from 20 μM by several orders of magnitude. All stocks and dilutions of stimulants and compounds were stored at -80°C and repeated freeze thaw cycles were avoided.

2.4 STIMULATION OF PBMCS

Stimulation is defined broadly as the exposure of PBMC cells to a ligand which has the potential to perturb resting state cell signalling dynamics by either increasing or decreasing the expression of cell signalling epitopes. PBMCs were pelleted and resuspended (via 30μm cell strainer (Partec) for TC and AI studies) at 90 μl/well in 96-well polypropylene plates using complete RPMI media without penicillin-streptomycin. The resuspended cell concentrations were $2*10^6$ cells/ml (TC), $0.75*10^6$ cells/ml (AI), $1.2*10^6$ cells/ml (FDA) and $3.2*10^6$ cells/ml (DD). The cells were rested for 90 min (TC, AI) or 45 min (FDA and DD studies) at 37°C before ligand exposure. For the FDA study, this resting period was used to preincubate the cells with the extended FDA library compounds prior to stimulation.

Stimulants and vehicle were reconstituted in complete RPMI media without penicillin-streptomycin and added to the cells using a Biomek NX liquid handler (Beckman Coulter) with integrated compact shaker-heater-cooler system (Inheco). The ligand cocktail anti-CD3/CD28-XL was added in a two-step process (DD). First, anti-CD3/CD28 antibodies were added for 2 min at 37°C, and then the cross-linking Neutravidin (-XL) was added simultaneously with the rest of the stimulants. The final concentration of DMSO in all conditions including vehicle was 0.10 % (TC, AI and DD studies) and 0.21% (FDA). Vehicle wells represented one eighth of the total wells assayed (TC, AI and DD studies) or one sixth of the total wells assayed (FDA) and were spaced evenly across each 96-well plate. The cells were exposed to the stimulants at 37°C for 1, 5, 15 and 30 min (TC) or 30 min (AI, FDA and DD

studies). Ligand exposure was halted by fixation for 10 min at 37°C using paraformaldehyde (Sigma-Aldrich) at a final concentration of 1.6 % in PBS.

2.5 FLUORESCENT CELL BARCODING

Stock solutions of barcoding dyes CBD 450 (BD Biosciences), CBD 500 (BD Biosciences) and DL800 (Thermo Scientific) were prepared as per the manufacturer's instructions in DMSO in polypropylene 96-well plates and stored at -80°C. Different combinations of these dyes were used to produce a different number of barcoded cell populations specific to each study as follows. For the TC study 80 populations were resolved using final concentrations of CBD 450 (0.000, 0.015, 0.075, 0.300 μg/ml) combined with CBD 500 (0.000, 0.038, 0.188, 0.750 μg/ml) and DL800 (0.000, 0.011, 0.033, 0.100, 0.300 μg/ml). For the AI study 64 populations were resolved using final concentrations of CBD 450 (0.000, 0.015, 0.050, 0.150 μg/ml) combined with CBD 500 (0.000, 0.038, 0.125, 0.375 μg/ml) and DL800 (0.000, 0.017, 0.050, 0.150 μg/ml). For the DD study 16 populations were resolved using final concentrations of CBD 450 (0.000, 0.015, 0.050, 0.150 μg/ml) combined with CBD 500 (0.000, 0.038, 0.125, 0.375 μg/ml). For the FDA study four populations were resolved using final concentrations of DL800 (0.000, 0.017, 0.050, 0.150 μg/ml).

Fixed cells were washed with PBS and permeabilized in 100 μl ice cold methanol for 20 min at 2°C using a Biomek NX liquid handler. The barcoding dyes were diluted in ice cold PBS and 100 μl/well added to the suspension of cells in methanol. The final concentration of DMSO from the barcoding dyes at this stage was 3.5%. The barcoding reaction was incubated for 30 min at 2°C and the cells were washed five times (TC, AI, DD), or four times (FDA), in ice cold FACS buffer (PBS with bovine serum albumin 0.05 % (Sigma-Aldrich)). The barcoding wells were pooled, washed in a total volume of 45 ml (TC, AI), 2 ml (DD) or 0.28 ml (FDA) FACS buffer and resuspended at $1*10^6$ cells/ml in FACS buffer.

2.6 INTRACELLULAR STAINING OF CELL SIGNALLING EPITOPES IN PBMC SUBSETS

The suspension of fixed-permeabilized-barcoded cells was either stained using PBMC subtyping antibodies directly (TC, AI, FDA) or following pre-incubation with human Fc receptor binding inhibitor (DD; eBioscience). The pre-incubation consisted of 20 min at $1*10^7$ cells/ml in FACS buffer

with 12.5% human Fc receptor binding inhibitor, followed by resuspension for staining in FACS buffer at $1*10^6$ cells/ml (DD). The cell suspension was stained with either 0.5 µl/ml anti-human CD3 (UCHT1) PE-Cy7 (eBioscience) (TC, AI), or 1 µl/ml anti-human CD3 (UCHT1) PE-Cy7 and 1 µl/ml anti-human CD4 (SK3) PerCP-eFluor 710 (eBioscience) (DD), or 1 µl/ml anti-human CD3 (UCHT1) APC (eBioscience) (FDA). The suspension was distributed across a 96 well polypropylene plate at 90 µl/well (TC, AI and DD) or 60 µl/well (FDA). The cells were stained using a Biomek NX liquid handler (Beckman Coulter) with fluorescently-conjugated anti-human antibodies against intracellular signalling epitopes **(Table 2.3)** for 45 min at room temperature, as per the manufacturer's instructions. Antibodies were purchased from BD Biosciences, Cell Signalling Technology, Merck Millipore and Bioss. Antibodies against intracellular epitopes were used either individually (TC, FDA) or in groups of three antibodies per plex (AI, DD). The cells were washed twice with FACS buffer and resuspended in a final volume of 150 µl/well (TC, AI, and DD) or 100 µl (FDA) using FACS buffer.

2.7 IMMUNOPHENOTYPING

PBMCs were resuspended at 1 $x10^6$ cells/ml in 100 µl of FACS buffer, with 20 % human Fc receptor binding inhibitor and incubated for 20 min at room temperature in 5ml polystyrene FACS tubes. The PBMCs were stained in a total volume of 135 µl/tube with 0.5 µl of anti-human CD3 (UCHT1) PE-Cy7 (eBioscience), 0.5 µl of anti-human CD4 (SK3) PerCP-eFluor 710 (eBioscience), 0.5 µl of anti-human CD8 (SK1) APC-eFluor780 (eBioscience). The cells were incubated for 30 min at room temperature. They were washed twice with 3 ml of FACS buffer and resuspended in 0.5 ml of FACS buffer with 1 µM DAPI (Sigma-Aldrich).

2.8 DATA ACQUISITION USING FLOW CYTOMETRY

PBMC cell suspensions were acquired using an eight colour FACS Verse flow cytometer (BD Biosciences) with 405, 488 and 640 nm laser excitation at an average flow rate of 2 µl/sec and an average threshold event rate of 1000-2000 events/sec. The average number of viable single cell events collected per barcode population was 500 events (TC, AI), 3000 events (DD) and 2000 events (FDA). Multicolour Cytometer Setup and Tracking (CST) beads (BD Biosciences) were used for quality control and standardization of photomultiplier tube (PMT) detector voltages across multiple experimental runs. Fluorescence compensation for immunophenotyping was conducted using anti-mouse IgGκ antibody capture beads (Bangs Laboratories) labelled separately with each antibody.

Fluorescence compensation for barcoding dyes was conducted using single stain controls with maximum and minimum concentrations of each barcoding dye per PBMC sample. Fluorescence compensation for intracellular cell signalling epitopes in different PBMC subsets was conducted using anti-mouse IgGκ antibody capture beads labelled separately with individual antibodies for each study as follows. For the TC and AI studies, anti-human CD3 (UCHT1) PeCy7 (eBioscience), anti-human STAT3 (pY705) (4/P-STAT3) AlexaFluor488 (AF 488; BD Biosciences), anti-human STAT3 (pY705) (4/P-STAT3) PE (BD Biosciences) and anti-human STAT3 (pY705) (4/P-STAT3) AlexaFluor647 (AF647; BD Biosciences) were used. For the DD study, anti-human CD3 (UCHT1) PeCy7 (eBioscience), anti-human CD4 (SK3) PerCP-eFluor 710 (eBioscience), anti-human STAT3 (pY705) (4/P-STAT3) AlexaFluor488 (AF 488; BD Biosciences), anti-human STAT3 (pY705) (4/P-STAT3) PE (BD Biosciences) and anti-human STAT3 (pY705) (4/P-STAT3) AlexaFluor647 (AF647; BD Biosciences) were used. For the FDA study, anti-human CD3 (UCHT1) APC (eBioscience) and anti-human PLC-γ1 (10/PLCgamma) PE (BD Biosciences) were used.

2.9 STATISTICAL DATA ANALYSIS

Flow cytometry data was analyzed in FCS 3.0 file format using Flow Jo v. 10.0.8 (Tree Star) and Kaluza Analysis v. 1.3 (Beckman Coulter) software. Statistical analysis was conducted using R v. 3.1.2 software (R Core Team). PBMC samples in which the lymphocyte gate contained less than 30% of events, measured by forward scatter (FSC-A)/side scatter (SSC-A), were excluded from further analysis. Within each PBMC sample, individual treatment-epitope combinations (nodes) for which the cell count was lower than 50 cells (TC, AI, DD) or 200 cells (FDA) were excluded from further analysis. Across PBMC samples, nodes with fewer than 4 data points (i.e. 4 PBMC samples; TC, FDA) or fewer than 8 data points (i.e. 8 PBMC samples; AI, DD) were excluded from further analysis. Negative median fluorescence intensities (MFIs) caused by background and spectral overlap compensation were replaced by the minimum positive node value (DD). MFIs in the DD study were $\log_2$ transformed to approximate normality before statistical analysis. MFIs in the TC, AI and FDA studies were analysed untransformed. For the clinical studies, batch effects in MFIs, caused by running samples on different days (AI, DD) and by using samples collected in different clinical centres (DD), were normalized for each epitope using the empirical Bayes algorithm- ComBat. Experimental variables including positional effects within and across 96 well plates, barcoding dye fluorescence spillover, sample viability, cell counts, clinical group and sample source were controlled for by principal component and Z factor analyses. Matching of clinical groups was

conducted using the Mann-Whitney U test for continuous variables or the Fisher's exact test for categorical variables.

For the determination of stimulant activity, the MFIs across PBMC samples, per stained epitope, were compared between each stimulant and the vehicle treatment using the unpaired Wilcoxon rank-sum test. To account for the unknown distribution of the data, the small sample size and the presence of outliers, the null distribution of the test statistic was estimated by randomly permuting sample labels 10,000 times for each node. The same test was also applied for each stimulant per functional fluorescence channel (AF 488, PE and AF647) in the unstained condition to determine whether the stimulant activity was an artefact of fluorescence spillover from adjacent channels or ligand auto-fluorescence (collectively termed background fluorescence). In cases where the stimulant MFI was significantly (permuted $p<0.05$) altered with respect to vehicle MFI in the unstained condition, the epitopes labelled in the corresponding functional channel were only counted as active if the MFI response was in a different direction or had a 10% greater fold change than the unstained condition. For stimulants with significant activity (permuted $p<0.05$) which superseded the background fluorescence, the response ratio was quantified as the MFI of the stimulant divided by the MFI of the vehicle across PBMC samples. For responses <1 (i.e. where the stimulant caused a decrease in MFI with respect to the vehicle) the response is reported as a negative fold change (-1/ response ratio). The stain index of each antibody was calculated across PBMC samples, in the absence of stimulation, as the median MFI of the antibody stained sample divided by the median MFI of the corresponding unstained control. The two-tailed Spearman's rank test was used to assess the correlation in fold change responses for nodes replicated in independent experiments.

In the AI and DD studies, association of each signalling node MFI to clinical group status was investigated using linear fixed effects regression after adjusting for covariates. The predictive variables of clinical group and ligand presence were set as interaction terms within the regression model to determine epitopes which responded differently to individual ligand exposures across the clinical groups. Differences in basal epitope expression between clinical groups were defined as epitopes in which at least 30% of nodes tested significantly (permuted $p<0.05$) for a main effect of the clinical group variable, independently of the ligand identity variable. Where basal epitope expression differences were detected between groups, the mean MFI of the vehicle condition per epitope and sample group was used to represent the fold change. Optional covariates, age and BMI, were selected in the regression model in a stepwise procedure for each node separately using Bayesian Information Criterion. The mean of eight measurements in the vehicle condition and a single measurement in the stimulant condition per donor were used for the analysis. To account for

the unknown distribution of the data, the small sample size and the presence of outliers, the null distribution of the test statistic was estimated by randomly permuting sample labels 10,000 times for each node. Due to the exploratory nature of the AI and DD study, nodes with an unadjusted permuted $p<0.05$ were considered significant. Unsupervised hierarchical clustering using the correlation similarity metric and average linkage clustering (R 'made4' package) was used to group nodes significantly associated to clinical status and group PBMC samples with different clinical identities. Nodes were represented for clustering as the ratio of MFI of the ligand treatment to MFI of the vehicle treatment (for ligand responses) or ratio of the MFI of the vehicle condition to mean MFI of the vehicle condition in the control group (for basal epitope expression) per condition and sample, scaled across all nodes. Missing data were replaced for clustering with the mean of the respective node and clinical group.

In the FDA study, association of phospholipase C (PLC)-γ1 MFI to compound and stimulant status was investigated using permutation-based linear fixed effects regression (n=10,000 permutations). The predictive variables of stimulant group (thapsigargin or vehicle) and compound exposure (compound or vehicle) were set as interaction terms in the regression model to determine compounds which modified the PLC-γ1 response to thapsigargin. For compounds which showed a significant interaction with the stimulant (permuted $p<0.05$), post-hoc one-way analysis of variance (ANOVA) tests and median values were used to determine the directionality of the effects. In the validation experiments, dose-response data was fitted with 4-parameter (thapsigargin dose-response experiments) or 5-parameter (drug dose-response experiments) logistic regression models (R 'nplr' package and GraphPad Prism 5).

Data was visualized using Flow Jo v. 10.0.8, Kaluza Analysis v. 1.3, R software, GraphPad Prism 5, Excel 2016, PubChem and Adobe Illustrator.

Ligands	Abbreviation	Function	Class	Assay conc.	Conc. unit	TC	AI	DD	FDA	CAS number	Supplier
anti-IgG/ anti-IgM/ anti-Igλ/ anti-Igκ	anti-BCR/FcR-XL	B cell R (BCR)/ Fc R cross-linker agonist	Antigen receptor ligand	2/ 2/ 2/ 4	ug/ml	TC	AI			NA	Sigma (3)/ ab-online
anti-IgG/ anti-IgM/ anti-Igλ/ anti-Igκ// MegaCD40L	anti-BCR/FcR-XL // CD40L	B cell R (BCR)/ Fc R cross-linker agonist// CD40 agonist	Antigen receptor ligand	2/ 2/ 2/ 4// 0.25	ug/ml			DD		NA	Sigma (3)/ ab-online/ Enzo
anti-CD3 (HIT3a)/ anti-CD28 (CD28.2)	anti-CD3/ CD28	T cell R (TCR)/ CD28 agonist	Antigen receptor ligand	0.5/ 0.5	ug/ml	TC	AI			NA	eBioscience (2)
anti-CD3 (OKT3)-biotin/ anti-CD28 (CD28.2)-biotin/ NeutrAvidin	anti-CD3/ CD28-XL	T cell R (TCR)/ CD28 cross-linker agonist	Antigen receptor ligand	2.5/ 2.5/ 12.5	ug/ml			DD		NA	eBioscience (2)/ Life Technologies
lipopolysaccharides *Escherichia coli* 055:B5	LPS	toll-like R 4 (TLR4) agonist	Antigen receptor ligand	0.1	ug/ml	TC	AI			NA	Sigma
staphylococcal enterotoxin B *Staphylococcus aureus*	SEB	T cell R (TCR) agonist	Antigen receptor ligand	1	ug/ml	TC	AI			NA	Sigma
(S)-3,5-DHPG	(S)-3,5-DHPG	metabotropic glutamate 1/5 (mGlu1/5) R agonist	CNS ligand	10	uM	TC				162870-29-3	Tocris
2-pyridylethylamine dihydrochloride	2-pyridylethylamine	histamine 1 (H1) R agonist	CNS ligand	10	uM	TC	AI			3343-39-3	Tocris
7-hydroxy-DPAT hydrobromide	7-OH-DPAT	dopamine 3 (D3) R agonist	CNS ligand	10	uM	TC	AI			74938-11-7	Tocris
agomelatine	agomelatine	melatonin 1/2 (MT1/2) R agonist	CNS ligand	10	uM	TC	AI			138112-76-2	abcam
AS 19	AS 19	5-hydroxytryptamine 7 (5-HT7) R agonist	CNS ligand	10	uM	TC	AI			1000578-26-6	Tocris
cis-ACPD// (S)-(-)-5-fluorowillardiine	cis-ACPD// (S)(-)-5-FW	N-methyl-D-aspartate (NMDA) R agonist, mGlu2/3 R agonist // α-amino-3-hydroxy-5-methyl-4-isoxazolepropionic acid (AMPA) R agonist	CNS ligand	10// 10	uM	TC				477331-06-9	Tocris (2)
isoproterenol hydrochloride	isoproterenol	β-adreno (β-A) R agonist	CNS ligand	10	uM	TC	AI			51-30-9	Tocris
L-AP4	L-AP4	metabotropic glutamate 4/6/7/8 (mGlu4/6/7/8) R agonist	CNS ligand	10	uM	TC				23052-81-5	Tocris
LY 354740 hydrate	LY 354740	metabotropic glutamate 2/3 (mGlu2/3) R agonist	CNS ligand	10	uM	TC				176199-48-7	Tocris
muscimol	muscimol	γ-Aminobutyric acid A (GABA-A) R agonist	CNS ligand	10	uM	TC				2763-96-4	Tocris
NECA	NECA	adenosine 1/2A/3 (A1/2A/3) R agonist	CNS ligand	10	uM	TC	AI	DD		35920-39-9	Tocris
PD 168077 maleate	PD 168077	dopamine 4 (D4) R agonist	CNS ligand	10	uM	TC				630117-19-0	Tocris
PHA 543613 hydrochloride	PHA 543613	α-7 nicotinic acetylcholine receptor (α-7nACh) R agonist	CNS ligand	10	uM	TC	AI			478149-53-0	Tocris
phencyclidine hydrochloride	phencyclidine	N-methyl-D-aspartate (NMDA) R antagonist, σ R agonist	CNS ligand	10	uM	TC	AI	DD		956-90-1	Sigma
SKF 83822 hydrobromide	SKF 83822	dopamine 1/5 (D1/5) R agonist	CNS ligand	10	uM	TC	AI			74115-08-5	Tocris
SR 57227 hydrochloride	SR 57227	5-hydroxytryptamine 3 (5-HT3) R agonist	CNS ligand	10	uM	TC	AI			77145-61-0	Tocris
sumanirole maleate	sumanirole	dopamine 2 (D2) R agonist	CNS ligand	10	uM	TC	AI			179386-43-7	Tocris
TCB-2	TCB-2	5-hydroxytryptamine 2A (5-HT2A) R agonist	CNS ligand	10	uM	TC	AI			912342-28-0	Tocris
WAY 161503 hydrochloride	WAY 161503	5-hydroxytryptamine 2C (5-HT2C) R agonist	CNS ligand	10	uM	TC				75704-24-4	Tocris
WAY 208466 dihydrochloride	WAY 208466	5-hydroxytryptamine 6 (5-HT6) R agonist	CNS ligand	10	uM	TC				633304-27-5	Tocris
xaliproden hydrochloride	xaliproden	5-hydroxytryptamine 1A (5-HT1A) R agonist	CNS ligand	10	uM	TC	AI			90494-79-4	Tocris
xanomeline oxalate	xanomeline	muscarinic 1 (M1) R agonist	CNS ligand	10	uM	TC	AI			141064-23-5	Tocris
interferon-α2c*	IFN-α2c	interferon α/β (IFNα/β) R agonist	Cytokine	0.1	ug/ml	TC	AI	DD		NA	eBioscience
interferon-γ*	IFN-γ	interferon γ (IFNγ) R agonist	Cytokine	0.1	ug/ml	TC	AI			NA	eBioscience
interleukin-10 *	IL-10	interleukin-10 (IL-10) R agonist	Cytokine	0.1	ug/ml	TC	AI	DD		NA	eBioscience
interleukin-1β *	IL-1β	interleukin-1β (IL-1β) R agonist	Cytokine	0.1	ug/ml	TC	AI			NA	eBioscience
interleukin-2 *	IL-2	interleukin-2 (IL-2) R agonist	Cytokine	0.1	ug/ml	TC	AI			NA	eBioscience
interleukin-23 *	IL-23	interleukin-23 (IL-23) R agonist	Cytokine	0.1	ug/ml	TC	AI			NA	eBioscience
interleukin-4 *	IL-4	interleukin-4 (IL-4) R agonist	Cytokine	0.1	ug/ml	TC	AI			NA	eBioscience
interleukin-6 *	IL-6	interleukin-6 (IL-6) R agonist	Cytokine	0.1	ug/ml	TC	AI	DD		NA	eBioscience
tumor necrosis factor-α *	TNF-α	tumor necrosis factor (TNF) R agonist	Cytokine	0.1	ug/ml	TC	AI			NA	eBioscience

Table 2.1 Ligands used to stimulate/ alter cell signalling dynamics in PBMCs. Ligands are ordered by class and then alphabetically. Time course (TC), Antipsychotic intervention (AI), Differential diagnosis (DD) and FDA compound library screening (FDA) columns denote the studies for which the ligands were used. (*) recombinant human protein. The antibodies in anti-CD3/ CD28 and anti-CD3/ CD28-XL stimulant cocktails are anti-human mouse monoclonal antibodies for which the clone is specified in brackets. The antibodies in anti-BCR/ FcR-XL and anti-BCR/ FcR-XL + CD40L stimulant cocktails are anti-human goat polyclonal antibodies. Receptor (R) subtypes and enzyme isotypes quoted represent those for which the ligand displays significantly higher binding affinity (Ki) or in vitro-potency (EC50) relative to other subtypes/ isotypes.

Ligands	Abbreviation	Function	Class	Assay conc.	Conc. unit	TC	AI	DD	FDA	CAS number	Supplier
17 β-estradiol	17 β-estradiol	Oestrogen (E) R agonist	Hormone/ growth factor	10	uM	TC	AI			50-28-2	Sigma
brain derived neurotrophic factor *	BDNF	tyrosine receptor kinase B (TrkB) R agonist	Hormone/ growth factor	0.1	ug/ml	TC	AI			NA	eBioscience
dexamethasone	dexamethasone	glucocorticoid (G) R agonist	Hormone/ growth factor	10	uM	TC	AI			50-02-2	Sigma
insulin*	insulin	insulin (I) R agonist	Hormone/ growth factor	0.1	uM	TC	AI			NA	Sigma
leptin*	leptin	leptin (LEP) R agonist	Hormone/ growth factor	1	ug/ml	TC	AI			NA	R&D Systems
platelet-derived growth factor-BB *	PDGF-BB	fibroblast proliferation agonist	Hormone/ growth factor	0.1	ug/ml	TC				NA	eBioscience
β-nerve growth factor*	β-NGF	tropomyosin receptor kinase A (TrkA) agonist	Hormone/ growth factor	0.1	ug/ml	TC				NA	Life Technologies
aripiprazole	aripiprazole	dopamine 2 (D2) R and 5-HT1A R partial agonist, 5-HT2A R antagonist	Neuropsychiatric treatment	10	uM	TC	AI			129722-12-9	abcam
carbamazepine	carbamazepine	voltage-gated sodium channel inhibitor	Neuropsychiatric treatment	10	uM	TC				298-46-4	Sigma
clozapine	clozapine	5-hydroxytryptamine 2A/2C (5-HT2A/2C) R and dopamine 4 (D4) R antagonist	Neuropsychiatric treatment	10	uM	TC	AI			5786-21-0	Tocris
desipramine hydrochloride	desipramine	noradrenaline (NA) reuptake inhibitor	Neuropsychiatric treatment	10	uM	TC	AI			58-28-6	Sigma
desvenlafaxine succinate	desvenlafaxine	5-hydroxytryptamine (5HT) reuptake inhibitor	Neuropsychiatric treatment	10	uM	TC	AI			386750-22-7	Tocris
fluoxetine hydrochloride	fluoxetine	5-hydroxytryptamine (5HT) reuptake inhibitor	Neuropsychiatric treatment	10	uM	TC	AI			56296-78-7	Tocris
haloperidol	haloperidol	dopamine 2/3 (D2/3) R inverse agonist	Neuropsychiatric treatment	10	uM	TC	AI			52-86-8	Sigma
lithium chloride	lithium	glycogen synthase kinase-3β (GSK-3β) inhibitor	Neuropsychiatric treatment	10000	uM	TC	AI			7447-41-8	Sigma
olanzapine	olanzapine	5-hydroxytryptamine 2A (5-HT2A) R and dopamine 1-5 (D1-5) R antagonist	Neuropsychiatric treatment	10	uM	TC	AI			132539-06-1	Tocris
quetiapine hemifumarate	quetiapine	5-hydroxytryptamine 2A (5-HT2A) R and dopamine 2/3 (D2/3) R antagonist	Neuropsychiatric treatment	10	uM	TC				111974-72-2	Tocris
risperidone	risperidone	5-hydroxytryptamine 2A (5-HT2A) R and dopamine 2-4 (D2-4) R antagonist	Neuropsychiatric treatment	10	uM	TC	AI			106266-06-2	Tocris
sodium valproic acid	valproic acid	sodium channel and histone deacetylase inhibitor	Neuropsychiatric treatment	1000	uM	TC	AI			1069-66-5	Sigma
740 Y-P	740 Y-P	Phosphatidylinositol-4,5-bisphosphate 3-kinase activator	Positive control - activator	3	uM	TC				1236188-16-1	Tocris
sodium 8-bromo-cAMP	8-Br-cAMP	protein kinase A activator	Positive control - activator	700	uM	TC	AI			76939-46-3	Tocris
calyculin A	calyculin A	protein phosphatase 1/2A (PP1/2A) inhibitor	Positive control - activator	1	uM	TC	AI	DD		101932-71-2	Tocris
forskolin	forskolin	adenylyl cyclase activator	Positive control - activator	10	uM	TC	AI	DD		66575-29-9	Tocris
GW 9508	GW 9508	free fatty acid receptor 1 (FFA1) R agonist	Positive control - activator	10	uM	TC				885101-89-3	Tocris
sodium orthovanadate	orthovanadate	protein tyrosine phosphatase (PTPase), alkaline phosphatase (ALPase) and adenosine triphosphatase (ATPase) inhibitor	Positive control - activator	150	uM	TC	AI			13721-39-6	Tocris
phorbol 12-myristate 13-acetate/ calcium ionomycin *Streptomyces conglobatus*	PMA/ ionomycin	protein kinase C (PKC) activator / extracellular calcium ionophore	Positive control - activator	0.1/ 1	uM	TC	AI	DD		56092-82-1	Tocris/ Sigma
PS 48	PS 48	Phosphoinositide-dependent protein kinase-1 (PDK1) activator	Positive control - activator	10	uM	TC	AI			1180676-32-7	Tocris
SC-9	SC-9	protein kinase C (PKC) activator	Positive control - activator	10	uM	TC	AI			102649-78-5	Tocris
simvastatin	simvastatin	3-hydroxy-3-methyl-glutaryl-CoA reductase (HMGCR) inhibitor	Positive control - activator	10	uM	TC	AI			79902-63-9	Tocris
thapsigargin	thapsigargin	sarco-endoplasmic reticulum Ca2+-ATPase inhibitor	Positive control - activator	1 (0.5 for FDA)	uM	TC	AI	DD	FDA	67526-95-8	Tocris
CHIR 99021	CHIR 99021	glycogen synthase kinase-3β (GSK-3β) inhibitor	Positive control - inhibitor	10	uM	TC	AI			252917-06-9	Collaborator
GSK 690693	GSK 690693	protein kinase B (AKT) inhibitor	Positive control - inhibitor	10	uM	TC	AI			937174-76-0	Tocris
JB1121	JB1121	glycogen synthase kinase-3β (GSK-3β) inhibitor	Positive control - inhibitor	10	uM	TC	AI	DD			Collaborator
rapamycin	rapamycin	mammalian target of rapamycin (mTOR) inhibitor	Positive control - inhibitor	5	uM	TC	AI	DD		53123-88-9	Tocris
staurosporine	staurosporine	protein kinase inhibitor	Positive control - inhibitor	5	uM	TC	AI	DD		62996-74-1	Enzo

Table 2.1 continued. Ligands used to stimulate/ alter cell signalling dynamics in PBMCs. Ligands are ordered by class and then alphabetically. Time course (TC), Antipsychotic intervention (AI), Differential diagnosis (DD) and FDA compound screening (FDA) columns denote the studies for which the ligands were used. *recombinant human protein. Receptor (R) subtypes and enzyme isotypes quoted represent those for which the ligand displays significantly higher binding affinity (Ki) or in vitro-potency (EC50) relative to other subtypes/ isotypes.

Table 2.2: Extended FDA compound library (n=946). Source refers to the original compound library. The majority come from the FDA approved drug library v.2-Enzo Life Sciences (n=786; FDA). Experimental compounds (n=160) include those from collaborators (Broad Institute (BI), John's Hopkins University/ McMaster University (JH/ M), Royal Holloway University (RH)) and positive controls and neutraceuticals from the Cambridge Centre for Neuropsychiatric Research library (CCNR). The choice of a final assay concentration of 20 µM is consistent with established protocols for high-throughput functional screening of small molecule (<900 Da) drug libraries in PBMCs and other cell types[127,128.] It also represents the maximum assay concentration of compound obtainable, following dilution of the 10 mM FDA library stock, which does not exceed the threshold toxicity concentration for functional assays of 0.2% DMSO[128–131]. Compounds assayed at concentrations other then 20 µM (5%, n=47) reflected either dilutions of existing 20 µM library compounds or compounds for which in vitro EC50 data differed from 20 µM by several orders of magnitude.

ID	Source	Ligand	Assay conc. (uM)
1	FDA	(±) Isoproterenol·HCl	20
2	FDA	(±)-Atenolol	20
3	FDA	(S)-Timolol Maleate	20
4	FDA	4-Aminosalicylic Acid	20
5	FDA	Abacavir Sulfate	20
6	FDA	Acamprosate	20
7	FDA	Acarbose	20
8	FDA	Acebutolol·HCl	20
9	FDA	Acetaminophen	20
10	FDA	Acetazolamide	20
11	FDA	Acetohexamide	20
12	FDA	Acetohydroxamic Acid	20
13	FDA	Acetylcholine Chloride	20
14	FDA	Acetylcysteine	20
15	FDA	Acitretin	20
16	FDA	Acrivastine	4
17	FDA	Acyclovir (Acycloguanosine) Zovirax	20
18	FDA	Adapalene	20
19	FDA	Adefovir Dipivoxil	20
20	FDA	Adenosine	20
21	FDA	Albendazole	20
22	FDA	Alendronate·Na Trihydrate	20
23	FDA	Alfuzosin	20
24	FDA	Alitretinoin	20
25	FDA	Allopurinol	20
26	FDA	Almotriptan	20
27	FDA	Alosetron·HCl	20
28	FDA	Alprostadil	20
29	FDA	Altretamine	20
30	FDA	Amantadine·HCl	20
31	FDA	Ambrisentan	20
32	FDA	Amcinonide	20
33	FDA	Amifostine	20
34	FDA	Amikacin Disulfate	20
35	FDA	Amiloride·HCl·2H2O	20
36	FDA	Aminocaproic Acid	20
37	FDA	Aminohippurate·Na	20
38	FDA	Aminolevulinic Acid·HCl	20
39	FDA	Aminophylline	20
40	FDA	Amiodarone·HCl	20
41	FDA	Amitriptyline·HCl	20
42	FDA	Amlexanox	20
43	FDA	Amlodipine	20
44	FDA	Amoxapine	20
45	FDA	Amoxicillin	20
46	FDA	Amphotericin B	20
47	FDA	Ampicillin Trihydrate	20
48	FDA	Amrinone	20
49	FDA	Anagrelide	20
50	FDA	Anastrozole	20
51	FDA	Apomorphine·HCl Hemihydrate	20
52	FDA	Aprepitant	20
53	FDA	Argatroban	20
54	FDA	Aripiprazole	20
55	FDA	Arsenic Trioxide	20
56	FDA	Artemether	20
57	FDA	Articaine·HCl	20
58	FDA	Asenapine Maleate	20
59	FDA	Aspirin (Acetylsalicylic Acid)	20
60	FDA	Atazanavir	20
61	FDA	Atomoxetine·HCl	20
62	FDA	Atorvastatin Calcium	20
63	FDA	Atovaquone	20
64	FDA	Atracurium Besylate	20
65	FDA	Atropine Sulfate Monohydrate	20
66	FDA	Auranofin	20
67	FDA	Azacitidine	20
68	FDA	Azathioprine	20
69	FDA	Azelaic Acid	20
70	FDA	Azelastine·HCl	20
71	FDA	Azithromycin	20
72	FDA	Aztreonam	20
73	FDA	Bacitracin	20
74	FDA	Baclofen	20
75	FDA	Balsalazide	20
76	FDA	Beclomethasone Dipropionate	20
77	FDA	Benazepril·HCl	20
78	FDA	Bendamustine·HCl	20
79	FDA	Bendroflumethiazide	20
80	FDA	Benztropine Mesylate	20
81	FDA	Betaine	20
82	FDA	Betamethasone	20
83	FDA	Betaxolol·HCl	20
84	FDA	Bethanechol Chloride	20
85	FDA	Bexarotene	20
86	FDA	Bicalutamide	20
87	FDA	Bimatoprost	20
88	FDA	Biperiden·HCl	20
89	FDA	Bisacodyl	20
90	FDA	Bisoprolol Fumarate	20
91	FDA	Bleomycin Sulfate	20
92	FDA	Bortezomib	20
93	FDA	Bosentan	20

94	FDA	Brimonidine	20
95	FDA	Bromfenac	20
96	FDA	Bromocriptine Mesylate	20
97	FDA	Brompheniramine Maleate	20
98	FDA	Budesonide	20
99	FDA	Bumetanide	20
100	FDA	Bupivacaine·HCl	20
101	FDA	Bupropion	20
102	FDA	Buspirone·HCl	20
103	FDA	Busulfan	20
104	FDA	Butenafine·HCl	20
105	FDA	Butoconazole Nitrate	20
106	FDA	Butorphanol-(+)-Tartrate (Schedule Iv)	20
107	FDA	Cabergoline	20
108	FDA	Caffeine	20
109	FDA	Calcipotriene	20
110	FDA	Calcitriol	20
111	FDA	Candesartan	20
112	FDA	Capecitabine	20
113	FDA	Capreomycin Sulfate	20
114	FDA	Capsaicin	20
115	FDA	Captopril	20
116	FDA	Carbachol (Carbamylcholine) Chloride	20
117	FDA	Carbamazepine	20
118	FDA	Carbidopa	20
119	FDA	Carbinoxamine Maleate	20
120	FDA	Carboplatin	20
121	FDA	Carglumic Acid	20
122	FDA	Carmustine	20
123	FDA	Carvedilol	20
124	FDA	Cefaclor	20
125	FDA	Cefadroxil	20
126	FDA	Cefazolin·Na	20
127	FDA	Cefdinir	20
128	FDA	Cefditoren Pivoxil	20
129	FDA	Cefepime·HCl Hydrate	20
130	FDA	Cefixime	20
131	FDA	Cefotaxime Acid	20
132	FDA	Cefotetan Disodium	20
133	FDA	Cefoxitin·Na	20
134	FDA	Cefpodoxime Proxetil	20
135	FDA	Cefprozil	20
136	FDA	Ceftazidime	20
137	FDA	Ceftibuten	20
138	FDA	Ceftizoxim·Na	20
139	FDA	Ceftriaxone·Na	20
140	FDA	Cefuroxime Axetil	20
141	FDA	Cefuroxime·Na	20
142	FDA	Celecoxib	20
143	FDA	Cephalexin Monohydrate	20
144	FDA	Cetirizine 2HCl	20
145	FDA	Chenodiol (Chenodeoxycholic Acid)	20
146	FDA	Chlorambucil	20
147	FDA	Chloramphenicol	20
148	FDA	Chlorhexidine Dihydrochloride	20
149	FDA	Chloroquine Diphosphate	20
150	FDA	Chlorothiazide	20
151	FDA	Chlorpheniramine Maleate	20
152	FDA	Chlorpromazine·HCl	20
153	FDA	Chlorpropamide	20
154	FDA	Chlorthalidone	20
155	FDA	Chlorzoxazone	20
156	FDA	Ciclesonide	20
157	FDA	Ciclopirox	20
158	FDA	Cidofovir	20
159	FDA	Cilastatin·Na	20
160	FDA	Cilostazol	20
161	FDA	Cimetidine	20
162	FDA	Cinacalcet·HCl	20
163	FDA	Ciprofloxacin	20
164	FDA	Cisatracurium Besylate	20
165	FDA	Cisplatin (Cis-Diamineplatinum(Ii) Dichloride)	20
166	FDA	Citalopram·HBr	20
167	FDA	Cladribine	20
168	FDA	Clarithromycin	20
169	FDA	Clavulanate Potassium	20
170	FDA	Clemastine Fumarate	20
171	FDA	Clindamycin Palmitate·HCl	20
172	FDA	Clindamycin·HCl	20
173	FDA	Clobazam	20
174	FDA	Clobetasol Propionate	20
175	FDA	Clofarabine	20
176	FDA	Clofazimine	20
177	FDA	Clomiphene Citrate	20
178	FDA	Clomipramine·HCl	20
179	FDA	Clonazepam	20
180	FDA	Clonidine·HCl	20
181	FDA	Clopidogrel Hydrogen Sulfate	20
182	FDA	Clotrimazole	20
183	FDA	Cloxacillin·Na	20
184	FDA	Clozapine	20
185	FDA	Colchicine	20
186	FDA	Colistimethate·Na	20
187	FDA	Colistin Sulfate	20
188	FDA	Cortisone Acetate	20
189	FDA	Cromolyn·Na (Disodium Cromoglycate)	20
190	FDA	Crotamiton	20
191	FDA	Cyclobenzaprine·HCl	20
192	FDA	Cyclopentolate	20
193	FDA	Cyclophosphamide (Free Base)	20
194	FDA	Cycloserine	20
195	FDA	Cyclosporine A	20
196	FDA	Cyproheptadine·HCl Sesquihydrate	20
197	FDA	Cysteamine·HCl	20
198	FDA	Cytarabine	20
199	FDA	Dacarbazine	20
200	FDA	Dactinomycin (= Actinomycin D)	20
201	FDA	Dalfampridine (4-Aminopyridine)	20
202	FDA	Danazol	20
203	FDA	Dantrolene·Na	20
204	FDA	Dapsone	20
205	FDA	Daptomycin	20
206	FDA	Darifenacin·HBr	20
207	FDA	Darunavir	20
208	FDA	Dasatinib	20
209	FDA	Daunorubicin·HCl	20
210	FDA	Decitabine	20
211	FDA	Deferasirox	20
212	FDA	Deferoxamine Mesylate	20
213	FDA	Delavirdine Mesylate	20
214	FDA	Demeclocycline·HCl	20
215	FDA	Desipramine·HCl	20
216	FDA	Desloratadine	20
217	FDA	Desogestrel	20
218	FDA	Desonide	20
219	FDA	Desoximetasone	20
220	FDA	Desvenlafaxine Succinate	20

		Hydrate	
221	FDA	Dexamethasone	20
222	FDA	Dexchlorpheniramine Maleate	20
223	FDA	Dexmedetomidine·HCl	20
224	FDA	Dexrazoxane	20
225	FDA	Dextromethorphan	20
226	FDA	Diatrizoate Meglumine	20
227	FDA	Diazepam	20
228	FDA	Diazoxide	20
229	FDA	Diclofenac·Na Salt	20
230	FDA	Dicloxacillin·Na Salt Monohydrate	20
231	FDA	Dicyclomine·HCl	20
232	FDA	Didanosine	20
233	FDA	Dienogest	20
234	FDA	Diflunisal	20
235	FDA	Difluprednate	20
236	FDA	Digoxin	20
237	FDA	Dihydroergotamine Mesylate	20
238	FDA	Diltiazem·HCl	20
239	FDA	Dimenhydrinate	20
240	FDA	Dinoprostone	20
241	FDA	Diphenhydramine·HCl	20
242	FDA	Dipyridamole	20
243	FDA	Disopyramide	20
244	FDA	Disulfiram	20
245	FDA	Dobutamine·HCl	20
246	FDA	Docetaxel (Taxotere)	20
247	FDA	Dofetilide	20
248	FDA	Dolasetron	20
249	FDA	Donepezil·HCl	20
250	FDA	Dopamine·HCl	20
251	FDA	Doripenem	20
252	FDA	Dorzolamide·HCl	20
253	FDA	Doxapram·HCl	20
254	FDA	Doxazosin Mesylate	20
255	FDA	Doxepin·HCl	20
256	FDA	Doxorubicin·HCl	20
257	FDA	Doxycycline Monohydrate	20
258	FDA	Droperidol	20
259	FDA	Drospirenone	20
260	FDA	Duloxetine·HCl	20
261	FDA	Dutasteride	20
262	FDA	Dyphylline	20
263	FDA	Econazole Nitrate	20
264	FDA	Efavirenz	20
265	FDA	Eflornithine·HCl	20
266	FDA	Emtricitabine	20
267	FDA	Enalapril	20
268	FDA	Enalaprilat Maleate	20
269	FDA	Entacapone	20
270	FDA	Epinastine·HCl	20
271	FDA	Epinephrine (L-(-)-Epinephrine-(+)-Bitartrate)	20
272	FDA	Epirubicin·HCl	20
273	FDA	Eplerenone	20
274	FDA	Eprosartan Mesylate	20
275	FDA	Eptifibatide	20
276	FDA	Ergotamine Tartrate	20
277	FDA	Erlotinib	20
278	FDA	Erythromycin	20
279	FDA	Escitalopram	20
280	FDA	Esmolol	20
281	FDA	Esomeprazole Potassium	20
282	FDA	Estradiol	20
283	FDA	Estramustine Phosphate·Na	20
284	FDA	Estrone	20
285	FDA	Estropipate	20
286	FDA	Eszopiclone	20
287	FDA	Ethacrynic Acid	20
288	FDA	Ethambutol Dihydrochloride	20
289	FDA	Ethinyl Estradiol	20
290	FDA	Ethionamide	20
291	FDA	Ethosuximide	20
292	FDA	Etidronate Disodium	20
293	FDA	Etodolac	20
294	FDA	Etomidate	20
295	FDA	Etonogestrel	20
296	FDA	Etoposide	20
297	FDA	Everolimus	20
298	FDA	Exemestane	20
299	FDA	Ezetimibe	20
300	FDA	Famciclovir	20
301	FDA	Famotidine	20
302	FDA	Febuxostat	20
303	FDA	Felbamate	20
304	FDA	Felodipine	20
305	FDA	Fenofibrate	20
306	FDA	Fenoldopam Mesylate	20
307	FDA	Fenoprofen Calcium	20
308	FDA	Fexofenadine·HCl	20
309	FDA	Finasteride	20
310	FDA	Fingolimod	20
311	FDA	Flavoxate·HCl	20
312	FDA	Flecainide Acetate	20
313	FDA	Floxuridine	20
314	FDA	Fluconazole	20
315	FDA	Flucytosine	20
316	FDA	Fludarabine Phosphate	20
317	FDA	Fludrocortisone Acetate	20
318	FDA	Flumazenil	20
319	FDA	Flunisolide	20
320	FDA	Fluocinolone Acetonide	20
321	FDA	Fluocinonide	20
322	FDA	Fluorometholone	20
323	FDA	Fluorouracil (5-Fluorouracil)	20
324	FDA	Fluoxetine·HCl	20
325	FDA	Fluphenazine·HCl	20
326	FDA	Flurandrenolide	20
327	FDA	Flurbiprofen	20
328	FDA	Flutamide	20
329	FDA	Fluticasone Propionate	20
330	FDA	Fluvastatin·Na	20
331	FDA	Fluvoxamine Maleate	20
332	FDA	Fomepizole	20
333	FDA	Formoterol	20
334	FDA	Foscarnet·Na (Sodium Phosphonoformate Tribasic Hexahydrate)	20
335	FDA	Fosfomycin Calcium	20
336	FDA	Fosinopril·Na	20
337	FDA	Fosphenytoin·Na Pentahydrate	20
338	FDA	Fulvestrant	20
339	FDA	Furosemide	20
340	FDA	Gabapentin	20
341	FDA	Galantamine·HBr	20
342	FDA	Ganciclovir	20
343	FDA	Gatifloxacin	20
344	FDA	Gefitinib	20
345	FDA	Gemcitabine·HCl	20
346	FDA	Gemfibrozil	20
347	FDA	Gemifloxacin	20
348	FDA	Gentamycin Sulfate	20
349	FDA	Glimepiride	20
350	FDA	Glipizide	20

351	FDA	Glyburide	20
352	FDA	Glycopyrrolate Iodide	20
353	FDA	Goserelin Acetate	20
354	FDA	Granisetron·HCl	20
355	FDA	Griseofulvin	20
356	FDA	Guanabenz Acetate	20
357	FDA	Guanfacine·HCl	20
358	FDA	Guanidine·HCl	20
359	FDA	Halcinonide	20
360	FDA	Halobetasol Propionate	20
361	FDA	Haloperidol	20
362	FDA	Hexachlorophene	20
363	FDA	Homatropine Methylbromide	20
364	FDA	Hydralazine·HCl	20
365	FDA	Hydrochlorothiazide	20
366	FDA	Hydrocortisone	20
367	FDA	Hydrocortisone Acetate	20
368	FDA	Hydroflumethiazide	20
369	FDA	Hydroxocobalamin·HCl	20
370	FDA	Hydroxychloroquine Sulfate	20
371	FDA	Hydroxyurea	20
372	FDA	Hydroxyzine Dihydrochloride	20
373	FDA	Ibandronate·Na Monohydrate	20
374	FDA	Ibuprofen	20
375	FDA	Ibutilide Fumarate	20
376	FDA	Idarubicin·HCl	20
377	FDA	Idoxuridine	20
378	FDA	Ifosfamide	20
379	FDA	Iloperidone	20
380	FDA	Imatinib Mesylate	20
381	FDA	Imipenem	20
382	FDA	Imipramine·HCl	20
383	FDA	Imiquimod	20
384	FDA	Indapamide	20
385	FDA	Indinavir	20
386	FDA	Indomethacin	20
387	FDA	Ipratropium·Br	20
388	FDA	Irbesartan	20
389	FDA	Irinotecan·HCl	20
390	FDA	Isocarboxazid	20
391	FDA	Isoniazid	20
392	FDA	Isosorbide Dinitrate	20
393	FDA	Isotretinoin (13-Cis-Retinoic Acid)	20
394	FDA	Isradipine	20
395	FDA	Itraconazole	20
396	FDA	Ivermectin	20
397	FDA	Kanamycin Sulfate	20
398	FDA	Ketoconazole	20
399	FDA	Ketoprofen	20
400	FDA	Ketorolac Tromethamine	20
401	FDA	Ketotifen Fumarate	20
402	FDA	Labetalol·HCl	20
403	FDA	Lacosamide	20
404	FDA	Lactulose	20
405	FDA	Lamivudine	20
406	FDA	Lamotrigine	20
407	FDA	Lansoprazole	20
408	FDA	Lapatinib Ditosylate	20
409	FDA	L-Ascorbic Acid	20
410	FDA	Latanoprost	20
411	FDA	Leflunomide	20
412	FDA	Lenalidomide	20
413	FDA	Letrozole	20
414	FDA	Leucovorin Calcium Pentahydrate	20
415	FDA	Levalbuterol·HCl	20
416	FDA	Levetiracetam	20
417	FDA	Levobunolol·HCl	20
418	FDA	Levocarnitine	20
419	FDA	Levocetirizine Dihydrochloride	20
420	FDA	Levofloxacin·HCl	20
421	FDA	Levonorgestrel	20
422	FDA	Levothyroxine·Na	20
423	FDA	Lidocaine·HCl·H2O	20
424	FDA	Lincomycin·HCl	20
425	FDA	Lindane	20
426	FDA	Linezolid	20
427	FDA	Liothyronine·Na	20
428	FDA	Lisinopril·2H2O	20
429	FDA	Lomustine	20
430	FDA	Loperamide·HCl	20
431	FDA	Lopinavir	20
432	FDA	Loratadine	20
433	FDA	Lorazepam	20
434	FDA	Losartan Potassium	20
435	FDA	Loteprednol Etabonate	20
436	FDA	Lovastatin	20
437	FDA	Loxapine Succinate	20
438	FDA	Mafenide·HCl	20
439	FDA	Malathion	20
440	FDA	Mannitol	20
441	FDA	Maprotiline·HCl	20
442	FDA	Maraviroc	20
443	FDA	Mebendazole	20
444	FDA	Mechlorethamine·HCl	20
445	FDA	Meclizine Dihydrochloride	20
446	FDA	Meclofenamate·Na	20
447	FDA	Medroxyprogesterone Acetate	20
448	FDA	Mefenamic Acid	20
449	FDA	Mefloquine·HCl	20
450	FDA	Megestrol Acetate	20
451	FDA	Meloxicam	20
452	FDA	Melphalan	20
453	FDA	Memantine·HCl	20
454	FDA	Mepenzolate Bromide	20
455	FDA	Mepivacaine·HCl	20
456	FDA	Meprobamate (Schedule Iv)	20
457	FDA	Mequinol	20
458	FDA	Mercaptopurine Hydrate	20
459	FDA	Meropenem	20
460	FDA	Mesalamine (5-Aminosalicylic Acid)	20
461	FDA	Mesna	20
462	FDA	Mestranol	20
463	FDA	Metaproterenol Hemisulfate (Orciprenaline)	20
464	FDA	Metaraminol Bitartrate	20
465	FDA	Metaxalone	20
466	FDA	Metformin·HCl	20
467	FDA	Methacholine Chloride	20
468	FDA	Methazolamide	20
469	FDA	Methenamine Hippurate	20
470	FDA	Methimazole	20
471	FDA	Methocarbamol	20
472	FDA	Methotrexate	20
473	FDA	Methoxsalen (Xanthotoxin)	20
474	FDA	Methscopolamine Bromide ((–)-Scopolamine Methyl Bromide)	20
475	FDA	Methsuximide	20
476	FDA	Methyclothiazide	20
477	FDA	Methyl Aminolevulinate·HCl	20
478	FDA	Methyldopa Sesquihydrate (L-A-Methyl-Dopa Sesquihyrate)	20

479	)A	Methylergonovine Maleate	20
480	FDA	Methylprednisolone	20
481	FDA	Metoclopramide·HCl	20
482	FDA	Metolazone	20
483	FDA	Metoprolol Tartrate	20
484	FDA	Metronidazole	20
485	FDA	Metyrapone	20
486	FDA	Mexiletine·HCl	20
487	FDA	Micafungin	20
488	FDA	Miconazole	20
489	FDA	Midodrine·HCl	20
490	FDA	Mifepristone	20
491	FDA	Miglitol	20
492	FDA	Miglustat (N-Butyldeoxynojirimycin·HCl)	20
493	FDA	Milnacipran·HCl	20
494	FDA	Milrinone	20
495	FDA	Minocycline	20
496	FDA	Minoxidil	20
497	FDA	Mirtazapine	20
498	FDA	Misoprostol	20
499	FDA	Mitomycin C	20
500	FDA	Mitotane	20
501	FDA	Mitoxantrone·HCl	20
502	FDA	Modafinil (Schedule Iv)	20
503	FDA	Moexipril·HCl	20
504	FDA	Mometasone Furoate	20
505	FDA	Montelukast·Na	20
506	FDA	Moxifloxacin·HCl	20
507	FDA	Mupirocin	20
508	FDA	Mycophenolate Mofetil	20
509	FDA	Mycophenolic Acid	20
510	FDA	Nabumetone	20
511	FDA	Nadolol	20
512	FDA	Nafcillin·Na	20
513	FDA	Naftifine·HCl	20
514	FDA	Nalbuphine·HCl Dihydrate	20
515	FDA	Naloxone·HCl	20
516	FDA	Naltrexone·HCl	20
517	FDA	Naphazoline·HCl	20
518	FDA	Naproxen	20
519	FDA	Naratriptan·HCl	20
520	FDA	Natamycin	20
521	FDA	Nateglinide	20
522	FDA	Nebivolol·HCl	20
523	FDA	Nefazodone·HCl	20
524	FDA	Nelarabine	20
525	FDA	Nelfinavir Mesylate	20
526	FDA	Neomycin Sulfate	20
527	FDA	Nepafenac	20
528	FDA	Nevirapine	20
529	FDA	Niacin (Known As Vitamin B3, Nicotinic Acid And Vitamin Pp)	20
530	FDA	Nicardipine·HCl	20
531	FDA	Nicotine	20
532	FDA	Nifedipine	20
533	FDA	Nilotinib	20
534	FDA	Nilutamide	20
535	FDA	Nimodipine	20
536	FDA	Nisoldipine	20
537	FDA	Nitazoxanide	20
538	FDA	Nitisinone	20
539	FDA	Nitrofurantoin	20
540	FDA	Nizatidine	20
541	FDA	Norepinephrine Bitartrate Monohydrate	20
542	FDA	Norethindrone	20
543	FDA	Norfloxacin	20
544	FDA	Nortriptyline·HCl	20
545	FDA	Nystatin	20
546	FDA	Ofloxacin	20
547	FDA	Olanzapine	20
548	FDA	Olmesartan	20
549	FDA	Olopatadine	20
550	FDA	Olsalazine·Na	20
551	FDA	Omeprazole	20
552	FDA	Ondansetron	20
553	FDA	Orlistat (Tetrahydrolipstatin)	20
554	FDA	Orphenadrine Citrate	20
555	FDA	Oseltamivir Phosphate	20
556	FDA	Oxacillin·Na	20
557	FDA	Oxaliplatin	20
558	FDA	Oxaprozin	20
559	FDA	Oxazepam	20
560	FDA	Oxcarbazepine	20
561	FDA	Oxiconazole Nitrate	20
562	FDA	Oxtriphylline	20
563	FDA	Oxybutynin Chloride	20
564	FDA	Oxytetracycline·HCl	20
565	FDA	Paclitaxel (Taxol)	20
566	FDA	Paliperidone	20
567	FDA	Palonosetron·HCl	20
568	FDA	Pamidronate Disodium Pentahydrate (Pamidronic Acid)	20
569	FDA	Pancuronium·2Br	20
570	FDA	Pantoprazole	20
571	FDA	Paromomycin Sulfate	20
572	FDA	Paroxetine·HCl	20
573	FDA	Pazopanib·HCl	20
574	FDA	Pemetrexed Disodium	20
575	FDA	Pemirolast Potassium	20
576	FDA	Penciclovir	20
577	FDA	Penicillamine (D-Penicillamine)	20
578	FDA	Penicillin G Potassium (Benzylpenicillin)	20
579	FDA	Penicillin V Potassium	20
580	FDA	Pentamidine Isethionate	20
581	FDA	Pentostatin	20
582	FDA	Pentoxifylline	20
583	FDA	Perindopril Erbumine	20
584	FDA	Permethrin	20
585	FDA	Perphenazine	20
586	FDA	Phenelzine Sulfate	20
587	FDA	Phenoxybenzamine·HCl	20
588	FDA	Phentolamine·HCl	20
589	FDA	Phenylephrine	20
590	FDA	Phenytoin	20
591	FDA	Phytonadione	20
592	FDA	Pilocarpine·HCl	20
593	FDA	Pimecrolimus	20
594	FDA	Pimozide	20
595	FDA	Pindolol	20
596	FDA	Pioglitazone·HCl	20
597	FDA	Piperacillin	20
598	FDA	Piroxicam	20
599	FDA	Pitavastatin Calcium	20
600	FDA	Podofilox	20
601	FDA	Posaconazole	20
602	FDA	Pralidoxime Chloride	20
603	FDA	Pramipexole Dihydrochloride Monohydrate	20
604	FDA	Prasugrel	20
605	FDA	Pravastatin·Na	20
606	FDA	Praziquantel	20

607	FDA	Prazosin·HCl	20
608	FDA	Prednisolone	20
609	FDA	Prednisone	20
610	FDA	Pregabalin	20
611	FDA	Prilocaine·HCl	20
612	FDA	Primaquine Phosphate	20
613	FDA	Primidone	20
614	FDA	Probenecid	20
615	FDA	Procainamide·HCl	20
616	FDA	Procarbazine·HCl	20
617	FDA	Progesterone	20
618	FDA	Promethazine·HCl	20
619	FDA	Propafenone·HCl	20
620	FDA	Proparacaine·HCl	20
621	FDA	Propofol	20
622	FDA	Propranolol·HCl	20
623	FDA	Propylthiouracil	20
624	FDA	Protriptyline·HCl	20
625	FDA	Pyrazinamide	20
626	FDA	Pyridostigmine Bromide	20
627	FDA	Pyrimethamine	20
628	FDA	Quetiapine Fumarate	20
629	FDA	Quinapril·HCl	20
630	FDA	Quinidine·HCl·H2O	20
631	FDA	Quinine·HCl·H2O	20
632	FDA	Rabeprazole·Na	20
633	FDA	Raloxifene·HCl	20
634	FDA	Raltegravir	20
635	FDA	Ramelteon	20
636	FDA	Ramipril	20
637	FDA	Ranitidine·HCl	20
638	FDA	Ranolazine·2HCl	20
639	FDA	Rasagiline Mesylate	20
640	FDA	Regadenoson	20
641	FDA	Repaglinide	20
642	FDA	Reserpine	20
643	FDA	Ribavirin	20
644	FDA	Rifabutin	20
645	FDA	Rifampin (Rifampicin)	20
646	FDA	Rifapentine	20
647	FDA	Rifaximin	20
648	FDA	Riluzole·HCl	20
649	FDA	Rimantadine·HCl	20
650	FDA	Risperidone	20
651	FDA	Risredonic Acid	20
652	FDA	Ritonavir	20
653	FDA	Rivastigmine Tartrate	20
654	FDA	Rizatriptan Benzoate	20
655	FDA	Rocuronium Bromide	20
656	FDA	Ropinirole·HCl	20
657	FDA	Ropivacaine·HCl Monohydrate	20
658	FDA	Rosiglitazone	20
659	FDA	Rosuvastatin Calcium	20
660	FDA	Rufinamide	20
661	FDA	Salbutamol Hemisulfate	20
662	FDA	Salmeterol	20
663	FDA	Saquinavir Mesylate	20
664	FDA	Scopolamine·HBr	20
665	FDA	Selegiline·HCl	20
666	FDA	Sertaconazole	20
667	FDA	Sertraline·HCl	20
668	FDA	Sildenafil Citrate	20
669	FDA	Silver Sulfadiazine	20
670	FDA	Simvastatin	20
671	FDA	Sirolimus (Rapamycin)	20
672	FDA	Sitagliptin Phosphate	20
673	FDA	Sodium Phenylbutyrate	20
674	FDA	Sorafenib Tosylate	20
675	FDA	Sotalol·HCl	20
676	FDA	Spectinomycin·HCl Pentahydrate	20
677	FDA	Spironolactone	20
678	FDA	Stavudine	20
679	FDA	Streptomycin Sulfate	20
680	FDA	Streptozocin	20
681	FDA	Succinylcholine Chloride·2H2O	20
682	FDA	Sulconazole Nitrate	20
683	FDA	Sulfacetamide·Na	20
684	FDA	Sulfadiazine	20
685	FDA	Sulfamethoxazole	20
686	FDA	Sulfanilamide	20
687	FDA	Sulfasalazine	20
688	FDA	Sulindac	20
689	FDA	Sumatriptan Succinate	20
690	FDA	Sunitinib Malate	20
691	FDA	Tacrine·HCl	20
692	FDA	Tacrolimus (Fk506)	20
693	FDA	Tadalafil	20
694	FDA	Tamoxifen Citrate	20
695	FDA	Tamsulosin·HCl	20
696	FDA	Tazarotene	20
697	FDA	Telbivudine	20
698	FDA	Telithromycin	20
699	FDA	Telmisartan	20
700	FDA	Temazepam	20
701	FDA	Temozolomide	20
702	FDA	Temsirolimus	20
703	FDA	Teniposide	20
704	FDA	Tenofovir	20
705	FDA	Terazosin·HCl	20
706	FDA	Terbinafine·HCl	20
707	FDA	Terbutaline Hemisulfate	20
708	FDA	Terconazole	20
709	FDA	Testosterone Enanthate	20
710	FDA	Tetrabenazine	20
711	FDA	Tetracycline	20
712	FDA	Tetrahydrozoline·HCl	20
713	FDA	Thalidomide	20
714	FDA	Theophylline	20
715	FDA	Thioguanine (6-Thioguanine)	20
716	FDA	Thioridazine·HCl	20
717	FDA	Thiotepa	20
718	FDA	Tiagabine·HCl	20
719	FDA	Ticlopidine·HCl	20
720	FDA	Tigecycline	20
721	FDA	Tiludronate Disodium	20
722	FDA	Tinidazole	20
723	FDA	Tiopronin	20
724	FDA	Tiotropium Bromide Monohydrate	20
725	FDA	Tirofiban·HCl	20
726	FDA	Tizanidine·HCl	20
727	FDA	Tobramycin	20
728	FDA	Tolazamide	20
729	FDA	Tolbutamide	20
730	FDA	Tolcapone	20
731	FDA	Tolmetin·Na	20
732	FDA	Tolterodine Tartrate	20
733	FDA	Tolvaptan	20
734	FDA	Topiramate	20
735	FDA	Topotecan·HCl	20
736	FDA	Toremifene Base	20
737	FDA	Torsemide	20
738	FDA	Tramadol·HCl	20
739	FDA	Trandolapril	20

740	FDA	Tranexamic Acid	20
741	FDA	Tranylcypromine Hemisulfate	20
742	FDA	Travoprost	20
743	FDA	Trazodone·HCl	20
744	FDA	Tretinoin	20
745	FDA	Triamcinolone Acetonide	20
746	FDA	Triamterene	20
747	FDA	Triazolam	20
748	FDA	Trientine Dihydrochloride	20
749	FDA	Trifluoperazine·HCl	20
750	FDA	Trihexyphenidyl·HCl	20
751	FDA	Trimethadione	20
752	FDA	Trimethobenzamide·HCl	20
753	FDA	Trimethoprim	20
754	FDA	Trimipramine Maleate	20
755	FDA	Triptorelin Acetate	20
756	FDA	Tropicamide	20
757	FDA	Trospium Chloride	20
758	FDA	Ursodiol	20
759	FDA	Valacyclovir·HCl	20
760	FDA	Valganciclovir·HCl	20
761	FDA	Valproate·Na	20
762	FDA	Valproic Acid	20
763	FDA	Valsartan	20
764	FDA	Vancomycin·HCl	20
765	FDA	Vardenafil	20
766	FDA	Varenicline Tartrate	20
767	FDA	Vecuronium Bromide	20
768	FDA	Venlafaxine·HCl	20
769	FDA	Verapamil·HCl	20
770	FDA	Vigabatrin	20
771	FDA	Vinblastine Sulfate	20
772	FDA	Vincristine Sulfate	20
773	FDA	Vinorelbine	20
774	FDA	Voriconazole	20
775	FDA	Vorinostat	20
776	FDA	Warfarin·Na	20
777	FDA	Zafirlukast	20
778	FDA	Zalcitabine (2',3'-Dideoxycytidine)	20
779	FDA	Zaleplon	20
780	FDA	Zanamivir	20
781	FDA	Zidovudine (3'-Azido-3'-Deoxythymidine)	20
782	FDA	Zileuton	20
783	FDA	Ziprasidone	20
784	FDA	Zoledronic Acid Monohydrate	20
785	FDA	Zolmitriptan	20
786	FDA	Zonisamide	20
787	BI	BRD_1 (TV062569)	20
788	BI	BRD_10 (TV062581)	20
789	BI	BRD_11 (TV062567)	20
790	BI	BRD_12 (TV062568)	20
791	BI	BRD_13 (TV062203)	20
792	BI	BRD_14 (TV062240)	20
793	BI	BRD_15 (TV062245)	20
794	BI	BRD_16 (TV062246)	20
795	BI	BRD_17 (TV062582)	20
796	BI	BRD_18 (TV062192)	20
797	BI	BRD_19 (TV062193)	20
798	BI	BRD_2 (TV062570)	20
799	BI	BRD_20 (TV062194)	20
800	BI	BRD_21 (TV062195)	20
801	BI	BRD_22 (TV062196)	20
802	BI	BRD_23 (TV062197)	20
803	BI	BRD_24 (TV062202)	20
804	BI	BRD_25 (TV062207)	20
805	BI	BRD_26 (TV062208)	20
806	BI	BRD_27 (TV062209)	20
807	BI	BRD_28 (TV062200)	20
808	BI	BRD_29 (TV062201)	20
809	BI	BRD_3 (TV062572)	20
810	BI	BRD_30 (TV062198)	20
811	BI	BRD_31 (TV062199)	20
812	BI	BRD_4 (TV062573)	20
813	BI	BRD_5 (TV062574)	20
814	BI	BRD_6 (TV062577)	20
815	BI	BRD_7 (TV062578)	20
816	BI	BRD_8 (TV062579)	20
817	BI	BRD_9 (TV062580)	20
818	BI	CHIR 99021	20
819	BI	SJH2	20
820	BI	SJH3	20
821	BI	SJH4	20
822	BI	SJH5	20
823	BI	JB 1121	20
824	JH/M	5C10	20
825	JH/M	78-3	20
826	JH/M	86-1	20
827	JH/M	86-2	20
828	JH/M	86-3	20
829	JH/M	87-1	20
830	JH/M	87-2	20
831	JH/M	87-3	20
832	JH/M	87-4	20
833	JH/M	90-2	20
834	JH/M	90-3	20
835	JH/M	90-4	20
836	JH/M	90-5	20
837	JH/M	CPH2-102	20
838	JH/M	CPH2-103	20
839	JH/M	CPH2-128	20
840	JH/M	CPH2-141	20
841	JH/M	CPH2-48	20
842	JH/M	CPH2-49	20
843	JH/M	CPH2-52	20
844	JH/M	CPH2-53	20
845	JH/M	CPH2-56	20
846	JH/M	CPH3-27	20
847	JH/M	CPH6-60	20
848	JH/M	FTY720 HCL	20
849	JH/M	JDG3-82	20
850	JH/M	JGD-13W(3f)	20
851	JH/M	JGD3-142	20
852	JH/M	JGD3-143	20
853	JH/M	JGD4-11Y(3e)	20
854	JH/M	JGD4-12W(3c)	20
855	JH/M	JGD4-13Y(3d)	20
856	JH/M	JGD4-20W	20
857	JH/M	Toxo-0027	20
858	JH/M	Toxo-0028	20
859	RH	RW_121	3000
860	RH	RW_26	3000
861	RH	RW_43	3000
862	RH	RW_44	3000
863	RH	RW_54	3000
864	RH	RW_60	3000
865	RH	RW17	3000
866	CCNR	2-pirydylethylamine	20
867	CCNR	7-hydroxy-DPAT	20
868	CCNR	8-bromo-cAMP	1400
869	CCNR	agomelatine	20
870	CCNR	AICAR (+GW5015160.1uM)	20
871	CCNR	anti-CD3/CD28	0.006
872	CCNR	AS19	20

873	CCNR	BCR stim	0.056
874	CCNR	BDNF	0.008
875	CCNR	calyculin	2
876	CCNR	clozapine	20
877	CCNR	cucurbitacin I	20
878	CCNR	Curcumin	20
879	CCNR	fenobam	20
880	CCNR	forskolin	20
881	CCNR	FPL 64176	0.2
882	CCNR	FPL 64176	2
883	CCNR	FPL 64176	20
884	CCNR	GSK690693	20
885	CCNR	GW7647	20
886	CCNR	haloperidol	20
887	CCNR	idebenone	20
888	CCNR	IFNalpha2C	0.01
889	CCNR	IFNgamma	0.012
890	CCNR	IL-10	0.01
891	CCNR	IL-1beta	0.012
892	CCNR	IL-2	0.014
893	CCNR	IL-23	0.004
894	CCNR	IL-4	0.014
895	CCNR	IL-6	0.008
896	CCNR	insulin	0.2
897	CCNR	isoproterenol	20
898	CCNR	KT 5720	0.8
899	CCNR	leptin	0.126
900	CCNR	LPS	0.0002
901	CCNR	LY-294,002 hydrochloride	20
902	CCNR	m-3M3FBS	0.2
903	CCNR	m-3M3FBS	2
904	CCNR	m-3M3FBS	20
905	CCNR	NECA	20
906	CCNR	Nefiracetam	0.2
907	CCNR	Nefiracetam	2
908	CCNR	Nefiracetam	20
909	CCNR	NNC 55-0396 dHCl	0.2
910	CCNR	NNC 55-0396 dHCl	2
911	CCNR	NNC 55-0396 dHCl	20
912	CCNR	olanzapine	20
913	CCNR	orthovanadate	300
914	CCNR	PCP	20
915	CCNR	Penfluridol	0.2
916	CCNR	Penfluridol	2
917	CCNR	Penfluridol	20
918	CCNR	PHA543613	20
919	CCNR	PMA/ionomycin	2
920	CCNR	PS48	20
921	CCNR	resveratrol	20
922	CCNR	risperidone	20
923	CCNR	ryanodine	0.2
924	CCNR	ryanodine	2
925	CCNR	ryanodine	20
926	CCNR	SB 239063	10
927	CCNR	SB202190	20
928	CCNR	SC9	20
929	CCNR	SEB	0.07
930	CCNR	SKF83822	20
931	CCNR	SR57227	20
932	CCNR	staurosporine	10
933	CCNR	sumanirole	20
934	CCNR	TCB-2	20
935	CCNR	TC-G 24	20
936	CCNR	thapsigargin	2
937	CCNR	TNFalpha	0.01
938	CCNR	trolox	20
939	CCNR	U0126	20
940	CCNR	U73122	0.2
941	CCNR	U73122	2
942	CCNR	U73122	20
943	CCNR	Vitamin D3 solution	0.2
944	CCNR	WHI-P154	20
945	CCNR	xaliproden	20
946	CCNR	xanomeline	20

Epitopes	Clone	Isotype	Gene	Class	Fluoro-chrome	Stain index	TC	AI	DD	FDA	Supplier
4EBP1 (pT36/pT45)	M31-16	Ms IgG_1, κ	EIF4EBP1	AKT	AF 488	5.3	TC	AI	DD		BD Biosciences
4EBP1 (pT69)	M34-273	Ms IgG_1, κ	EIF4EBP1	AKT	PE	1.9	TC	AI			BD Biosciences
Akt (pS473)	M89-61	Ms IgG_1, κ	AKT1	AKT	AF 647	22.4	TC	AI	DD		BD Biosciences
Akt (pT308)	J1-223.371	Ms IgG_1, κ	AKT1	AKT	PE	8.6	TC	AI	DD		BD Biosciences
Akt1	55/PKBa/Akt	Ms IgG_1, κ	AKT1	AKT	AF 488	12.4	TC	AI	DD		BD Biosciences
β-Catenin (pS45)	K63-363	Ms IgG_1, κ	CTNNB1	AKT	AF 647	72.8	TC	AI	DD		BD Biosciences
CD221 (pY1131)	K74-218	Ms IgG_1, κ	IGF1R	AKT	AF 647	7.2	TC	AI			BD Biosciences
eIF4E (pS209)	J77-925	Ms IgG_1, κ	EIF4E	AKT	PE	1.7	TC	AI			BD Biosciences
Ezrin (pY353)	I66-386	Ms IgG_1	EZR	AKT	PE	1.4	TC	AI			BD Biosciences
FAK (pS910)	K73-480	Ms IgG_{2b}, κ	PTK2	AKT	AF 488	118.9	TC				BD Biosciences
GSK-3α/β	4G-1E	Ms IgG_1	GSK3B	AKT	FITC	8.7	TC	AI	DD		Merck Millipore
GSK-3β (pSer9)	D85E12	R IgG	GSK3B	AKT	PE	2.9	TC	AI	DD		Cell Signaling Technology
GSK-3β (pThr390)	polyclonal	R IgG	GSK3B	AKT	PE	23.1	TC	AI			Bioss
GSK-3β (pTyr216)	polyclonal	R IgG	GSK3B	AKT	AF 647	498.6	TC				Bioss
IRS-1 (pY896)	K9-211	Ms IgG_{2a}, κ	IRS1	AKT	AF 647	9.8	TC	AI			BD Biosciences
PDPK1 (pS241)	J66-653.44.17	Ms IgG_1, κ	PDPK1	AKT	AF 488	29.7	TC	AI	DD		BD Biosciences
S6 (PS235/PS236)	N7-548	Ms IgG_1, κ	RP26	AKT	AF 647	9.9	TC	AI	DD		BD Biosciences
S6 (PS240)	N4-41	Ms IgG_1, κ	RPS6	AKT	AF 488	1.4	TC	AI			BD Biosciences
IκBα	25/IkBa/MAD-3	Ms IgG_1	NFKBIA	IL1R/ TLR	PE	25.9	TC	AI	DD		BD Biosciences
IRAK4	L29-525	Ms IgG_1, κ	IRAK4	IL1R/ TLR	PE	33.3	TC				BD Biosciences
IRF-7 (pS477/pS479)	K47-671	Ms IgG_1, κ	IRF7	IL1R/ TLR	AF 488	32.2	TC	AI	DD		BD Biosciences
NF-κB p65 (pS529)	K10-895.12.50	Ms IgG_{2b}, κ	RELA	IL1R/ TLR	AF 647	23.1	TC	AI	DD		BD Biosciences
STAT1 (N-Terminus)	1/Stat1	Ms IgG_1	STAT1	JAK/ STAT	PE	45.6	TC	AI	DD		BD Biosciences
STAT1 (pS727)	K51-856	Ms IgG_1, κ	STAT1	JAK/ STAT	AF 488	5.9	TC	AI	DD		BD Biosciences
STAT1 (pY701)	4a	Ms IgG_{2a}	STAT1	JAK/ STAT	AF 647	10.6	TC	AI	DD		BD Biosciences
STAT3	M59-50	Ms IgG1, λ	STAT3	JAK/ STAT	PE	4.5	TC	AI	DD		BD Biosciences
STAT3 (pS727)	49/p-Stat3	Ms IgG_1	STAT3	JAK/ STAT	AF 488	9.7	TC	AI	DD		BD Biosciences
STAT3 (pY705)	4/P-STAT3	Ms IgG_{2a}, κ	STAT3	JAK/ STAT	AF 647	14.4	TC	AI	DD		BD Biosciences
STAT4 (pY693)	38/p-Stat4	Ms IgG_{2b}	STAT4	JAK/ STAT	PE	5.8	TC	AI	DD		BD Biosciences
STAT5 (pY694)	47/Stat5(pY694)	Ms IgG_1, κ	STAT5A, STAT5B	JAK/ STAT	AF 647	61.5	TC	AI	DD		BD Biosciences
STAT6 (pY641)	18/P-Stat6	Ms IgG_{2a}	STAT6	JAK/ STAT	PE	1.5	TC	AI			BD Biosciences
Bcl-2 (pS70)	N46-467	Ms IgG_1	BCL2	MAPK	AF 647	14.5	TC	AI	DD		BD Biosciences
ERK1/2 (pT202/pY204)	20A	Ms IgG_1	MAPK1, MAPK3	MAPK	AF 647	79.1	TC	AI	DD		BD Biosciences
JNK (pT183/pY185)	N9-66	Ms IgG_1, κ	MAPK8	MAPK	AF 647	23.9	TC				BD Biosciences
MAPKAPK-2 (pT334)	P24-694	Ms IgG_1, κ	MAPKAPK	MAPK	AF 488	1.1	TC	AI			BD Biosciences
MEK1 (pS218)/MEK2 (pS222)	O24-836	Ms IgG_1, κ	MAP2K1, MAP2K2	MAPK	AF 647	18.4	TC	AI			BD Biosciences
MEK1 (pS298)	J114-64	Ms IgG_1, κ	MAP2K1	MAPK	PE	2.1	TC	AI			BD Biosciences
p38 MAPK (pT180/pY182)	36/p38 (pT180/pY182)	Ms IgG_1, κ	MAPK14, MAPK13, MAPK12	MAPK	AF 647	12.4	TC	AI	DD		BD Biosciences
p53 (acK382)	L82-51	Ms IgG_1, κ	TP53	MAPK	AF 647	21.5	TC	AI	DD		BD Biosciences
p53 (pS37)	J159-641.79	Ms IgG_1, κ	TP53	MAPK	AF 488	6.2	TC	AI			BD Biosciences
CD140b (pY857)	J24-618	Ms IgG_1, κ	PDGFRB	Other	AF 488	1.2	TC	AI			BD Biosciences
Rb (pS780)	J146-35	Ms IgG_1, κ	RB1	Other	AF 488	2.6	TC	AI			BD Biosciences
Smad2 (pS465/pS467)/Smad3 (pS423/pS425)	O72-670	Ms IgG_1, κ	SMAD2	Other	PE	2.8	TC	AI			BD Biosciences
CREB (pS133) / ATF-1 (pS63)	J151-21	Ms IgG_1, κ	CREB1	PKA	AF 647	15	TC	AI	DD		BD Biosciences
DARPP32	polyclonal	R IgG	PPP1R1B	PKA	PE	27	TC				Bioss
DARPP32 (pThr34)	polyclonal	R IgG	PPP1R1B	PKA	AF 647	188.7	TC				Bioss
DARPP32 (pThr75)	polyclonal	R IgG	PPP1R1B	PKA	AF 488	57	TC				Bioss
PKA RII-α (pS99)	I65-856.286	Ms IgG_1, κ	PRKAR2A	PKA	AF 647	91.7	TC	AI	DD		BD Biosciences
PKA RII-β (pS114)	47/PKA	Ms IgG_1	PRKAR2B	PKA	AF 488	5	TC	AI	DD		BD Biosciences
p120 Catenin (pS268)	9a.390	Ms IgG_{2b}, κ	CTNND1	PKC	AF 488	1.4	TC	AI			BD Biosciences
p120 Catenin (pS879)	K114-1011	Ms IgG_1, κ	CTNND1	PKC	PE	4.1	TC	AI			BD Biosciences
p120 Catenin (pT310)	22/p120 (pT310)	Ms IgG_1, κ	CTNND1	PKC	AF 488	10.2	TC	AI	DD		BD Biosciences
PKC-α	3/PKCα	Ms IgG_{2b}	PRKCA	PKC	AF 488	43.6	TC	AI	DD		BD Biosciences
PKC-α (pT497)	K14-984	Ms IgG_1, κ	PRKCA	PKC	AF 647	33.4	TC	AI	DD		BD Biosciences
PKC-α/βII (pThr638/641)	polyclonal	R IgG	PRKCA, PRKCB	PKC	PE	14.8	TC				Bioss
PKC-β1/2 (pThr500)	polyclonal	R IgG	PRKCB	PKC	PE	1.9	TC				Bioss
PKC-δ (pThr505)	polyclonal	R IgG	PRKCD	PKC	AF 488	18.6	TC				Bioss
PKC-θ	27/PKCθ	Ms IgG2a, κ	PRKCQ	PKC	PE	2.8	TC	AI	DD		BD Biosciences
PKC-θ (pT538)	polyclonal	R IgG	PRKCQ	PKC	PE	16.4	TC	AI			Bioss
PKC-θ(pSer695)	polyclonal	R IgG	PRKCQ	PKC	AF 488	9.1	TC				Bioss
PLC-γ1	10/PLCgamma	Ms IgG_1	PLCG1, PLCG2	PKC	PE	15.1	TC	AI	DD	FDA	BD Biosciences
PLC-γ1 (pY783)	27/PLC	Ms IgG_1	PLCG1	PKC	AF 647	12.4	TC	AI	DD		BD Biosciences
PLC-γ2	K86-1161	Ms IgG_1, κ	PLCG2	PKC	AF 488	1.7	TC	AI	DD		BD Biosciences
PLC-γ2 (pY759)	K86-689.37	Ms IgG_1, κ	PLCG2	PKC	AF 647	9.4	TC	AI	DD		BD Biosciences
BLNK (pY84)	J117-1278	Ms IgG_{2b}, κ	BLNK	TCR/ BCR	PE	1.2	TC	AI			BD Biosciences
Btk (pY551) & Itk (pY511)	24a/BTK (Y551)	Ms IgG_1	BTK	TCR/ BCR	AF 647	16.4	TC				BD Biosciences
c-Cbl (pY700)	47/c-Cbl	Ms IgG_1	CBL	TCR/ BCR	PE	2.2	TC	AI			BD Biosciences
c-Cbl (pY774)	29/c-Cbl	Ms IgG_1	CBL	TCR/ BCR	PE	1.9	TC	AI			BD Biosciences
CrkL (pY207)	K30-391.50.80	Ms IgG_{2a}, κ	CRKL	TCR/ BCR	AF 488	14.1	TC	AI	DD		BD Biosciences
LAT (pY226)	J96-1238.58.93	Ms IgG_1, κ	LAT	TCR/ BCR	AF 488	1.5	TC	AI			BD Biosciences
Lck (pY505)	4/LCK-Y505	Ms IgG_1	LCK	TCR/ BCR	AF 488	2.4	TC	AI			BD Biosciences
Pyk2 (pY402)	L68-1256.272	Ms IgG_{2b}, κ	PTK2B	TCR/ BCR	PE	8.9	TC	AI	DD		BD Biosciences
SHP2 (pY542)	L99-921	Ms IgG_1, κ	PTPN11	TCR/ BCR	AF 647	31	TC	AI	DD		BD Biosciences
SLP-76 (pY128)	J141-668.36.58	Ms IgG_1, κ	LCP2	TCR/ BCR	AF 647	11.4	TC	AI	DD		BD Biosciences
Src (pY418)	K98-37	Ms IgG_1, κ	SRC	TCR/ BCR	AF 488	4.9	TC	AI	DD		BD Biosciences
WIP (pS488)	K32-824	Ms IgG_1, κ	WIPF1	TCR/ BCR	PE	9.2	TC	AI	DD		BD Biosciences
Zap70 (pY292)	J34-602	Ms IgG_1, κ	ZAP70	TCR/ BCR	AF 488	2	TC	AI			BD Biosciences
Zap70 (pY319)/Syk (pY352)	17A/P-ZAP70	Ms IgG_1	SYK, ZAP70	TCR/ BCR	AF 647	12.7	TC	AI	DD		BD Biosciences
CD3	UCHT1	Ms IgG1, κ	CD3E	Subtyping	PE Cy7	NA	TC	AI	DD		eBioscience
CD3	UCHT1	Ms IgG1, κ	CD3E	Subtyping	APC	NA				FDA	eBioscience
CD4	SK3	Ms IgG1, κ	CD4	Subtyping	PerCP-eF710	NA		AI	DD		eBioscience
CD8a	SK1	Ms IgG1, κ	CD8A	Subtyping	APC-eF780	NA		AI	DD		eBioscience
CD14	MφP9	IgG2b, κ	CD14	Subtyping	V500	NA		AI	DD		BD Biosciences

Table 2.3: Antibodies used to detect intracellular cell signalling epitopes and PBMC subtypes. Antibodies are grouped by class, in terms of which cell signalling pathways they are ascribed to, and then ordered alphabetically. Time course (TC), Antipsychotic intervention (AI), Differential diagnosis (DD) and FDA compound screening (FDA) columns denote the studies for which the antibodies were used. Gene IDs are taken from NCBI Gene database. Stain index refers to median MFI of the stained samples/ median MFI of the unstained samples in the vehicle condition across eight PBMC donors for each epitope, based on data from the TC study. Abbreviations: Rabbit (R), Mouse (Ms), protein kinase B (AKT), interleukin-1 receptor/ toll-like receptor (IL1R/ TLR), Janus kinase/signal transducer and activator of transcription (JAK/ STAT), mitogen-activated protein kinase (MAPK), protein kinase A (PKA), protein kinase C (PKC), T cell receptor/ B cell receptor (TCR/ BCR).

CHAPTER 3

ESTABLISHING THE HIGH-CONTENT PLATFORM

3.1 INTRODUCTION

In this section we aim to evaluate the robustness of the high-content functional cytomics platform in terms of its multiplexing capacity and the reproducibility of the single-cell signalling response across different donors and experimental runs. Furthermore we aim to select the most relevant kinetics and cell signalling responses **(time course- 'TC'; Chapter 1 Fig. 1.3b)** for application to clinical samples in later stages of the project. We will also evaluate the sensitivity and specificity of the platform in terms of kinetic cytokine responses in previously well characterized T cell signalling networks. Finally we seek to explore its potential for identifying surrogate models of CNS drug efficacy including cellular responses to neuropsychiatric medications and experimental drug candidates.

3.2 RESULTS

3.2.1 MULTIPLEXING OF T CELL SIGNALLING MODULATORS

We employed fluorescent cell barcoding (FCB) technology to enable analysis of single-cell signalling responses of up to 80 ligands simultaneously in peripheral blood mononuclear cells (PBMCs) by flow cytometry **(Fig. 3.1)**[105]. FCB allows reproducible antibody staining across the ligand conditions, increased dimensionality for high content analysis and also efficient use of the limited PBMC samples. Briefly PBMCs were dispensed into 80 wells of a 96 well plate and each well was treated with a different ligand relevant to neuropsychiatric pathology or the vehicle. The PBMCs in each

well were then stained with different intensities of three fluorescent barcoding dyes (CBD 450, CBD 500 and DL 800) in combination, such that PBMCs in each treatment well had a unique fluorescent signature. The cells from all wells were pooled and the different combinations of the barcoding dye intensities (4 x 4 x 5) enabled the resolution of 80 independent PBMC populations corresponding to the 80 ligands or vehicle conditions with which the cells had been treated **(Fig. 3.2)**. Subsequently the pooled cells were permeabilized, stained with anti-CD3 PE-Cy7 to resolve T cells and distributed across an array of antibodies against 78 different intracellular signalling epitopes to determine signalling pathway responses to each ligand.

To test the accuracy of this multiplexing methodology for the purpose of functional profiling of T cell signalling responses in neuropsychiatric diseases we defined the induction of STAT3 phosphorylation at residue pY705 in response to 15 min stimulation with 50 ng/ml interleukin-6 (IL-6) as a positive control. IL-6 has been repeatedly implicated as an inflammatory mediator of neuropsychiatric disease[132]. IL-6 signalling through STAT3 (pY705) is also well characterized in T cells using this technology[116,133]. Firstly we assessed whether responses to IL-6 could be reproducibly measured across each of the 80 positions in the barcoding matrix and in each of the three fluorescent channels used for functional antibody detection (representative antibody detection fluorophores in each channel include PE, AF 647 and AF 488). CVs across the 80 wells were 5% for STAT3 (pY705) PE, 6% for STAT3 (pY705) AF 647 and 8% for STAT3 (pY705) AF 488 **(data reflects mean of 4 replicate plates; Fig. 3.3)**. Furthermore we dispensed IL-6 and vehicle alternately in rows or columns across the PBMC stimulation plate. Following multiplexing and deconvolution of the barcode signatures, the orientation of IL-6 wells with respect to vehicle wells could be accurately determined based on the STAT3 (pY705) response profile **(Fig. 3.4)**. The Z' factor values, which account for the reproducibility and dynamic range of the assay[134], were 0.75 and 0.68 for STAT3 (pY705) PE, 0.70 and 0.64 for STAT3 (pY705) AF 647 and 0.68 and 0.46 for STAT3 (pY705) AF 488 for row and column orientations respectively. This indicates that cell signalling responses can be measured with precision independently of the position of the ligand within the barcoding matrix or the antibody detection fluorophore used.

3.2.2 TIME COURSE SELECTION OF OPTIMAL LIGAND AND EPITOPE ARRAYS

A mechanistically diverse set of functional ligands and cell signalling epitopes was selected for this study with a view to identifying surrogate functional markers which reflect systemic abnormalities in cell signalling in neuropsychiatric disease **(Chapter 2: Tables 2.1 and 2.3)**. However the functional relationships of many of these ligand-epitope combinations (especially those related to CNS

pathology) have never been systematically screened in PBMCs. Phosphorylation changes in cell signalling proteins in response to ligand binding reveal transient kinetic profiles[135]. Thus determination of the optimal time point for measuring cellular responses was crucial to characterizing this novel set of functional ligands and cell signalling epitopes. Previous high-content screens have suggested that phosphorylation of cell signalling proteins in response to many prototypical ligands (including immunomodulatory cytokines or antigen receptor stimulants) in PBMCs reaches a peak at 15-30 min post stimulation[127,135,136], with even earlier (1-10 min) peak responses observed for specific subsets of proteins following T cell receptor stimulation[79,137,138]. Concurrently, maximal phosphorylation changes of signalling proteins in response to CNS ligands in neurons have also been reported to occur within 1-30 min [139,140]. Therefore we set the maximum response time to 30 min and sought to explore kinetic responses within this time window. We conducted a time course experiment to measure the effects of 70 cellular stimulants (in addition to 10 vehicle controls) on the expression of 78 cell signalling epitopes at 1, 5, 15 and 30 min time points post stimulation in PBMCs obtained from eight healthy donors. The ligands included a variety of CNS receptor agonists, neuropsychiatric medications, cytokines, hormones/ growth factors, antigens and intracellular signalling modulators. The epitopes spanned a wide variety of cell signalling pathways broadly including Akt/GSK-3β, PKA, PKC, MAPK, JAK/STAT, IL1R/TLR and TCR/BCR pathways. Putative expression of the target in lymphocytes and its potential implication in neuropsychiatric disease mechanisms were fundamental criteria for the inclusion of each ligand and epitope in the array. This created a total of 5460 diverse ligand-epitope combinations, or "signalling nodes", measured at each time point per donor **(Chapter 1 Fig. 1.4a)**. 68 of the cell signalling epitopes represented phosphorylation sites linked to the activation state of the protein and the remaining 10 epitopes were included to quantify the total levels of key proteins independently of phosphorylation status.

A significant response to ligand was defined as an increase or decrease in the levels of a specific epitope relative to the vehicle control across the eight donor samples (unpaired Wilcoxon $p<0.05$, fold change >10%) after accounting for background fluorescence. Maximal induction of significant cell signalling responses was observed at 30 min where 228/ 5460 nodes were active compared to 97, 146 and 211 nodes at 1, 5 and 15 min respectively **(Fig. 3.5)**. In addition, the fold change distributions of significant nodes revealed an increased magnitude of responses at later time points with maximum negative and positive responses of -6.1 fold and 95.4 fold respectively at 30 min **(Fig. 3.6)**. This is consistent with published data for induction of phosphorylation of cell signalling proteins using conventional PBMC ligands[135]. Moreover the distribution of significant nodes with respect to ligand or epitope class was largely preserved across time points such that 30 min

represented the maximal induction of nodes for the majority of classes **(Fig. 3.7)**. Thus 30 min was selected as the optimal time point for the exploration of cell signalling nodes in clinical samples.

Ranking of active ligands and epitopes at 30min **(Table 3.1, Fig. 3.5d)** revealed that positive controls calyculin (phosphatase inhibitor) and PMA/ionomycin (calcium flux/ PKC activator) were among the most effective ligands for inducing widespread increases in phosphorylation across cell signalling epitopes. This is consistent with their published role as broad spectrum cell signalling activators[141]. Conversely staurosporine, a known non-specific kinase inhibitor, had opposing effects resulting in widespread decreases in phosphorylation status across cell signalling epitopes. The kinetic induction of nodes by these positive controls was largely unidirectional. Interestingly the widespread signalling modulator thapsigargin, which raises cytosolic calcium concentrations by blocking calcium reuptake into the endoplasmic reticulum, displayed a bidirectional activity profile. 32% of responses had a positive fold change and 68% had a negative fold change. Furthermore 15% of the responses which were sustained across at least two time points displayed a biphasic profile with increases in the earlier time points and decreases in the later time points. This is likely to reflect negative feedback regulation in which the initial activation is subsequently quenched by dephosphorylation or sequestration of the active protein. Taken together these findings suggest that thapsigargin is a relevant ligand for exposing regulatory interactions. Finally epitopes were ranked by activity **(Table 3.2)** and their respective stain indices ((mean MFI of the stained samples/ mean MFI of the unstained samples) in the vehicle condition across eight PBMC donors) **(Fig. 3.8)**. This allowed the identification of basal epitope expression, inactive epitopes and potentially nonspecific antibody clones.

3.2.3 REPRODUCIBILITY

Having examined the variation of cell signalling responses across different stimulation wells and positions of the barcoding matrix (as described above), we sought to define the variability of responses measured in the same PBMC donor across time. For this purpose, in the subsequent antipsychotic intervention (AI) and differential diagnosis (DD) studies, we measured responses for the total ligand and epitope arrays in the same PBMC sample from a healthy donor (quality control) across six and nine days respectively. Single measurements each day were taken for the AI study and duplicate measurements were taken for all except two days of the DD study (on which single measurements were taken instead). For the AI and DD studies, the mean CVs across all nodes for the quality control samples were 11% and 10% respectively, while the proportion of nodes with CVs

under 15% was 78% and 90% respectively **(Fig. 3.9a, b)**. Considering the mechanistic scope of the ligands and epitopes used, the wide of range of fold changes across nodes and the challenges of reproducing functional responses *ex vivo*, this level of variation was considered satisfactory for assessment of clinical samples.

We also sought to assess whether the functional responses and epitope staining patterns were reproducible in independent cohorts of healthy PBMC donors derived from different collection sites. To this end, we compared responses at 30 min and stain indices for control PBMCs in the time course (TC) study (n = 8 donors) and the AI study (n = 12 donors) for nodes (n = 3696 responses and n = 66 basal epitope expression levels) which were measured in both studies. Of the 259 nodes which were active in the TC study 75% were reproduced and displayed the same direction of change in the AI study. Furthermore there was a strong correlation between the studies in terms of the fold changes for nodes which were replicated ($r_s = 0.94$, $p < 1x10^{-15}$) and the epitope stain indices ($r_s = 0.96$, $p < 1x10^{-15}$) **(Fig. 3.9c, d)**. This shows that functional responses and epitope staining patterns across the ligand-epitope array are robust even in studies with small sample sizes, low cell counts and reformatting of ligands and antibodies across different positions in the barcoding matrix and detection fluorophores respectively. Finally we verified that this % replication and correlation of responses was preserved in the nodes selected for comparison of cytokine activity (100% replication, $r_s = 0.86$, $p = 6.1x10^{-10}$; **Fig. 3.10**) and the effects of Akt/GSK-3β pathway inhibitors (85% replication, $r_s = 0.90$, $p = 2.8x10^{-13}$; **Fig. 3.13**) which are presented subsequently as key aspects of the platform validation.

3.2.4 SENSITIVITY, SPECIFICITY AND DYNAMIC REGULATION OF CYTOKINE SIGNALLING RESPONSES

To validate the specificity of the platform and ensure that 30 min was the optimal time point to capture regulatory interactions between proteins, we examined the kinetic responses obtained across JAK/STAT signalling pathways in response to immuno-modulatory cytokines **(Fig. 3.10a)**. Characteristic responses were obtained at the activation residues of the key STAT isotypes consistent with published data[116,141,142]. For example maximal phosphorylation at STAT1 (pY701) was induced by IFN-α2c, at STAT3 (pY705) by IL-6 and IL-10, at STAT5 (pY694) by IL-2 and at STAT6 (pY641) by IL-4. Furthermore changes at multiple epitopes on STAT1 and STAT3 proteins in response to IL-6, IL-10 and IFN-α2c treatment revealed the dynamic regulation of JAK/STAT signalling. While induction of phosphorylation at the activation sites STAT1 (pY701) and STAT3 (pY705) was frequently present at earlier time points (1 and 5 min) and sustained until 30 min, phosphorylation

of the regulatory sites STAT1 (pS727) and STAT3 (pS727) was induced later and reached its maximum observed level at 30 min. Decreases in the levels of total STAT1 and STAT3 were also observed at later time points (15 and 30 min) indicative of dimerization, sequestration by downstream signalling partners or negative feedback regulation of the signalling response. The dynamic regulation of STAT signalling, including different kinetic profiles for the activation, regulatory and total protein sites, is exemplified by responses to IFN-α2c at STAT1 and STAT3 **(Fig. 3.10b, c)**. Taken together these findings suggest that 30 min is an optimal time point to capture both specific activation profiles and regulatory interactions within the T cell signalling repertoire and provides a suitable reference point for the novel ligand-epitope combinations targeted in the clinical phase of this study. Finally to optimise use of the assay for clinical samples, in which cell numbers are limited, 12 epitopes and 14 ligands which showed minimal activity were excluded from the subsequent AI and DD studies **(Chapter 2: Tables 2.1 and 2.3)**. This represented a reduction of the size of the functional matrix by a third and ensured that only the nodes with greater functionality, and hence greater potential for revealing disease-related drug targets, were carried forward to the clinical application stage of the study.

3.2.5 KINETIC EXPLORATION OF CNS LIGANDS

Significant novelty of the functional cytomics platform resides in the potential to use blood cells as a surrogate model for functional interactions at CNS drug targets, specifically neurotransmitter receptors, which are otherwise unavailable for *ex vivo* analysis. Kinetic screening of the T cell signalling repertoire revealed 59 significant responses (Wilcoxon $p<0.05$) for CNS receptor ligands relative to the vehicle at different time points. The response range for CNS ligands (-1.3 to 1.4 fold) was modest compared to the positive controls and cytokines described earlier. The CNS ligand class was the only one which did not display a rising activity profile at later time points. Instead many compounds in this class showed transient epitope effects at a single time point. The most robust responses were prioritized as those with activity at a minimum of two consecutive time points in the same direction **(Fig. 3.11)**. Seven nodes satisfied this criteria including adenosine receptor agonist (NECA)/ CREB (pS133)- ATF-1 (pS63) (mean FC 1.25, 5-30 min), D3 receptor agonist (7-OH-DPAT)/ MEK1 (pS298) (mean FC 1.26, 5-15 min), NMDA receptor antagonist (phencyclidine)/ CrkL (pY207) (mean FC 1.10, 1-5 min) and Lck (pY505) (mean FC 1.09, 1-5 min), 5-HT3 receptor agonist (SR 57227)/ S6 (pS240) (mean FC 1.15, 15-30 min) and CrkL (pY207) (mean FC 1.07, 1-5 min) and 5-HT7 receptor agonist (AS 19)/ b-Catenin (pS45) (mean FC -1.08, 15-30 min).

Ligands which showed sporadic fold changes above 10% and convergent mechanisms at signalling epitopes traditionally located downstream of their receptors in the CNS are also noteworthy. These included reduction in PKA RIIα (pS99) in response to adenosine receptor agonist (NECA) and β-adrenoreceptor agonist (isoproterenol) at 1 min, indicative of cAMP signalling. These also included convergence of 5-HT2C receptor agonist (WAY 161503) and 5-HT2A receptor agonist (TCB-2) on 4EBP1 (pT36/ pT45) at 15 and 30 min respectively, indicative of mammalian target of rapamycin complex 1 (mTORC1) signalling.

3.2.6 KINETIC EXPLORATION OF NEUROPSYCHIATRIC TREATMENTS AND NOVEL INHIBITORS

Compounds which are commonly used to treat neuropsychiatric disorders, and have primary mechanisms of action in the brain, also revealed significant interactions at signalling epitopes within the T cell repertoire during the time course analysis. In total 77 significant interactions (Wilcoxon $p<0.05$) were found across different time points with fold changes ranging from -1.5 to 3.3. The epitopes 4EBP1 (pT36/pT45), CrkL (pY207) and GSK3-B (pS9) were enriched, accounting for 13%, 9% and 8% of responses respectively, compared to less than 1% expected assuming a random distribution of responses across all 78 epitopes. We further prioritized 15 responses which displayed changes in epitope expression across two consecutive time points in the same direction **(Fig. 3.12)**. 4EBP1 (pT36/pT45), CrkL (pY207) and GSK3-B (pS9) were the only epitopes for which more than one drug was active suggesting that the initial enrichment represented genuine kinetic profiles and not sporadic activation of these epitopes.

Analysis of activities by therapeutic indication revealed convergent inhibition of phosphorylation at mTORC1 target, 4EBP1 (pT36/pT45), across antidepressant (fluoxetine, desipramine), mood stabilizing (lithium) and antipsychotic (risperidone) drug classes. Additionally inhibition was shared within the antidepressant class (fluoxetine, desipramine) at GSK-3β. Conversely potentiation at CrkL (pY207) was shared within the antipsychotic class. Olanzapine was also active at a single time point (30 min) at CrkL (pY207) with a similar fold change to haloperidol and clozapine. Aripiprazole was unique in its induction of PDPK1 (pS241). Notable heterogeneity was observed among additional sites for the mood stabilizers lithium, valproic acid and carbamazepine. Lithium was active at Smad2 (pS465/pS467)/Smad3 (pS423/pS425) and STAT3, while valproic acid was active at Rb (pS780) and carbamazepine was inactive. The induction of MEK1 (pS298) by desipramine at 15-30min (1.5-3.3

FC respectively) represented the highest positive fold change of phosphorylation status across all the neuropsychiatric treatments.

To further explore the potential of the platform to detect interactions of approved neuropsychiatric medications with relevant CNS pathways and to determine whether these interactions could be applied to the discovery of novel drugs, we focused on the Akt/GSK-3β pathway as one of the most widely implicated cell signalling pathways in neuropsychiatric drug discovery[80,90,143,144]. We compared the kinetic profile of compounds which are known to modulate Akt/GSK-3β pathway activity with established neuropsychiatric treatments and novel drug candidates. Signalling proteins within the Akt/GSK-3β pathway have been repeatedly linked to pathological changes in the brain of neuropsychiatric patients and are thought to represent principal mediators of clinical efficacy of antidepressant, antipsychotic and mood stabilizing medication[80,90,143–146]. Furthermore changes in Akt/GSK-3β pathway proteins have been linked to treatment response in PBMCs from patients with affective and psychotic disorders[147,148].

We measured kinetic interactions of different cellular ligands with Akt/GSK-3β pathway members and downstream effectors at 1, 5, 15 and 30min **(Fig. 3.13)**. Calyculin (phosphatase inhibitor) and the PMA/ ionomycin cocktail (PKC activator/ calcium flux inducer) caused widespread activation of proteins within the canonical signalling pathway with induction of phosphorylation at 30 min reaching 95 fold at AKT (pT308) in response to calyculin and 80 fold at S6 (PS235/PS236) in response to PMA/ ionomycin. In addition to the characteristic kinetic profile of incremental response at later time points, dynamic regulation of the calyculin response was observed through -1.3 and -1.6 fold decreases in total Akt1 levels at 15 and 30 min suggestive of sequestration of the active Akt1 by downstream effectors.

Having defined the limits of pathway activation using these positive controls we sought to reproduce phosphorylation inhibition patterns characteristic of known Akt/GSK-3β pathway inhibitors. Staurosporine displayed widespread inhibition of phosphorylation at 6 of the 13 epitopes, GSK 690693 inhibited phosphorylation downstream of Akt1 at GSK-3β (pS9) and rapamycin inhibited phosphorylation downstream of mTORC1 at 4EBP1 (pT36/pT45). This is consistent with the roles of staurosporine as a broad spectrum kinase inhibitor, GSK 690693 as a specific Akt1 inhibitor and rapamycin as a specific mTORC1 complex inhibitor. The fact that the inhibition profiles observed for GSK690693 and rapamycin relate to specific sites, immediately downstream of the primary drug target, support the utility of the platform in determining causative signalling relationships in response to pharmacological intervention. In contrast CHIR 99021, a highly selective GSK-3β inhibitor, displayed inhibition of phosphorylation directly at the pS9 residue

on GSK-3β suggesting that the binding site of the drug is functionally coupled to the GSK-3β activation site itself.

Several compounds used clinically to treat neuropsychiatric disorders displayed kinetic inhibition profiles which overlapped with those described for GSK 690693, rapamycin and CHIR 99021. Antidepressant medications fluoxetine and desipramine showed significant inhibition of phosphorylation at both GSK-3β (pS9) (max 32% and 26% respectively) and 4EBP1 (pT36/pT45) (max 35% and 26% respectively). Antipsychotic medications aripiprazole and risperidone inhibited phosphorylation at either GSK-3β (pS9) (17%) or 4EBP1 (pT36/pT45) (35%) respectively. The mood stabilizer lithium, commonly prescribed for treatment of bipolar disorder, exhibited phosphorylation inhibition at 4EBP1 (pT36/pT45) (30%) but not at either of the GSK-3β phospho-epitopes. However several of these treatment drugs also displayed inhibitory effects on phosphorylation at key sites of other Akt/GSK-3β signalling proteins. For example lithium showed inhibition at PDPK1 (pS241) (5%), aripiprazole at Akt (pT308) (8%) and desipramine at NF-κB p65 (pS529) (21%). In contrast novel compound JB 1121 showed a highly selective 20-30% phosphorylation inhibition of GSK-3β (pS9) across all the time points with no inhibition at any of the other selected pathway sites. This profile closely matched that of CHIR 99021, one of the most potent and selective GSK-3β inhibitors available.

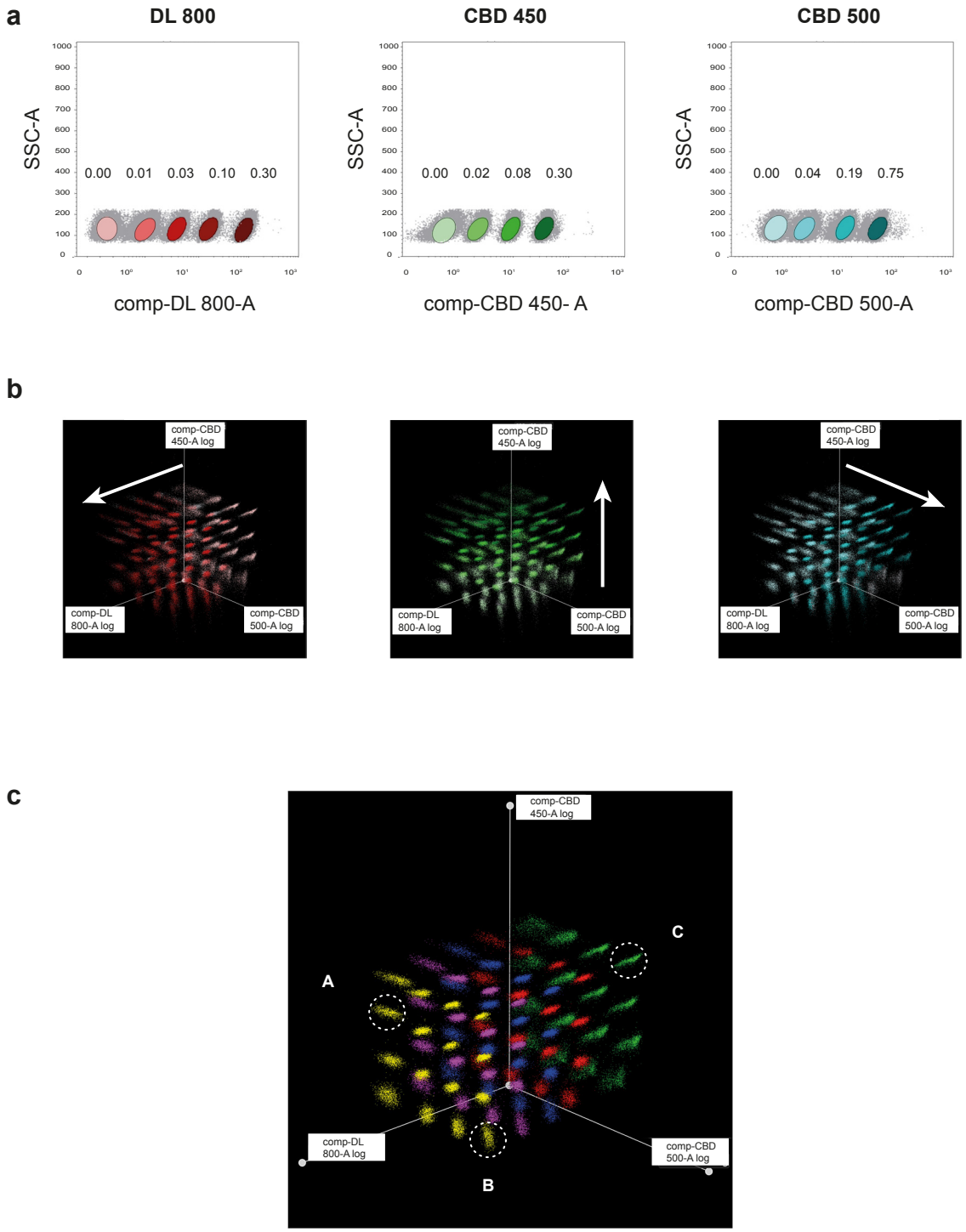

Figure 3.1 Construction of a three dimensional fluorescent cell barcoding matrix for multiplexing of 80 cellular treatments. **(a)** PBMCs in each treatment (ligand or vehicle) well of a 96 well plate were stained with different intensities of each of three fluorescent barcoding dyes (DL 800, CBD 450 and CBD 500). **(b)** Combination of the three dyes produced the 80 population barcoding matrix in which the contribution of each dye can be visualized as a distinct fluorescence intensity gradient along the x, y and z axes. The 80 populations were then pooled and stained for intracellular signalling epitopes. **(c)** Three dimensional deconvolution of the 80 barcoded populations as individual ligand or vehicle treatments, for example A = staurosporine, B = calyculin and C= vehicle. Data represents one PBMC sample.

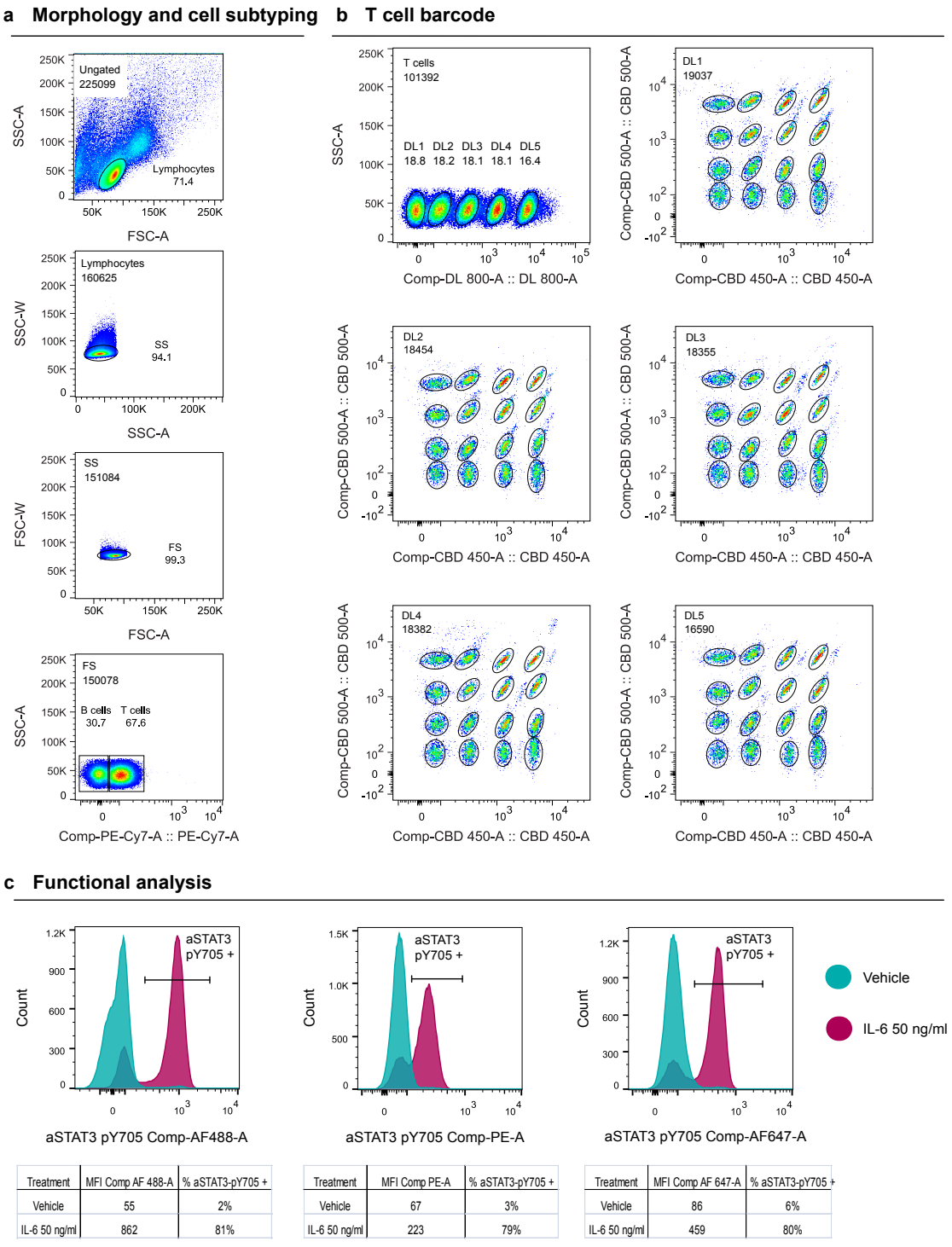

Treatment	MFI Comp AF 488-A	% aSTAT3-pY705 +
Vehicle	55	2%
IL-6 50 ng/ml	862	81%

Treatment	MFI Comp PE-A	% aSTAT3-pY705 +
Vehicle	67	3%
IL-6 50 ng/ml	223	79%

Treatment	MFI Comp AF 647-A	% aSTAT3-pY705 +
Vehicle	86	6%
IL-6 50 ng/ml	459	80%

Figure 3.2 Gating strategies for the functional analysis of 80 barcoded T cell populations. (a) Viable cells were gated (FSC-A vs. SSC-A), followed by single cell discrimination (SSC-A vs. SSC-W and FSC-A vs. FSC-W) and T vs. B lymphocyte cell subtyping using anti-CD3 PE-Cy7. **(b)** 80 populations, each corresponding to a different ligand or vehicle condition, were resolved within the T lymphocyte gate following fluorescent cell barcoding using DL 800, CBD 450 and CBD 500 dyes. T cells were gated first for DL 800 populations (DL 1-5) and subsequently for CBD 450 vs. CBD 500 populations (V1-16). **(c)** Within each barcoded T cell population functional analysis of intra-cellular signalling epitopes (n=78) was conducted across AF 488, PE and AF 647 channels. Induction of STAT3 (pY705) phosphorylation in response to 15 min stimulation with IL-6 50 ng/ml is shown as an example. Data represents one PBMC sample.

a

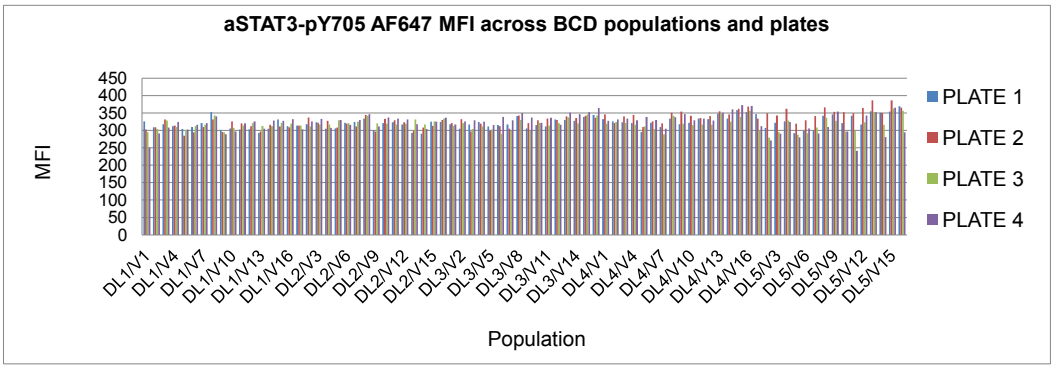

b

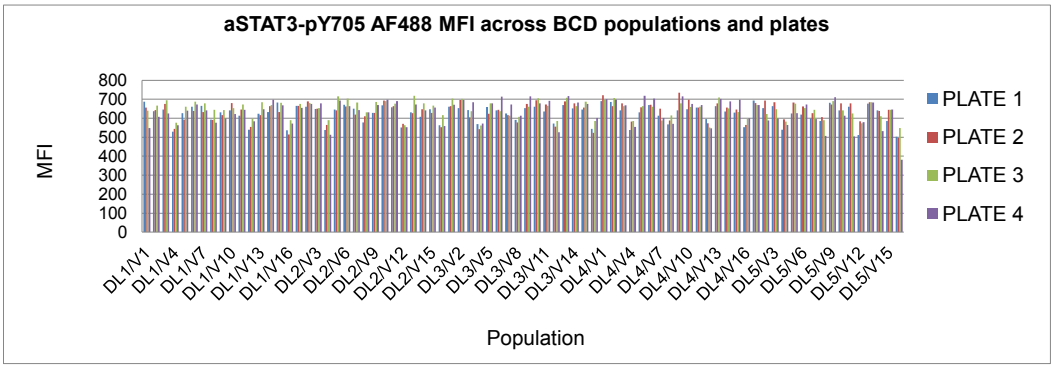

c

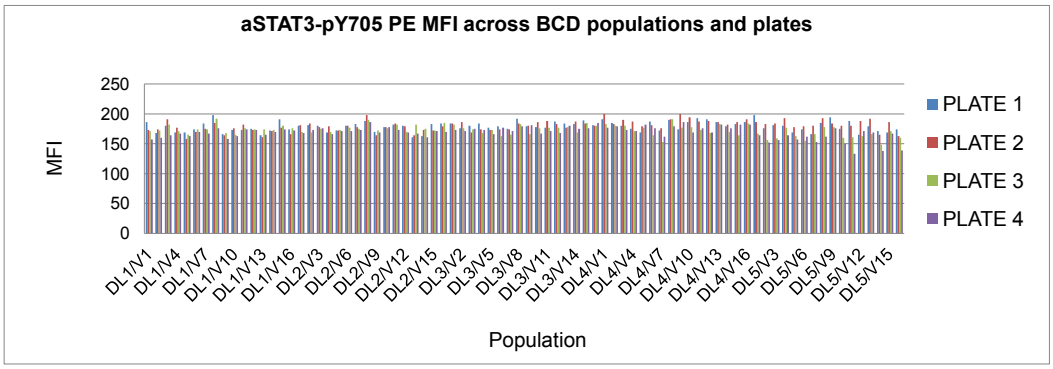

d

Antibody	PLATE 1	PLATE 2	PLATE 3	PLATE 4	Mean
aSTAT3-pY705 AF647	5	7	5	8	6
aSTAT3-pY705 AF488	8	8	7	10	8
aSTAT3-pY705 PE	5	5	5	6	5

Figure 3.3 Median fluorescence intensities (MFIs) and CVs across 80 barcoded (BCD) T cell populations for each functional fluorescence channel. 80 wells in four different plates were treated with IL-6 50 ng/ml for 15 min. Each plate was barcoded separately and the pooled sample from each plate was stained with anti-STAT3 (pY705) AF 647 **(a),** anti-STAT3 (pY705) AF488 **(b)** and anti-STAT3 (pY705) PE **(c)**. **(d)** The % CVs for each plate and the mean are shown for each functional channel. Data represents one PBMC sample.

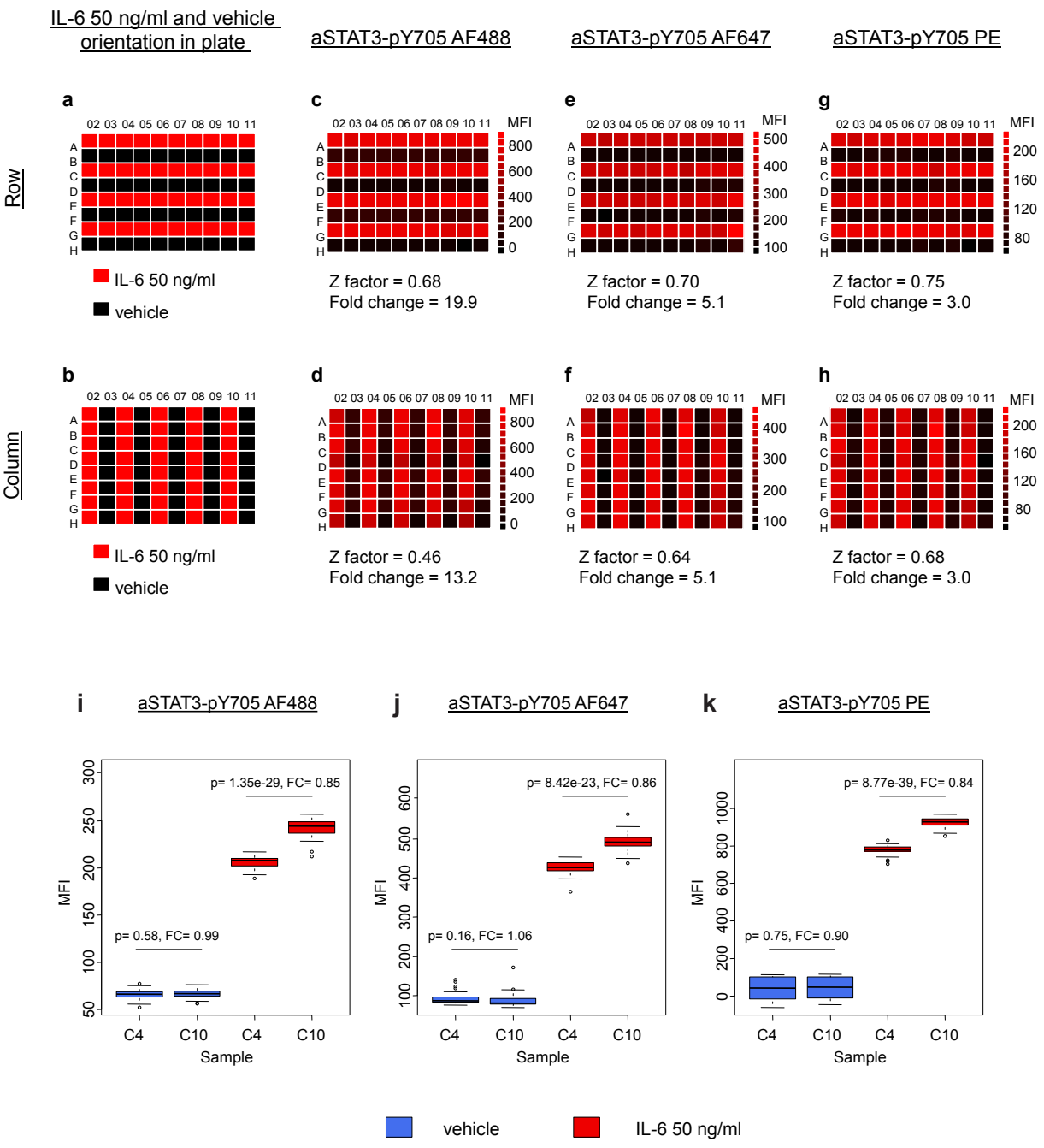

Figure 3.4 Z factor analyses across 80 barcoded T cell populations for each functional fluorescence channel. PBMCs were treated with IL-6 50 ng/ml or vehicle arranged alternately in rows **(a)** or columns **(b)** for 15 min. Mean MFIs of two PBMC donors for each barcode population were used to calculate the Z factor and fold change for each orientation after staining with anti-STAT3 (pY705) AF488 **(c,d)**, anti-STAT3 (pY705) AF 647 **(e,f)**, and anti-STAT3 (pY705) PE **(g,h)**. Differences in STAT3 (pY705) phosphorylation between PBMC donors (C4 and C10) were significant (t test, $p < 0.05$) following IL-6 50 ng/ml stimulation but not in vehicle condition across anti-STAT3 (pY705) AF488 **(i)**, anti-STAT3 (pY705) AF 647 **(j)**, and anti-STAT3 (pY705) PE **(k).**

a **1 min**

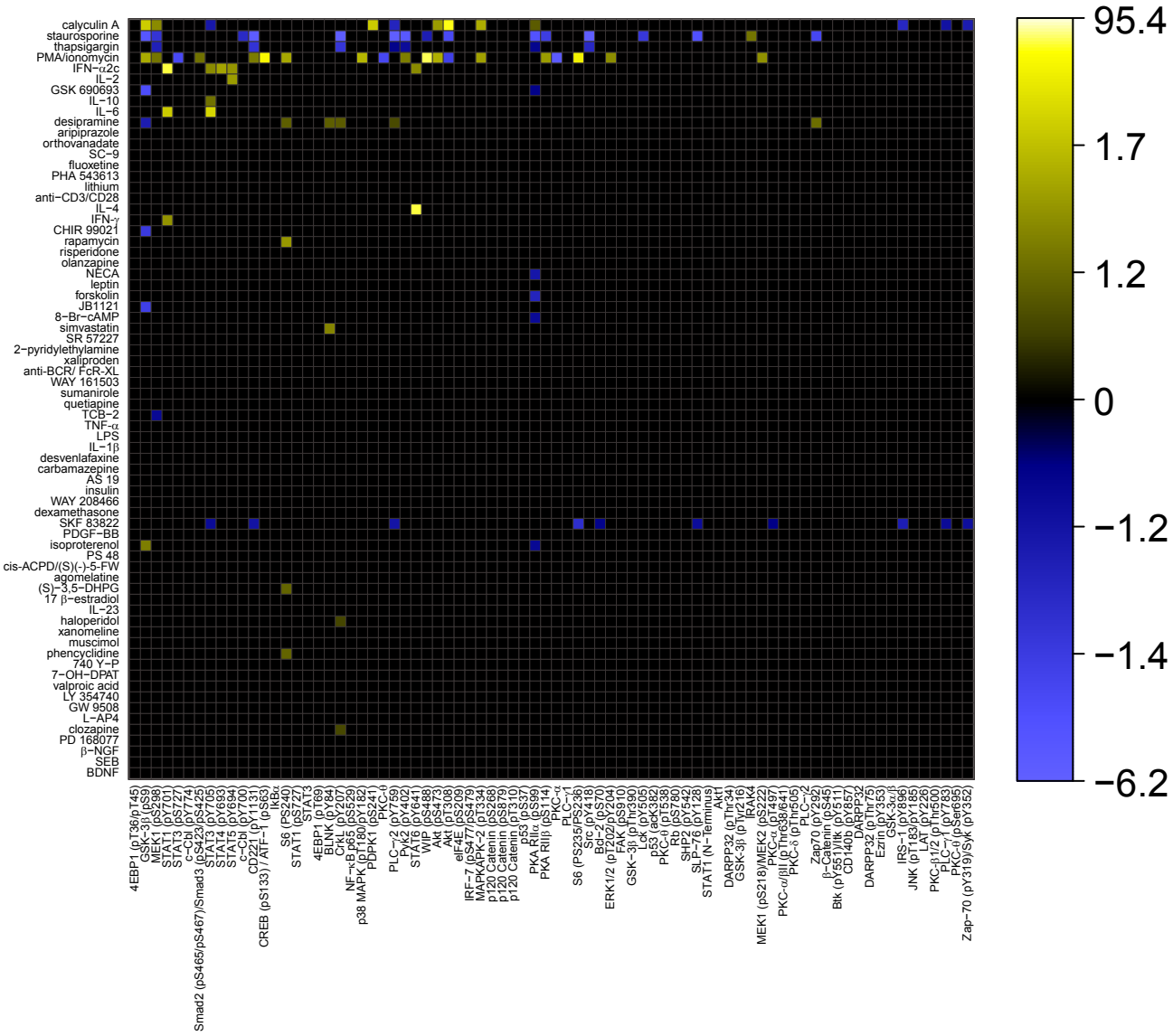

Figure 3.5 Kinetic induction of cell signalling responses across the ligand and epitope array (n = 5460 nodes). Responses in T cells to 70 diverse functional ligands (y axes) were measured at 78 intracellular signalling epitopes (x axes) following 1 min **(a)**, 5 min **(b)**, 15 min **(c)** or 30 min **(d)** ligand incubation times. Legend shows fold change in epitope expression, calculated as median MFI of the ligand treatment/ median MFI of the vehicle treatment across eight PBMC donors, with labels distributed evenly across the quantile range. For each epitope only ligands which showed significant responses (Wilcoxon $p < 0.05$) with a minimum fold change of 10%, relative to the vehicle, are shown. Ligands and epitopes are ranked in terms of the number of significantly responding nodes at 30min.

b **5 min**

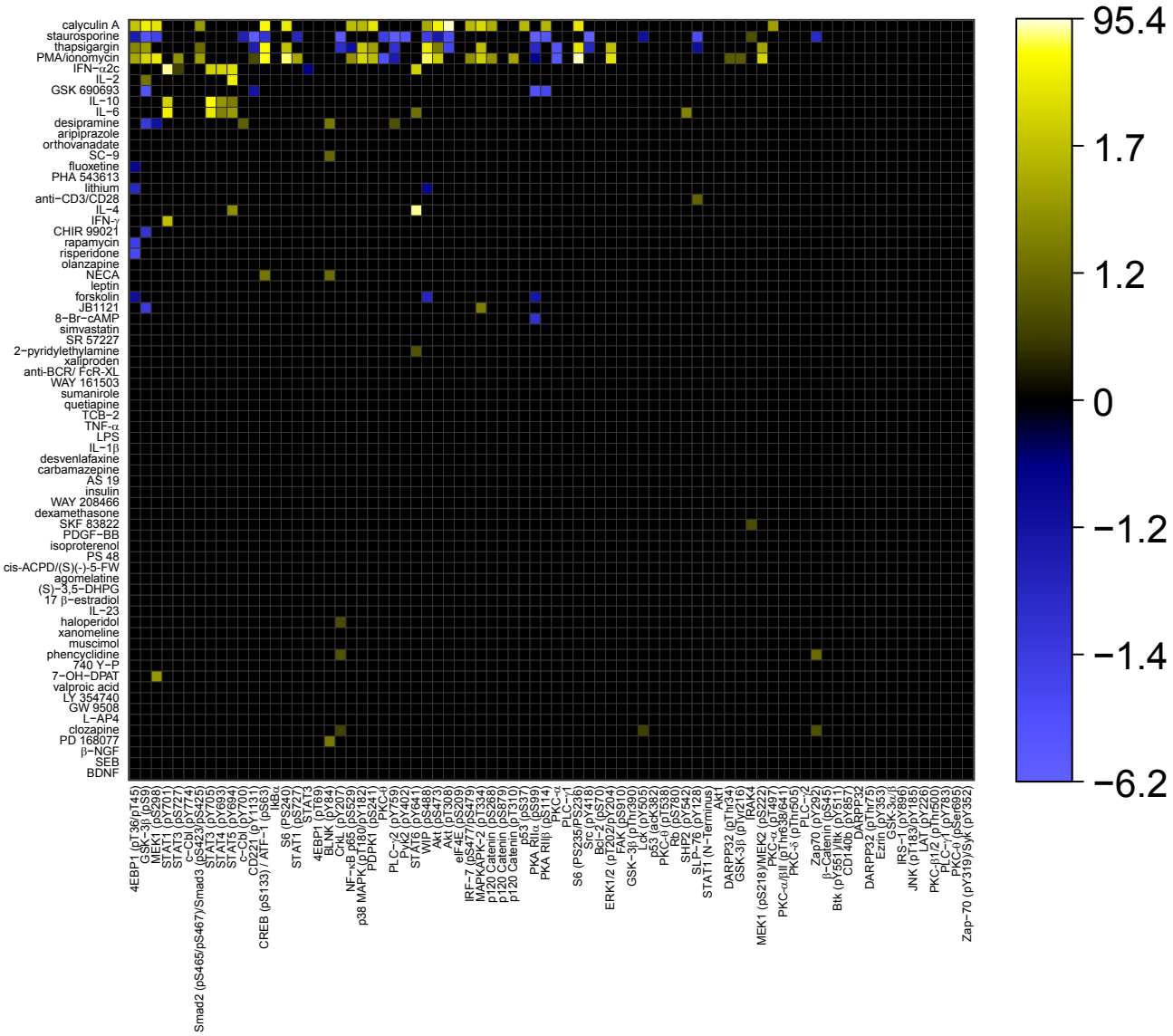

Figure 3.5 Kinetic induction of cell signalling responses across the ligand and epitope array (n = 5460 nodes) continued.

c **15 min**

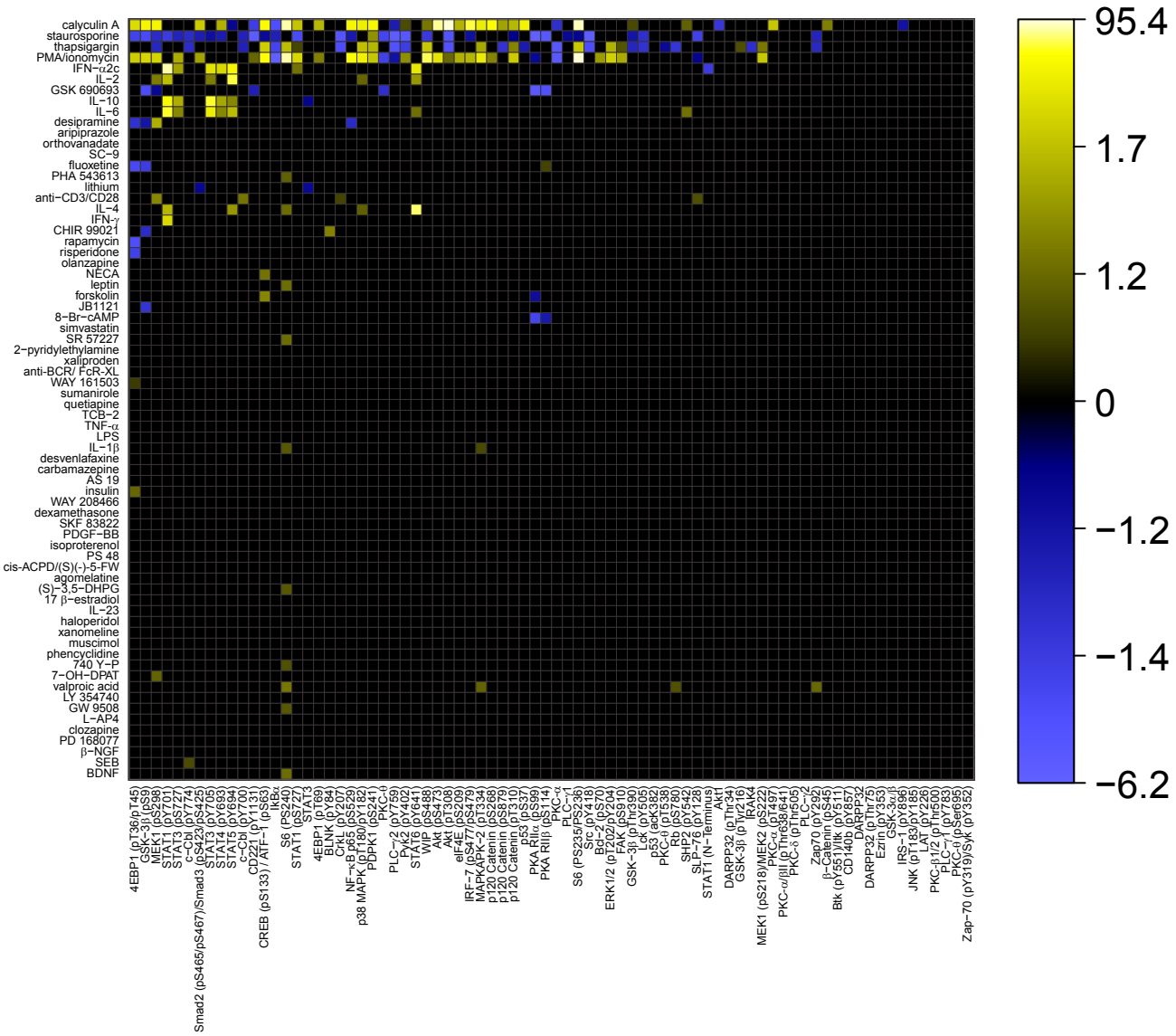

Figure 3.5 Kinetic induction of cell signalling responses across the ligand and epitope array (n = 5460 nodes) continued.

d **30 min**

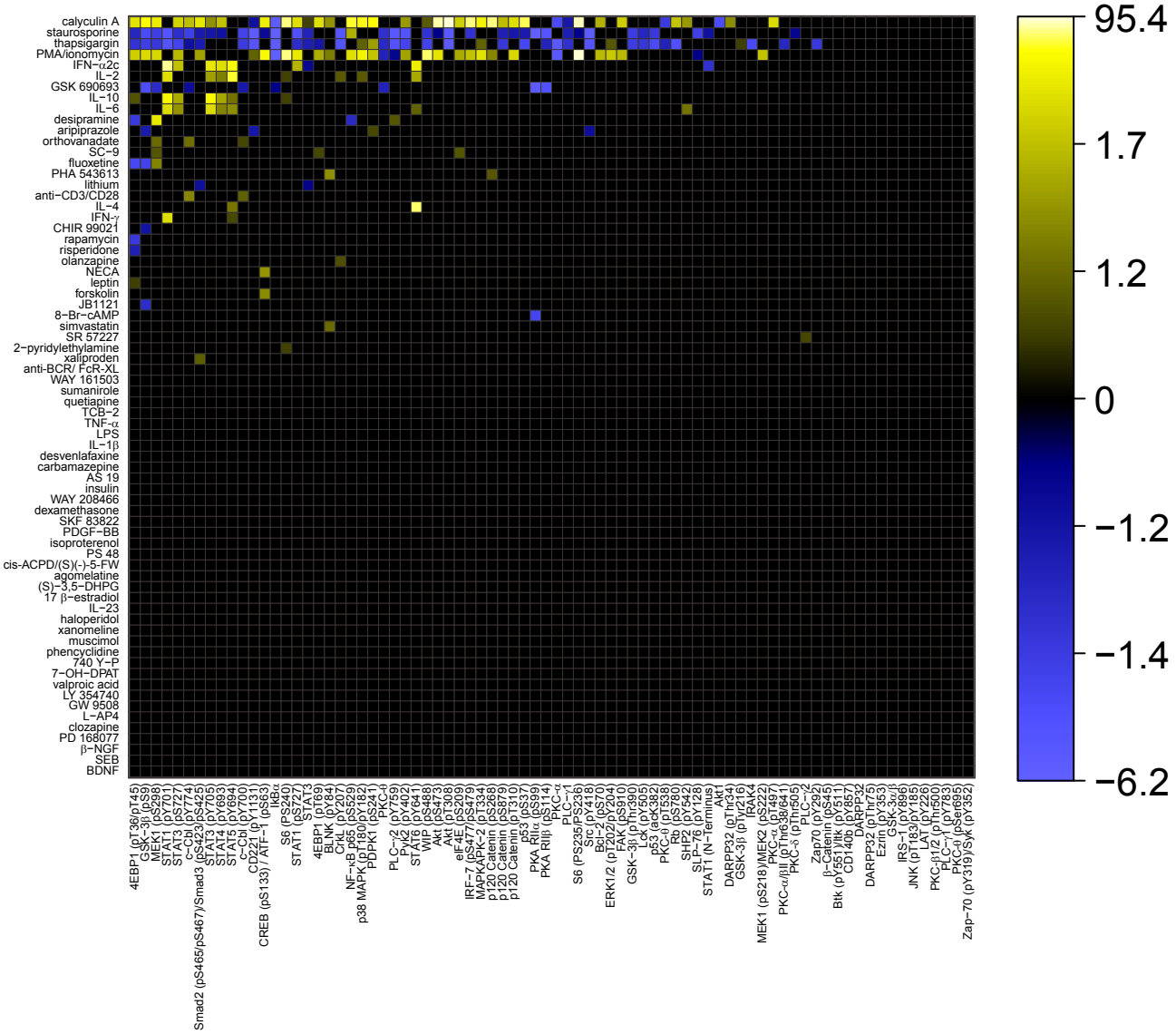

Figure 3.5 Kinetic induction of cell signalling responses across the ligand and epitope array (n = 5460 nodes) continued.

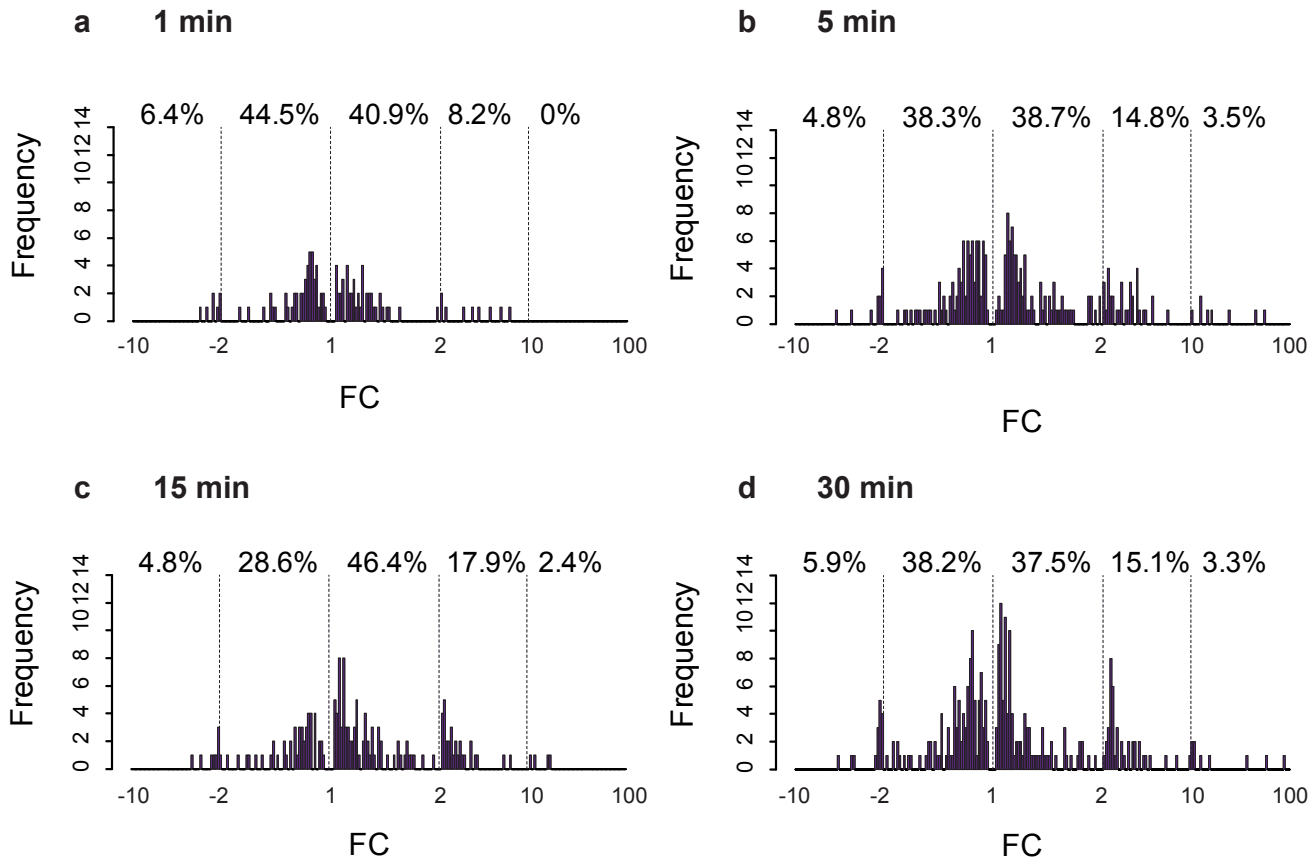

Figure 3.6 Distribution of fold changes for T cell signalling responses across time points. The proportion of responses (%) in each fold change interval is shown for 1 min **(a)**, 5 min **(b)**, 15 min **(c)** and 30 min **(d)** time points. The data is binned in different increments for each FC interval as follows: -10 to -2 (0.2), -2 to 2 (0.05), 2 to 10 (0.2) and 10 to 100 (2). Only significant responses (Wilcoxon $p < 0.05$) with a minimum fold change of 10%, relative to the vehicle, are shown. Data represents median responses of eight PBMC donors.

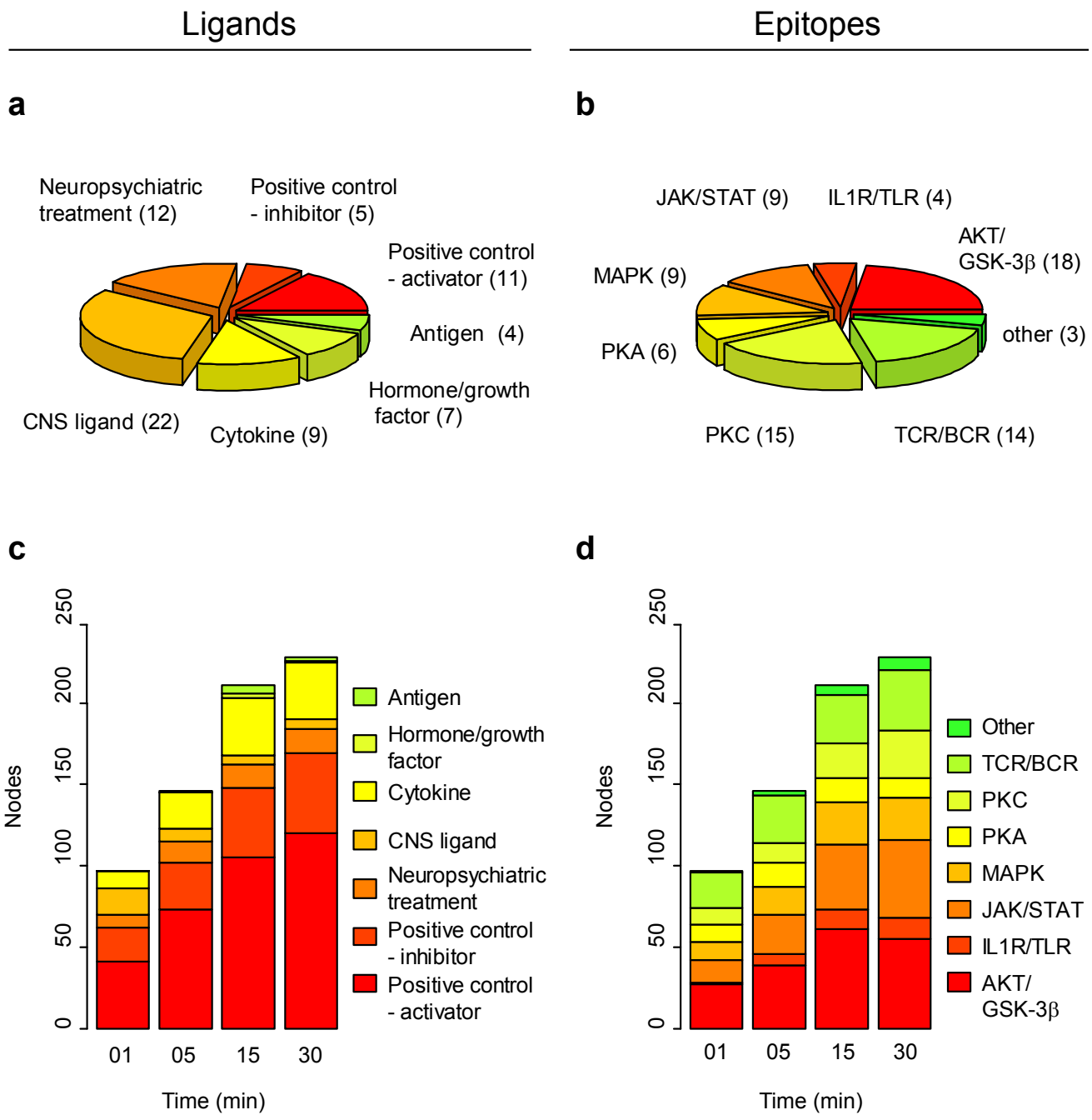

Figure 3.7 Kinetic distribution of T cell signalling responses across ligand and epitope categories. Relative composition of the ligand **(a)** and epitope **(b)** arrays by class or pathway respectively. Composition of the total number of significant responses (nodes) for each time point by ligand class **(c)** or epitope pathway **(d).** Only significant responses (Wilcoxon $p < 0.05$) with a minimum fold change of 10%, relative to the vehicle, are shown. Data represents median of eight PBMC donors

Ligand	1 min	5 min	15 min	30 min
calyculin A	12	19	35	41
staurosporine	16	21	33	38
thapsigargin	7	22	31	38
PMA/ionomycin	19	27	33	32
IFN-alpha 2c	5	7	8	9
GSK 690693	2	4	6	8
IL-2	1	2	6	8
IL-10	1	4	6	7
IL-6	2	6	7	7
aripiprazole	0	0	0	4
desipramine hydrochloride	6	5	4	4
fluoxetine	0	1	3	3
SC-9	0	1	0	3
sodium orthovanadate	0	0	0	3
anti-CD3/CD28	0	1	4	2
IFN gamma	1	1	1	2
IL-4	1	2	5	2
lithium chloride	0	2	2	2
PHA 543613 hydrochloride	0	0	1	2
2-pyridylethylamine dihydrochloride	0	1	0	1
8-bromo-cAMP	1	1	2	1
forskolin	1	3	2	1
leptin	0	0	1	1
NECA	1	2	1	1
olanzapine	0	0	0	1
rapamycin	1	1	1	1
risperidone	0	1	1	1
simvastatin	1	0	0	1
SJH 6 (JB1121)	1	2	1	1
SJH1 (CHIR 99021)	1	1	2	1
SR 57227 hydrochloride	0	0	1	1
xaliproden hydrochloride	0	0	0	1
(S)-3,5-DHPG	1	0	1	0
17 beta-estradiol	0	0	0	0
740 Y-P	0	0	1	0
7-hydroxy-DPAT hydrobromide	0	1	1	0
agomelatine	0	0	0	0
AS 19	0	0	0	0
BCR stim	0	0	0	0
BDNF	0	0	1	0
beta-NGF	0	0	0	0
carbamazepine	0	0	0	0
cis-ACPD/(S)-(-)-5-fluorowillardiine	0	0	0	0
clozapine	1	3	0	0
desvenlafaxin succinate (WY 45233)	0	0	0	0
dexamethasone	0	0	0	0
GW 9508	0	0	1	0
haloperidol	1	1	0	0
IL-1 beta	0	0	2	0
IL-23	0	0	0	0
insulin	0	0	1	0
isoproterenol hydrochloride	2	0	0	0
L-AP4	0	0	0	0
LPS	0	0	0	0
LY 354740 hydrate	0	0	0	0
muscimol	0	0	0	0
PD 168077 maleate	0	1	0	0
PDGF-BB	0	0	0	0
phencyclidine hydrochloride	1	2	0	0
PS 48	0	0	0	0
quetiapine	0	0	0	0
SEB	0	0	1	0
SKF 83822 hydrobromide	10	1	0	0
sumanirole maleate	0	0	0	0
TCB-2	1	0	0	0
TNF alpha	0	0	0	0
valproic acid	0	0	4	0
WAY 161503 hydrochloride	0	0	1	0
WAY 208466 dihydrochloride	0	0	0	0
xanomeline oxalate	0	0	0	0
Total	97	146	211	228

Table 3.1 Activity of ligands across the time course. Shows the number of significant responses (Wilcoxon $p < 0.05$) with a minimum fold change of 10% relative to the vehicle, across 1, 5, 15 and 30 min time points. Ligands are ranked in ascending order of activity at 30 min. Data represents median of eight PBMC donors.

Epitope	1 min	5 min	15 min	30 min
4EBP1 (pT36/pT45)	0	9	9	10
GSK-3β (pSer9)	8	9	8	9
MEK1 (pS298)	5	5	9	9
stat1 (pY701)	3	4	7	7
stat3 (pS727)	1	2	5	7
c-Cbl (pY774)	0	0	3	6
Smad2 (pS465/pS467)/Smad3 (pS423/pS425)	1	3	4	6
stat3 (pY705)	5	3	5	6
stat4 (pY693)	1	3	5	6
stat5 (pY694)	2	5	6	6
c-Cbl (pY700)	1	2	3	5
CD221 (pY1131)	4	4	4	5
CREB (pS133) / ATF-1 (pS63)	1	5	6	5
IkBα	0	0	4	5
S6 (pS240)	5	3	13	5
stat1 (pS727)	0	2	5	5
Stat3	0	1	2	5
4EBP1 (pT69)	0	0	2	4
BLNK (pY84)	2	4	1	4
CrkL (pY207)	5	5	3	4
NF-κB p65 (pS529)	0	3	4	4
p38 MAPK (pT180/pY182)	1	3	5	4
PDPK1 (pS241)	1	3	4	4
PKC theta	1	2	3	4
PLC-γ2 (pY759)	5	4	4	4
Pyk2 (pY402)	3	1	4	4
stat6 (pY641)	2	4	4	4
WIP (pS488)	2	6	4	4
Akt (pS473)	2	4	2	3
AKT (pT308)	3	3	4	3
eIF4E (pS209)	0	0	2	3
IRF-7 (pS477/pS479)	0	2	3	3
MAPKAPK-2 (pT334)	2	4	5	3
p120 Catenin (pS268)	0	2	2	3
p120 Catenin (pS879)	0	0	2	3
p120 Catenin (pT310)	0	1	4	3
p53 (pS37)	0	1	2	3
PKA RII-α (pS99)	8	6	5	3
PKA RII-β (pS114)	2	3	4	3
PKC-α	1	2	3	3
PLC-γ1	0	0	1	3
S6 (pS235/pS236)	2	3	4	3
Src (pY418)	2	2	2	3
Bcl-2 (pS70)	1	0	1	2
ERK1/2 (pT202/pY204)	1	2	2	2
FAK (pS910)	0	0	2	2
GSK-3β (pThr390)	0	0	3	2
Lck (pY505)	1	2	2	2
p53 (acK382)	0	0	0	2
PKC-θ (pT538)	0	0	1	2
Rb (pS780)	0	0	2	2
SHP2 (pY542)	0	1	2	2
SLP-76 (pY128)	2	3	3	2
stat1 (N-Terminus)	0	0	1	2
Akt1	0	0	1	1
DARPP32(pThr34)	0	1	0	1
GSK-3β (pTyr216)	0	1	1	1
IRAK4	1	2	1	1
MEK1 (pS218)/MEK2 (pS222)	1	2	2	1
PKC-α (pT497)	1	1	1	1
PKC-α/βII (pThr638/641)	0	0	0	1
PKC-δ (pThr505)	0	0	0	1
PLC-γ2	0	0	0	1
Zap70 (pY292)	2	3	3	1
β-Catenin (pS45)	0	0	1	0
Btk (pY551) & Itk (pY511)	0	0	0	0
CD140b (pY857)	0	0	0	0
DARPP32	0	0	0	0
DARPP32(pThr75)	0	0	0	0
Ezrin (pY353)	0	0	0	0
GSK-3α/β	0	0	0	0
IRS-1 (pY896)	2	0	1	0
JNK (pT183/pY185)	0	0	0	0
LAT (pY226)	0	0	0	0
PKC-β1/2(pThr500)	0	0	0	0
PLC-γ1 (pY783)	2	0	0	0
PKC-θ (pSer695)	0	0	0	0
Zap-70 (pY319)/Syk (pY352)	2	0	0	0
Total	97	146	211	228

Table 3.2 Activity of epitopes across the time course. Shows the number of significant responses (Wilcoxon $p < 0.05$) with a minimum fold change of 10% relative to the vehicle, across 1, 5, 15 and 30 min time points. Epitopes are ranked in ascending order of activity at 30 min. Data represents median of eight PBMC donors.

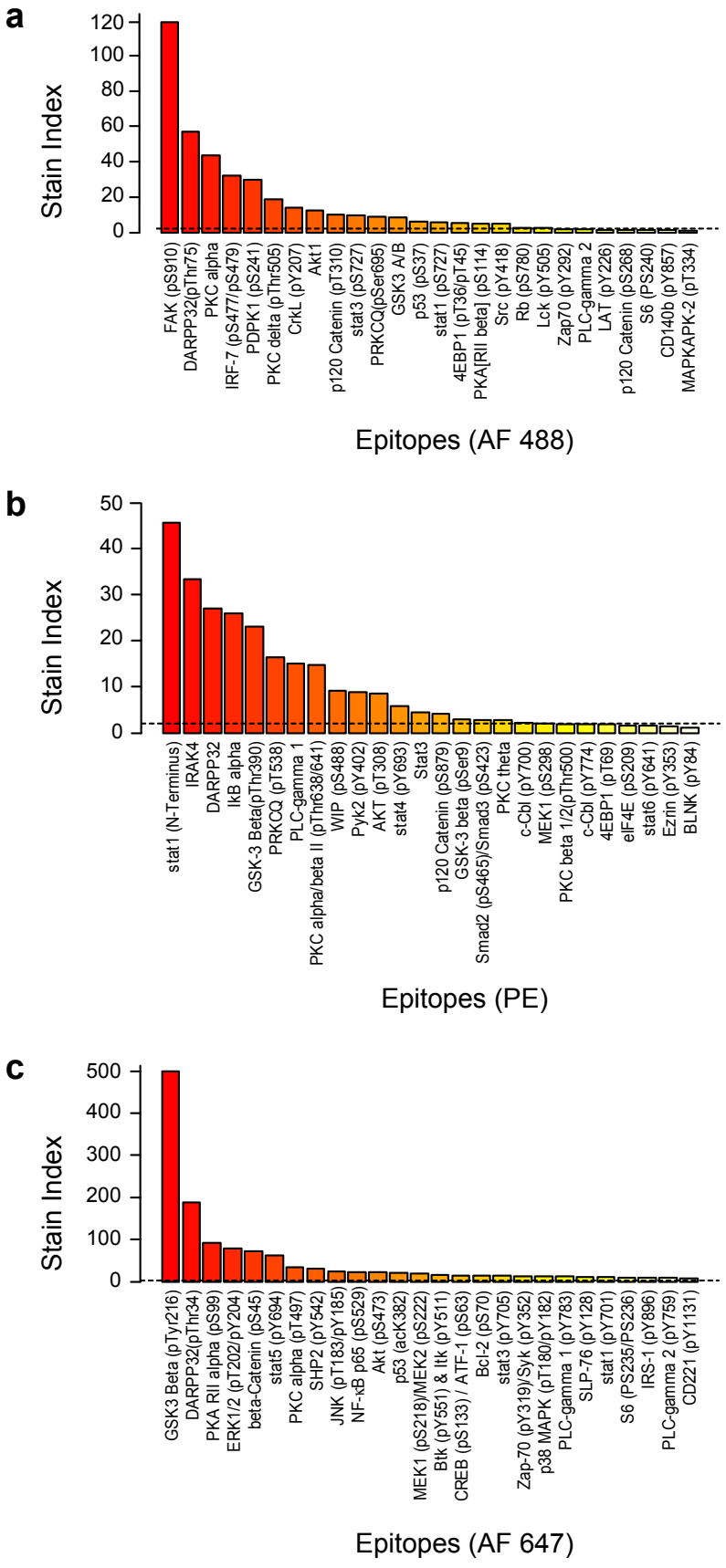

Figure 3.8 Stain index of antibody clones against T cell signalling epitopes used in the time course. Shows the median MFI of the stained samples/ median MFI of the unstained samples in the vehicle condition across eight PBMC donors for each epitope. Stain indices are ranked per functional fluorescence detection channel as labelled with a representative fluorochrome: Alexa Fluor 488 (AF 488) **(a)**, Phycoerythrin (PE) **(b)** and Alexa Fluor 647 (AF 647) **(c)**. Dotted line marks a threshold stain index of two.

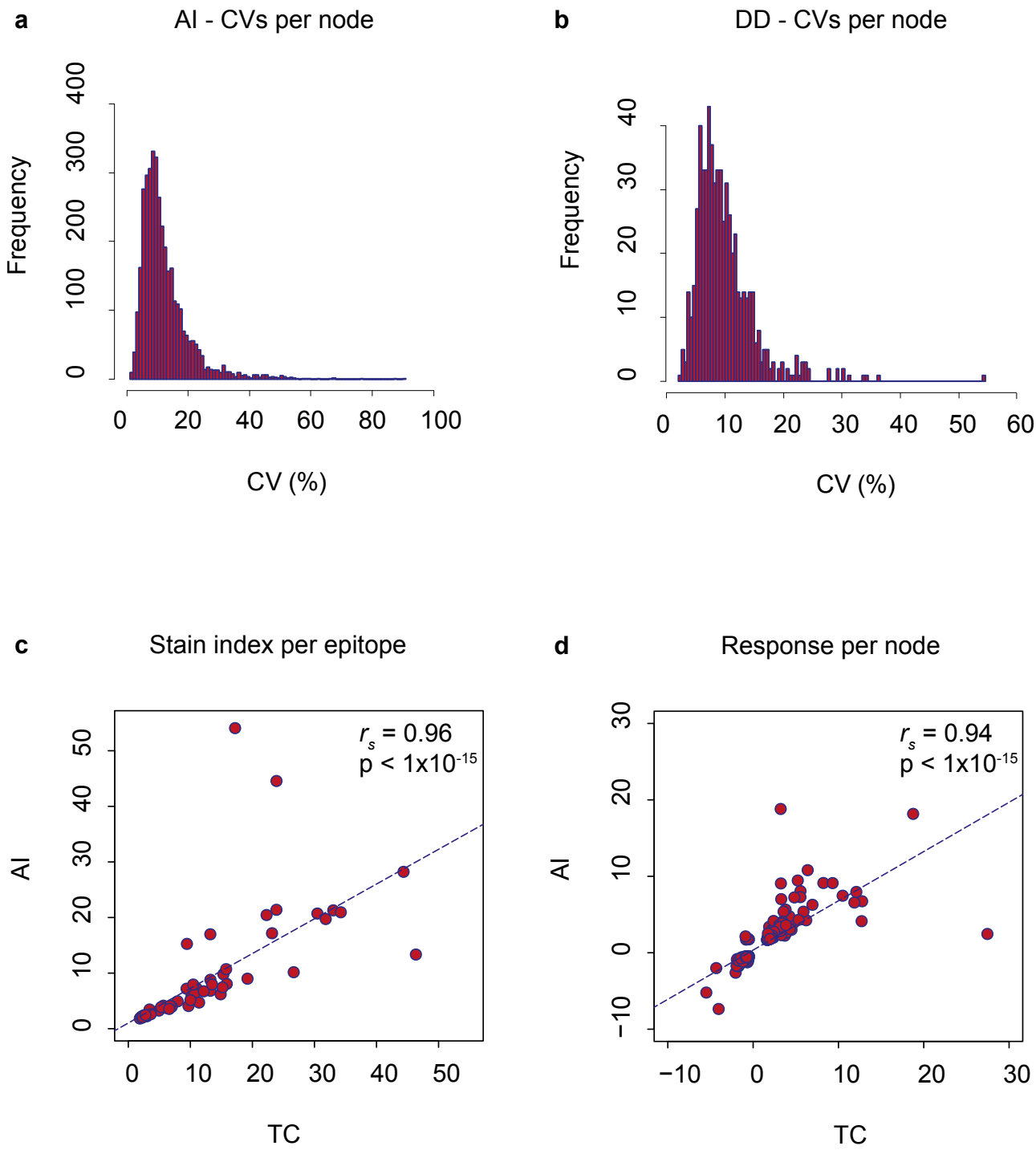

Figure 3.9 Reproducibility across time and independent PBMC cohorts. CVs for each T cell signalling node in the same quality control PBMC sample from a healthy donor measured across six days in the antipsychotic intervention study (AI) **(a)** and nine days in the differential diagnosis study (DD) **(b)**. Single measurements each day were taken for the AI study and duplicate measurements were taken for all except two days of the DD study (on which single measurements were taken instead). Spearman's rank correlation of stain indices (n = 66 epitopes) **(c)** and fold change signalling responses (n = 197 nodes) **(d)** in healthy control PBMC donors for nodes which were active in the time course (TC) at 30min (n = 8 donors) and validated in the same direction in the AI study (n = 12 donors). Three nodes (Akt (pT308)/calyculin, S6 (pS235/pS236)/calyculin, S6 (pS235/pS236)/PMA-ionomycin) with fold changes above 40 were removed from **(d)** for representation, however r_S and p values are reported for the full data set.

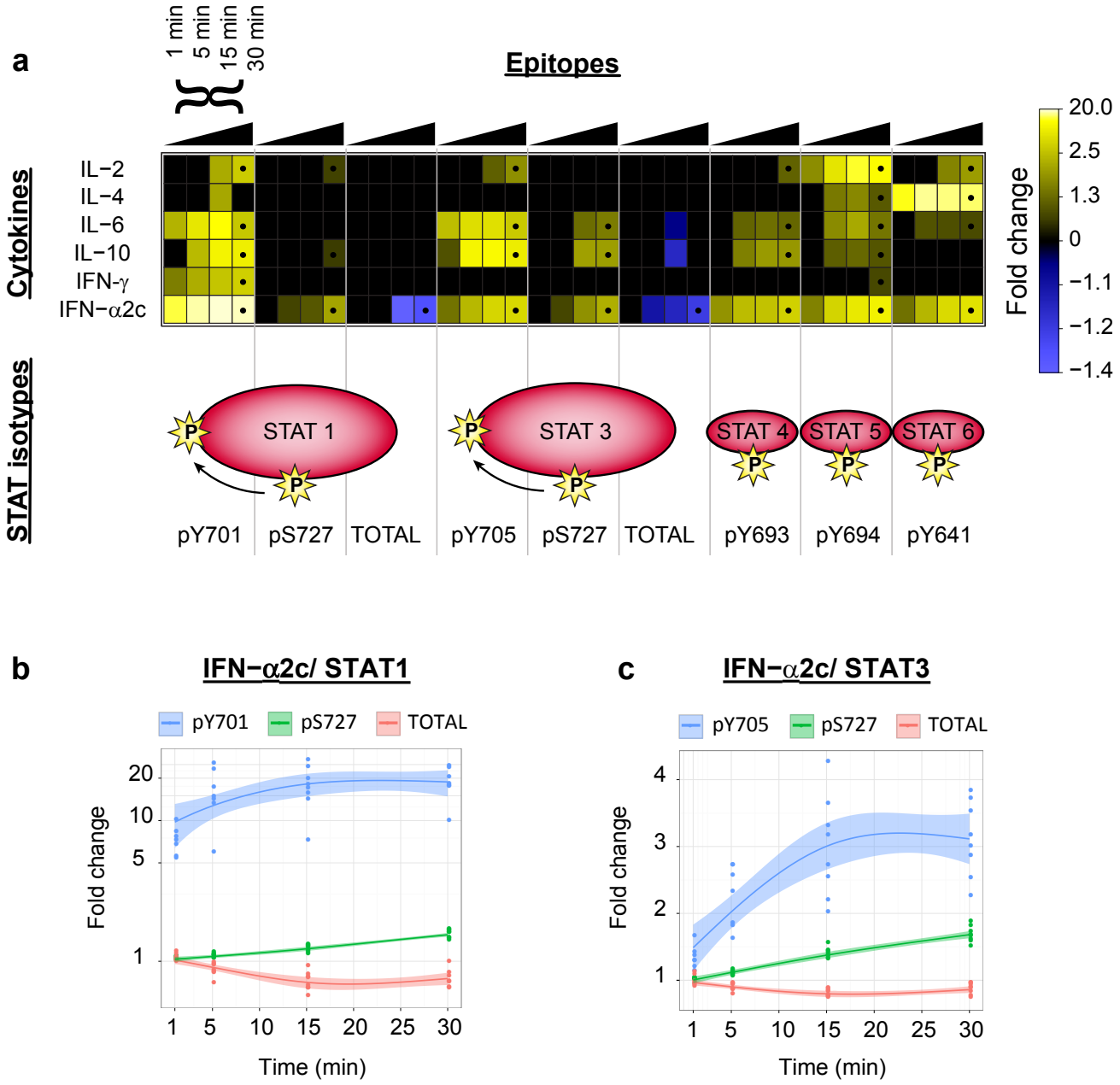

Figure 3.10 Dynamic regulation of JAK/STAT T cell signalling across time course. (a) Specific responses across STAT isotypes were observed for different cytokines. Kinetic induction of phosphorylation at activation sites (STAT1 (pY701), STAT3 (pY705), STAT4 (pY693), STAT5 (pY694) and STAT6 (pY641)) and regulatory sites (STAT1 (pS727) and STAT3 (pS727)) was followed by decreases in total protein epitope availability (STAT1 and STAT3). Black dots at 30 min time points represent replication in an independent PBMC cohort (n =12). Arrows represent regulatory activity between sites. Legend shows fold change in epitope expression, calculated as median MFI of the ligand treatment/ median MFI of the vehicle treatment, with labels distributed evenly across the quantile range. Only significant responses (Wilcoxon $p < 0.05$) are shown. Dynamic regulation of all three sites on STAT1 **(b)** and STAT3 **(c)** in response to IFN-α2c. All data represents median across eight PBMC donors.

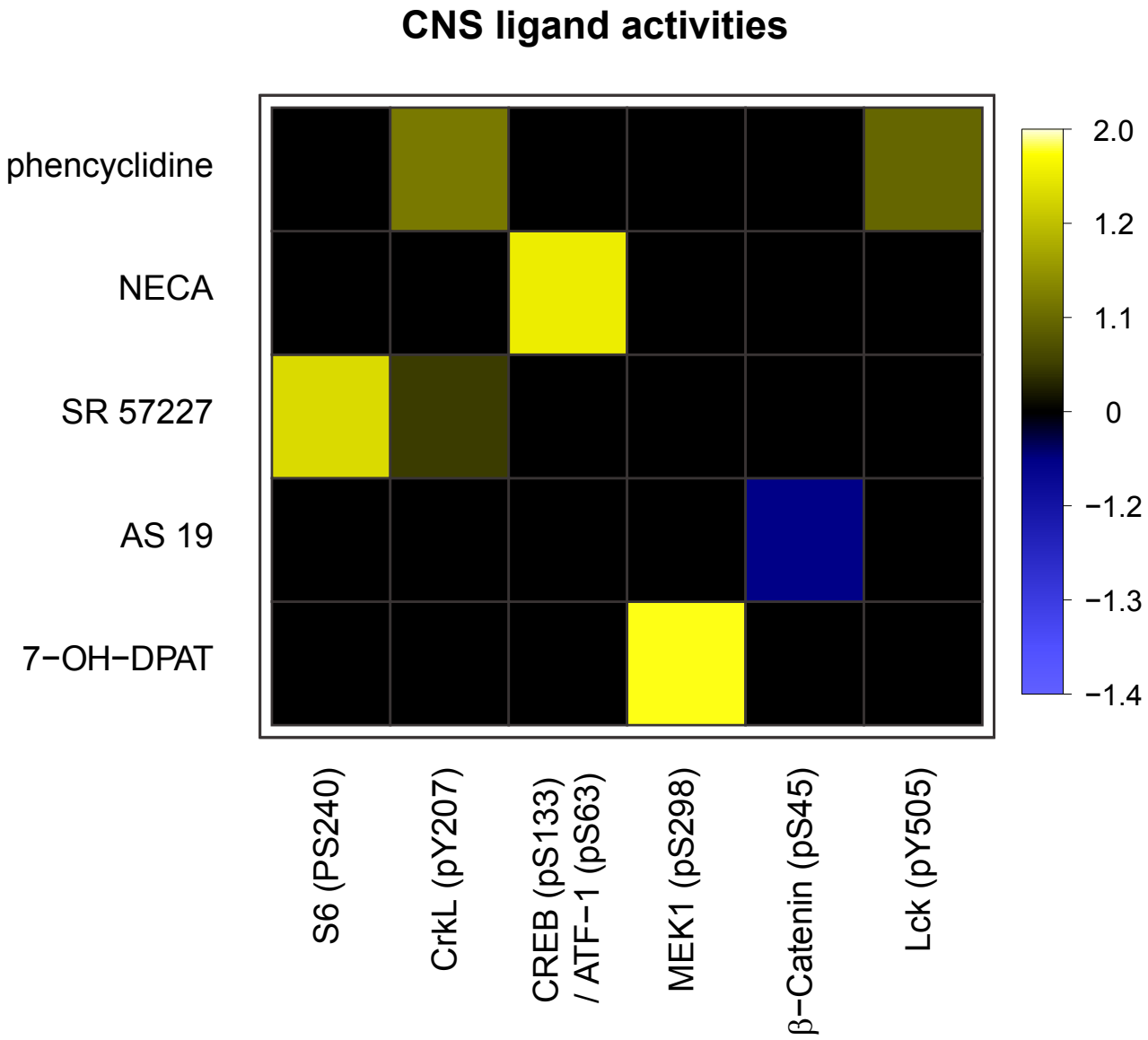

Figure 3.11 Responses to CNS ligands in T cells. Only significant responses (Wilcoxon $p < 0.05$) which were sustained in the same direction for a minimum of two consecutive time points are shown. Legend shows mean fold change in epitope expression across active time points, calculated as median MFI of the ligand treatment/ median MFI of the vehicle treatment, with labels distributed evenly across the quantile range. Data represents median across eight PBMC donors. Targets of the compounds include phencyclidine (NMDA receptor antagonist/ σ receptor agonist), NECA (adenosine A1/2A/3 receptor agonist), SR 57227 (5-HT3 receptor agonist), AS 19 (5-HT7 receptor agonist) and 7-OH-DPAT (D3 receptor agonist).

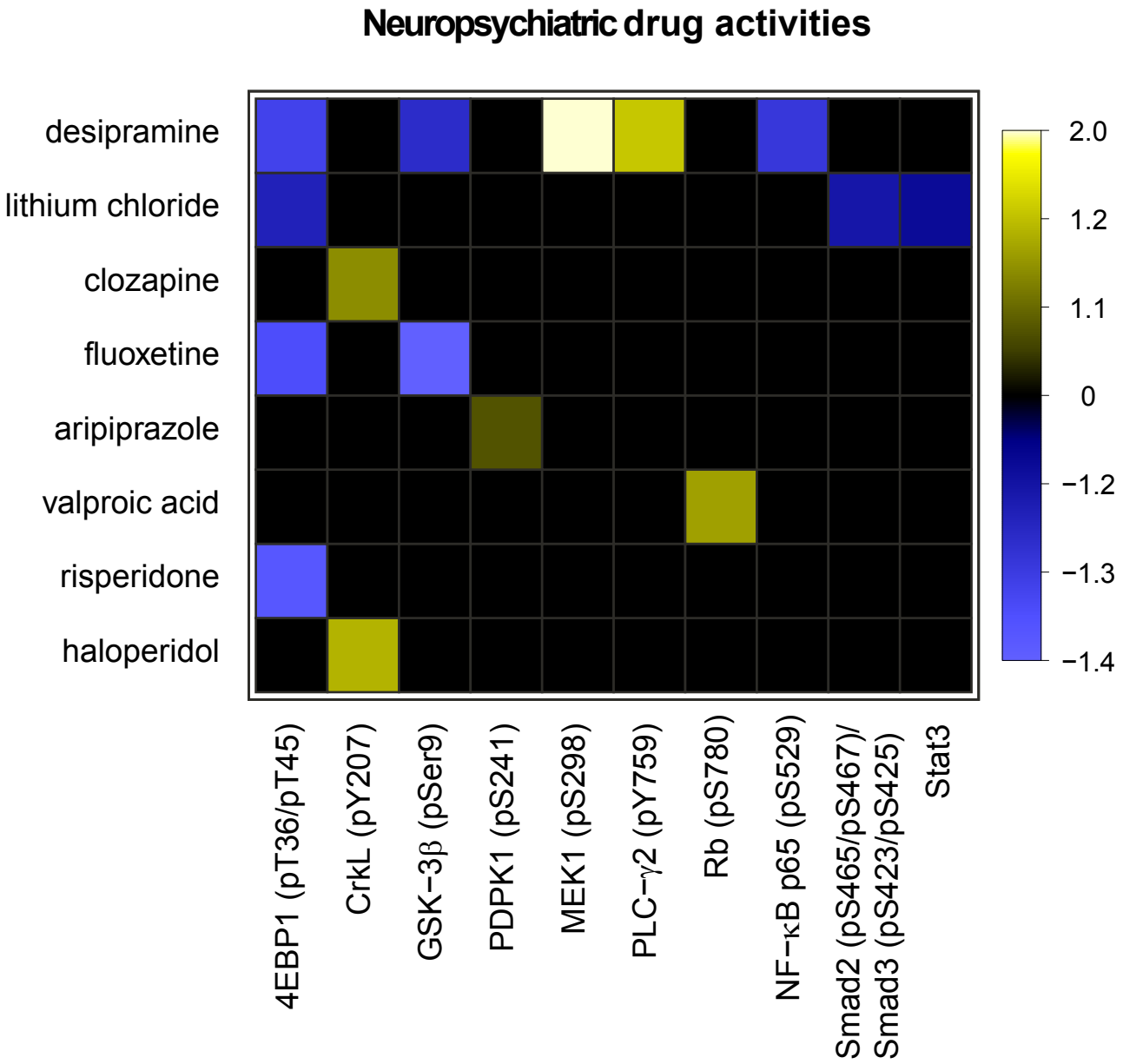

Figure 3.12 Responses to neuropsychiatric treatments in T cells. Only significant responses (Wilcoxon $p < 0.05$) which were sustained in the same direction for a minimum of two consecutive time points are shown. Legend shows mean fold change in epitope expression across active time points, calculated as (MFI of the ligand treatment/ MFI of the vehicle treatment), with labels distributed evenly across the quantile range. Data represents median across eight PBMC donors. Clinical indications of the compounds include desipramine and fluoxetine (antidepressant), lithium and valproic acid (mood stabilizer) and clozapine, risperidone, aripiprazole and haloperidol (antipsychotics).

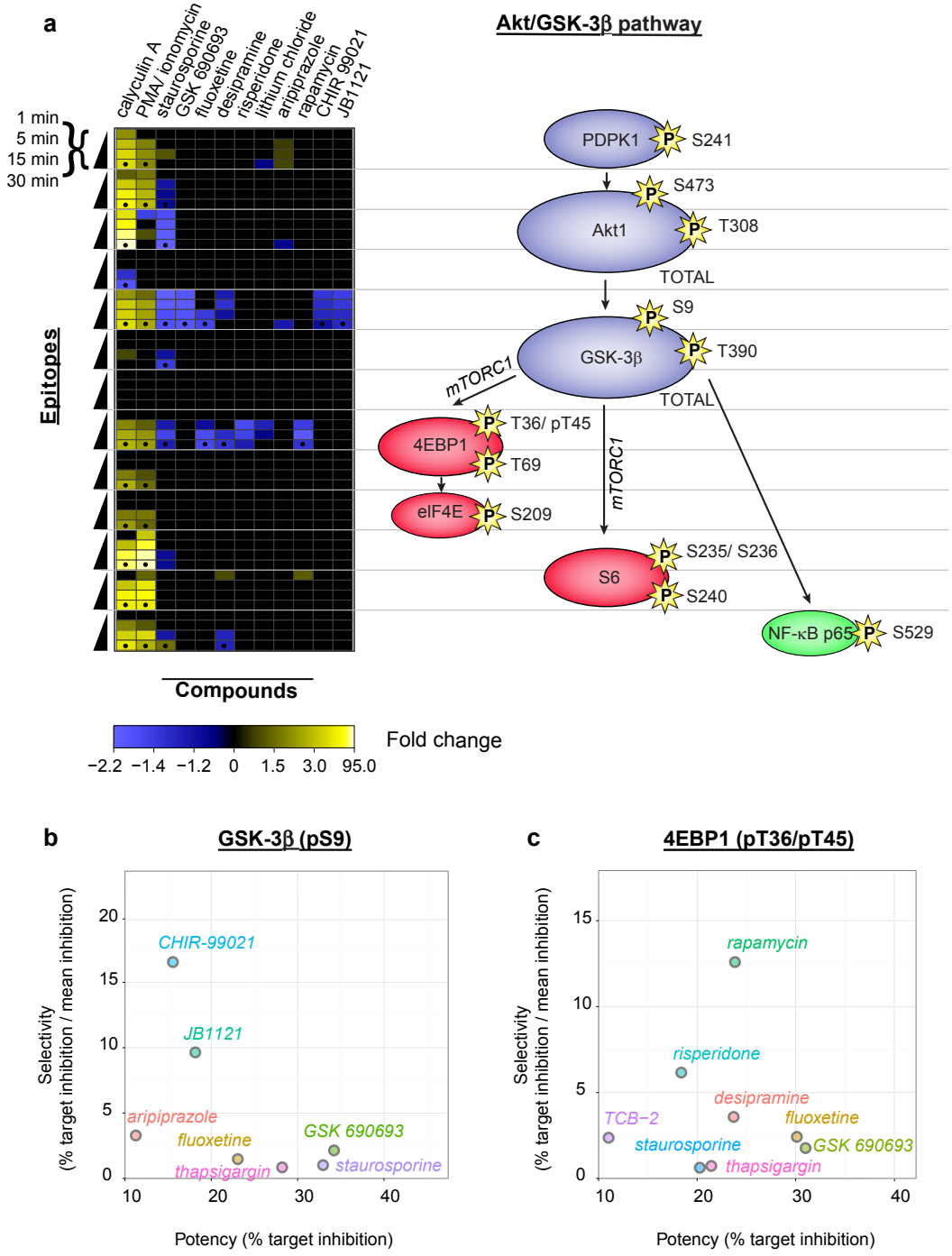

Fig. 3.13 Kinetic exploration of neuropsychiatric treatments and novel inhibitors of the Akt/GSK-3β pathway in T cells. **(a)** Kinetic induction of responses (left) at key Akt/GSK-3β pathway epitopes (right) for positive controls (calyculin A, PMA/ ionomycin, staurosporine and GSK 690693) as compared to neuropsychiatric treatments (fluoxetine, desipramine, risperidone, lithium and aripiprazole) and specific novel inhibitors (rapamycin, CHIR 99021 and JB1121). Only significant responses ($p<0.05$, Wilcoxon rank-sum test; n=8 healthy control PBMC donors) are shown. Black dots at 30 min time points represent replication in an independent PBMC cohort (n=12). Legend shows fold change in epitope expression (calculated as median MFI of the ligand treatment/median MFI of the vehicle treatment across PBMC donors), with labels distributed evenly across the quantile range for negative and positive fold changes separately. Fold change is converted to -1/fold change for downregulated epitopes. Proteins are coloured with respect to their cellular function: blue (kinase), red (translation) and green (transcription). The position of mammalian target of rapamycin complex 1 (mTORC1) is shown for mechanistic interpretation although no epitopes were measured on this protein. The epitopes which form the Akt/GSK-3β pathway (right) represent a small subset of the possible cell signalling protein interactions in PBMCs. They are selected based on prior hypotheses of signalling alterations and drug treatment effects in neuropsychiatric disorders as opposed to emergent properties of the experimental data. **(b)** Inhibition potency and selectivity across all 70 ligands used in the time course for targets GSK-3β (pS9) and **(c)** 4EBP1 (pT36/pT45) at 30 min. Potency reflects % inhibition of phosphorylation at target site calculated as (1 – MFI of the ligand treatment/mean MFI of the vehicle treatment)*100%, averaged across PBMC donors (n=8). Selectivity reflects the ratio of % inhibition of phosphorylation at the target site to mean % inhibition across Akt (pS473), Akt (pT308), GSK-3β (pS9) and 4EBP1 (pT36/pT45) sites, averaged across 8 donors. Only ligands with >10% potency are shown. MFI - median fluorescence intensity.

3.3 DISCUSSION

Three main types of results have been presented in this chapter. The first set of results focuses on the establishment of a platform capable of high content functional screening of T cell responses *ex vivo*. The second set relates to an application of the platform for detection of responses at CNS receptors. Exploration of the activities of approved and novel neuropsychiatric treatments comprises the third set of results. This discussion will focus on the third set of results **(Fig. 3.12 and 3.13)**, due to the direct clinical implications for treatment response prediction and novel drug discovery.

The results showed heterogeneity with respect to the pharmacological profile of neuropsychiatric treatments. This is consistent with clinical findings in which even compounds which are almost structurally identical can have very different clinical properties and efficacies. For example clozapine is more effective in treating psychosis and suicidality in schizophrenia, and yet is uniquely associated with the potentially fatal side effect of agranulocytosis, compared to its close structural relative olanzapine[21,149]. Furthermore patients with the same diagnoses do not always respond in the same way to similar treatment[9,14,15]. Thus the heterogeneity which we observe in this *ex vivo* assay lies at the heart of one of the most pressing unmet medical needs in neuropsychiatry, that of personalized medicine. Consequently there are two primary objectives in the interpretation of this data. The first is to identify core functional signalling motifs, which are common to different drugs, and assess their potential as a scaffold for novel drug discovery across disease indications. The second is to identify divergent functional signalling motifs for drugs within the same indication and explore their potential for targeting subpopulations of treatment resistant patients. In line with these objectives we also seek to address the persistent question of whether *ex vivo* responses in T lymphocytes can be correlated to existing or plausible mechanisms of CNS drug efficacy or side effects? First the main differences between the current system and published research in neuropsychiatric drug effects on cell signalling will be discussed. Subsequently we examine the relevance of convergent activity detected at 4EBP1 across drugs with different indications. Finally we explore the functional signatures unique to each indication or specific drugs and the potential for novel combinatorial treatment strategies.

3.3.1 COMPARISON OF THE PRESENT *EX VIVO* METHODOLOGY TO THE STATE OF THE ART

Clinical response to the majority of approved neuropsychiatric treatments is only apparent after several weeks of administration[8,14]. This corresponds to the time necessary for changes in synaptic plasticity and neurogenesis, which are thought to mediate clinical efficacy, to occur[9,19,144]. In line with this the majority of research into the cell signalling changes evoked by neuropsychiatric medications has been conducted through chronic drug administration (2-6 weeks) in animal models[150–154]. Leaving aside the controversies surrounding the behavioural correlates of cell signalling changes in these animals, these *in vivo* systems at least investigate the neuronal infrastructure which is thought to be fundamental to clinical efficacy. The importance of the physiological environment is evident from the heterogeneous results obtained through *in vitro* cell culture experiments. For example the majority of neuropsychiatric treatments across different drug classes increase the phosphorylation of GSK-3β at the (pS9) residue and therefore inhibit GSK-3β activity[90,144]. However while this trend is relatively well replicated across animal administration paradigms, the results in cell culture are more contradictory across drug classes and different cell lineages[90,144]. This is not to mention the likely proportion of negative findings which have remained unpublished as they do not subscribe to the current dogma. Nevertheless the majority of these *in vitro* studies have used primary neurons, such as cerebellar granule cells, or neuronal cell lines, such as SH-SY5Y[139,155–158]. These cell cultures at least benefit from the confirmed expression and downstream coupling of cell surface receptors, for example 5-HT, dopamine and glutamate receptors, which are traditionally implicated in neuropsychiatric treatment response. In contrast there is scarce published data on the cell signalling effects of neuropsychiatric treatments in blood cells. Furthermore these neuronal *in vitro* studies, like their *in vivo* counterparts, have also focused on chronic drug administration protocols. For example the majority of *in vitro* studies relating to the putative neuroprotective functions of mood stabilizers and second generation antipsychotics have measured changes in GSK-3β or Akt1 phosphorylation status following 2 – 96 h of drug incubation[139,155–158]. Even high throughput screening of novel compounds such as CHIR 99021 and JB1121 against GSK-3β activity involved overnight drug incubations[159]. The current data, on the other hand, reflects an acute drug response within 30 min.

The present *ex vivo* system is therefore substantially different from the current state of the art. Firstly we are devoid of the surrounding neuronal infrastructure which is essential to putative clinical effects in humans and animal models. Secondly we are operating in a completely different cell lineage in which it is still not clear to what extent traditional CNS receptors are expressed or functionally coupled. Thirdly we are looking at kinetic effects on much shorter time scale than the majority of published data. Thus we are looking for changes at the most basic common denominator

of immediate and direct drug interactions with cell signalling epitopes under the premise that some of these are shared at a systemic level *in vivo*. Also as the drugs are tested here individually, without exogenous stimulants, it is likely that we are manipulating constitutive phosphorylation mechanisms.

A final consideration is that, independently of which model system is used, the cell signalling mechanisms which underlie the clinical efficacy of neuropsychiatric treatments are still not thoroughly defined. As discussed in the introduction their molecular mechanisms of action have emerged several decades after their incorporation into clinical practice[1]. For example, while the discovery that lithium can inhibit GSK-3β ostensibly revolutionized our understanding of cell signalling in neuropsychiatry, the precise mechanism which mediates its clinical effect is still a matter of intense debate and controversy[88]. Likewise the interaction between D2 receptor antagonism, considered central to antipsychotic efficacy, and the range of other putative molecular disease targets suggested by recent GWAS studies is scarcely understood[24,160]. Therefore while we seek to relate the present *ex vivo* findings to known drug or disease mechanisms it is also possible that some of the observed effects have not yet been characterized.

3.3.2 MODULATION OF CONSTITUTIVE ACTIVITY

The phosphorylation status of many cell signalling epitopes does not represent a binary switch, for which the respective protein function is either on or off, but instead a dynamic equilibrium in which a certain level of basal phosphorylation and activity is always present. This homeostatic control is maintained through auto-phosphorylation and the activity of regulatory kinases and phosphatases[88,117,161]. It is possible that enrichment of neuropsychiatric drug activity at certain epitopes, without exogenous stimulants present, is due to the fact that these proteins show higher levels of constitutive activity. Nevertheless the modulation of constitutive activity could provide a valuable surrogate measurement of the therapeutic window of pathway inhibitors.

This is exemplified by two opposing mechanisms of action in the well characterized neuropsychiatric drug target GSK-3β: pseudo-substrate inhibition and auto-activation[88]. Pseudo-substrate inhibition refers to the competitive blocking of the primed substrate recognition site by GSK-3β's own N-terminal tail when phosphorylated at pS9. Auto-activation refers to the inhibition of upstream Akt kinase and activation of protein phosphatase 1 (PP1) which provides a feed-forward mechanism for GSK-3β to reduce its own inhibitory S9 phosphorylation. In neuropsychiatric

diseases this auto-activation mechanism has been suggested to amplify the effects of an initial insult towards pathological manifestations[88].

In contrast the mood stabilizer lithium is thought to achieve clinical efficacy by dampening these self-activating mechanisms and promoting pseudo-substrate association[88,90]. The vital feature of this interaction is that lithium does not completely abrogate the activity of GSK-3β. Instead it establishes a new steady state in which the constitutive activity of the enzyme is reduced but it is still able to execute its wide range of cellular functions, hence avoiding toxicity. Therefore, in manipulating the constitutive activity and phosphorylation status of key proteins *ex vivo*, it is possible that we are probing the same mechanisms which determine the therapeutic window of pathway inhibitors *in vivo*. This is supported by the observation that changes in phosphorylation at most epitopes, in response to neuropsychiatric ligands, were not maximal compared to the positive controls (calyculin, PMA/ionomycin and staurosporine). This suggests that these changes are still within the dynamic range of phosphorylation for these site and consequently subject to regulatory control.

3.3.3 Convergent inhibition of 4EBP1 (pT36/pT45) across neuropsychiatric drug indications

The convergent inhibition of phosphorylation at 4EBP1 (pT36/pT45) in T cells, across several drugs with different clinical indications, is one of the prominent findings revealed by the *ex vivo* assay **(Fig. 3.12 and 3.13)**. These drugs included fluoxetine and desipramine (antidepressants), lithium (mood stabilizer) and risperidone (antipsychotic). 4EBP1 (pT36/pT45), along with p70S6K, is directly phosphorylated by mTORC1 to promote mRNA translation. The direction, magnitude and kinetic profile of the responses observed at 4EBP1 (pT36/pT45) for these neuropsychiatric drugs closely resembled that of the highly specific mTORC1 inhibitor rapamycin. This suggests that inhibition of phosphorylation at 4EBP1 (pT36/pT45) by these drugs potentially represents inhibition of mTORC1 directly upstream.

mTORC1 is a cell signalling hub and a well characterized mediator of long-term potentiation/ depression in the synaptic milieu[162–164]. For example it has been shown to mediate defining aspects of the pathogenesis of depression, such as stress susceptibility and early life mood disturbances[165,166]. It has also been implicated as a convergent target of classical antidepressants, such as fluoxetine and desipramine, and experimental antidepressants, such as ketamine or mGlu2/3 receptor antagonists[167–171]. However there are no reports of direct mTORC1 inhibition by

these neuropsychiatric drugs outside the synaptic environment where the appropriate neurotransmitter receptors are expressed. This raises the intriguing possibility that these drugs are interacting with cell signalling protein complexes such as mTORC1, which lie downstream of their traditional targets, via completely different mechanisms. Whether this inhibition of mTORC1 reflects collateral efficacy or a side effect is an intriguing question[172].

mTORC1 inhibition has two well characterized physiological effects, immuno-suppression and induction of autophagy, which could represent as yet underappreciated facets of the efficacy of these neuropsychiatric drugs[162,173]. Immune activation has been implicated in the pathogenesis of several disorders including schizophrenia, bipolar disorder, major depression and autism. The drugs which display putative mTORC1 inhibition activity in the present study, have all been attributed with immunosuppressive properties. For example, fluoxetine, desipramine and lithium have all been shown to protect mice against an otherwise lethal dose of lipopolysaccharide-induced sepsis with efficacy comparable to prednisolone[174,175]. Fluoxetine has also been shown to reduce transplant rejection via T cell immuno-suppression and induce apoptosis in Burkitt lymphoma B cells[176–178]. These results are consistent with an alternative application of our platform in which fluoxetine suppressed the inflammatory burst capacity in T cells and increased the expression of pro-apoptotic markers Annexin V and DAPI in B cells following 72hr incubation with T cell mitogenic cocktail SEB (1ug/ml)/anti-CD28 (0.1ug/ml). Interestingly, risperidone has also distinguished itself from other antipsychotics in lymphoblastoid growth inhibition assays[179].

The immuno-modulatory potential of these drugs could be related to collateral efficacy in several ways. Firstly immuno-suppression could potentially reduce the secretion by peripheral immune cells of proinflammatory cytokines such as IL-6, TNF-α, IFN-γ, MCP-1, IL-12 and IL-1β, which are able to cross the blood brain barrier and exacerbate neuropsychiatric symptoms[132,180]. Secondly it could suppress aberrant pruning of dendritic spines and production of reactive oxygen species by M1-activated microglia in the brain[181,182]. Finally the pro-apoptotic propensities of these drugs in specific cell subtypes could regulate the relative proportions of different immune cell subsets, both in the brain and periphery, to mitigate the effects of the pathogenic subtypes[56,183].

Autophagy, the second potential mechanism of collateral efficacy suggested by the current study, has been extensively studied in neurodegenerative disorders[184,185]. Autophagy (meaning 'self eating') is the regulated digestion of damaged cellular components for their subsequent recycling as functional biomolecules. It lies at the crossroads of apoptosis and cellular resilience[186,187]. It prevents neuronal toxicity in the early stages of Alzheimer's, Huntington's and Parkinson's diseases by reducing the accumulation of phosphorylated tau, huntingtin or a-synuclein protein aggregates respectively[162,184]. Very recently autophagy has also been implicated in the pathophysiology of

neuropsychiatric disorders. For example mRNA expression of the autophagic regulator beclin-1 was reduced in post-mortem brains of schizophrenia patients relative to controls suggesting an impaired autophagic response in these patients[188]. In animal models of major depression, the induction of autophagy via FKBP51 has been shown to mediate antidepressant efficacy[189,190]. Promotion of autophagy has also been associated to the therapeutic efficacy of lithium in bipolar disorder[191]. This raises the possibility that the shared inhibition of mTORC1 by drugs from different indications in the *ex vivo* assay reflects the initial stages of an autophagic response which could be related to their clinical efficacy *in vivo*.

If it is the case that the immuno-modulatory and pro-autophagic effects of these drugs are related to their therapeutic profile, it would support the utility of rapamycin as a potential novel treatment candidate for neuropsychiatric disorders, either alone or as an add-on therapy. There are several features which make rapamycin attractive in this respect. Firstly it is an FDA approved medication (sirolimus) with a well documented pharmacokinetic and safety profile, consistent with the focus on drug repurposing in the current work. Secondly it has shown promising results in the treatment of different aspects of neurodegenerative disorders which share many of the pathological hallmarks of neuropsychiatric disorders[192]. These include normalization of neuronal stem cell quiescence, neuronal migration, cortical patterning, synaptic plasticity and aberrant inflammasome activation and reactive oxygen species production in microglia[162,192]. Furthermore it has also shown clinical efficacy in the reduction of epileptic seizures associated with 'mTORopathies' such as tuberous sclerosis[193]. Not only do these mTORopathies have high comorbidity with neuropsychiatric disorders; but there is also a shared heritage of drug discovery between anticonvulsant and mood stabilizing drug classes[194,195]. Thirdly the correlation of rapamycin's *in vivo* efficacy with the phosphorylation status of mTORC1 substrates, such as p70S6K, in lymphocytes using flow cytometry is well established in other indications, expediting a similar application in neuropsychiatry[196]. Finally mTORC1 activity in lymphocytes has been shown to correlate with cognitive impairment suggesting that systemic alterations in mTORC1 activity can reflect core neuropsychiatric symptoms[197]. The utility of compounds, such as rapamycin, are likely to have very different effects depending on the stage of the disease at which they are implemented and the chronicity of the treatment[162].

However if we are to propose rapamycin or related 'rapalogs' as viable therapeutic strategies in neuropsychiatry, we also have to propose a model in which its mTORC1 inhibition does not functionally antagonize the mTORC1 activation necessary for synaptic plasticity and treatment response. One such model could involve a low level of systemic mTORC1 inhibition, which promotes neuronal 'housekeeping' through autophagy, neurogenesis and stabilization of microglial reactivity,

and at the same time does not exceed the threshold for localized and activity-dependent mTORC1 activation in response to stimulation through neurotransmitter receptors. Preliminary studies suggest that this is feasible[198].

3.3.4 *EX VIVO* CORRELATES FOR BIPOLAR DISORDER TREATMENTS

Divergent *ex vivo* cell signalling signatures, consistent with known differences in their pharmacological profiles, were observed for mood stabilizers lithium and valproic acid **(Fig. 3.12)**. Neither of the mood stabilizers displayed the expected increase in GSK-3β (pS9) phosphorylation. This is likely due to the fact that the majority of evidence for this effect has been derived from chronic administration (4-8 weeks) *in vivo* in either humans or animal models as discussed earlier. However in the control PBMC samples used in the antipsychotic intervention study, activity was detected at 30min for lithium at Akt (pT308).This is relevant as a recent study suggests that destabilization of the Akt- βarrestin 2- protein phosphatase 2A (Akt-Barr2-PP2A) complex, which promotes the accumulation of active Akt phosphorylated at key regulatory site pT308, is the primary mechanism of action of lithium[87,94]. This is supported by an elegant recent study using strains of mice which differ in their responsiveness to lithium in behavioural tasks[94]. Specific Akt inhibition (using AKTI-17) abolished lithium sensitivity in the responsive mouse strain (C57BL/6J). Meanwhile viral-mediated over-expression of Akt restored sensitivity in the unresponsive mouse strain (DBA/2J). Lithium response was also correlated with levels of Akt (pT308) in the striatum. Thus while we do not detect the downstream GSK-3β (pS9) phosphorylation for lithium there is preliminary evidence that the preceding and fundamental Akt (pT308) phosphorylation is detectable in the current time frame *ex vivo*.

Furthermore lithium was active at putative downstream partners of Akt/ GSK-3β including 4EBP1 (pT36/pT45) (discussed earlier), Smad2 (pS465/pS467)/Smad3 (pS423/pS425) and STAT3. The reduction in phosphorylation at Smad2 (pS465/pS467)/Smad3 (pS423/pS425) is consistent with a direct interaction of Smad 3 within a complex with GSK-3β and Axin. Furthermore lithium has been shown to mediate the transcriptional activities of Smad proteins in response to TGF-β signalling[199]. A poignant recent study showed that TGF-B signalling was the principle mediator of gene expression changes related to antidepressant responses in mice. Moreover genetic polymorphisms in TGF-B signalling pathway members (including Smad 3) were found to predict antidepressant response latency in a large longitudinal cohort of patients (n=575) with major depression[200]. This raises the intriguing possibility that the effects on Smad 3 detected in the current *ex vivo* system could underlie the antidepressant aspect of lithium's concurrent anti-manic and antidepressive profile[201].

If that is the case this *ex vivo* interaction could be used to predict response to lithium in bipolar patients with more prominent depressive symptomatology. The inhibition of STAT3 by lithium has also been reported in primary astrocytes, microglia and neural progenitor cells from rodents suggesting potentially clinically relevant mediation of neuro-inflammation and astrogliogenesis[202,203].

Valproic acid showed an *ex vivo* signature which was very different to that of lithium. It displayed exquisite specificity for increasing retinoblastoma - Rb (pS780) phosphorylation. This is consistent with its role as a histone deacetylase (HDAC) inhibitor, a feature which prominently distinguishes its mechanism of action from that of lithium [204–206]. Phosphorylation at Rb (pS780) disrupts the HDAC-Rb complex which allows chromatin acetylation and gene transcription to occur [207] . Thus we are potentially witnessing in this 15-30 min kinetic window the initial stages of epigenetic reprogramming associated with the therapeutic profile of valproic acid. HDACs are thought to mediate the epigenetic memory of stressful early life events contributing to the pathogenesis of mood disorders in subsets of patients[204]. For example suicide victims with a history of child abuse, compared to those without, showed epigenetic downregulation of the glucocorticoid receptor in the hippocampus *post mortem*[208]. Altered HDAC mRNA expression in peripheral leukocytes has also been implicated as a state marker for depressive symptomatology in BD and MDD[209]. Taken together these findings illustrate the role of HDACs as dynamic epigenetic sensors of adverse environmental stressors with clinically relevant expression in PBMCs. This raises the exciting possibility that the *ex vivo* response of Rb (pS780) to valproic acid could be used to predict treatment response in bipolar patients with different disease aetiologies. For example it is possible that patients with a higher environmental stress loading (e.g. comorbid post-traumatic stress syndrome[210]) respond better to valproic acid than those with a dominant congenital loading. To our knowledge, there is no treatment response prediction assay in neuropsychiatry which links direct drug interactions with environmental aetiology. The same *ex vivo* response, in light of Rb's role in mediating cell cycle progression, could also be used to predict potential side effects of valproic acid such as teratogenicity or polycystic ovarian syndrome[211].

Potent novel GSK-3β inhibitors, CHIR 99021 and JB 1121, distinguished themselves in the *ex vivo* assay from lithium and valproic acid in several ways. This is important as their alternative mechanism of action has been proposed as a potential solution for treatment resistant patients with bipolar disorder. The first difference relates to their specificity towards GSK-3β. Whereas lithium and valproic acid collectively displayed effects at several epitopes related to GSK-3β, CHIR 99021 and JB 1121 showed activity specifically at GSK-3β (pS9) **(Fig. 3.12 and 3.13)**. This is consistent with their provenance in drug discovery. CHIR 99021 was originally discovered for type II diabetes,

where it was shown to restore insulin sensitivity in insulin-resistant ZDF rats[212]. It has an IC50 of 0.1 μM for glycogen synthase stimulation in cell culture and is over 500 times more selective for GSK compared to closely related kinases[212]. JB 1121 was discovered following a large-scale drug library (320,000 compounds) screen followed by optimization using co-crystal structure with GSK-3β. It preserves the potency of CHIR 99021, while inhibiting a smaller fraction of the kinome (2.3% vs. 6.8% of >300 kinases respectively)[159]. Correspondingly both inhibitors were highly selective with respect to the 78 epitopes tested *ex vivo*. While JB1121 showed no additional activity outside GSK-3β (pS9), CHIR 99021 additionally inhibited only STAT1 (p727).

The second difference is that CHIR 99021 and JB 1121 showed a sustained decrease in inhibitory GSK-3β (pS9) phosphorylation, whereas the prevailing model for therapeutic efficacy of mood stabilizers, at least *in vivo*, stipulates an increase in inhibitory GSK-3β (pS9) phosphorylation[90]. How then do we reconcile the decrease in inhibitory GSK-3β (pS9) phosphorylation observed *ex vivo* with the known inhibitory effects of CHIR 99021 and JB 1121? One possible explanation relates to their role as ATP-competitive inhibitors of GSK-3β[213]. It is possible that their binding at the ATP site, in close proximity to the binding site of the N-terminal (pS9) pseudosubstrate, stabilizes the pseudo-substrate within the substrate association pocket. This would have the potential to deactivate the enzyme, by outcompeting endogenous primed substrates, and at the same time make the pS9 residue inaccessible for antibody detection due to steric hindrance of the binding pocket or the drug itself. The activity of these inhibitors is so quick that it would suggest direct chemical interactions, as opposed to inhibition via regulatory kinases (e.g. Akt in the case of lithium), which would have a longer kinetic profile, in line with other nodes in the time course study and published data. By extension it would imply that the oscillation of the N-terminal (pS9) pseudo-substrate in and out of the binding pocket is rapid and continuous. This could have important implications for the design of future inhibitors.

Alternative explanations could involve stabilization of the GSK-3β-Axin complex in which the (pS9) residue is notoriously inaccessible or changes in the subcellular localization of GSK-3β. However as only 10% of cellular GSK-3β is estimated to be associated with Axin[88] and the sequestration profiles observed for other proteins had a higher latency, it is unlikely that these factors are decisive. A final possibility is that these compounds display a biphasic phosphorylation response as has been observed for several neuropsychiatric compounds[139,144]. In this case the initial decrease in GSK-3β (pS9), for example during the first two hours of exposure, might be succeeded by an increase, for example at 24 - 96hrs. Taken together, these findings allow us to re-evaluate the role of GSK-3β (pS9) phosphorylation in the development of enhanced inhibitors of this pathway.

The different mechanisms of action of CHIR 99021 and JB 1121 relative to lithium and valproic acid have vital implications for the clinical potential of these novel compounds. While compounds like lithium exert their effect on GSK-3β via interacting proteins such as Akt, CHIR 99021 and JB 1121 can bypass this requirement and act directly on GSK-3β. This direct action on GSK-3β by CHIR 99021 was sufficient to provide putative mood stabilizing effects in a lithium insensitive mouse strain (DBA/2J). Furthermore CHIR 99021 normalized the behaviour of this mouse strain in paradigms used to model both manic and depressive symptoms[94]. This suggests the CHIR 99021, and by extension JB 1121, could provide a much needed therapeutic intervention for bipolar patients who don't respond to or don't tolerate standard lithium treatment. It is particularly interesting that the lithium insensitive DBA/2J mice responded even better to CHIR 99021 compared to their lithium responsive CB57BL/6J murine counterparts[94]. This mirrors a feature observed across several neuropsychiatric disorders, which is that often the patients with the most severe symptoms show the greatest response to treatment[68]. Thus if we are able to target these resistant phenotypes correctly at the cell signalling level, using novel compounds such as CHIR 99021 and JB1121, these patients could potentially show the highest therapeutic response.

The dependence on Akt for lithium's mechanism of action could explain why, despite atypical antipsychotics being used for the treatment of acute mania and psychosis in bipolar disorder, lithium is ineffective against psychotic symptoms in schizophrenia[55]. Reduced Akt and phospho-Akt has been reported in *post mortem* brains, lymphocytes and lymphoblastoid cell lines from patients with schizophrenia[84,214]. This could explain why they are non-responsive to lithium. At the same time it raises the possibility the inhibitors such as CHIR 99021 and JB 1121 could have future indications in schizophrenia. Introduction of these inhibitors to the clinic will depend on their pharmacokinetic and safety profiles which are still being characterized. Nevertheless, in the *ex vivo* assay they provide a mechanistic scaffold for Akt-independent modulation of GSK-3β which could drive a much needed new generation of neuropsychiatric medications with a radically different mechanism of action.

3.3.5 *EX VIVO* CORRELATES FOR ANTIPSYCHOTIC TREATMENTS

Convergent activity was detected at consecutive time points for typical (haloperidol) and atypical (clozapine) antipsychotics at v-crk avian sarcoma virus CT10 oncogene homolog-like (CrkL) (pY207) **(**mean FC=1.12 and 1.11 for 1-5 min, respectively; **Fig. 3.12)**. Olanzapine also showed activity at this epitope (FC 1.13) at 30 min. CrkL is not an established target of these medications. However several recent lines of evidence strongly support its involvement in schizophrenia. The largest genome wide

association study performed in schizophrenia to date (36,989 cases vs. 113,075 controls) revealed micro RNA-137 as one of two genes in the second most significant locus[24]. A parallel study found CrkL to be one of the top four genes whose expression was regulated by micro RNA-137 in human neural progenitor cells[215]. A third study which contrasted the results of available GWAS data with a meta-analysis of genes which were disrupted by copy number variations (CNVs) in schizophrenia also identified CrkL as one of the top candidates[29]. Interestingly in this study CrkL was highly connected using network analysis with other identified risk genes including ERBB3, ERBB4, NPAS3 and ANK3. Furthermore it has been linked to schizophrenia and ASD in large exome sequencing studies which reported *de novo* and rare disruptive mutations[106,107,216]. Finally it is one of the key genes, within the schizophrenia-associated 22q11.2 microdeletion locus, which affect embryonic retinoic acid homeostasis, reelin signalling and neuronal migration[217–220]. Despite indications that clozapine and haloperidol modulate reelin levels in the rat brain[221], CrkL itself has not yet been implicated as a primary target of existing antipsychotics. Taken together these findings suggest that the activity detected at CrkL (pY207) in the *ex vivo* assay represents a potentially novel mechanism of action of approved antipsychotic medications. Moreover this putative target is shared by both typical and atypical antipsychotic drug classes and phencyclidine **(Fig. 3.11)** which induces psychosis like symptoms in humans. Finally its involvement in neurodevelopmental pathogenesis raises the exciting possibility that it could be used as response predictor *ex vivo* in early intervention strategies for patients with more prominent neurodevelopmental disease aetiology or ASD comorbidity.

The progressive induction of phosphorylation at 3-phosphoinositide dependent protein kinase-1 (PDPK1) (pS241) at 5 -30 min specifically by aripiprazole is the second main finding within the antipsychotic drug class. PDPK1 is considered a master upstream kinase in metabolic signalling as it phosphorylates several substrates, including Akt, PKC and p70S6K, in response to insulin and insulin-like growth factor-1 (IGF-1)[222,223]. The activation of PDPK1 at (pS241) by aripiprazole corresponds to a putative insulin sensitizing effect. In contrast antagonistic dephosphorylation of insulin and IGF-1 signalling epitopes, AKT (pT308), CD221 (pY1131) and GSK-3β (S9), was observed at 30 min suggesting compensatory mechanisms in response to the initial PDPK1 activation. While the direction of these changes requires further investigation across a longer kinetic course, it is notable that aripiprazole was the only antipsychotic to produce this effect. Compared to other atypical antipsychotics, aripiprazole is associated with a relatively lower risk of weight gain and metabolic side effects[224]. This has been conventionally explained by a lower relative affinity for histamine 1 (H1) receptors in the CNS[225]. However the present results suggest that it might also have a differential interaction directly with insulin signalling in the periphery. This interaction *ex vivo* could potentially be used to predict which patients would benefit from reduced metabolic side effects if treated with aripiprazole as compared to other atypical antipsychotics. This would

represent a significant innovation as the adverse metabolic effects of many atypical antipsychotic drugs currently result in serious morbidity and mortality[13].

Risperidone showed a divergent profile with respect to the other active antipsychotics (clozapine, haloperidol and aripiprazole). It is noteworthy that while potentiation of CrkL (pY207) was shared across individual members of both the atypical and typical antipsychotic drug classes, this effect was not shared by risperidone. While risperidone shows an intermediate effect, relative to other antipsychotic drugs, in meta-analyses of clinical efficacy and side effects (extrapyramidal symptoms, weight gain, prolactin release, sedation and cardiac arrhythmias)[17], several *in vitro* and biochemical studies suggest that it has a divergent molecular activity profile. Risperidone has been shown to have a differential effects on the secretion of Th1 vs. Th2 cytokines from dendritic cells, relative to haloperidol[226], and in terms of growth inhibition in lymphoblastoid cell lines, relative to other antipsychotics[179]. The latter is concurrent with a differential expression of cell proliferation related proteins in the rat cerebral cortex following chronic *in vivo* administration of risperidone, relative to clozapine[227]. The evidence of an anti-proliferative and anti-inflammatory profile of risperidone is concurrent with its unique inhibition of the mTORC1 pathway at 4EBP1 (pT36/pT45) in the current results. Receptor binding affinity studies have also indicated differences in the affinity of risperidone to 5HT2C and 5HT2A receptors, relative to other antipsychotics[225]. These divergent molecular activities are supported by the relatively different chemical structure of risperidone (Tanimoto 2D similarity score of <0.68, PubChem; **Chapter 5 Fig 5.6**) in comparison with other antipsychotics.

Taken together, these findings suggest that, although the divergent cell signalling profile of risperidone does not equate to drastically biased activity in clinical meta-analyses, its divergent molecular profile may contribute to variable responses, in terms of efficacy or side effects, observed between individuals. By extension the data also suggests that the commonly adopted experimental design, in which the molecular profiles of single members of either typical or atypical antipsychotic drug classes are generalized to represent that of other class derivatives, potentially obscures divergent molecular profiles with significant clinical impact. This is compounded by a biased distribution of specific class derivatives across previous clinical trials of comparative efficacy, which are dominated by haloperidol, risperidone and olanzapine[17]. The direct comparison of multiple class relatives, at both the molecular and clinical level, in future studies would serve to elucidate the divergent profiles of antipsychotic medications, beyond the current paradigm for typicality, and address the vital question of interpersonal variation in treatment response.

3.3.6 *EX VIVO* CORRELATES OF ANTIDEPRESSANT TREATMENTS

The induction of MEK1 (pS298) at 15-30min (1.5 - 3.3 FC) by desipramine and at 30min by fluoxetine (1.25 FC) represented the highest positive fold changes in phosphorylation status across all the neuropsychiatric treatments measured *ex vivo* **(Fig. 3.12)**. Decreases in MEK1 phosphorylation and catalytic activity have been found in the hippocampus and prefrontal cortex brain regions of suicide victims *post mortem*[228]. In two separate studies pharmacological inhibition of MEK, using PD184161, produced depressive-like behaviour in mice and blocked the ability of either desipramine or ketamine to reverse this phenotype[229,230]. Potentiation of the MEK signalling cascade, downstream of 5-HT1A and 5-HT4 receptors, has also been shown to improve emotional memory in rat models of depression[231]. Thus the potentiation of MEK (pS298) in the presence desipramine and fluoxetine *ex vivo* represents a direct functional antagonism of the putative disease process. These findings also suggest that MEK is a convergent target of conventional and novel antidepressant mechanisms of action consistent with its role in synaptic plasticity. Furthermore its implication in restoring emotional memory suggests that it could be a valuable drug target for ameliorating cognitive deficits, which are common to several neuropsychiatric disorders, and are notoriously difficult to treat using current psychiatric medications. Taken together these findings indicate that MEK (pS298) could be a valuable treatment response predictor for major depression and a surrogate drug target for screening of novel compounds. Interestingly IL-2, anti-CD3/CD28 and D3 agonist (7-OH-DPAT) shared the MEK1 (pS298) potentiation signal. This suggests that convergent cell signalling mechanisms could be involved in T cell survival and proliferation and also the neurotrophic effects of neurotransmitters and antidepressants. Fluoxetine and desipramine also shared inhibition of both GSK-3β (pS9) and 4EBP1 (pT36/pT45). This will be discussed below in the wider context of functional coupling across neuropsychiatric medications.

3.3.7 FUNCTIONAL COUPLING AS A NOVEL THERAPEUTIC STRATEGY

In the pathway structure investigated **(Fig. 3.13)** the relationships between signalling proteins are depicted as unidirectional for clarity. Signals are shown travelling from receptors at the cell surface, down the canonical signalling pathway to proteins involved in gene transcription and translation. In fact many bidirectional relationships have been reported. For example GSK-3β can regulate Akt activity in several ways including phosphorylation of the inhibitory site Akt (pT312), activation of protein phosphatase 1 (PP1) which dephosphorylates the activation site Akt (pS473), or by promoting the Akt-Barr2-PP2A complex which dephosphorylates the regulatory site Akt (pT308)[88]. This bidirectionality is not limited to adjacent proteins but can also occur across several proteins in

the signalling hierarchy. For example GSK-3β can regulate mTORC2 'downstream' and mTORC2 can phosphorylate Akt (pS473) several levels 'upstream'[108]. There are likely to be countless other bidirectional relationships between proteins shown which will help to redefine the concept of the canonical signalling pathway towards an interconnected network.

This concept allows us to assess whether the off-target effects at 4EBP1 (pT36/pT45), for drugs which are known to modulate GSK-3β (pS9), indicate functional coupling between these two epitopes. The fact that the specific GSK-3β and mTORC1 inhibitors, CHIR 99021 and rapamycin respectively, do not reciprocally interact with both epitopes suggests that the two epitopes are not directly coupled in a compulsory manner. This is supported by differential kinetics between the two epitopes for compounds which interact with both, such as fluoxetine and desipramine. In addition, the causality of the relationship between GSK-3β and mTORC1 is likely to vary across compounds. However it is possible that enrichment of these two epitopes in the activity profile of neuropsychiatric treatments represents parallel targeting of a holistic disease process.

A pertinent recent oncology study showed that specific inhibition of GSK-3β, using 3 μM CHIR 99021, affected the sensitivity of cancer cell lines to a range of FDA approved antineoplastic drugs (NCI Approved Oncology Drug Set II, n=89)[108]. GSK-3β inhibition altered the apoptotic profile of nearly half of the library compounds with the highest variation observed for kinase inhibitors. Notably CHIR 99021 completely desensitized the cells to rapamycin, and its closely related analogue everolimus, suggesting a strong mechanistic interaction between their respective drug targets. Interestingly the mechanism of action was independent of the conventional target of rapamycin (mTORC1). This interaction also explained why many colorectal cancer cells, with reduced GSK-3β activity, are resistant to rapamycin treatment relative to healthy epithelial cells. On the other hand the combination of GSK-3β inhibition with a different compound, polo-like kinase 1 (PLK1) inhibitor, was able to overcome cellular resistance to apoptosis.

This study taken from the field of oncology has several vital implications for the current results. Firstly that compounds which are active at these two sites, mTORC1 and GSK-3β, can have a profound mechanistic relationship which is not immediately apparent in the traditional framework of canonical signalling. Secondly that combined targeting of these two sites, with precisely the same inhibitors which showed *ex vivo* activity in the present study (CHIR 99021 and rapamycin), can reveal the molecular basis of resistant cellular phenotypes. Conversely combinatorial drug treatment can be used to overcome cellular resistance or mitigate toxicity. For example while the interaction between CHIR 99021 and rapamycin reduces the desired apoptotic effect in cancer, it could provide precisely the neuroprotective qualities sought in a neuropsychiatric medication. The

shared pattern of cellular response between CHIR 99021, rapamycin and the efficacious neuropsychiatric medications in the current studies suggests that this interaction could be positive in neuropsychiatry. Interestingly synergistic effects on Akt/ GSK-3β signalling have been reported for fluoxetine and risperidone, which shared 4EBP1 activity in the current system, and are known to modulate GSK-3β[82]. Moderate GSK-3β inhibition has also been shown to potentiate the effects of a subthreshold dose of ketamine on mTORC1 dependent behavioural responses in animal models of treatment resistant depression[232].

The authors of the oncology study also raise an interesting point about the ultimate specificity of the inhibitors. Using a kinome-wide RNAi screen, they showed that selective GSK-3β inhibition modulates the activity of 50% of the kinases targeted by drugs which are FDA-approved or in clinical trials. Many of these kinases are likely to be shared targets of neuropsychiatric medications thus supporting the exploration of these interactive relationships between specific inhibitors and approved neuropsychiatric treatments. Furthermore, as kinases represent the largest class of protein drug targets after GPCRs, the potential of specific GSK-3β modulation to affect drug sensitivity extends beyond neuropsychiatric indications. However it also raises the question of whether specific inhibition of pleiotropic kinases, such as GSK-3β and mTORC1, represents a feasible drug target given the likelihood of toxicity and non-specific side effects. The safe therapeutic use of GSK-3β inhibitor lithium for over 60 years in the clinic suggests that this is possible in neuropsychiatry[201]. Furthermore many of these pleiotropic kinases require their substrates to be pre-phosphorylated or complexed by other regulatory proteins for phosphorylation to occur[88]. Therefore a low level of specific inhibition by compounds such as CHIR 99021, JB 1121 or rapamycin might not necessarily evoke the cellular cataclysm predicted by a promiscuous kinome-interaction profile. Instead the threshold at which master cellular regulators, such as GSK-3β and mTORC1, compute intervening signals might be modified leading to a normalization of aberrant responses only when they occur.

Many approved chemical entities in neuropsychiatry have been described as 'magic shotguns'[112]. In other words this relates to drugs which have effects on multiple targets, many of which are poorly understood, yet their combined effect is essential to clinical efficacy. The present *ex vivo* results allow us to dissect the individual targets, such as mTORC1 and GSK-3β, of these 'magic shotgun' treatments. We can then use specific inhibitors against these targets, such as CHIR 99021, JB 1121 and rapamycin, to individually modulate their behaviour. As the targets themselves are promiscuous, this in turn could normalize a variety of cellular processes. However the vital distinction is that the input to the therapeutic system is specific and controlled. To extend the shotgun treatment metaphor, this would constitute parallel 'silver bullets'. Moreover if the efficacy

of these so called 'silver bullets' can be correlated *ex vivo* to clinical outcomes it would allow the selection and combination of specific inhibitors to be tailored to specific patient groups. The *in vivo* potential of this strategy has been demonstrated using CHIR 99021 to improve the behavioural profile of lithium treatment resistant mice in an animal model of BD, as described earlier[94]. The current results have applied this strategy using only a handful of specific inhibitors and their similarity to the cell signalling patterns of approved treatments as the clinical correlate. Expanding this strategy to see how the approved medications behave in the signalling milieu of patient cells *ex vivo,* as compared to controls, and using whole libraries of specific inhibitors will potentially provide a wealth of novel pharmacophores.

CHAPTER 4

CLINICAL DRUG TARGET DISCOVERY FOR SCHIZOPHRENIA

4.1 INTRODUCTION

To determine whether the functional cytomic platform is capable of identifying changes in cell signalling that constitute novel drug targets for schizophrenia, we applied the most active ligand-epitope combinations from the time course study (as outlined in **Chapter 3**) to patient and control PBMCs *ex vivo*. This was conducted in two separate, discovery and validation, stages. The discovery stage involved the identification of cell signalling responses which were altered in PBMCs from individuals with schizophrenia, relative to healthy controls, and subsequently normalized by *in vivo* antipsychotic therapy (antipsychotic intervention study- 'AI'; **Chapter 1 Fig. 1.3c**). The validation stage involved the replication of these findings in an independent cohort of schizophrenia patients and assessment of their relative specificity for schizophrenia as compared to other major neuropsychiatric disorders including bipolar disorder, autism spectrum disorder and major depressive disorder (differential diagnosis study –'DD'; **Chapter 1 Fig. 1.3d**). By combining these two types of clinical exploration (AI and DD) we sought to extend the findings of the time course study by defining which cell signalling responses correlate to therapeutic efficacy on a clinically relevant timescale (six weeks) *in vivo* and moreover whether these responses represent potentially specific drug targets or treatment response predictors for schizophrenia relative to related neuropsychiatric disorders.

4.2 RESULTS

4.2.1 DRUG TARGET DISCOVERY USING AN *IN VIVO* ANTIPSYCHOTIC INTERVENTION

STUDY DESIGN

We compared PBMC cell signalling responses obtained from a cohort of male healthy controls (n=12) to drug-naive male schizophrenia patients before (T0) (n=12) and after six weeks (T6) (n=10) of mono-therapy with the atypical antipsychotic medication olanzapine. The patient and control samples were matched for age, gender, BMI, ethnicity, cannabis use, blood pressure and hip vs. waist circumference but not for smoking or alcohol consumption **(Table 4.1)**. Comparison of PBMC responses in samples from schizophrenia patients before treatment to responses from controls allowed the identification of putative signalling mechanisms altered in the disease state. Comparison of PBMC responses in samples from schizophrenia patients before and after treatment allowed the determination of surrogate markers of drug efficacy *in vivo* **(Fig. 4.1)**. Finally the overlap between these two data sets allowed the prioritization of putative drug targets.

We incubated PBMCs from each of the clinical groups (CTRL, T0 and T6) for 30 min with the 56 most active ligands (and 8 vehicle controls) identified in the time course screening **(Chapter 3 Fig. 3.5d and Table 3.1)**. The ligands included a variety of CNS receptor agonists, neuropsychiatric medications, cytokines, hormones/ growth factors, antigens and intracellular signalling modulators **(Chapter 2: Table 2.1)**. Subsequently we measured changes in T cell signalling evoked by the ligands using the 66 most active cell signalling epitopes determined in the time course **(Chapter 3 Fig. 3.5d and Table 3.2)**. The epitopes spanned a wide variety of cell signalling pathways broadly including Akt/GSK-3β, PKA, PKC, MAPK, JAK/STAT, IL1R/TLR and TCR/BCR pathways **(Chapter 2; Table 2.3)**. This produced a total of 3696 cell signalling responses, in addition to basal expression levels of the 66 epitopes, which were measured in T cells for each PBMC donor **(Chapter 1: Fig. 1.4b)**. As in the time course study, fluorescent cell barcoding was used to multiplex the different ligand and vehicle conditions, followed by T cell subtyping using anti-CD3 and functional analysis using antibodies specific for different cell signalling epitopes **(Fig. 4.2)**. Additionally the PBMC samples were immunophenotyped prior to ligand stimulation to establish the relative abundance of helper (CD4+) and cytotoxic (CD8+) T cell subsets and assure that the samples had sufficient viability for functional analysis **(Fig. 4.3)**.

Two types of cell signalling changes, ligand response and basal epitope expression, were identified across the clinical group comparisons. Ligand response alterations relate to ligand-epitope combinations or 'signalling nodes' in which there was a statistical interaction between clinical group status and the response to ligand. In other words PBMCs from different clinical groups showed different epitope responses to a specific ligand. Basal epitope alterations relate to nodes in which there was a statistical association between clinical group status and epitope expression, which was independent of the ligand activity. In other words PBMCs from different clinical groups showed different levels of epitope expression in the resting unstimulated state. Epitopes for which over 30% of the nodes satisfied this condition were categorized as displaying differences in basal epitope expression **(Chapter 2: Statistical analysis)**.

4.2.2 SIGNATURE FOR ALTERED CELL SIGNALLING AND CLINICAL ANTIPSYCHOTIC TREATMENT RESPONSE IN SCHIZOPHRENIA

In total, across both group comparisons (SCZ T0 vs. CTRL and SCZ T0 vs. SCZ T6), 27 ligand responses and 19 basal epitope levels were found to be significantly altered representing 1% of the conditions screened (46/ 3762 nodes). Unsupervised hierarchical clustering of these 46 nodes and the PBMC sample IDs revealed three distinct clusters, corresponding to the three clinical groups (with the exception of three healthy control samples in the schizophrenia T6 group; **Fig. 4.4**). The fact that these clinical groups can be separated based on their cell signalling profiles suggests that there is a significant clinical representation of schizophrenia pathology and antipsychotic treatment effects within the T cell signalling repertoire. The order of the clinical groups within the clustering hierarchy, with schizophrenia T0 and healthy controls at opposite ends of the tree and schizophrenia T6 samples in the middle and adjacent to healthy controls, suggests a normalization of the altered T signalling repertoires over the course of olanzapine treatment. This is concurrent with an overall improvement of symptoms in the schizophrenia T6 group **(Fig. 4.1)**. Conversely, clustering of the cell signalling nodes revealed two main groups. The upper group consisted primarily of ligand responses (19 responses vs. 3 basal epitopes), including several CNS ligands and neuropsychiatric treatments, and appeared to drive the separation of the schizophrenia T0 group from the rest. In contrast the lower group was comprised mostly of basal epitope expression levels (16) relative to ligand responses (8) and appeared to drive the separation of schizophrenia T6 from T0 and healthy controls. This indicates a dichotomy between disease and clinical treatment effects at the level of T cell signalling.

To investigate this further we prioritized the ligand responses obtained from the interaction testing by selecting only ligands which produced a significant (unpaired Wilcoxon $p<0.05$ adjusted for background fluorescence) fold change over 5% compared to the vehicle in at least one of the comparison groups **(Table 4.2)**. Basal epitopes with a minimum stain index of two, relative to the unstained sample, were also prioritized **(Table 4.3)**.

The prioritized ligand responses and epitopes with altered basal expression derived from the schizophrenia T0 vs. CTRL group comparison revealed several cell signalling alterations already associated with schizophrenia **(Fig. 4.5a)**. Altered basal epitopes included decreased Akt1 and IRF-7 (pS477/pS479) and increased STAT3 (pY705). Ligand responses in schizophrenia T cells were attenuated at PLC-γ1, in response to the calcium flux inducer (thapsigargin), and at PKA RII-α (pS99), in response to the adenosine agonist (NECA). Conversely the response to cyclic adenosine monophosphate (cAMP) inducer (forskolin) was potentiated at Src (pY418). Finally the glutamate receptor antagonist (phencyclidine), known to induce psychosis-like symptoms in humans and animal models, provoked a different direction of response at PLC-γ1 in each of the clinical groups.

Comparison of the prioritized ligand responses and basal epitope levels between schizophrenia T0 and T6 groups revealed cell signalling alterations associated with the six week olanzapine treatment course **(Fig. 4.5b).** Basal expression was altered for 14 epitopes across mechanistically diverse signalling pathways including Akt/GSK3-β (5 epitopes), PKC (1 epitope), MAPK (2 epitopes), JAK/STAT (3 epitopes), IL1R/TLR (1 epitope) and TCR/BCR (3 epitopes). All of these changes represented increased epitope levels, except for STAT3 (pY705) which was decreased, following *in vivo* olanzapine treatment. Several ligand responses were also modified by *in vivo* olanzapine treatment. These included attenuated responses to D3 receptor agonist (7-OH-DPAT) and sex hormone (17 β-estradiol) at PKA RII-α (pS99), forskolin at Src (pY418) and antidepressant medication (desipramine) at CrkL (pY207). Responses which were potentiated included thapsigargin at PLC-γ1, STAT5 (pY694) and CrkL (pY207) and PKC/ calcium flux activator (PMA/ ionomycin) at WIP (pS488).

4.2.3 PRIORITIZATION OF PUTATIVE DRUG TARGETS BASED ON NORMALIZATION OF DISEASE SIGNALLING NODES FOLLOWING CLINICAL ANTIPSYCHOTIC TREATMENT

In order to identify which of the prioritized nodes represented potential drug targets for schizophrenia we assessed which of the cell signalling alterations, present in schizophrenia T0 samples relative to controls, were reversed over the course of clinical olanzapine treatment **(Fig. 4.6)**. Four nodes were found to be reversed ('reversal nodes') which represented 15% (4/26) of the total prioritized nodes. These included basal epitope expression at Akt1 and STAT3 (pY705) and ligand responses for thapsigargin at PLC-γ1 and forskolin at Src (pY418) **(Fig. 4.7)**. Considering that the number of prioritized nodes was 0.2% (7/ 3762 nodes) and 0.6% (23/ 3762 nodes) of the total nodes assayed, for schizophrenia and olanzapine treatment comparisons respectively, this represents a significant enrichment of nodes for which the signalling profile was reversed. It is notable that all of the nodes which overlapped between schizophrenia vs. control and treatment follow up comparisons reflected reversal or 'normalization' of aberrant responses and not potentiation. The combined likelihood of the enrichment and unanimous reversal patterns observed at these nodes occurring by chance was extremely low ($p = 1.8x10^{-8}$).

Thapsigargin-PLC-γ1 was especially noteworthy as it was the most significant ligand response altered in schizophrenia T0 vs. control by a factor of 20 fold (p=0.001). PLC-γ1 was also the only epitope to show multiple ligand interactions in the schizophrenia vs. control comparison, one of which involved the known psychosis-inducing compound phencyclidine. Moreover thapsigargin was the only ligand to induce multiple changes across different epitopes (PLC-γ1, STAT5 (pY694) and CrkL (pY207)) in either of the clinical group comparisons. Taken together these results clearly implicate the thapsigargin- PLC-γ1 response as the top drug target to emerge from the clinical stage of the study.

4.2.4 Symptom subscale segregation of cell signalling responses

To better characterize the putative drug targets and determine whether specific schizophrenia symptoms can be linked to altered cellular responses, we correlated changes in the four normalized nodes (described above) to changes (δ) in positive and negative syndrome scale (PANSS) scores across the olanzapine treatment course. Syndrome subscales included PANSS positive (PANSSp), PANSS negative (PANSSn), PANSS general (PANSSg) and PANSS total (PANSSt). Basal STAT3 (pY705) expression was the only reversal node which correlated to a syndrome subscale and showed a

significant reduction associated with an improvement in negative symptoms (δ–PANSSn; ANCOVA: p = 0.010, Spearman: p = 0.001, rho= -0.93, n= 9 samples). This raised the possibility that different cell signalling pathways reflect changes in the different symptom subscales. Despite low sample numbers (n = 6-9) for many nodes, we conducted an exploratory analysis to determine which epitopes were independently linked to positive or negative syndrome subscales. Epitopes for which at least 25% of the nodes showed an association to δ–PANSSp or δ–PANSSn, independently of their respective ligand activities, included S6 (pS240), PDPK1 (pS241) and NF-κB p65 (pS529) for δ–PANSSp **(Fig. 4.8a)** and STAT3 (pY705), STAT3 (pS727), NF-kb p65 (pS529) and Zap-70 (pY319)/Syk (pY352) for δ–PANSSn **(Fig. 4.8b)**. NF-κB p65 (pS529) was the only epitope to meet this criteria for both symptom subscales, yet was correlated in opposite directions in δ–PANSSp vs. δ–PANSSn. The direction of change and epitopes implicated across the rest of the array further suggested distinct cell signalling patterns associated to changes in each symptom subscale.

4.2.5 Comparison of *ex vivo* and *in vivo* effects of olanzapine on cell signalling epitopes

The profound imprint of *in vivo* olanzapine treatment on the T cell signalling repertoire raised the question of whether these cell signalling changes represented direct effects of the drug or complex changes in patient physiology. To address this we examined the direct effects on signalling epitope expression of olanzapine 10 μM at 30 min in each of the clinical comparison groups. Potentiation of epitope expression was observed for Src (pY418), PKC-α, CrkL (pY207) and PKA RII-α (pS99) in the CTRL group and Akt1 in the SCZ T0 group **(Fig. 4.9)**. In the case of Src (pY418), CrkL (pY207) and Akt1 these rapid (30 min) *ex vivo* effects of olanzapine were mirrored by similar increases in basal epitope expression after six weeks of clinical olanzapine administration. Notably the normalization of response to forskolin at Src (pY418), identified as one of the primary drug activities of clinical olanzapine treatment, involved an increase in basal Src (pY418) similar to that observed after 30 min of olanzapine exposure *ex vivo*. The only epitopes which displayed multiple ligand interactions in the schizophrenia T0 vs. T6 comparison were CrkL (pY207) and PKA RII- α (pS99). The *ex vivo* responses of these epitopes to olanzapine at 30 min were correlated to changes in positive (p ANCOVA = 0.017, n= 6 samples) and negative (p ANCOVA = 0.011, n= 6 samples) symptoms respectively following *in vivo* drug administration. Overall the epitopes which were responsive to acute olanzapine exposure *ex vivo* comprised 27% (7/26) of the nodes altered by olanzapine *in vivo*. This represented a significant enrichment considering that only 0.6% of the total nodes assayed

(23/ 3762) were altered following *in vivo* olanzapine treatment. Conversely no *ex vivo* effects of olanzapine were observed in the SCZ T6 group.

4.2.6 VALIDATION OF PUTATIVE SCHIZOPHRENIA DRUG TARGET SPECIFICITIES USING A DIFFERENTIAL DIAGNOSIS STUDY DESIGN

We compared four neuropsychiatric disease cohorts, including drug-naive schizophrenia (SCZ, n=25), bipolar disorder (BD, n=25), major depressive disorder (MDD, n=25) and autism spectrum disorder (ASD, n=25), in parallel to healthy control samples collected at their respective clinical centres (n=25 each). Each cohort was matched for age, gender and BMI to their respective controls and also to the schizophrenia cohort. The only clinical parameters for which matching was not possible were age and BMI in the MDD cohort relative to SCZ **(Table 4.4)**. Comparison of the SCZ samples to controls allowed independent validation of the four prioritized drug targets from the antipsychotic intervention (AI) study to be tested (basal Akt1 and STAT3 (pY705) and ligand responses for thapsigargin at PLC-γ1 and forskolin at Src (pY418)). Furthermore exploration of these drug targets in the other neuropsychiatric disease cohorts allowed us to determine their specificity towards schizophrenia.

The experimental protocol used for the differential diagnosis (DD) study was similar to that described above for the AI study with three primary modifications. Firstly a subset of 14 ligands (and two vehicle controls) was used for incubation with PBMCs. These ligands included two additional cocktails, anti-BCR/FcR-XL/CD40L and anti-CD3/CD28-XL, which were not examined previously and provided enhanced activation of T and B cell receptors. **(Chapter 2: Table 2.1)**. Secondly a subset of 42 epitopes was used relative to the AI study. The epitopes spanned a wide variety of cell signalling pathways broadly including Akt/GSK-3β, PKA, PKC, MAPK, JAK/STAT, IL1R/TLR and TCR/BCR pathways **(Chapter 2: Table 2.3)**. Finally whereas the AI study examined cell signalling changes in T cells alone the DD study examined changes in subtypes of T cells, CD4+ (T helper) and CD4- (predominantly T cytotoxic-CD8+) cells, in addition to B cells. This produced a total of 1764 PBMC subtype-resolved cell signalling responses and 126 basal epitope expression levels measured in each PBMC donor **(Chapter 1: Fig. 1.4c)**.

4.2.7 VALIDATION OF ALTERED BASAL EPITOPE EXPRESSION IDENTIFIED IN THE AI STUDY

Both Akt1 and STAT3 (pY705), which were altered in schizophrenia and reversed by *in vivo* olanzapine treatment in T cells in the AI study, were also altered in the SCZ vs. CTRL comparison of the DD study **(Table 4.5)**. These alterations were further resolved in the DD study to CD4- (Akt1) and CD4+ (STAT3 (pY705)) T cell subtypes in addition to B cells (Akt1 and STAT3 (pY705) **(Fig. 4.10a-d)**. Notably the association of AKt1 to schizophrenia was several orders of magnitude more significant (p=0.0001 vs. p=0.0430) with a greater fold change (-1.60 vs. -1.06) in B cells relative to CD4- cells. While Akt1 was reduced in both the AI and DD studies, in the associated cell subtypes, STAT3 (pY705) was increased in the AI study (1.22 fold for T cells) and decreased in the DD study (-1.13 fold for CD4+ T cells and -1.08 fold for B cells). To expand the scope of analysis and take advantage of the power provided by increased sample numbers in the DD study we investigated possible associations to schizophrenia, or any of the other neuropsychiatric diseases, at all of the measured sites on Akt1 and STAT3 proteins. These included the activation sites pT308 and pS473 on Akt, and regulatory pS727 and non-phosphorylated total protein detection sites on STAT3. The only additional indication of altered basal epitope expression, at any of the Akt1 or STAT3 sites across the diseases, was decreased STAT3 (pS727) in CD4+ T cells for MDD. This confirms the specificity of changes in total Akt1 and STAT3 (pY705) epitopes to schizophrenia. However it also raises the possibility that schizophrenia and MDD converge mechanistically on STAT3, albeit at different epitopes.

4.2.8 EXPLORATION OF LIGAND RESPONSES AT EPITOPES WHICH WERE NORMALIZED BY ANTIPSYCHOTIC THERAPY IN THE AI STUDY

A total of ten ligand responses were significantly altered in PBMCs across the neuropsychiatric cohorts relative to CTRLs at the four normalized epitopes from the AI study (Akt1, STAT3 (pY705), PLC-γ1 and Src (pY418)). PLC-γ2 was also included in this comparison as it shares 99.9% sequence homology and similar biological activity to PLC-γ1(UniProt P19174 vs. P16885)[233,234] **(Table 4.6)**. Responses at these epitopes were all specific to schizophrenia with no significant interactions detected in any of the other disease groups. Responses at the PLC-γ1/2 isotypes accounted for 60% of the abnormal ligand responses in schizophrenia supporting the implication of altered PLC-γ signalling as the top drug target to emerge from the AI study. Interestingly the response to thapsigargin in T cell subsets was not detected at PLC-γ1, as in the AI study, but instead at PLC-γ2 **(Fig. 4.10e).** This can be attributed to the fact that the responses at PLC-γ1 for thapsigargin were likely saturated in the DD study due to a more potent batch of the stock ligand despite similar

concentrations. This is supported by the fact that the maximal group response in the AI study was 1.25 whereas in the DD study it was 1.46 across all the clinical groups, corresponding to the maximal plateau of the thapsigargin/ PLC-γ1 dose response curve **(Chapter 5 Fig. 5.2)**. However it is remarkable in the DD study that the only schizophrenia-associated response to thapsigargin, despite widespread activity at over 30% of the epitopes, was specifically at the close functional and structural homologue of PLC-γ1 (PLC-γ2). Furthermore the direction and magnitude of the fold changes at PLC-γ2 in DD study (-1.23 CTRL vs. -1.05 SCZ) closely matches those observed at PLC-γ1 in the AI study (-1.25 CTRL vs. -1.09 SCZ). Thus both studies suggest that schizophrenia patient PBMCs, relative to controls, show a blunted response to thapsigargin at PLC-γ isotypes. Moreover this attenuated response was specific to schizophrenia **(Fig. 4.11)**.

The attenuated PLC-γ1/2 response was also detected in the DD study using other ligands and in other cell types for example IL-10 in CD4+ and CD4- T cells and calyculin, PMA/ionomycin and anti-CD3/CD28-XL in B cells. Interestingly while the effect of these ligands relative to the vehicle in T cell subsets was to reduce PLC-γ isotype expression, in B cells they served to increase PLC-γ isotype expression, in both clinical groups **(Fig. 4.10f)**. However while the absolute directions of the ligand responses were different in T and B cell subsets the attenuation of response, independently of the direction, was a consistent feature of the schizophrenia PBMCs relative to controls **(Fig.4.10e,f)**. Depending on the cell subtype and ligand this attenuation in schizophrenia PBMCs ranged from -2.47 to -10.28 fold. This suggests that PLC-γ signalling is not simply increased or decreased in the disease state but instead is dysregulated across a varied response range. Interestingly one of the affected PLC-γ isotype responses in B cells was evoked by the T cell receptor (TCR) stimulant anti-CD3/CD28-XL. While it is impossible to rule out direct effects of this ligand cocktail on B cells, it is possible that the response represents communication between different cell subsets following the initial T cell stimulation. This is consistent with the rapid kinetic profile of cell signalling changes downstream of the T cell receptor (1-5 min) and also published reports of cell-to-cell communication with similar assay systems[135,137].

No interaction was detected between clinical group status and the response to forskolin at Src (pY418) in T cell subsets in the DD study. An interaction was detected at Src (pY418) in response to staurosporine in B cells. However it is likely that this was due to reduced basal epitope expression in schizophrenia, as was the case for the interaction in B cells of the response to calyculin at Akt1. In contrast while basal expression of STAT3 (pY705) in CD4+ T cells was reduced in schizophrenia (-1.13 fold, discussed earlier), the cells from this subset nevertheless showed an enhanced phosphorylation response (1.32 fold) specifically to the cognate STAT3 (pY705) inducer IL-6. Notably

levels of the STAT3 total protein were not changed in schizophrenia. This raises the intriguing possibility that while constitutive levels of STAT3 (pY705) phosphorylation may be reduced in schizophrenia patients they paradoxically show a hyper-sensitive response to proinflammatory cytokine stimulation.

	SCZ	CTRL	p SCZ-CTRL
N	12	12	na
Age (years)*	26.4 ± 6.2	27.0 ± 6.5	1.000
Gender (male/female)	12/0	12/0	na
BMI (kg/m^2)*	24.0 ± 4.8	23.5 ± 1.6	0.419
Ethnicity (white/other)**	8/4	11/1	0.317
Smoking (y/n)**	8/4	2/10	**0.036**
Cannabis (y/n)**	2/10	4/8	0.640
Alcohol (y/n)**	4/8	11/1	**0.009**
Blood pressure systolic (mmHg)*	131.3 ± 11.0	124.8 ± 14.0	0.203
Blood pressure diastolic (mmHg)*	78.4 ± 10.3	76.7 ± 9.2	0.908
Hip (cm)*	95.9 ± 9.5	92.5 ± 5.7	0.435
Waist (cm)*	86.8 ± 10.5	88.2 ± 5.6	0.339

Table 4.1 Demographic characteristics and matching of PBMC donors used in the antipsychotic intervention study. Matching was achieved for male drug-naive schizophrenia (SCZ) vs. male control (CTRL) samples for all demographic variables except smoking and alcohol consumption. Statistical tests included Mann-Whitney U test (*) and Fisher's exact test (**). Table shows mean values ± standard deviation.

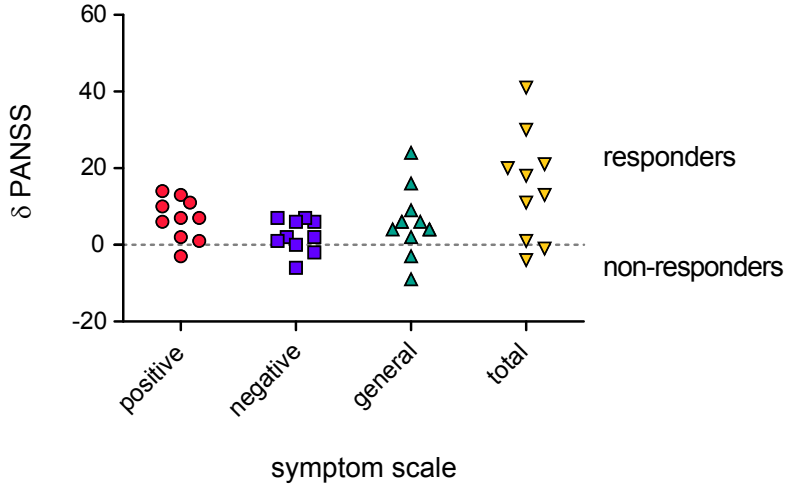

PANSS	positive	negative	general	total
Drug-naive	20.5± 5.3	22.1± 5.4	39.6± 6.0	82.2± 13.9
6 weeks olanzapine	13.7± 4.8	19.8± 5.1	33.7± 8.6	67.2± 15.4
δ	6.8± 5.5	2.3± 4.3	5.9± 9.2	15.0± 14.2

Figure 4.1 Clinical response to antipsychotic treatment with olanzapine in schizophrenia patients at 6 weeks. Ten out of the twelve schizophrenia patients were measured after 6 weeks of treatment (T6) with atypical antipsychotic medication olanzapine. 70% of these patients were classed as responders showing overall improvements in psychopathological symptoms, as measured by total Positive and Negative Syndrome Scale scores (δPANSSt), relative to before treatment initiation (T0). Concurrently symptom improvements for these patients were also observed for positive, negative and general PANSS subscales. Table shows mean values ± standard deviation. δPANSS refers to (PANSS T0-PANSS T6) with positive values indicating symptom improvement.

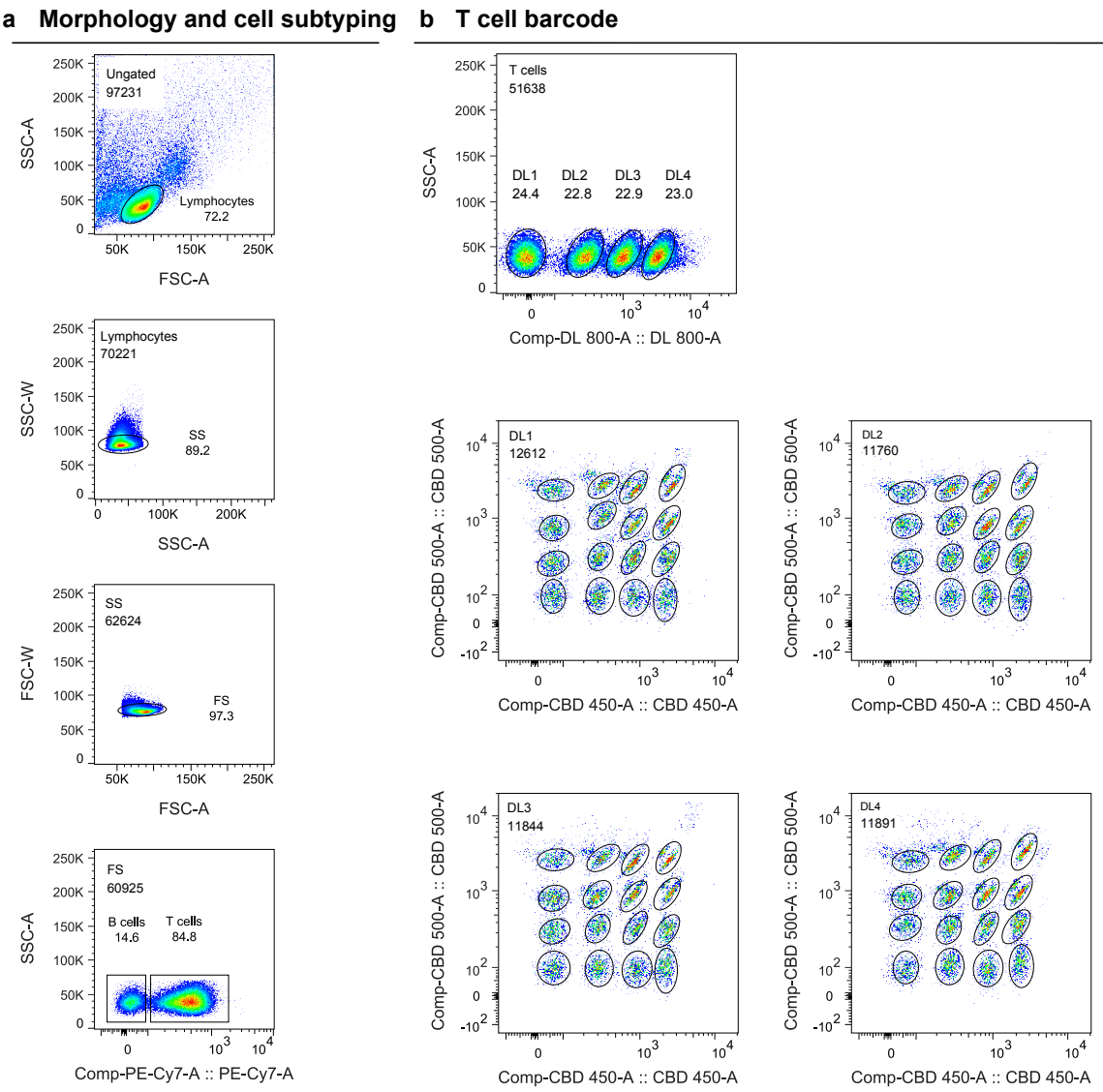

Figure 4.2 Gating strategies for functional analysis of 64 barcoded T cell populations. (a) Viable cells were gated (FSC-A vs. SSC-A), followed by single cell discrimination (SSC-A vs. SSC-W and FSC-A vs. FSC-W) and T vs. B lymphocyte cell subtyping using anti-CD3 PE-Cy7. **(b)** 64 populations, each corresponding to a different ligand or vehicle condition, were resolved within the T lymphocyte gate following fluorescent cell barcoding using DL 800, CBD 450 and CBD 500 dyes. T cells were gated first for DL 800 populations (DL 1-4) and subsequently for CBD 450 vs. CBD 500 populations (V1-16). (c) Within each barcoded T cell population functional analysis of intracellular signalling epitopes (n=66) was conducted across AF 488, PE and AF 647 channels. Induction of STAT3 (pY705) phosphorylation in response to 15 min stimulation with IL-6 50 ng/ml is shown as an example. Data represents one PBMC sample.

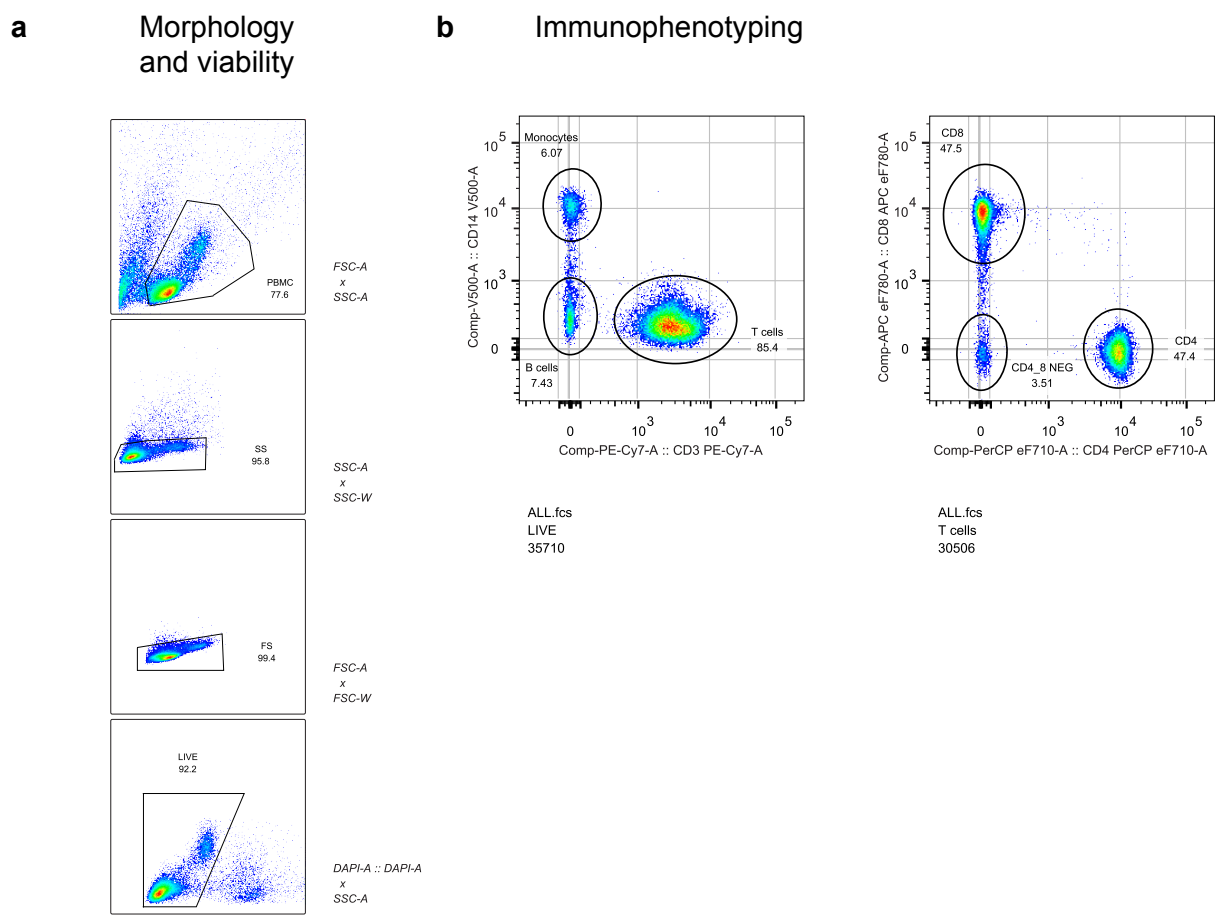

Figure 4.3 Gating strategy for cell viability and immunophenotyping. (a) PBMCs were gated (FSC-A vs. SSC-A), followed by single cell discrimination (SSC-A vs. SSC-W and FSC-A vs. FSC-W) and viability measurement (DAPI-A vs. SSC-A). **(b)** Within the live cell gate relative proportions of T cells, B cells and monocytes were quantified using anti-CD3 PE-Cy7 and anti-CD14 V500. Within the T cell gate relative proportions of CD4+, CD8+ and CD4-/CD8- cells were quantified using anti-CD4 PerCP-eF710 and anti-CD8 APC-eF780.

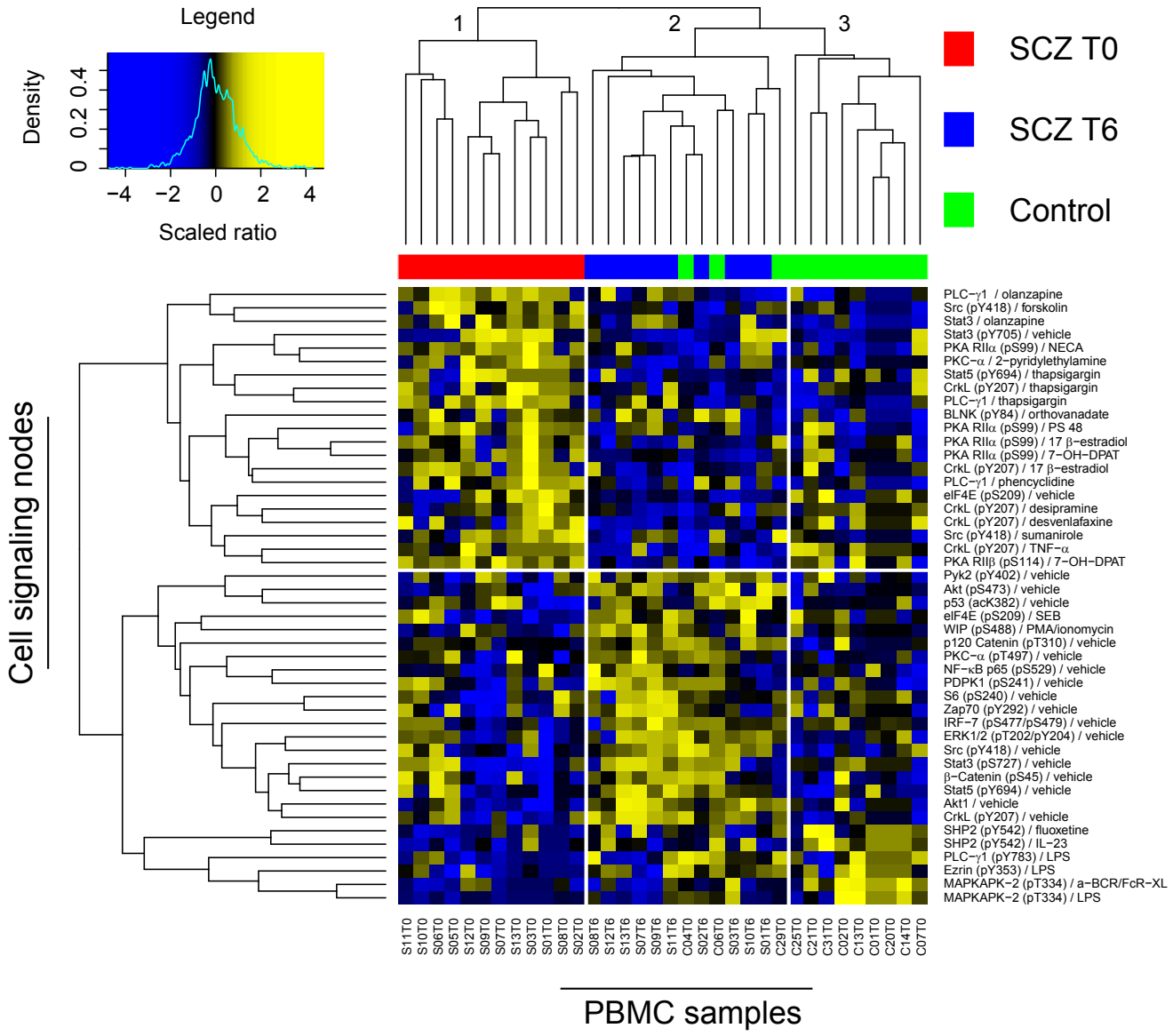

Figure 4.4 Hierarchical clustering of clinically associated T cell signalling nodes (AI study). Cell signalling nodes (defined as individual ligand-epitope combinations) (n=46) which displayed a significant interaction between clinical group status and either ligand response (n=27) or basal epitope expression (n=19), for either of the group comparisons (CTRL vs. SCZ T0 (drug-naive) or SCZ T0 (drug-naive) vs. T6 (olanzapine 6 weeks)), were subjected to unsupervised hierarchical clustering. Clustering of PBMC samples (x axis) revealed segregation of the three clinical groups (SCZ T0, SCZ T6 and CTRL) suggesting that the T cell signalling repertoire is indicative of clinical status. The position of the SCZ T6 group predominantly between the SCZ T0 and CTRL groups suggests a normalization of aberrant cell signalling following treatment with olanzapine. Clustering of cell signalling nodes (y axis) revealed that abnormal ligand responses primarily drive the separation of SCZ T0 samples from the rest while alterations in basal epitope expression primarily drive the separation of SCZ T6 samples. Legend reflects ratio of MFI of the ligand treatment to mean MFI of the vehicle treatment (for ligand responses) or ratio of mean MFI of the vehicle condition to mean MFI of the vehicle condition in the control group (for basal epitope expression) per condition and sample, scaled across all nodes. MFI - median fluorescence intensity. Total PBMC sample numbers in each group include CTRL (n=12), SCZ T0 (n=12) and SCZ T6 (n=10).

Reference vs. comparison group	Epitope	Ligand	PBMC subtype	n reference group (vehicle)	n reference group (ligand)	n comp. group (vehicle)	n comp. group (ligand)	Covariates	p interaction	p group	p ligand	Ligand response (reference group)	Ligand response (comp. group)	Response direction (across groups)	Response ratio (comp./ reference group)	Potentiation/ attenuation fold change (comp vs. reference)	Stain index	Node QC (%CV)	Spearman rho (node vs CD4:CD8 ratio)	Spearman p (node vs CD4:CD8 ratio)
CTRL vs T0	PLC-γ1	thapsigargin	T	9	9	11	10	age	0.001	0.020	2.55E-07	0.80	0.92	↓	0.38	-2.61	7.20	10.37	0.10	0.69
CTRL vs T0	PLC-γ1	phencyclidine	T	9	9	11	9	age	0.021	0.130	0.963	0.94	1.03	↑↓	-0.53	-0.53	7.20	5.53	0.31	0.22
CTRL vs T0	PKA RIIα (pS99)	NECA	T	10	10	11	10	-	0.035	0.527	0.002	0.80	0.94	↓	0.29	-3.43	65.40	13.00	0.39	0.09
CTRL vs T0	Src (pY418)	forskolin	T	11	9	12	10	-	0.050	0.112	0.018	1.03	1.11	↑	3.33	3.33	3.28	7.51	-0.29	0.22
T0 vs T6	WIP (pS488)	PMA/ionomycin	T	10	9	9	9	age	0.006	0.341	1.03E-19	8.55	9.95	↑	1.18	1.18	4.28	11.64	-0.11	0.66
T0 vs T6	CrkL (pY207)	thapsigargin	T	11	10	10	10	bmi	0.028	0.351	2.46E-11	0.83	0.73	↓	1.54	1.54	5.33	5.53	-0.34	0.15
T0 vs T6	Src (pY418)	forskolin	T	12	10	10	9	-	0.030	0.449	0.003	1.11	1.01	↑	0.07	-14.39	3.28	7.51	0.18	0.46
T0 vs T6	PKA RIIα (pS99)	17 β-estradiol	T	11	10	10	10	age	0.040	0.841	0.055	1.12	0.96	↑↓	-0.32	-0.32	65.40	8.14	-0.01	0.96
T0 vs T6	PLC-γ1	thapsigargin	T	11	10	10	10	-	0.041	0.892	4.85E-05	0.92	0.82	↓	2.33	2.33	7.20	10.37	0.13	0.59
T0 vs T6	Stat5 (pY694)	thapsigargin	T	9	9	10	10	age	0.047	0.440	0.018	1.00	0.93	↑↓	-271.95	-271.95	35.83	8.29	-0.39	0.10
T0 vs T6	PKA RIIα (pS99)	7-OH-DPAT	T	11	10	10	9	age	0.048	0.961	0.000	1.20	1.04	↑	0.22	-4.48	65.40	9.57	0.26	0.29
T0 vs T6	CrkL (pY207)	desipramine	T	11	10	10	10	bmi	0.049	0.169	0.003	1.11	1.05	↑	0.44	-2.26	5.33	7.68	0.15	0.52

Table 4.2 Altered ligand responses at T cell signalling epitopes in control vs. pre-treatment schizophrenia (CTRL vs. T0) and pre- vs. post-treatment schizophrenia (T0 vs. T6) comparisons (AI study). Shows ranked nodes (individual ligand-epitope combinations) for which there was a statistical interaction between group status and the response to ligand (*'p interaction'*<0.05, two-way ANOVA; terms in *'italics'* represent column headings) in either of the group comparisons CTRL vs. T0 (drug-naïve) or T0 (drug-naïve) vs. T6 (6 weeks of treatment with olanzapine). The clinical groups were assigned as *'reference'* or *'comparison'* for interpretation of subsequent columns. *'p group'* and *'p ligand'* refer to main effects of group status and ligand response, respectively, within the statistical model. The number of peripheral blood mononuclear cell (PBMC) samples (*'n'*) in each comparison group is cited in columns 5-8. *'Ligand response'* represents median MFI of the ligand treatment/median MFI of the vehicle treatment within the respective clinical group. Only nodes which displayed a significant *'ligand response'* (p<0.05, Wilcoxon rank-sum test; min. fold change 5%), after adjusting for background fluorescence, in either clinical group, are shown. *'Response direction'* refers to the increase (↑) or decrease (↓) in epitope expression evoked by the ligand. Arrows in both directions (↑↓) indicate responses in different directions in the reference and comparison groups. *'Response ratio'* represents (1-*'ligand response in the comparison group'*)/(1-*'ligand response in the reference group'*). For the majority of responses, this represents a means of expressing the relative potentiation or attenuation of response independently of its direction. This is expressed in the following column as *'potentiation/attenuation fold change'* (*'response ratio'* converted to -1/*'response ratio'* for response ratios between 0 and 1), whereby a positive value represents potentiation and a negative value represents attenuation or reversal of response. *'Stain index'* refers to the median MFI of the stained samples/median MFI of the unstained samples for the vehicle condition in the CTRL group. *'Node QC'* refers to the %CV in MFIs across the quality control (QC) samples from a single healthy PBMC donor run alongside the clinical samples on different days. The *'Spearman'* statistics reflect the correlation of each node MFI with the respective CD4:CD8 ratio in the immunophenotyping test. Total PBMC sample numbers in each group include CTRL (n=12), T0 (n=12) and T6 (n=10). MFI = median fluorescence intensity.

Reference vs. comparison group	Epitope	PBMC subtype	Node count (p group < 0.05)	Expression ratio (comp./ reference group)	Potentiation/ attenuation fold change (comp vs. reference)	Stain index	Node QC (%CV)	Spearman rho (node vs CD4:CD8 ratio)	Spearman p (node vs CD4:CD8 ratio)
CTRL vs T0	Stat3 (pY705)	T	34	1.22	1.22	6.57	20.00	0.35	0.12
CTRL vs T0	IRF-7 (pS477/S479)	T	26	0.95	-1.05	20.43	6.32	-0.54	0.01
CTRL vs T0	Akt1	T	21	0.93	-1.07	16.13	6.03	-0.49	0.03
T0 vs T6	Akt1	T	55	1.12	1.12	16.13	6.03	-0.25	0.28
T0 vs T6	Akt (pS473)	T	52	1.14	1.14	16.31	6.38	0.27	0.24
T0 vs T6	PDPK1 (pS241)	T	52	1.12	1.12	19.85	16.06	-0.32	0.16
T0 vs T6	Stat3 (pS727)	T	51	1.21	1.21	7.08	9.70	-0.06	0.79
T0 vs T6	p120 Catenin (pT310)	T	48	1.06	1.06	6.39	4.57	-0.12	0.65
T0 vs T6	CrkL (pY207)	T	47	1.07	1.07	5.33	3.40	-0.07	0.76
T0 vs T6	ERK1/2 (pT202/pY204)	T	44	1.05	1.05	34.73	4.19	-0.31	0.16
T0 vs T6	Stat5 (pY694)	T	41	1.05	1.05	35.83	6.42	-0.25	0.31
T0 vs T6	Stat3 (pY705)	T	38	0.86	-1.16	6.57	20.00	0.12	0.61
T0 vs T6	NF-κB p65 (pS529)	T	36	1.04	1.04	20.53	10.22	0.05	0.82
T0 vs T6	Pyk2 (pY402)	T	34	1.07	1.07	3.22	6.19	-0.05	0.84
T0 vs T6	Src (pY418)	T	34	1.07	1.07	3.28	4.33	-0.32	0.15
T0 vs T6	PKC-α (pT497)	T	28	1.04	1.04	20.09	1.61	0.04	0.88
T0 vs T6	β-Catenin (pS45)	T	25	1.06	1.06	44.61	8.11	-0.36	0.13
T0 vs T6	p53 (acK382)	T	20	1.01	1.01	19.59	3.98	-0.05	0.85

Table 4.3 Altered basal expression of T cell signalling epitopes in control vs. pre-treatment schizophrenia (CTRL vs. T0) and pre- vs. post-treatment schizophrenia (T0 vs. T6) comparisons (AI study). Shows ranked epitopes for which over 30% of the nodes (individual ligand-epitope combinations) displayed an association between clinical group status and epitope expression (p for the main effect of the group<0.05, two-way ANOVA), independently of ligand activity, in either of the group comparisons CTRL vs. T0 (drug-naïve) or T0 (drug-naïve) vs. T6 (6 weeks of treatment with olanzapine). The number of nodes, out of a total of 56 for each epitope, which satisfied these criteria is cited in the *'node count (p group <0.05)'* column (terms in *'italics'* represent column headings). In both comparisons (CTRL vs. T0 and T0 vs. T6), the clinical groups were assigned as *'reference'* or *'comparison'* for interpretation of subsequent columns. The *'expression ratio'* refers to the median epitope MFI for the vehicle condition in the comparison vs. reference groups. The *'potentiation/attenuation fold change'* is the *'expression ratio'* converted to -1/*'expression ratio'* for ratios below 1, whereby a positive fold change represents an increase and a negative fold change represents a decrease in epitope expression. *'Stain index'* refers to the median MFI of the stained samples/median MFI of the unstained samples for the vehicle condition in the CTRL group. *'Node QC'* refers to the node %CV in MFIs across the quality control (QC) samples from a single healthy peripheral blood mononuclear cell (PBMC) donor run alongside the clinical samples on different days. The *'Spearman'* statistics reflect the correlation of each node MFI with the respective CD4:CD8 ratio in the immunophenotyping test. Total PBMC sample numbers in each group include CTRL (n=12), T0 (n=12) and T6 (n=10). MFI = median fluorescence intensity.

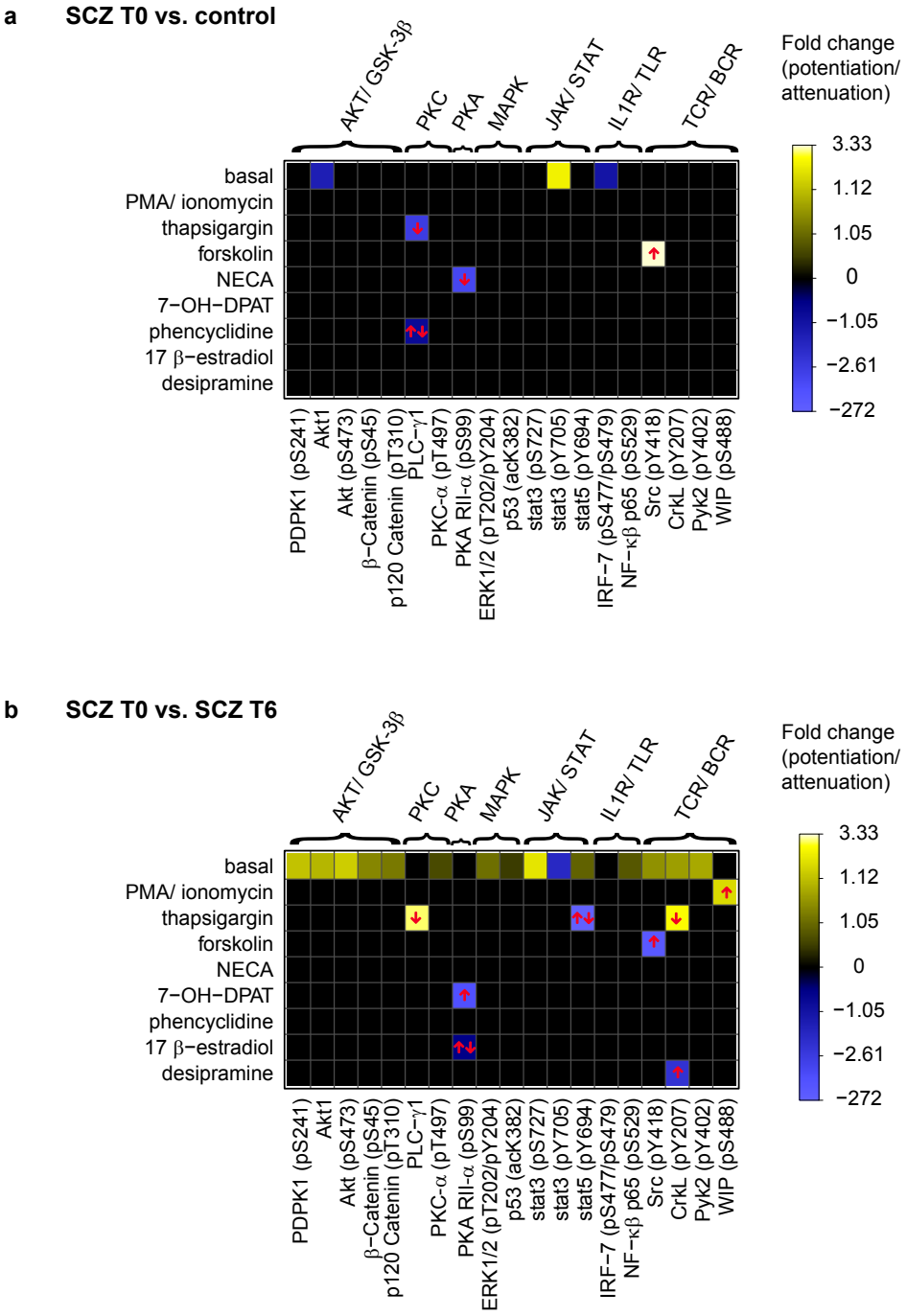

Figure 4.5 Altered T cell signalling nodes in SCZ T0 vs. CTRL and SCZ T0 vs. T6 comparisons (AI study). Shows significant differences between clinical groups, in either SCZ T0 (drug-naive) vs. CTRL **(a)** or SCZ T0 (drug-naive) vs. T6 (olanzapine 6 weeks) **(b)** comparisons, for cell signalling epitope expression under basal conditions or in response to ligand exposure. Significantly altered basal epitopes were defined as those in which over 30% of the nodes displayed an association between clinical group status and epitope expression, independently of ligand activity (*'node count (p group<0.05)'*). The vehicle condition is used for representation of altered basal epitopes. Significantly altered ligand responses were defined as nodes for which there was a statistical interaction between clinical group status and the response to ligand (*'p interaction'*<0.05). Only nodes which displayed a significant *'ligand response'*, defined as median (MFI of the ligand treatment/ MFI of the vehicle treatment) (p<0.05, fold change >5%) after adjusting for background fluorescence, in either clinical group are shown. The arrows denote the direction of the *'ligand response'* relative to vehicle (↓↑). A single arrow represents a similar ligand response direction in both clinical groups, while double arrows represent different directions of ligand response in each clinical group. Node is defined as a single ligand-epitope combination. The legend shows relative *'potentiation (yellow) or attenuation (blue) fold change'* of basal epitope expression or ligand response. Terms in *'italics'* represent column headings in **Tables 4.2 and 4.3** for referencing of absolute values. Total PBMC sample numbers in each group include CTRL (n=12), SCZ T0 (n=12) and SCZ T6 (n=10). MFI = median fluorescence intensity.

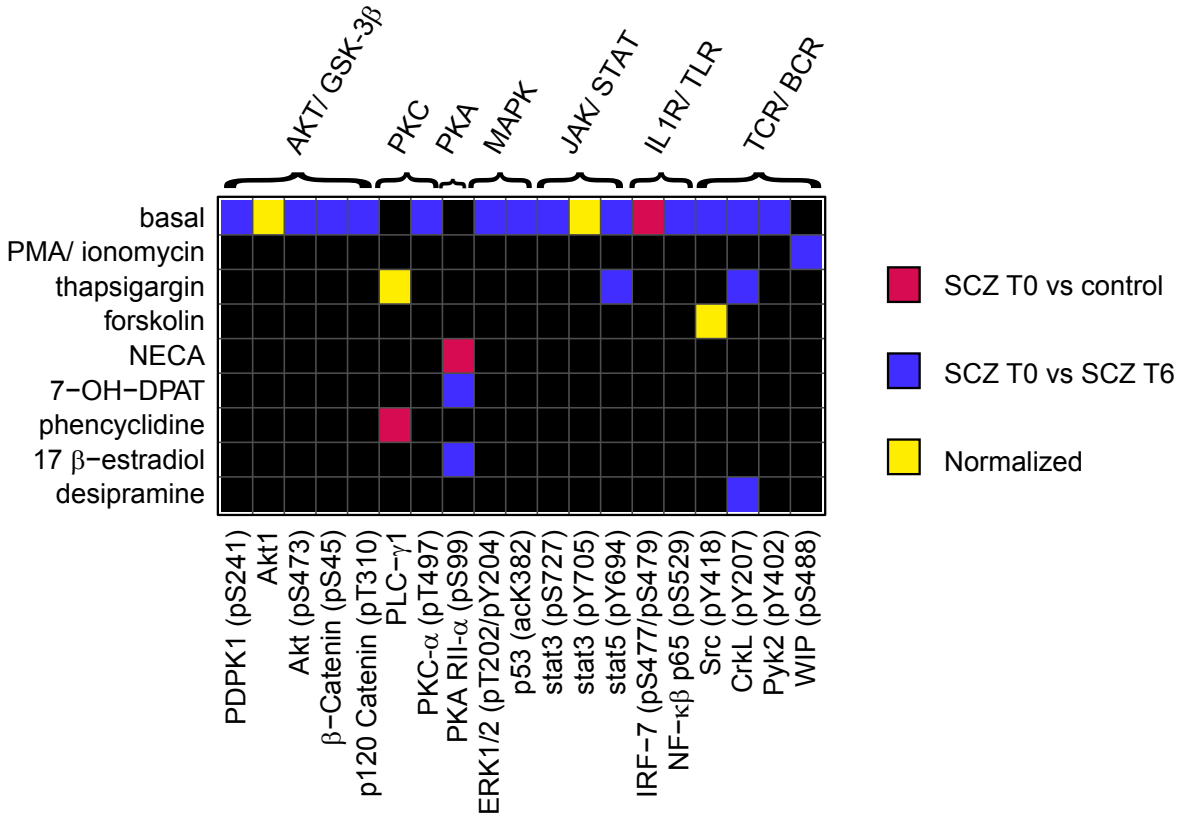

Figure 4.6 Overlay of T cell signalling nodes altered in schizophrenia and following clinical antipsychotic therapy (AI study). Overlay of data from **Fig. 6a and b**. Shows significant differences between clinical groups for cell signalling epitope expression under basal conditions or in response to ligand exposure (as defined in **Fig. 4.5a, b)**. Nodes (individual ligand-epitope combinations) altered in the SCZ T0 (drug-naive) vs. CTRL comparison are pink and nodes altered in the SCZ T0 (drug-naive) vs. T6 (olanzapine 6 weeks) comparison are blue. Nodes altered in both comparisons in opposite directions (i.e. 'reversed') are yellow. These yellow nodes represent putative normalization of schizophrenia cell signalling alterations and form the basis for drug target selection. Total PBMC sample numbers in each group include CTRL (n=12), SCZ T0 (n=12) and SCZ T6 (n=10).

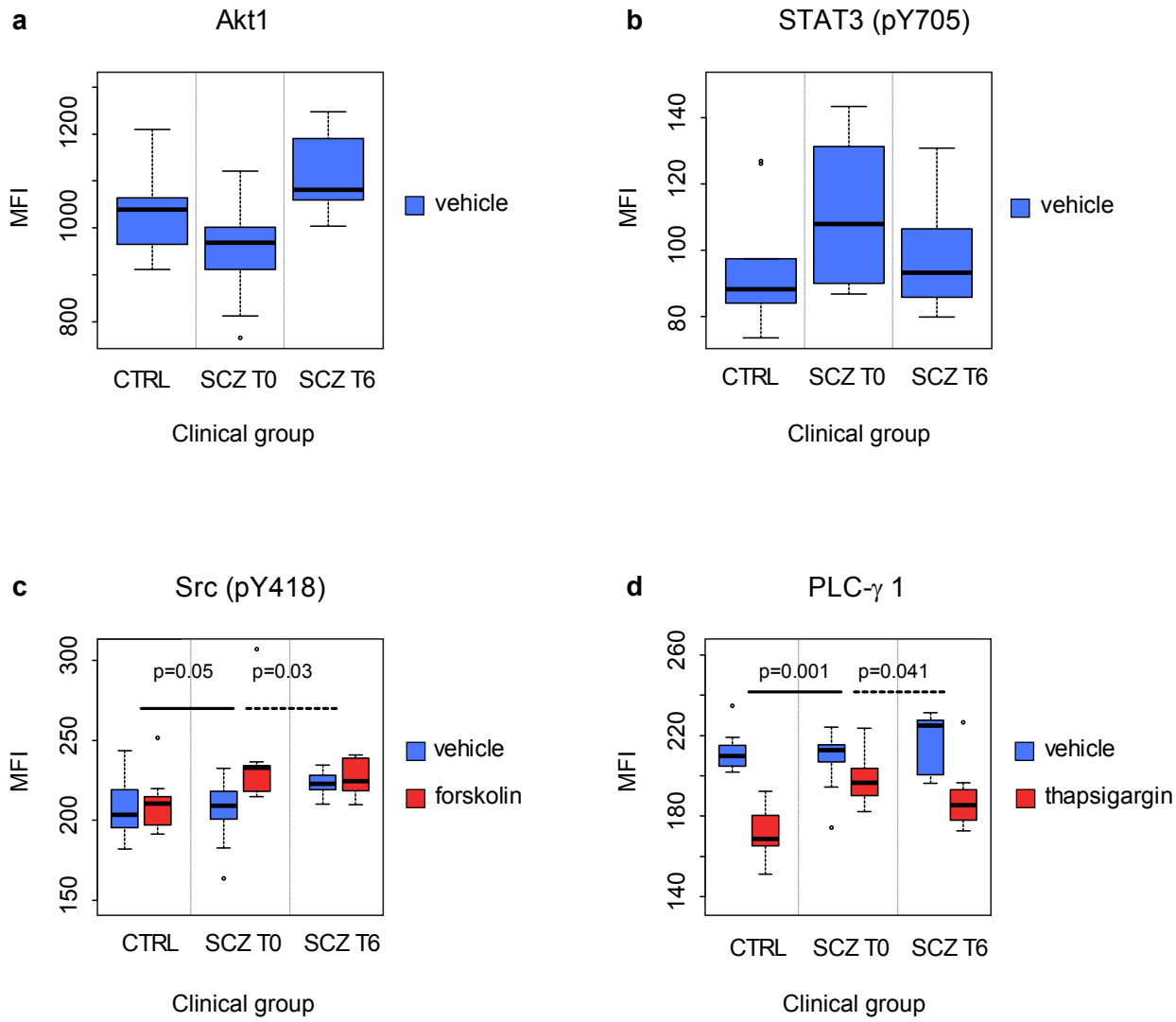

Figure 4.7 T cell signalling nodes altered in schizophrenia and normalized following clinical antipsychotic therapy (AI study). Shows the four T cell signalling nodes identified in **Fig. 4.6** as 'normalized' (i.e. altered in the SCZ T0 (drug-naive) vs. CTRL comparison and subsequently reversed in SCZ T0 (drug-naive) vs. T6 (olanzapine 6 weeks) comparison). Normalized nodes include basal epitope expression **(a, b)** and ligand responses **(c, d)** as defined for **Fig. 4.5**. The vehicle condition is used for representation of basal epitope expression. Statistical interactions between ligand responses and clinical group status (p) are shown for SCZ T0 (drug-naive) vs. CTRL and SCZ T0 (drug-naive) vs. T6 (olanzapine 6 weeks) comparisons. Total PBMC sample numbers in each group include CTRL (n=12), SCZ T0 (n=12) and SCZ T6 (n=10). MFI = median fluorescence intensity.

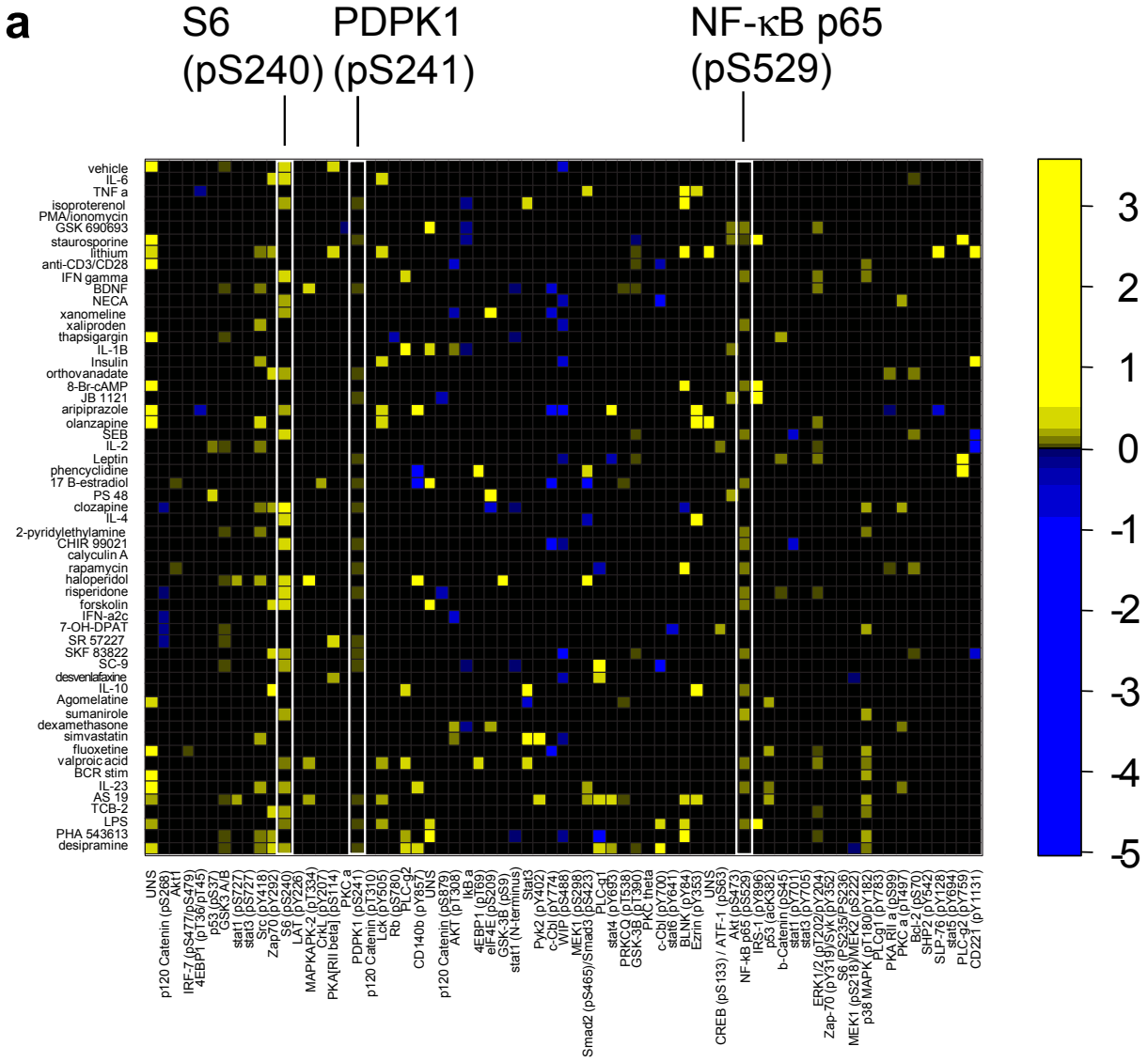

Figure 4.8 Correlation of changes in T cell signalling nodes to changes in schizophrenia symptom subscales following clinical antipsychotic therapy *in vivo* (AI study). Shows regression analysis of changes in median fluorescence intensity (MFI) for T cell signalling nodes (individual ligand-epitope combinations) (δNode) with changes in positive **(a)** and negative **(b)** syndrome subscales (δPANSSp and δPANSSn respectively) following 6 week olanzapine treatment. Legend represents regression estimate. Only nodes which showed a significant ($p<0.05$) correlation between δNode and δPANSSp or δPANSSn are coloured. Epitopes (x axis) for which over 25% of nodes showed a significant correlation are marked with white vertical bands and labelled above. Total PBMC sample numbers in each group include CTRL (n=12), SCZ T0 (n=12) and SCZ T6 (n=10). Continued overleaf.

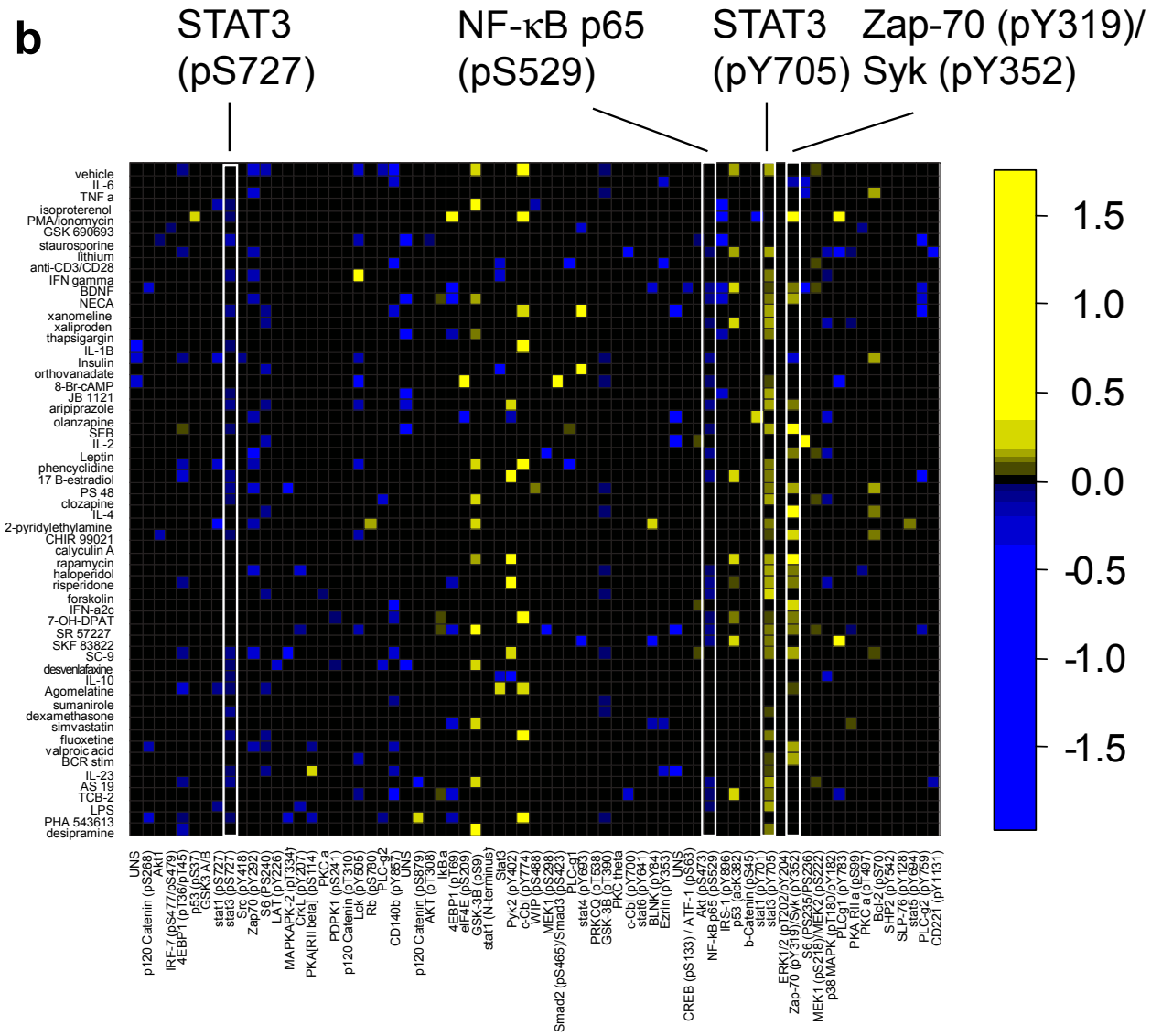

Figure 4.8 Correlation of changes in T cell signalling nodes to changes in schizophrenia symptom sub-scales following clinical antipsychotic therapy *in vivo* (AI study) continued.

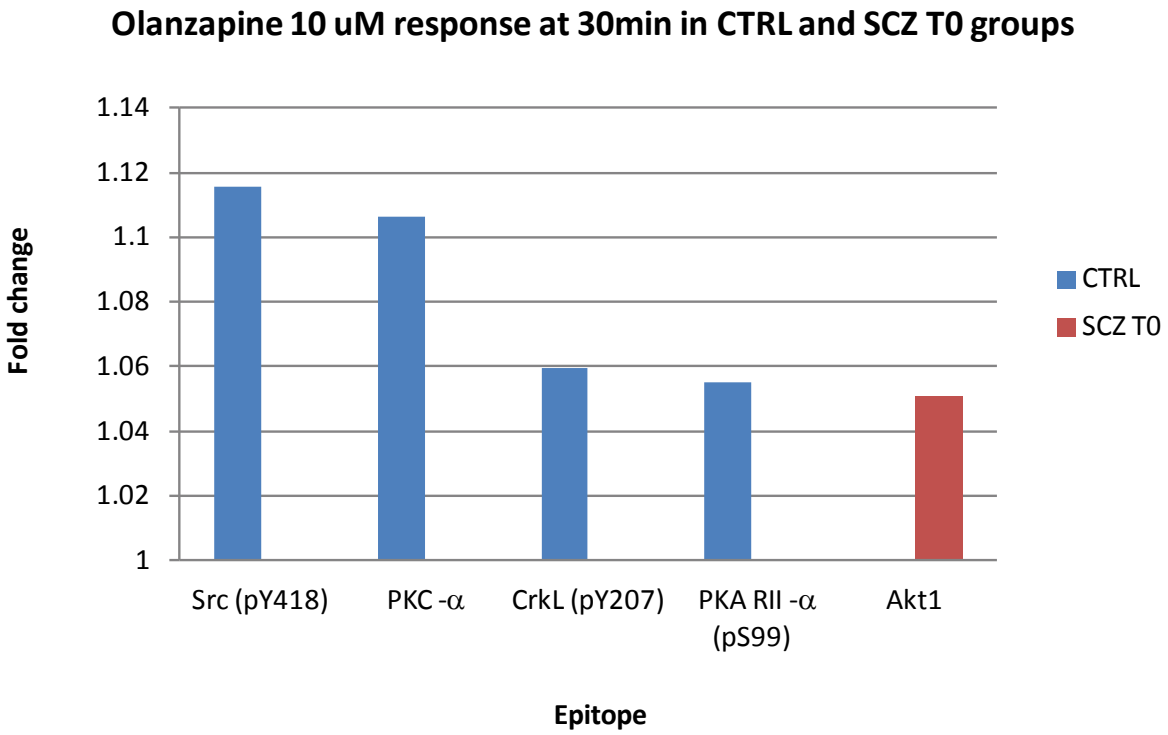

Figure 4.9 T cell signalling epitopes respond to olanzapine after 30 min incubation *ex vivo* (AI study). Shows T cell signalling epitopes which displayed a significant response, defined as median MFI of the ligand treatment/ median MFI of the vehicle treatment ($p<0.05$, fold change >5%) after adjusting for background fluorescence, to 30 min incubation with olanzapine 10 µM in either CTRL or SCZ T0 groups. No responses were detected to olanzapine in the SCZ T6 group. Total PBMC sample numbers in each group include CTRL (n=12), SCZ T0 (n=12) and SCZ T6 (n=10). MFI = median fluorescence intensity.

	SCZ			BD				ASD				MDD			
	SCZ	**CTRL**	**$p_{SCZ-CTRL}$**	**BD**	**CTRL**	**$p_{BD-CTRL}$**	**p_{BD-SCZ}**	**ASD**	**CTRL**	**$p_{ASD-CTRL}$**	**$p_{ASD-SCZ}$**	**MDD**	**CTRL**	**$p_{MDD-CTRL}$**	**$p_{MDD-SCZ}$**
N	25	25	na	25 (12/13)	25 (10/15)	na	na	25	25	na	na	25	25	na	na
Age (years)*	27.3 ± 6.7	30.4 ± 7.8	0.116	32.6 ± 9.5	33.2 ± 8.2	0.712	0.050	31.5 ± 8.3	27.8 ± 6.3	0.127	0.071	40.5 ± 10.0	41.6 ± 12.2	0.771	**<0.001**
Gender (male/female)**	17/8	12/13	0.252	12/13	11/14	1.000	0.252	14/11	14/11	1.000	0.561	12/13	12/13	1.000	0.252
BMI (kg/m^2)*	22.9 ± 6.4[+]	23.8 ± 3.5	0.108	24.2 ± 4.3	24.3 ± 4.2	0.992	0.132	23.9 ± 4.4	22.2 ± 3.3	0.342	0.223	26.6 ± 4.5	25.6 ± 3.9	0.587	**0.002**

Table 4.4 Demographic characteristics and matching of PBMC donors used in the differential diagnosis (DD) study. Each cohort was matched for age, gender and BMI to their respective controls and also to the schizophrenia cohort. The only clinical parameters for which matching was not possible were age and BMI in the MDD cohort relative to SCZ (bold). Statistical tests included Mann-Whitney U test (*) and Fisher's exact test (**). Table shows mean values ± standard deviation.

Reference vs. comparison group	Epitope	PBMC subtype	n CTRL (vehicle)	n disease (vehicle)	Covariates	p group	Expression ratio (disease/ CTRL)	Potentiation/ attenuation fold change (comp vs. reference)	Stain index	Node QC (%CV)
CTRL vs. SCZ	Akt1	B	21	23	-	1.00E-04	0.62	-1.60	11.04	10.22
CTRL vs. SCZ	Akt1	T CD4-	23	23	gender	0.043	0.94	-1.06	12.91	6.21
CTRL vs. SCZ	STAT3 (pY705)	T CD4+	23	23	age	0.029	0.88	-1.13	22.11	18.43
CTRL vs. SCZ	STAT3 (pY705)	B	20	23	-	0.038	0.93	-1.08	18.02	13.69
CTRL vs. MDD	STAT3 (pS727)	T CD4+	22	24	-	0.040	0.92	-1.09	10.43	3.98

Table 4.5 Altered basal expression of selected cell signalling epitopes in PBMC subtypes across four neuropsychiatric diseases (DD study). Shows epitopes with a significant association to group status (*'p group'* <0.05, two-way ANOVA; terms in *'italics'* represent column headings) in the vehicle condition for any of the diagnostic group comparisons (SCZ (drug-naive) vs. CTRL, BD vs. CTRL, MDD vs. CTRL and ASD vs. CTRL) in any of the PBMC subtypes (CD4+ T cells, CD4- T cells and B cells). Epitopes assessed included Akt1 total, Akt (pS473), Akt (pT308), STAT3 total, STAT3 (pY705) and STAT3 (pS727) and are grouped by identity. The clinical groups were assigned as *'reference'* or *'comparison'* for interpretation of subsequent columns. The number of PBMC samples (*'n'*) in each comparison group is cited in columns 4-5 The *'expression ratio'* refers to the median epitope MFI for the vehicle condition in the comparison/ reference groups. The *'potentiation/ attenuation fold change'* is (-1/ *'expression ratio'*), whereby a positive fold change represents an increase and a negative fold change represents a decrease in epitope expression. *'Stain index'* refers to the median (MFI of the stained samples/ MFI of the unstained samples) for the vehicle condition in the CTRL group. *'Node QC'* refers to the %CV in MFIs across the QC samples from a single healthy PBMC donor run alongside the clinical samples on different days. Total PBMC sample numbers in each group include CTRL (n=25 per disease), SCZ (n=25), BD (n=25), MDD (n=25) and ASD (n=25). MFI = median fluorescence intensity.

Reference vs. comparison group	Epitope	Ligand	PBMC subtype	n CTRL (vehicle)	n CTRL (ligand)	n disease (vehicle)	n disease (ligand)	Covariates	p interaction	p group	p ligand	Ligand response (CTRL)	Ligand response (SCZ)	Response direction (across groups)	Response ratio (SCZ/ CTRL)	Potentiation/ attenuation fold change (comp vs. reference)	Stain index	Node QC (%CV)
CTRL vs SCZ	Akt1	calyculin A	B	21	18	23	18	-	0.025	1.00E-04	2.28E-10	0.59	0.79	↓	0.52	-1.93	11.04	10.04
CTRL vs SCZ	PLC-γ1	calyculin A	B	22	20	22	20	-	0.037	0.741	2.47E-04	1.22	1.09	↑	0.41	-2.47	1.95	15.13
CTRL vs SCZ	PLC-γ1	PMA/ionomycin	B	22	20	22	20	-	0.013	0.530	0.004	1.18	1.02	↑	0.10	-10.28	1.95	11.88
CTRL vs SCZ	PLC-γ2	anti-CD3/CD28-XL	B	21	20	23	22	-	0.037	0.096	0.004	1.27	1.11	↑	0.41	-2.41	2.88	20.95
CTRL vs SCZ	PLC-γ2	IL-10	T CD4+	23	23	23	23	age	0.033	0.822	5.37E-06	0.66	0.86	↓	0.41	-2.46	1.54	23.35
CTRL vs SCZ	PLC-γ2	IL-10	T CD4-	23	23	23	23	-	0.044	0.484	6.16E-07	0.70	0.94	↓	0.19	-5.28	1.52	18.71
CTRL vs SCZ	PLC-γ2	thapsigargin	T CD4+	23	23	23	23	-	0.035	0.728	0.073	0.81	0.95	↓	0.29	-3.41	1.54	16.34
CTRL vs SCZ	Src (pY418)	staurosporine	B	21	21	22	23	-	0.012	0.059	3.95E-36	0.43	0.45	↓	0.98	-1.03	2.67	12.34
CTRL vs SCZ	STAT3 (pY705)	IL-6	T CD4+	23	23	23	23	-	0.047	0.588	8.45E-35	7.31	9.34	↑	1.32	1.32	22.11	10.35
CTRL vs SCZ	STAT3 (pY705)	staurosporine	T CD4+	23	23	23	23	age	0.038	0.200	5.26E-10	0.62	0.73	↓	0.70	-1.43	22.11	16.09

Table 4.6 Altered ligand responses at selected cell signalling epitopes in PBMC subtypes across four neuropsychiatric diseases (DD study). Shows ranked nodes (individual ligand-epitope combinations) for which there was a statistical interaction between group status and the response to ligand *('p interaction'*<0.05, two-way ANOVA; terms in *'italics'* represent column headings) for any of the diagnostic group comparisons (SCZ (drug-naive) vs. CTRL, BD vs. CTRL, MDD vs. CTRL and ASD vs. CTRL) in any of the PBMC subtypes (CD4+ T cells, CD4- T cells and B cells). Epitopes assessed included Akt1, PLC–γ1, PLC–γ2, Src (pY418) and STAT3 (pY705). The clinical groups were assigned as *'reference'* or *'comparison'* for interpretation of subsequent columns. *'p group'* and *'p ligand'* refer to main effects of group status and ligand response respectively within the statistical model. The number of PBMC samples (*'n'*) in each comparison group is cited in columns 5-8. '*Ligand response'* represents median (MFI of the ligand treatment/ MFI of the vehicle treatment) within the respective clinical groups. Only nodes which displayed a significant *'ligand response'* (p<0.05, fold change >5%) after adjusting for background fluorescence, in either clinical group are shown. *'Response direction'* refers to the increase (↑) or decrease (↓) in epitope expression evoked by the ligand. *'Response ratio'* represents (1-*'ligand response in the comparison group'*)/ (1-*'ligand response in the reference group'*). For the majority of responses this represents a means of expressing the relative potentiation or attenuation of response independently of its direction. This is expressed in the following column as *'potentiation/ attenuation fold change'* (-1/ *'response ratio'*), whereby a positive fold change represents potentiation and a negative fold change represents attenuation of response. *'Stain index'* refers to the median (MFI of the stained samples/ MFI of the unstained samples) for the vehicle condition in the CTRL group. *'Node QC'* refers to the %CV in MFIs across the QC samples from a single healthy PBMC donor run alongside the clinical samples on different days. Total PBMC sample numbers in each group include CTRL (n=25 per disease), SCZ (n=25), BD (n=25), MDD (n=25) and ASD (n=25). MFI = median fluorescence intensity.

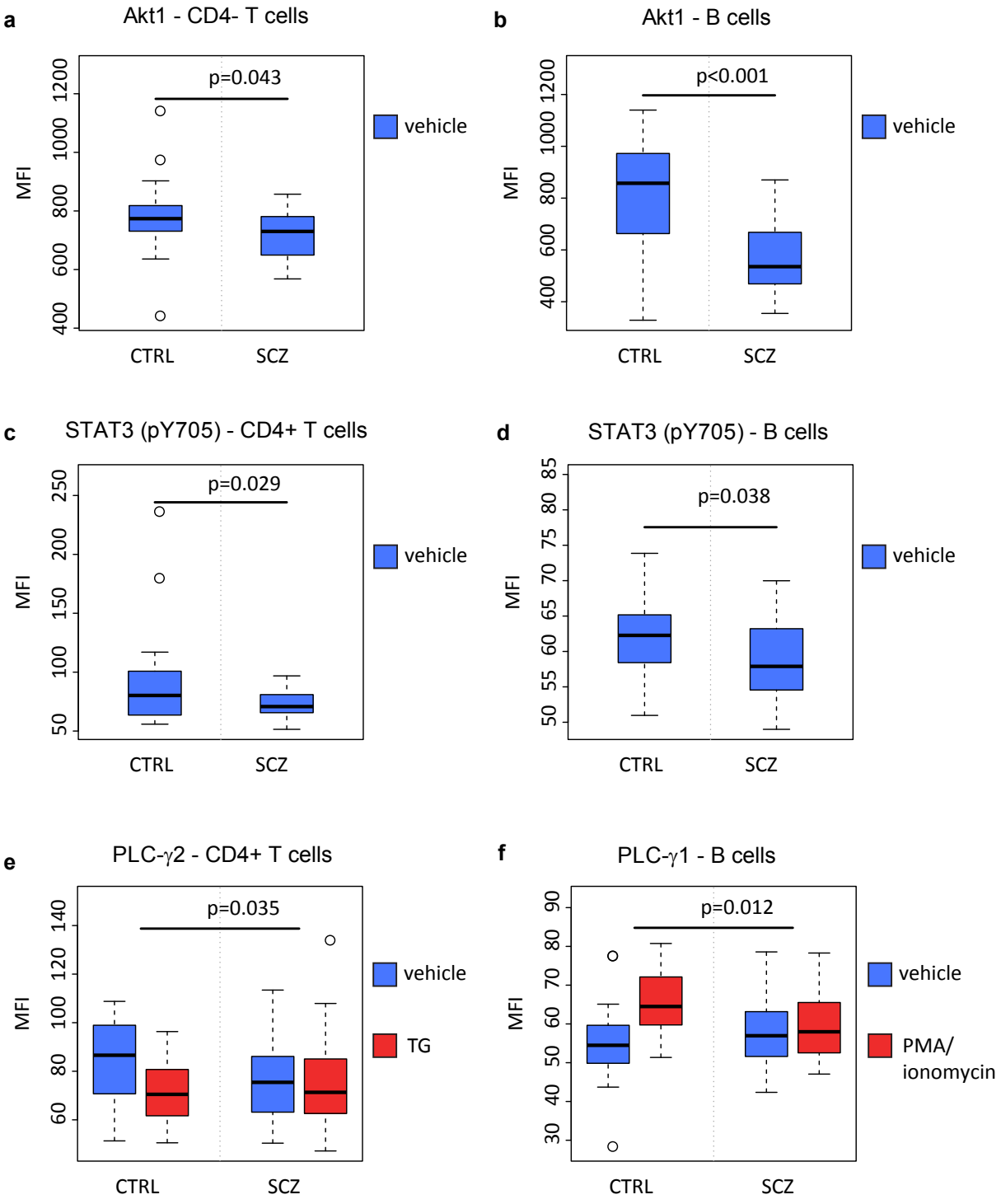

Figure 4.10 Validation of normalization nodes derived from the AI study in an independent cohort of drug-naive schizophrenia patients and controls (DD study). Shows PBMC subtypes (CD4+ T cells, CD4- T cells or B cells) for which basal (vehicle condition) epitope expression of Akt1 **(a, b)** or STAT3 (pY705) **(c, d)** was significantly (*'p group'* <0.05) altered in drug-naive SCZ vs. CTRL. Significantly altered responses (*'p interaction'*) to calcium flux ligands in drug-naive SCZ relative to CTRL PBMC subtypes, including thapsigargin (TG) at PLC–γ2 in CD4+ T cells **(e)** and PMA/ ionomycin at PLC–γ1 in B cells **(f)**. Terms in *'italics'* represent column headings in **Tables 4.5 and 4.6** for referencing of absolute values. Total PBMC sample numbers in each group include CTRL (n=25) and SCZ (n=25). MFI = median fluorescence intensity.

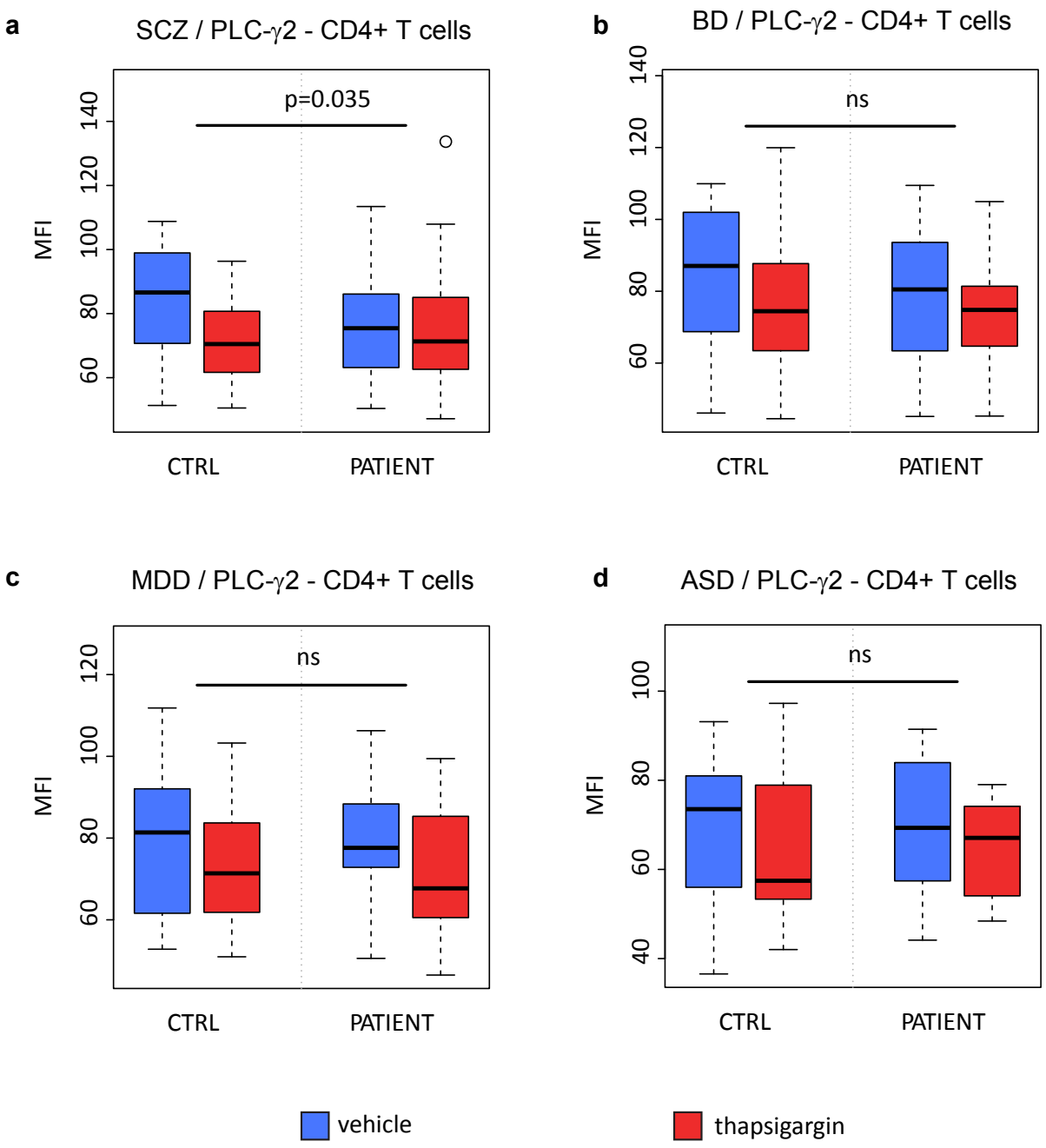

Figure 4.11 Altered response to thapsigargin at PLC-γ2 in CD4+ T cells is specific to schizophrenia relative to other major neuropsychiatric disorders. Shows response to thapsigargin at PLC–γ2 in CD4+ T cells in SCZ (drug-naive) **(a)**, BD **(b)**, MDD **(c)** and ASD **(d)** patient cohorts relative to CTRL. A significantly altered response *('p interaction')* was observed only for SCZ. Absolute values provided in **Table 4.6**. Total PBMC sample numbers in each group include CTRL (n=25) and PATIENT (n=25). MFI = median fluorescence intensity.

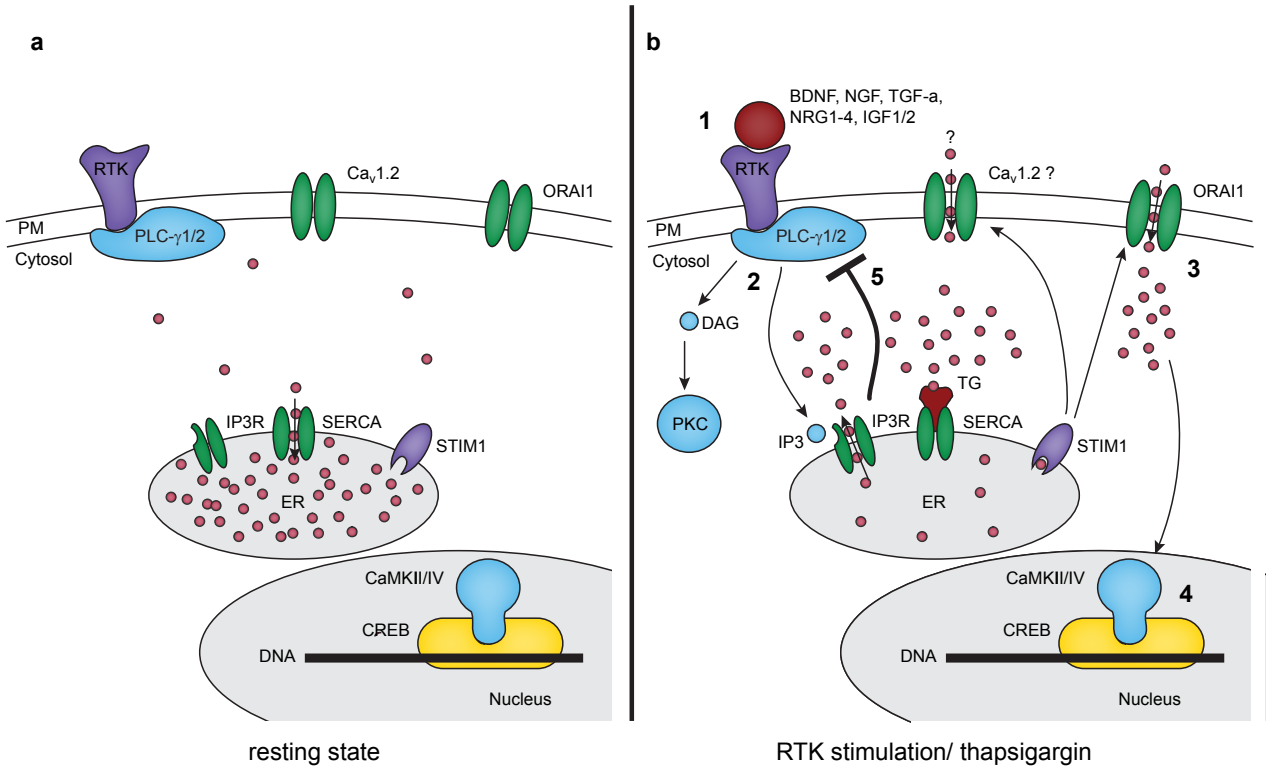

Figure 14.12 Impaired regulatory response at PLC-γ1/2 to calcium release from the endoplasmic reticulum in schizophrenia. Figure shows proposed mechanism of action in neuronal cells based on the altered response to thapsigargin (TG) at phospholipase C γ1/2 (PLC-γ1/2) in T cells from schizophrenia patients and controls in the AI and DD studies. **(a)** In resting neurons low calcium concentration is maintained in the cytosol (~100nM), relative to the endoplasmic reticulum (ER ~ 0.5 mM) and extracellular space (~1 mM), by active calcium transporter sarco-endoplasmic reticulum Ca^{2+}-ATPase (SERCA). **(b) 1)** Receptor tyrosine kinase (RTK) ligand activation by cytokines, hormones or growth factors (selected examples shown) activates PLC-γ1/2. **2)** PLC-γ1/2 catalyzes the degradation of phosphatidylinositol 4,5-biphosphate into intracellular second messengers inositol 1,4,5-triphosphate (IP3) and 1,2 diacylglycerol (DAG), which induce the release of calcium stored in the endoplasmic reticulum (ER), via IP3 receptors (IP3Rs), and the activation of protein kinase C (PKC) respectively. Analogous depletion of ER calcium stores is achieved by SERCA blockade using TG 1 µM. **3)** Reduction of ER calcium is sensed by stromal interaction molecule 1 (STIM1) which subsequently promotes the influx of extracellular calcium via the ORAI1 plasma membrane channel. **4)** Elevated cytosolic calcium activates gene transcription via Ca^{2+}/calmodulin-dependent protein kinase II/IV (CaMKII/IV) and transcription factor cAMP response element-binding protein (CREB). **5)** Elevated cytosolic calcium causes the downregulation or sequestration of PLC-γ1/2 to desensitize RTK signal transduction. In schizophrenia either the initial calcium flux from the ER or the negative feedback regulation of PLC-γ1/2 is proposed to be disrupted and restored by clinical treatment with olanzapine 6 weeks **(Fig. 4.7d)**. Voltage-gated calcium channels (e.g. L-type Ca_V 1.2) are included based on the association of calcium channel subunits (e.g. CACNA1C, CACNB2 and CACNA1I) to schizophrenia in GWAS studies and their role in neuronal excitation-transcription coupling. Their contribution to the altered TG-PLC-γ1/2 response and reported interactions with STIM1 remain to be defined (?).

4.3 DISCUSSION

The discussion will focus specifically on the four cell signalling nodes which were altered in T cells from schizophrenia patients relative to healthy controls, and subsequently normalized by clinical antipsychotic therapy with olanzapine in the AI study **(Fig. 4.6 and 4.7).** These include the altered responses to thapsigargin at PLC-γ1and to forskolin at Src (pY418) and altered basal expression of Akt1 and STAT3 (pY705). Firstly we will assess the altered response to thapsigargin at PLC-γ1 as the primary novel drug target to emerge from the clinical screening phase of the project and the substrate of the subsequent drug discovery phase. Subsequently we will consider altered basal expression of Akt1, as a positive control for previously reported cell signalling abnormalities in schizophrenia PBMCs, and STAT3 (pY705) as a potentially novel mediator of inflammatory activation in the brain and periphery. Next we will consider Src (pY418) as a potential denominator of mechanistic interaction between these targets. Finally we will assess whether cell signalling changes induced by olanzapine during acute *ex vivo* exposure are relevant to its clinical effects *in vivo.* In assessing these findings we seek to answer several pertinent questions. Firstly are these cell signalling changes plausibly related to known pathogenic mechanisms or genetic risk factors within the CNS in schizophrenia? Secondly are the responses preferentially associated with specific symptom subscales (e.g. positive or negative symptoms) or side effect profiles? Thirdly what is the potential of these cell signalling targets to improve treatment response prediction and novel drug discovery? Finally, what is the specificity of the observed cell signalling changes for schizophrenia relative to related major neuropsychiatric disorders including major depression, bipolar disorder and autism spectrum disorder?

4.3.1 ALTERED PLC-γ1- THAPSIGARGIN RESPONSE AS THE PRIMARY DRUG TARGET IDENTIFIED BY FUNCTIONAL CYTOMIC SCREENING IN SCHIZOPHRENIA PBMCS

The attenuated response of phospholipase C γ1 (PLC-γ1) to thapsigargin (TG) in T cells of drug-naive schizophrenia patients, relative to controls, was the most significant finding in the AI study (p=0.001) **(Table 4.2, Fig. 4.7d)**. It is also in many ways the archetypal drug target sought by the current platform. First, basal expression of PLC-γ1 was not altered between the two clinical groups. This demonstrates the added value of functional testing, in the presence of an active ligand, to reveal clinically significant associations which would be otherwise undetectable by quantification of the signalling proteins alone. Second, the altered cellular response, in this case calcium signalling

induced by TG, is empirically measured in live cells from patients as opposed to imputed through *in silico* pathway analysis. Thirdly, the aberrant response was normalized over the course of efficacious clinical treatment with olanzapine in schizophrenia patients, suggesting that the *ex vivo* response in blood cells can be correlated to physiological changes in active CNS pathology (δPANSS). Fourth, the components of the functional response, TG and PLC-γ1, are known to be mechanistically coupled and relate to high profile CNS drug targets suggested by previous studies. Finally, the response appears specific to schizophrenia relative to other neuropsychiatric diseases. For all of these reasons combined the TG-PLC-γ1 response was selected as the substrate of the subsequent drug library screening stage of the project **(Chapter 5)**.

4.3.2 PLC-γ1- THAPSIGARGIN MECHANISM OF ACTION

PLC-γ1 serves as signal transducer for receptor tyrosine kinase (RTK) activation[234–236]. The RTK family responds to a wide range of neurotrophins, hormones, cytokines and growth factors which are relevant to neuropsychiatric pathogenesis. This includes BDNF and NT 3/4 at the TrkB receptor, NGF at the TrkA receptor, TGF-a and NRG 1-4 at ErbB 1-4 receptors, FGF at the FGF receptor and insulin/ IGF-1/2 at the insulin and IGF receptors [233,235–239]. Ligand binding to RTKs provokes the autophosphorylation of the intracellular loop of the receptor which allows PLC-γ1 to bind using its Src homology 2 (SH-2) domain. The activation of PLC-γ1 catalyzes the degradation of phosphatidylinositol 4,5-biphosphate into intracellular second messengers inositol 1,4,5-triphosphate (IP3) and 1,2 diacylglycerol (DAG), which induce the release of calcium stored in the endoplasmic reticulum (ER) and the activation of PKC respectively. Reduction of ER calcium is sensed by stromal interaction molecule 1 (STIM1) which subsequently promotes the influx of extracellular calcium via the ORAI1 plasma membrane channel[233,235–240]. TG (1 μM) drastically elevates the intracellular calcium concentration by non-competitively blocking the ability of the sarco/endoplasmic reticulum $Ca2^{+}$ ATPase (SERCA) to pump calcium back into the endoplasmic reticulum[241]. Thus its effect on increasing cytosolic calcium concentration is analogous to that of PLC-γ1-mediated RTK signalling.

It is possible therefore that the decrease in PLC-γ1, observed in response to TG in the current assay, represents negative feedback regulation designed to desensitize the cellular response to sustained RTK activation in a physiological environment. Desensitization of receptor transduction is a common feature of several signalling networks to ensure that cell signals are both spatially and temporally resolved[172,242]. If we extrapolate this cellular phenotype to neuronal cells in

schizophrenia it would suggest that they are potentially incapable of adequately switching off signalling events in response to neurotrophic, hormonal or cytokine ligands. It is also possible that the cells from schizophrenia patients display a reduced calcium flux in response to TG and that the reduced PLC-γ1 response is simply proportional. While the application of a near maximal concentration **(Fig. 5.2)** of TG (1 μM) for 30 min suggests that this is unlikely, this possibility cannot be excluded without parallel measurement of calcium release. The fact that ionomycin, which causes calcium influx from the extracellular space, did not elicit a clinically distinct phenotype in T cells suggests that the dysregulation of PLC-γ1 in this cell subtype in schizophrenia is specific to calcium release from the internal stores. However this would have to be confirmed in the absence of PMA, which was administered as part of a cocktail with ionomycin. Interestingly neither of the PKC isoforms, which have been repeatedly linked to neuropsychiatric disorders and are immediate downstream targets of PLC-γ1 (via DAG), were found to be dysregulated despite sensitivity to TG (-1.11 and –1.68 FC for PKC-θ and PKC-α)[77,243]. This suggests that the pathological phenotype is focused on the IP3-mediated branch of PLC-γ1 signalling. Finally the fact that expression of the phosphorylated activation site (pY783) on PLC-γ1 was not altered in patients relative to controls following TG exposure suggests that the dysregulated response involves sequestration of the total PLC-γ1 protein or binding to regulatory partners as opposed to changes in enzymatic activity. Taken together these findings suggest that there is an impaired regulatory response to calcium release from internal stores evident at PLC-γ1 in schizophrenia which is normalized following clinical treatment with olanzapine **(Fig. 4.12)**.

4.3.3 VOLTAGE-GATED CALCIUM CHANNELS AS PUTATIVE MEDIATORS OF THE PLC-γ1-THAPSIGARGIN RESPONSE IN SCHIZOPHRENIA

To further refine this hypothesis and understand which functional variants might contribute to the altered calcium response in schizophrenia we examined the disease-associated genes from the largest schizophrenia GWAS analysis to date (36,989 cases vs. 113,075 controls)[24]. The study found a total of 108 significant disease-associated genomic loci including three of which contain genes encoding voltage-gated calcium channel (Ca_v) subunits (CACNA1C, CACNB2 and CACNA1I). CACNA1C and CACNB2 encode L-type calcium channel subunits and CACNA1I encodes a T-type calcium channel subunit. These genes are among the most significant hits to emerge from this study for several reasons. Firstly they are ranked among the top risk loci which attained genome wide significance CACNA1C (4^{th}) CACNB2 (19^{th}) and CACNA1I (39^{th}). Secondly they are the only genes within their respective risk loci, whereas the majority (60%) of loci contain multiple genes. Thirdly

the primary risk single nucleotide polymorphism (SNP) for each gene is within the gene itself and not in a nearby genomic region. These features mean that they are readily identifiable as schizophrenia target genes as opposed to simply being in linkage disequilibrium with other alleles which are in fact the true causative variants.

The implication of voltage-gated calcium channel subunits in schizophrenia is supported by complementary results from the largest whole exome sequencing study in schizophrenia to date (2,536 cases vs. 2,543 controls)[244]. This study, looking for rare protein-coding mutations, found that the disruptive alleles associated with schizophrenia were enriched for voltage-gated calcium channel subunit genes (26 in total) including CACNA1B, CACNA1C, CACNA1H, CACNA1S, CACNB2/4 and CACNA2D1-4. The L-type calcium channel subunits were the most highly represented especially the CACNA1C (Ca_v 1.2) cited as the most significantly associated calcium channel hit in the previously described GWAS study. These mutations represent putative partial or complete loss of function[27]. Moreover a combined subset of ultra-rare calcium channel mutations (12 cases vs. 1 control) yielded a striking odds ratio of 8.4 (p=0.002) suggesting that when exon mutations in these genes occur they can have a profound impact on the risk of developing schizophrenia[244]. Several studies, focusing on carriers of the risk allele (rs1006737) within Ca_v1.2 L-type calcium channel have shown alterations in CACNA1C expression in the brain (cerebellum and dorsolateral prefrontal cortex) and in neurons induced from fibroblast cells[27,245]. Furthermore this risk allele has been associated to alterations in fMRI brain activation and connectivity of key schizophrenia associated brain regions in healthy volunteers and schizophrenia patients during working memory and emotional and reward response tasks[27,245]. Taken together these findings suggest that voltage-gated calcium channels, especially L and T-subtypes, represent some of the strongest known genetic risk factors with corresponding influences on higher order cognitive processes associated with schizophrenia. In light of this evidence we propose that these L- and/or T-type voltage-gated calcium channels are potentially involved, or at least have the therapeutic potential to mitigate, the altered response to thapsigargin at PLC-$\gamma 1$ in schizophrenia **(Fig. 4.12)**.

In support of this hypothesis there is evidence that these voltage-gated calcium channels play important roles in non-excitable blood cells in which calcium signalling is necessary for development, survival, activation, differentiation and cytokine production[240]. For example expression of all the subunits of Ca_v 1.1-4 L-type calcium channels has been demonstrated in T lymphocytes at levels comparable to excitable cells such as neurons[240]. Furthermore the expression of subtypes of L-type calcium channels is linked to the naive vs. effector activation status of different T cell subtypes and the balance between Th1 and Th2 T cell phenotypes[240]. For example the Ca_v 1.2 L-type channel, which contains the CACNA1C subunit described above as prominently linked to

schizophrenia, is specifically expressed in Th2 CD4+ effector cells[240]. Considering the repeated association of altered Th2 cell function in schizophrenia it is possible that the Ca_v 1.2 channel represents a convergent drug target between both CNS and peripheral disease aetiologies[72]. This is supported by the fact that both antipsychotic drugs and antihypertensive dihydropyridine (DHP) L-type calcium channel blockers can specifically mitigate over-activation of Th2 cells[240,246]. Finally with specific relevance to the mechanism of action of thapsigargin, peripheral naive and memory T cells from Ca_v 1.4 L-type calcium channel knockout mice showed significantly impaired calcium flux responses when exposed to thapsigargin and corresponding reductions in nuclear factor of activated T-cells (NFAT) activation and cytokine production[240]. Taken together these findings suggest that the altered response to thapsigargin in T cells from schizophrenia patients in the current study is plausibly mediated by L-type calcium channels. Furthermore these L-type calcium channels represent a convergent drug target for both CNS and peripheral schizophrenia disease mechanisms with the potential for drug repurposing.

4.3.4 PLC ISOTYPES IN SCHIZOPHRENIA AND RELATED NEUROPSYCHIATRIC DISORDERS

There is considerable evidence for the involvement of PLC isotypes in schizophrenia and related neuropsychiatric disorders. The genes coding for several PLC isotypes (PLCB2, PLCL1, PLCH2) were within the set of 108 loci associated with an increased risk of disease in the largest schizophrenia GWAS to date[24]. While these specific isotypes were not measured in the current study there is considerable overlap between their respective sequence homologies and functional repertoires with respect to PLC-$\gamma 1$ and PLC-$\gamma 2$[233] (UniProt). PLC-$\beta 1$ is the most widely studied of the isotypes in schizophrenia[247,248]. PLC-$\beta 1$ has a similar role to the PLC-γ isotypes in terms of producing IP3/calcium and DAG/PKC signals in response to cell surface receptor activation. However, PLC-$\beta 1$ responds primarily to GPCR receptor activation including mGluR 1/5, MR 1/3, 5-HT2A/C and D1/2/5[235,249,250]. PLC-$\beta 1$ expression is altered in the prefrontal and superior temporal cortex of post mortem brains from individuals with schizophrenia[247]. Furthermore PLC-$\beta 1$ knockout mice show several behavioural correlates of schizophrenia including hyperactivity, sensorimotor gating deficits and cognitive impairment. Notably these behavioural abnormalities are normalized by treatment with the antipsychotic clozapine, but not haloperidol[250]. This raises the possibility that the normalization of the related PLC-$\gamma 1$ activity observed in the present study is specific to atypical antipsychotics, especially structurally related olanzapine and clozapine. Conversely PLC-$\gamma 1$, which is expressed throughout the body and enriched in the brain (especially the cortex and hippocampus), has been frequently associated to a range of neurological disorders including major depression, bipolar

disorder, epilepsy, Alzheimer's and Huntington's disease[235,247]. For example PLC-γ1 represents a susceptibility locus for bipolar disorder and polymorphisms within this gene have been linked to lithium response in bipolar patients[251,252]. It has also been implicated in the response to antidepressant therapy in MDD[253] . Taken together these findings suggest that multiple PLC isotypes are affected across neuropsychiatric disorders including schizophrenia.

The fact that that the PLC isotype (PLC-γ1) detected in the AI study differs from the isotypes associated previously to schizophrenia (PLCB1, PLCB2, PLCL1, PLCH2), suggests that a convergent up- or downstream regulatory mechanism, which is shared between different PLC isotypes, might underlie the altered TG-PLC-γ1 response as opposed to altered function of the PLC-γ1 isotype itself. In other words PLC-γ1 is a surrogate marker for a more complex and integrated signalling response that affects different isotypes depending on the tissue type and ligand in question. This would also explain the emergence of a similar phenotype uniquely in response to TG at PLC-γ2 in the differential diagnosis study. PLC-γ2, which is primarily expressed in cells of the haematopoietic lineage, shares (99.9%) sequence homology and a similar functional repertoire to PLC-γ1 (UniProt P19174 vs. P16885)[233,235,236]. This suggests that both PLC-γ1 and PLC-γ2 have largely redundant roles in cell signalling. Therefore although they have a different dynamic range in relation to the potency of the TG response, as observed in the AI vs. DD studies, they nevertheless might serve as surrogate markers of the same fundamental signalling dysregulation in schizophrenia.

4.3.5 PLC-γ1/2- THAPSIGARGIN AS A FUNCTIONAL ENDOPHENOTYPE IN SCHIZOPHRENIA- SUMMARIZING COMPLEX GENETIC RISK

While the evidence provided for calcium channel and PLC isotype dysfunction in schizophrenia supports the validity of the putative drug target obtained in the AI and DD studies, it also serves to elucidate ways in which functional cytomic exploration can overcome specific limitations in the state of the art. Firstly the risk alleles in both voltage-gated calcium channels and PLC isotypes, described in some of the GWAS studies above, are relatively common (e.g. CACNA1C rs1006737 has a frequency of 33% in the general population) and are individually associated with a small incremental risk (OR <1.2)[23,27,254]. Conversely the highly penetrant mutations described above are rare[27,244]. Thus it is likely that the schizophrenia samples used in the AI and DD studies heterogeneously carry multiple common but weak risk alleles at these loci and possibly rare penetrant alleles in a minority of cases. In addition each patient will likely have been exposed to different environmental stressors and have different developmental trajectories. Nevertheless the

attenuated TG-PLC-γ isotype response is significant across the patient groups and shows the common feature of normalization by efficacious olanzapine treatment. This highlights the possibility that the functional cytomic platform summarizes different combinations of risk alleles and environmental insults in individual patients as common functional endophenotypes. It is intriguing in this respect that the abnormal TG-PLC-γ isotype cellular response was identified in small cohorts of patient samples (AI n=12 and DD n=25) while the detection of the plausibly related GWAS risk loci required tens of thousands of samples[23]. Clearly the cytomic analysis requires replication in larger sample cohorts to draw firm conclusions. However the striking coincidence that the top cytomic hits in the present study derived from a non-hypothesis driven functional screening approach, directly relate to some of the most significant and widely reproduced GWAS findings, suggests that the functional cellular endophenotype strategy could potentially provide advantages in terms of lower statistical power or at least be complementary. Furthermore the current best practice for validating the significance of GWAS risk loci in neuropsychiatry is to demonstrate a differential expression of the risk alleles in the brain, using expression quantitative trait loci (eQTL) mapping, and subsequently predict their mutual interaction *in silico*[31]. While this approach can provide valuable insight it is far from being a functional model against which the activity of novel drugs can be empirically tested. In other words the molecular networks discovered by these approaches subsequently have to be engineered into an *in vitro* drug screening assay. In contrast the functional endophenotypes derived from the present cytomic methodology constitute a screenable disease model by definition from their inception.

4.3.6 PLC-γ1/2- THAPSIGARGIN AS A FUNCTIONAL ENDOPHENOTYPE IN SCHIZOPHRENIA- INVESTIGATING DISEASE SPECIFICITY WITHIN THE NEUROPSYCHIATRIC SPECTRUM

Many of the genetic variants described above are common to several neuropsychiatric diseases. For example Ca_v channel subunits CACNA1C and CACNB2, in addition to being highly significant in the largest schizophrenia GWAS, were also two of the four top loci associated in a combined cohort of five different neuropsychiatric diseases (BD, MDD, SCZ, ASD and ADHD) relative to controls in the largest cross disorder GWAS[24,34]. Furthermore 20 of the 67 loci derived from the cross disorder GWAS at a lower significance threshold ($p<0.001$) corresponded to voltage-gated calcium channel subunits[34]. This suggests that altered calcium signalling could be a profoundly shared mechanism in several major neuropsychiatric diseases. In contrast the functional endophenotype represented by

the TG-PLC-γ isotype response in the present study was unique to schizophrenia. If indeed the aforementioned Ca_v channel subunits are involved in this response, there are several possible explanations for this specificity. The different Ca_v channels are associated to a greater or lesser extent to different neuropsychiatric diseases. For example whereas the other major neuropsychiatric diseases, aside from schizophrenia, show a highly heterogeneous rank order of association to CACNA1C and CACNB2 Ca_v subunits, schizophrenia is second at both loci suggesting that it is perhaps the most prominently associated to L-type channels overall[34]. In other words, the subsets of Ca_v channel alleles, which are collectively more likely in schizophrenia, interact to produce the specific TG-PLC-γ isotype response. Another plausible explanation is that the interaction of shared risk between Ca_v channels and PLC-γ isotypes defines the specificity of the TG-PLC-γ1/2 response in schizophrenia. This is supported by the fact that while TG was broadly active across all the disease groups (60% of epitopes) it is only clinically associated to PLC-γ isotypes in schizophrenia. In either case, the potential for deriving disease specific functional endophenotypes amidst overlapping neuropsychiatric genetic backgrounds is an invaluable feature for drug discovery.

4.3.7 FUNCTIONAL EXPLORATION OF PLC-γ ISOTYPE RESPONSES IN HETEROGENEOUS PRIMARY CELL POPULATIONS *EX VIVO*

The DD study revealed the importance of high content screening in heterogeneous primary cell populations. Whereas in the AI study clinical interactions of PLC-γ isotypes were analyzed only in T cells, in the DD study they were assessed in CD4+ T cells, CD4- T cells and B cells. This revealed a range of attenuated responses at PLC-γ isotypes in schizophrenia in different PBMC subsets in response to different ligands **(Table 4.6)**. While the increased sample number in the DD study (SCZ/ CTRL DD n=25 each vs. SCZ/ CTRL AI n=12 each) likely contributed to this feature, it is also possible that some of these cell type specific effects were not detectable when analyzing total T cells alone. Notably a much greater attenuation of response at PLC-γ1 in schizophrenia was observed in B cells following PMA/ ionomycin treatment in the DD study (**Fig. 4.10f**, -10.3 fold change) relative to T cells following TG treatment in the AI study (**Fig. 4.7d,** -2.6 fold change). The direction of the ligand response was also different between cell types (TG decreased PLC-γ1 while PMA/ ionomycin increased PLC-γ1). Both of these ligands induce cytosolic calcium flux although their mechanisms are different. Ionomycin induces extracellular calcium flux across the plasma membrane whereas as TG initially induces intracellular calcium flux via depletion of ER stores. While the end result of

each mechanism is similar, the fact that each one induces the schizophrenia-associated phenotype in different cell types highlights the fact that the same putative abnormality in cell signalling regulation can have divergent presentations in different cell lineages.

At the level of drug target discovery this is advantageous in terms of increasing the number of models for detecting pathological variants in cell signalling. It is also beneficial at the level of screening for novel drugs where pathway selectivity and cell type specificity are vital to the balance between therapeutic 'on –target' and toxic 'off-target' effects[127]. For example this feature would allow the targeting of anti-inflammatory drugs specifically to Th17 T helper cells, which have been proposed to cross the blood brain barrier and exacerbate neuroinflammation in schizophrenia, whilst avoiding toxicity to other immune cell subsets[71]. Interestingly the SNPs associated with schizophrenia in the largest GWAS study were differentially prevalent in gene expression-enhancer regions corresponding to different cell and tissue types. Notably the B cell lineage (CD19/ CD20) was the most enriched tissue type outside the brain[24]. This lends support to the prominent attenuation in PLC-$\gamma 1$ signalling observed in B cells in the DD study. It also advocates the inclusion of this PBMC subset in future functional cytomic screens in neuropsychiatry. However the enrichment of schizophrenia risk-associated SNPs was also present in other PBMC lineages including T cells. Taken together these findings suggest that different functional endophenotypes, which represent different aspects of altered brain pathology, are likely to be identifiable in different peripheral cell types. Therefore the inclusion of heterogeneous cell populations which can be discretely resolved affords a powerful contribution to drug target discovery and novel drug screening strategies using functional cytomics.

4.3.8 ALTERED AKT1 EXPRESSION AS A POSITIVE CONTROL IN SCHIZOPHRENIA

The finding that basal Akt1 was decreased in drug-naive first-onset schizophrenia patients relative to controls in both the AI and DD studies serves as a vital positive control for the validity of this novel functional cytomics platform **(Table 4.3 and 4.5)**. Decreased total Akt levels is the most widely replicated finding in studies which have assessed altered cell signalling protein expression in the PBMCs from schizophrenia patients. The first study[214] to make this link showed a decrease in both Akt1 protein level and the phosphorylation of its substrate GSK-3β (pS9) in lymphoblastoid cell lines derived from schizophrenia patients (n=28) relative to controls (n=28). Similar changes were confirmed by the same authors in the frontal cortex of *post-mortem* brains from schizophrenia patients in two independent cohorts (cohort 1: SCZ/CTRL n=10 each; cohort 2: SCZ/CTRL n=15 each).

They also showed that reduced Akt1 levels correlated to a putative disease haplotype in the Akt1 gene and that Akt1$^{-/-}$ mice showed disrupted sensory-motor gating reminiscent of perceptual alterations in schizophrenia. Finally they showed an increase in phosphorylation of Akt1 at (pS473) and (pT308), in addition to GSK-3β (pS9), but not total AKt1 levels in wild- type mice treated with antipsychotic haloperidol. These finding have subsequently been confirmed in multiple independent studies across patients from different ethnic backgrounds[255–259]. Notably several of these studies have associated the Akt1 risk haplotypes with alterations in executive function and fMRI responses during attentional processing[148,260].

The results obtained in the AI and DD studies support these findings in terms of the direction and magnitude of fold change across different PBMC subtypes in schizophrenia vs. controls **(Tables 4.3 and 4.5)**. For example the initial study by Emamian *et al.* found a -3.13 fold reduction in Akt1 protein expression in B lymphoblastoid cell lines (Western blot) whereas a recent publication by van Beveren *et al.* found a -1.20 fold reduction in total PBMCs (2.0 Gene Chip microarray)[84]. The present results similarly suggest a more pronounced reduction in B cells (DD -1.60 fold) relative to T cells (AI -1.07 and DD -1.08), with total PBMCs representing an intermediate value of -1.29 fold (estimated from DD data assuming an average 4.5 : 1 ratio of T : B cells[261] and excluding monocytes which were not measured).

In terms of the effect of antipsychotic treatment on Akt1 expression, the current results are in contrast to certain aspects of published data. Several reports suggest that antipsychotic treatment is associated with increases in Akt1 phosphorylation but not total levels of Akt1[92]. However, our *ex vivo* results suggest that antipsychotic treatment, at least with atypical olanzapine for six weeks, does provoke an increase in total Akt1 (1.12 fold) and that this increase is proportional to that of Akt (pS473) (1.14 fold) and regulatory PDPK1 (pS241) (1.12 fold). This discrepancy between the current results and published data is likely due to the predominant use of animal brain tissue vs. human PBMCs, use of different antipsychotics (usually typical antipsychotic haloperidol) and the dose and/or duration of treatment before sample collection. However closer examination of the aforementioned study from van Beveren *et al.* [84], which investigated human PBMCs, suggests that previous conclusions about total Akt1 levels following antipsychotic treatment could be compromised by a lack of assay sensitivity. This study showed that Akt1 mRNA in PBMCs is significantly reduced in the combined group of treated and untreated schizophrenia patients (n=41) relative to controls (n=29). At the same time there was no significant difference between antipsychotic drug-naive and treated patients. However there was an active-dose dependent trend towards increased mean Akt1 mRNA (log-transformed relative intensity –'RI') across antipsychotic naive (RI=482), antipsychotic free for over two weeks (RI=493), and medicated (RI=527) patients

relative to controls (RI=580)[84]. Interpretation of this in light of the AI and DD studies raises the possibility that normalization of total Akt1 following antipsychotic treatment is detectable specifically in T cells, where the initial disease perturbation is more moderate, and that this effect is diluted in analyses of total PBMCs by the presence of more extremely perturbed cellular subsets, such as B cells, which are potentially refractory to treatment. These conclusions require validation in larger cohorts with the vital correlation to changes in active symptomatology (δPANSS) across different antipsychotic classes. However the results highlight the potential of previously unexplored parallel assessments of individual cell subtypes, within heterogeneous PBMC populations, to derive clinically more accurate markers of disease progression. It is also notable that while the majority of studies, including this one, detect alterations in total levels of Akt1 in case/control comparisons, they do not detect alterations in the total level of phosphorylated epitopes such as Akt (pS473) and Akt (pT308). This would suggest that the proportion of phosphorylated, relative to unphosphorylated, Akt1 is higher in the disease samples under basal conditions, indicating a potential constitutive compensatory mechanism which is often overlooked.

4.3.9 AKT1 AS A SHARED CELL SIGNALLING SUBSTRATE FOR EFFICACY AND SIDE-EFFECTS OF CLINICAL ANTIPSYCHOTIC TREATMENT

As a key intracellular mediator of neurotransmission (notably D2 receptor signalling) and synaptic plasticity, altered Akt1 expression has potentially profound implications for schizophrenia pathogenesis and has been extensively reviewed as a drug target elsewhere[80,87,92,145,214,262–264]. However the relative importance of Akt signalling specifically with respect to positive and negative symptom subscales and metabolic side effects is less well documented. Data in the current AI study suggests that there is considerable segregation of the cell signalling repertoires which are associated with changes in positive vs. negative symptoms **(Fig. 4.8).** Interestingly PDPK1 (pS241) and S6 (pS240), which lie at proximal and distal ends of the canonical Akt pathway respectively, showed associations to positive but not negative symptoms. Metabolic side effects of atypical antipsychotic therapy, such as weight gain and insulin resistance, have traditionally been explained by the relative orexigenic potential of these drugs via CNS H1 receptor antagonism[225]. However recent data suggests that they also have direct effects on insulin signalling through the Akt pathway at peripheral sites including liver and adipose tissue[265,266]. This raises the possibility that while changes in the Akt pathway following olanzapine treatment in the AI study are associated with improvements in positive symptoms, they might also be associated with the metabolic side effects of the drug. This is concurrent with the concept that the D2 receptor, which is the main target of

drugs which are efficacious against positive symptoms, and insulin signalling converge on Akt. Thus efficacy and toxicity might share a common cell signalling substrate. Improved definition of this putative overlap in future applications of the *ex vivo* platform, with concurrent measurement of positive symptom changes and metabolic disturbances across different antipsychotic drug classes, potentially represents a valuable application for toxicity counter-screening in the development of novel drugs.

4.3.10 IMPLICATION OF ALTERED STAT3 ACTIVATION IN SCHIZOPHRENIA

In contrast to Akt which has an established association with schizophrenia, STAT3 is a novel cell signalling node which has scarcely been implicated in the disease. The best characterized mechanism of STAT3 function is as a mediator of cytokine signalling including IL-2, IL-5, IL-6, IL-10, IL-17A, IL-22, IFN-α/β [133,267–269]**(Chapter 3 Fig. 3.10)**. However it also responds to hormones, such as leptin, and growth factors, such as leukaemia inhibitory factor (LIF), epidermal growth factor (EGF), hepatocyte growth factor (HGF) and bone morphogenetic protein 2 (BMP-2)[269,270]. It controls a variety of cellular responses including proliferation, survival, differentiation and motility and has a central role in immune response, embryonic development (including CNS) and cancer[267,269,270]. Briefly its principal mechanism of activation, following cytokines or growth factor receptor binding, involves phosphorylation at pY705 by Janus kinases (JAKs), SRC family kinases (SRCs), growth factor receptors or other tyrosine kinases. This leads to dimerization and nuclear translocation where it acts as a transcription factor for a variety of genes. Phosphorylation at the pS727 regulatory site, by Akt and ERK1/2 kinases is also important for transcriptional activation. Downregulation of STAT3 signalling is mediated by suppressors of cytokine signalling (SOCS) and protein tyrosine phosphatases (PTPs) including SHP-2[267,269,271,272]. Below, two alternative hypotheses for alterations in the STAT3 (pY705) activation site in schizophrenia are discussed. The first is that altered STAT3 (pY705) phosphorylation is the effect of increased levels of circulating cytokines. The second is that STAT3 (pY705) phosphorylation represents a systemic alteration in cell signalling which is intrinsic to both immune and neuronal cells. Finally we compare alterations in STAT3 activation to similar cell signalling changes in MDD to propose a shared molecular substrate between MDD and the negative symptoms in schizophrenia.

4.3.11 STAT3 (PY705) ACTIVATION STATUS IS A REFLECTION OF ALTERED CIRCULATING CYTOKINES IN SCHIZOPHRENIA

Altered activation of STAT3 at pY705 in schizophrenia PBMCs, observed in the AI and DD studies, is potentially a reflection of altered circulating cytokine levels in patients. In a recent metanalysis (40 studies) the proinflammatory cytokine IL-6, which is the prototypical ligand for STAT3 (pY705) activation, was found to be the most prominently increased cytokine in drug-naive first-episode and acute relapse psychosis patients relative to controls. Furthermore IL-6 levels were normalized by antipsychotic therapy[132]. Therefore in the AI study it is possible that increased STAT3 (pY705) activation in drug-naive first-episode patients, with subsequent normalization following olanzapine treatment **(Table 4.3 and Fig. 4.7b)**, directly reflects changes in circulating IL-6 levels. In contrast in the DD study STAT3 (pY705) was found to be decreased in drug-naive first-episode patients relative to controls **(Table 4.5 and Fig. 4.10c, d)**. This could be explained by desensitization of STAT3 (pY705) following chronic stimulation by elevated circulating IL-6. In the DD study it is notable that while expression of STAT3 (pY705) was reduced, the response to IL-6 at this epitope *ex vivo* was enhanced in patients relative to controls. This raises the possibility that while basal regulation of STAT3 (pY705) phosphorylation is desensitized the rest of the cell signalling network up-/downstream of STAT3 (pY705) remains hyper-sensitive to ligand stimulation. This type of regulatory uncoupling, which could prove to be a key pathogenic mechanism, warrants further investigation.

Therefore despite the difference in the directionality of basal STAT3 (pY705) activation between the AI and DD, it is possible that both studies represent a common functional endpoint in the form of either increased inflammatory set-point or increased inflammatory response respectively as a result of sustained circulating IL-6 stimulation. It is also possible that differences in the proportion of monocytes secreting IL-6 in the *ex vivo* PBMC culture (as a result of PBMC isolation or donor variability) or the collection medium (sodium heparin vs. ACD) could influence the directionality between AI and DD studies. Standardization of these variables and correlation of STAT3 (pY705) to circulating and *ex vivo* IL-6 concentrations will help to clarify the influence of altered secreted cytokines on this epitope. Nevertheless these results extend our current knowledge on inflammatory alterations in schizophrenia by providing a putative link between altered circulating cytokines and T cell activation status. While IL-6 is presented by means of example, as the foremost inflammatory cytokine associated with schizophrenia and normalized following antipsychotic therapy, it is also worth considering that responses to anti-inflammatory cytokine IL-10, which is associated with acute psychotic relapse, are also mediated by STAT3 (pY705). Furthermore altered responses to IL-10 were observed at PLC-γ2 in CD4- and CD4+ T cells in the DD study. The

implications of altered STAT3 (pY705) activation status in future studies would therefore be best interpreted in conjunction with a full circulatory cytokine concentration profile which considers not only absolute levels but also relative cytokine ratios.

4.3.12 STAT3 (PY705) ACTIVATION STATUS REFLECTS AN INTRINSIC CELLULAR PHENOTYPE COMMON TO BOTH IMMUNE AND NEURONAL CELLS IN SCHIZOPHRENIA

It is possible that intrinsic dysregulation of STAT3 (pY705) activation in immune cells precedes and even provokes physiological alterations in cytokine ratios in schizophrenia. STAT3 mediates the transcription of a range of cytokines[273]. Intrinsic alterations in STAT3 transcriptional activation could therefore alter the secreted cytokine profile of specific immune cell subsets, which could in turn alter their relative proliferation or differentiation and further skew the circulatory cytokine profile. For example knock-out and knock-in studies of the related STAT1 protein have been shown to alter the balance between Th1, Th2 and Th17 T cell subsets all of which have been implicated in schizophrenia[71,226,262]. Likewise STAT3 affects the transcription of several cytokines which have been associated with schizophrenia pathogenesis even before the onset of overt psychological symptoms including circulating IL-8, IL-10 and matrix metalloproteinase 7 (MMP-7)[50,54,274]. Thus STAT3 (pY705) might be the cause of widely reported alterations in immune cell subtype ratios and cytokine secretion in schizophrenia, as opposed to the effect.

STAT3 has been implicated as a vital mediator of microglial activation in the brain. It is the only transcription factor currently reported to be involved in the phenotypic switching between resting microglia and both M1 and M2 microglia activation phenotypes[275]. M1 activation, mediated by IL-6-STAT3 signalling, results in proinflammatory microglial activity including release of inducible nitric oxide synthase (iNOS) and proinflammatory cytokines (TNF-α, IL-1β, IL-6, IL-12 and IL-23). M2 activation, mediated by IL-10-STAT3 signalling, results in restorative microglial activity including debris clearance, resolution of inflammation (via IL1R antagonist, IL-10 and chitinase-like protein secretion) and trophic factor release (TGF-β)[275]. Several studies using positron emission tomography (PET) *in vivo,* or immunocytochemistry and inflammatory cytokine mRNA expression *post mortem,* have suggested that increased M1 microglial activity in the brain might mediate the deleterious effects of schizophrenia in terms of cognition, negative symptoms and regional brain volume alterations in specific subgroups of patients[56,57,276]. Importantly subgroups of patients who suffer from these deleterious effects show concurrent elevation in the expression of proinflammatory cytokines in peripheral blood cells[57]. It is noteworthy that in the AI study there

was a heterogeneous expression of STAT3 (pY705) before treatment **(Fig. 4.7b)** suggesting the presence of potential subgroups of patients with more prominent STAT3 (pY705) activation. Furthermore STAT3 (pY705) expression was correlated to improvement in negative symptoms (δPANSSn) following olanzapine treatment **(Fig. 4.8b)**. Taken together these findings raise the possibility that the altered STAT3 (pY705) activation observed *ex vivo* could be associated with changes in brain microglial activation with consequent negative symptomatology in a subgroup of schizophrenia patients. In accordance with this hypothesis we have shown, in a parallel application of the functional cytomic platform, that serum from a subset of first-onset drug-naive schizophrenia patients (n=60) relative to controls (n=79) can induce STAT3 (pY705) activation in the SV-40 human microglial cell line (manuscript in preparation).

STAT3 also plays an important role in neuronal cells which is independent of its effects in neighbouring microglia. STAT3 has a uniquely high expression in the brain relative to the seven other STAT isotypes and is strongly upregulated in postnatal week one consistent with its role in neurogenesis, astrogliogenesis and axonal remodelling[271,277]. It is also reported to respond directly to neuronal depolarization and modulate the expression and function of key GPCRs including 5HT-2A, β-adreno, GABA, mAch, NMDA and AMPA receptors[271,277]. In addition it is a principal mediator of hypofunction at NMDA receptor synapses via effects on long-term depression and IL-6 mediated oxidative stress[278,279]. This is particularly relevant to schizophrenia as NMDA receptor hypofunction on GABAergic interneurons is thought to be a key pathogenic mechanism[25,280]. Interestingly several of these effects appear to be independent of STAT3 transcriptional activity, suggesting it is also involved in direct protein-protein interactions in the cytoplasm. Finally with relevance to the AI study, olanzapine has been shown to desensitize 5HT-2A receptors via induction of STAT3 (pS727) phosphorylation and transcription of regulators of G protein signalling 7 (RGS7) in rodent cortical cell lines and frontal cortex *in vivo* [281,282]. Taken together these findings suggest that STAT3 is a key mediator of neuronal processes which are known to be altered in schizophrenia and linked to antipsychotic response. Therefore it is possible that putative alterations in STAT3 activation status *ex vivo*, which would conventionally be confined to immunological interpretations of schizophrenia, could also reflect pathogenic mechanisms in neuronal cells.

4.3.13 STAT3 PHOSPHORYLATION REPRESENTS A SHARED CELL SIGNALLING SUBSTRATE BETWEEN NEGATIVE SYMPTOMS IN SCHIZOPHRENIA AND MAJOR DEPRESSIVE DISORDER

Altered IL-6-STAT3 signal transduction has been extensively implicated in the pathogenesis of MDD by several lines of investigation. Firstly elevated IL-6 in response to infection produces symptoms, such as low mood, lack of motivation and social withdrawal, similar to those which are characteristic of MDD[283]. Secondly IL-6 is elevated in response to acute stress in animals and humans and has been shown to mediate the social defeat phenotype in chronic mild stress animal models of MDD[153,284,285]. Concurrently maladaptive responses to stress via altered hypothalamic–pituitary–adrenal (HPA) axis function and deleterious effects of stress hormones on synaptic plasticity have also been shown to involve IL-6 in humans[286,287]. Thirdly, simulation of prenatal viral infection in rodents using polyinosinic: polycytidylic phosphate causes elevation of maternal IL-6 and consequently a reduction in hippocampal LTP, neurogenesis and neuronal survival with depressive-like symptoms and cognitive deficits in adult offspring[288]. Finally STAT3 has been shown to bind to the promoter of the serotonin transporter (SERT) in response to IL-6 and decrease the expression of SERT resulting in depressive like behaviour in rodents[289]. Polymorphisms in the STAT3 gene have also been associated with antidepressant response in humans[290]. Taken together these findings suggest a prominent role for IL-6-STAT3 signalling in both core symptomatology and the aetiology of MDD.

Several studies have suggested that IL-6-STAT3 signalling might play a similar role in the aetiology of negative symptoms and cognitive deficits in schizophrenia notably in terms of putative maternal viral infection and a maladaptive HPA-axis response to stress[10,288,291]. This is exemplified mechanistically by the association of increased blood cell and brain proinflammatory cytokine expression with microglial activation, brain volume changes and cognitive deficits in schizophrenia (described earlier)[56,57]. In the current study *ex vivo* changes in STAT3 (pY705) and STAT3 (pS727) were specifically correlated to improvements in negative symptoms (δPANSSn) following olanzapine treatment in the AI study **(Fig. 4.8b).** STAT3 (pY705) also had the largest dynamic range of any epitope in terms of the change in expression following treatment (-1.16 fold) compared to the initial difference with controls (1.22 fold) **(Table 4.3)**. Furthermore MDD was the only other neuropsychiatric disorder, in addition to SCZ, to show altered STAT3 phosphorylation in the DD study **(Table 4.5).** Finally the decreased basal STAT3 (pS727) expression (-1.09 fold) in MDD directly contrasts with the prominent increase in basal STAT3 (pS727) expression (1.21 fold), which accompanied a group-wide improvement in negative symptoms, following olanzapine treatment in

SCZ. Taken together these *ex vivo* findings, in conjunction with the well documented role of IL-6-STAT3 signalling in MDD, suggest that STAT3 signalling is a convergent target of negative symptomatology in both SCZ and MDD. Interestingly there seem to be different relative contributions of the two STAT3 activation sites, pY705 and pS727, in each of the diseases. This raises the possibility that different parallel pathways converge on STAT3 in MDD and SCZ respectively. Thus further elucidation of the relative upstream mechanisms of pY705 and pS727 activation, could provide vital insights into the cell signalling aetiology of MDD and SCZ.

The significance of being able to isolate a discrete cell signalling substrate for negative symptoms in schizophrenia is manifold. Firstly negative symptoms are notoriously difficult to ameliorate using current medications[16,292–294]. For example a recent meta-analysis on the comparative efficacy and tolerability of major antipsychotic medications excluded patients with predominant negative symptoms altogether[17]. Thus STAT3 (pY705) could represent a much needed drug target for the development of a novel drug series which specifically targets negative symptoms. To this end several mechanistically distinct potential STAT3 inhibitors have recently been described in the context of drug discovery including small molecule dimerization disruptors (SMDDs), tyrosine kinase inhibitors (TKis), decoy oligodeoxynucleotides (ODNs) and protein tyrosine phosphatase (PTP) inducers. There are over 40 compounds or biological molecules which are currently under investigation as potential STAT3 targeted therapies[267]. Many of these derive from natural products such as sanguarine (*Sanguinaria canadensis*- 'blood root'), berbamine (*Berberis amurensis*), resveratrol (*Vitis vinifera*), honokiol *(Magnolia officinalis)*, withaferin A (*Withania somnifera*) or curcumin (*Curcuma longa*). Notably the latter two compounds, which are STAT3 phosphorylation inhibitors, are in early stage (phase I/II) clinical trials for schizophrenia[267]. FDA approved medications which are phosphorylation inhibitors of other STAT family proteins, including pravastatin (STAT1) and pimozide (STAT5), and are also in clinical trials for schizophrenia ranging from phase II-IV[267]. Interestingly a decreased STAT5 (pY694) phosphorylation response to TG emerged specifically following clinical olanzapine treatment in the AI study, supporting the validity of this target. Furthermore the tetracycline antibiotic minocycline, which directly reduces STAT3 (pY705) phosphorylation, has been shown to mitigate microglial activation and improve negative symptoms when administered early in the course of schizophrenia[295–298]. Taken together this evidence suggests that there is substantial scope for novel drug discovery and drug repurposing targeted towards STAT isotypes for the amelioration of negative symptoms in schizophrenia. Moreover subgroups of patients with predominant negative symptoms often have worse prognoses and lesser responses to treatment[16,293,299]. Thus being able to identify these individuals early in the course of the disease could allow the best available treatments for negative symptoms to be applied

in time to avoid many of the deleterious effects on neuronal function (described earlier). Finally, the implication of STAT3 in stress susceptibility could mean that it provides a valuable prophylactic drug target for prodromal conversion to schizophrenia.

4.3.14 SRC & FUNCTIONAL INTEGRATION OF NODES NORMALIZED IN THE AI STUDY

Despite being one of the four nodes which was associated to schizophrenia and normalized by antipsychotic therapy in the AI study **(Table 4.2, Fig. 4.7c)**, the response to forskolin at Src (pY418) in T cells was not replicated in schizophrenia patients relative to controls in the DD study. Instead Src (pY418) was altered in B cells in response to staurosporine in the DD study **(Table 4.6)**. The heterogeneity of the response at this epitope combined with the higher overall significance of the TG-PLC-$\gamma 1$ response meant that it was not selected for the drug discovery phase of the study. However its identification raises the intriguing concept that the four normalized epitopes (Akt1, STAT3 (pY705), Src (pY418) and PLC-$\gamma 1$) might interact mechanistically. Src has been reported to activate Akt1, STAT3 and PLC-$\gamma 1$ in cell signalling processes which are central to schizophrenia[235,236,271,300]. For example inhibition of Src prevents phosphorylation of Akt and downstream GSK-3β in response to D2 and D3 receptor stimulation in Chinese hamster ovary (CHO) cells[300]. At glutamatergic synapses coincident calcium waves, mediated by NMDA receptors and L-type calcium channels, cause Src to activate STAT3, at pY705 (via Jak3) and pS727 (via Akt), hence contributing to neuronal excitation-transcription coupling, a process in which PLC-$\gamma 1$ has a well-documented role[235,271,301]. Interestingly STAT3 is one of the few transcription factors known to regulate Akt1 expression suggesting a feedback loop between these two proteins[302]. Recently Src has also been proposed as a mediator of neuregulin 1β-ErbB4 (NRG1β-ErbB4) inhibition of NMDA receptor transduction, therefore potentially implicating Src and its transcription coupling partners (Akt, STAT3 and PLC-$\gamma 1$) in NMDA receptor hypofunction[239,303]. Finally many of the main interactions of STAT3 and PLC-$\gamma 1$ with other proteins are mediated by their respective Src-homology (SH) domains[236,267]. This might explain reciprocal interactions between PLC-$\gamma 1$, STAT3 and Src, in addition to interactions with their common regulatory partners such as SHP-1 and SHP-2[304–309]. While there is considerable evidence for the interaction of these reversal nodes it is notable that in the AI study no single ligand induced changes in all of the four reversal epitopes simultaneously. Thus it seems that they are not obligate signalling partners in the canonical sense. Instead they are best viewed as disease-associated stress points within the cell signalling network that can contribute under varying physiological conditions to an integrated phenotype.

4.3.15 *EX VIVO* TREATMENT RESPONSE PREDICTION

The previous chapter highlighted the kinetic interaction of several neuropsychiatric medications with emergent drug targets in T cells from healthy donors following a 1-30 min drug incubation protocol *ex vivo* (TC study). However one of the major pending questions was whether these acute interactions would be reproduced in patient samples following chronic clinical drug administration. The AI study allowed this to be assessed with reference to six weeks of clinical olanzapine treatment. Among the cell signalling nodes changed after six weeks of olanzapine treatment *in vivo* (0.6% of the total nodes assayed; **Fig. 4.5b**), 27% of these involved epitopes which were altered by 30 min olanzapine incubation *ex vivo* in either CTRL or SCZ T0 groups (Src (pY418), PKC-α, CrkL (pY207), PKA RII-α (pS99) and Akt1, **Fig. 4.9**). This enrichment suggests that many of the clinical effects of olanzapine treatment are observable following acute *ex vivo* administration. Moreover the fact that no *ex vivo* effects of olanzapine were observed at the aforementioned epitopes in the SCZ T6 group suggests that *in vivo* administration of the drug potentially saturated the response capacity of these epitopes to olanzapine.

Notably changes in the acute *ex vivo* responses of PKA RII-α (pS99) and CrkL (pY207) to olanzapine were correlated to changes in positive (δPANSSp) and negative (δPANSSn) symptoms respectively across the clinical treatment course. The fact that these two epitopes were the only ones to display multiple alterations in ligand responses in the SCZ T0 vs. T6 comparison, suggests that epitopes which interact with olanzapine *ex vivo* are also those which show more profoundly altered functionality following treatment *in vivo.* This raises the exciting possibility, pending correlation of symptom changes (δPANSS) in larger patient cohorts, that these acute *ex vivo* olanzapine responses (30 min) could predict clinical response to chronic olanzapine treatment with positive and negative symptom subscale resolution. The implication of PKA RII-α (pS99) as a potential response prediction epitope is consistent with its role as a downstream signalling substrate (via cAMP) of D1-5 receptors in the CNS, which are known to mediate both clinical efficacy and extrapyramidal side effects of antipsychotic treatment. Conversely the implication of CrkL (pY207) is important as this protein has been strongly associated with schizophrenia via multiple genetic analyses (described in **Chapter 3**), but has not yet been implicated as a therapeutic target of current antipsychotic drugs. Moreover it was the only epitope to display a kinetic activation profile in response to both typical and atypical antipsychotic drug classes **(Chapter 3 Fig. 3.12)** in the TC study**.** Taken together these findings suggest that CrkL (pY207) has strong potential as a treatment predictor across antipsychotic drug classes and also as a novel drug target.

CHAPTER 5

DRUG REPURPOSING FOR SCHIZOPHRENIA

5.1 INTRODUCTION

To determine whether the putative drug targets discovered in schizophrenia patient PBMCs relative to controls in the clinical stages of the project could be translated into viable drug candidates, we modelled the abnormal cell signalling response to thapsigargin (TG) at PLC-$\gamma 1$ **(Chapter 4 Fig. 4.7d)** in control PBMCs and screened the extended FDA approved drug library for compounds capable of normalizing this response (FDA library screening- 'FDA'; **Chapter 1 Fig. 1.3e)**. As the response to TG at PLC-$\gamma 1$ was attenuated in drug-naive schizophrenia patients and restored following the clinical antipsychotic treatment course (six weeks) with olanzapine we sought to identify compounds capable of recapitulating this *in vivo* effect, in other words potentiating the response to TG at PLC-$\gamma 1$. Moreover as no alteration in basal expression was observed for PLC-$\gamma 1$ between schizophrenia patients and controls or following antipsychotic intervention *in vivo*, we further defined the desired compound profile as drugs which potentiated the PLC-$\gamma 1$ response only in the presence of TG and were inactive at this epitope by themselves **(Fig. 5.1)**. Thus the desired profile is broadly analogous to that of an allosteric modulator, a compound capable of modifying the response selectively in the presence of the primary ligand, by binding to an alternative site outside the orthosteric activation site, but which by itself is inactive[310,311]. This term is usually used to define alternative sites on the same protein as the primary orthosteric ligand binding domain. However as the molecular target responsible for the altered response in schizophrenia is unknown, we extend this concept to include ligands which selectively enhance the activity of TG via potentially alternative mechanisms ('functional allosteric modulation').

5.2 RESULTS

5.2.1 DRUG DISCOVERY AND REPURPOSING FOR SCHIZOPHRENIA

The FDA approved compound library (786 compounds) was extended to include experimental drugs with putative activity against CNS targets, nutraceuticals and positive controls related to the TG-PLC-γ1 response (160 compounds) **(Chapter 2 Table 2.2).** We preincubated PBMCs from control donors (n=6-12) with the extended FDA compound library (compounds at 20 μM final concentration unless stated otherwise and negative controls DMSO 0.2%) for 45min. Subsequently we stimulated the cells with TG 0.5 μM (circa half maximal concentration (EC_{50}) **Fig. 5.2**) or vehicle (stRPMI DMSO 0.01%) for 30 min. From this point onwards the samples were processed in the same way as the clinical samples in previous chapters with two exceptions. First the cells were barcoded with four concentrations of DL800. This allowed stimulant and vehicle wells with the same drug to be multiplexed for simultaneous staining hence removing the potentially confounding variation in cell counts between wells. Second the cells were stained only with CD3-APC and PLC-γ1 PE. This allowed the spectral isolation of the target response at PLC-γ1 **(Fig. 5.3) (Chapter 1 Fig. 1.4d)**. Similar to the statistical test used to define the aberrant clinical phenotype, which identified interactions between clinical group status and stimulant response, the test used to identify significant screening compounds identified interactions between compound status (negative control or compound) and TG stimulant response. Subsequently we prioritized the significant compounds in terms of the ones which displayed a selective potentiation profile (i.e. compounds which were inactive alone but potentiated the PLC-γ1 response selectively in the presence of TG) **(Fig. 5.1).** These potentially selective compounds were explored using an extended 14-point two-fold dose response of the compound (0.024-200 μM) prepared from a fresh stock in vehicle and TG (0.5 μM) conditions. Members of the same therapeutic class as the candidate compounds (e.g. Ca channel blockers, corticosteroids, antibiotics and antipsychotic medications) were included at this stage to explore potential structure activity relationships. The therapeutic window of these compounds was determined in terms of the dose range of each compound which induced a PLC-γ1 response selectively in the presence of TG relative to vehicle. Finally the compounds which displayed a putative therapeutic window for selective potentiation were ranked in terms of their potency to shift the EC_{50} of TG-PLC-γ1 dose response curves.

5.2.2 EXTENDED FDA LIBRARY SCREENING HITS

A total of 103 compounds from the extended FDA drug library were found to interact with the TG-PLC-γ1 response ($p<0.05$) (**Fig. 5.4b, d left panel**). The top hits ($p<0.0001$, n=11) were enriched for positive controls (36% of hits; including calyculin, TG, staurosporine and PMA/ionomycin) and calcium channel blockers (36% of hits; including NNC 55-0396, penfluridol, loperamide and nisoldipine) **(Fig. 5.5)**. This is consistent with the established functions of the positive controls as broad spectrum cell signalling modulators and the calcium channel blockers as mechanistic probes of calcium flux alterations. Furthermore the fact that TG (1 μM) was capable of further potentiating the PLC-γ1 response confirms that the background stimulation of TG (0.5 μM) was still within the dynamic range of the PLC-γ1 response. Therefore the potentiation effects of other compounds could be accurately determined. Other classes of compounds which were enriched among the 103 hits ($p<0.05$) included cephalosporin antibiotics, steroids and steroid derivatives, retinoids and antipsychotic medications. Notable other hits included selective inhibitors for Akt1 (GSK 690693), GSK-3β (TC-G 24), mTORC1 (Everolimus) and STAT3 (cucurbitacin I) and three instances of sphingosine-1-phosphate receptor modulator (fingolimod) from different sources. The Z' factor value, which accounts for the reproducibility and dynamic range of the assay[134], was 0.3 for TG (1 μM).

5.2.3 SELECTIVE POTENTIATION OF THE TG-PLC-γ1 RESPONSE

To refine the hits which interacted with the TG-PLC-γ1 response we identified a subset of 22 compounds which displayed the selective potentiation profile described above **(Fig. 5.4b; Table 5.1).** These included nisoldipine as the top hit ($p=0.0002$; 3.1-fold potentiation) and olanzapine ($p=0.0087$, ranked 7th; 2.9 fold potentiation) which was used clinically in the antipsychotic intervention study **(Chapter 4)**. The hits were also enriched for cephalosporin antibiotics (23%), corticosteroids (18%) and retinoids (9%). Eight of the initial 22 hits were validated in preliminary dose response testing. These compounds were carried through to the extended dose response stage, alongside 14 other members of the same therapeutic classes which were included to explore potential structure activity relationships (**Fig. 5.6**). These therapeutic classes included calcium channel blockers (nimodipine, nilvadipine, nisoldipine, nifedipine, nicardipine, amlodipine, verampil and NNC 55-0396), antipsychotic medications (penfluridol, haloperidol, risperidone, aripiprazole, olanzapine and clozapine), corticosteroids (fluorometholone, methylprednisolone, loteprednol and flunisolide) and antibiotics (cefixime, cefoxitin, gemifloxacin and capreomycin). The compounds loperamide and ibutilide, which independently showed the desired profile in

preliminary dose response testing, were also included in extended dose response stage while the retinoid compound class was not pursued due to clinical contraindications in schizophrenia.

In the extended dose response stage (**Fig. 5.4d centre panel**; 14-point two-fold dose response of the compound (0.024-200 μM) in vehicle and TG (0.5 μM) conditions) we identified 10 compounds which showed selective potentiation of the PLC-γ1 response in the presence of TG, at concentrations below those which were active in the vehicle condition alone, indicating a potential therapeutic window (1-25 μM, depending on the compound; **Fig. 5.7**). The selective TG-PLC-γ1 potentiation profile of olanzapine was also shared by other atypical antipsychotic drugs (risperidone, aripiprazole and clozapine), but not typical antipsychotics (haloperidol and penfluridol). Selective potentiation was observed also for 1,4-dihydropyridine (DHP) L-type calcium channel blockers with extended ester substitutions at the 3-position of the pyridine ring (nimodipine, nisoldipine and nicardipine), but not for the other members of the DHP class (no effect for nilvadipine; potentiation without therapeutic window for nifedipine; opposing effects for amlodipine), the phenylalkylamine L-type calcium channel blocker (verapamil) or highly specific T-type calcium channel blockers (NNC 55-0396 and penfluridol; **Fig. 5.8**). The last three compounds which showed the selective potentiation profile were the corticosteroids, methylprednisolone and flunisolide, and the potassium channel blocker, ibutilide.

Finally, we ranked the compounds which showed the selective potentiation profile in terms of their potency to shift the half maximal effective concentration (EC_{50}) of TG-PLC-γ1 dose response curves **(Fig. 5.4d right panel)**. Consistent with the previous results, all 10 drugs decreased the EC_{50} of the TG-PLC-γ1 response compared to the vehicle condition (**Fig. 5.4c**). The second-generation atypical antipsychotics displayed a rank order of potency ranging from risperidone (EC_{50}=223 nM) to aripiprazole (EC_{50}=233 nM), olanzapine (EC_{50}=270 nM) and clozapine (EC_{50}=311 nM). Furthermore, three drugs, namely nicardipine (EC_{50}=151 nM), nisoldipine (EC_{50}=168 nM) and methylprednisolone (EC_{50}=200 nM), showed stronger potentiation of the response than any of the measured antipsychotic medications. The effect of ibutilide (EC_{50}=258 nM), flunisolide (EC_{50}=286 nM) and nimodipine (EC_{50}=290 nM) was within the range of the atypical antipsychotic medications. These results demonstrate the potential of the *ex vivo* platform to stratify current schizophrenia medications, in terms of their ability to ameliorate disease-associated cellular responses, and moreover identify novel drug indications (nicardipine, nisoldipine and methylprednisolone) with putative enhanced therapeutic potency.

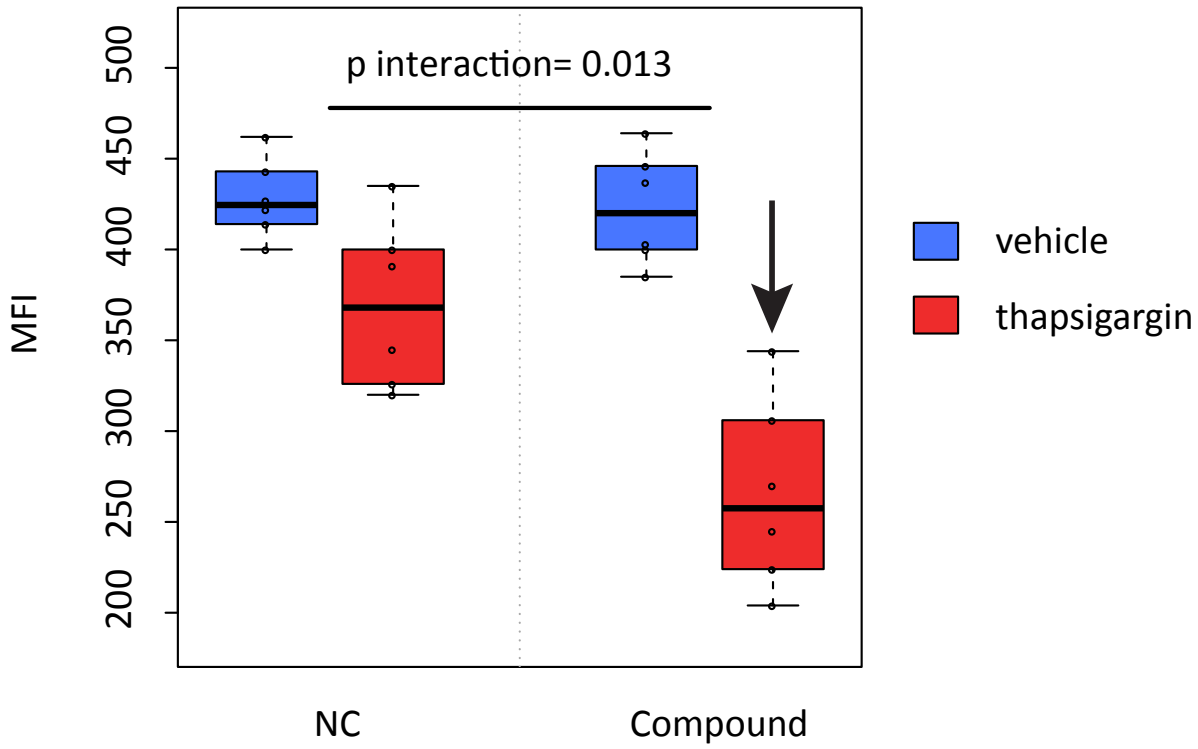

Figure 5.1 Selective potentiation of PLC–γ1 response in the presence of thapsigargin (TG). Compounds from the extended US Food and Drug Administration (FDA)-approved library were initially identified based on their interaction with the response to TG at PLC–γ1 independently of the direction of change. Subsequently these hits were refined to compounds which showed the desired directionality (decrease in PLC–γ1) specifically in the TG condition and were not active (at the concentration screened) in the vehicle condition. In other words these compounds showed no intrinsic activity but were capable of potentiating the PLC–γ1 response when coadministered with TG. Figure shows a representative selective potentiation compound (PBMC samples n=6). Compounds were at 20 μM final concentration unless otherwise stated in DMSO 0.2%. Negative control (NC) = DMSO 0.2%. TG was at 0.5 μM DMSO 0.01%. Vehicle= DMSO 0.01%. MFI = median fluorescence intensity.

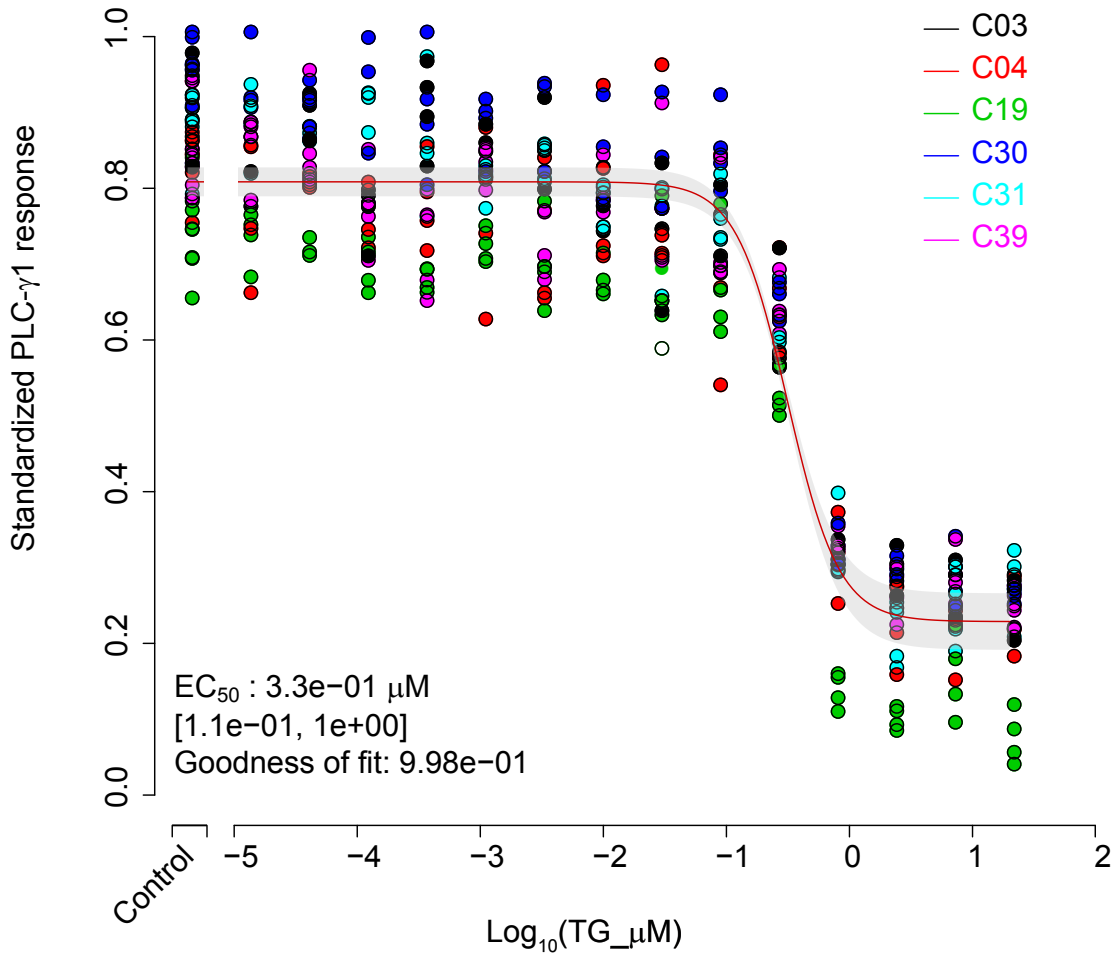

Figure 5.2 Thapsigargin (TG) dose response at phospholipase C PLC- 1. TG provokes a dose-dependent decrease in PLC–γ1 expression. Y axis represents the median fluorescence intensity standardized as a proportion of minimum and maximum values. TG stimulation circa the EC_{50} concentration (0.5 μM) determined from the four-parameter logistic curve (red) was used as a background condition for the extended FDA-approved library screen. Data represents six healthy control (C) peripheral blood mononuclear cell (PBMC) samples coloured by donor.

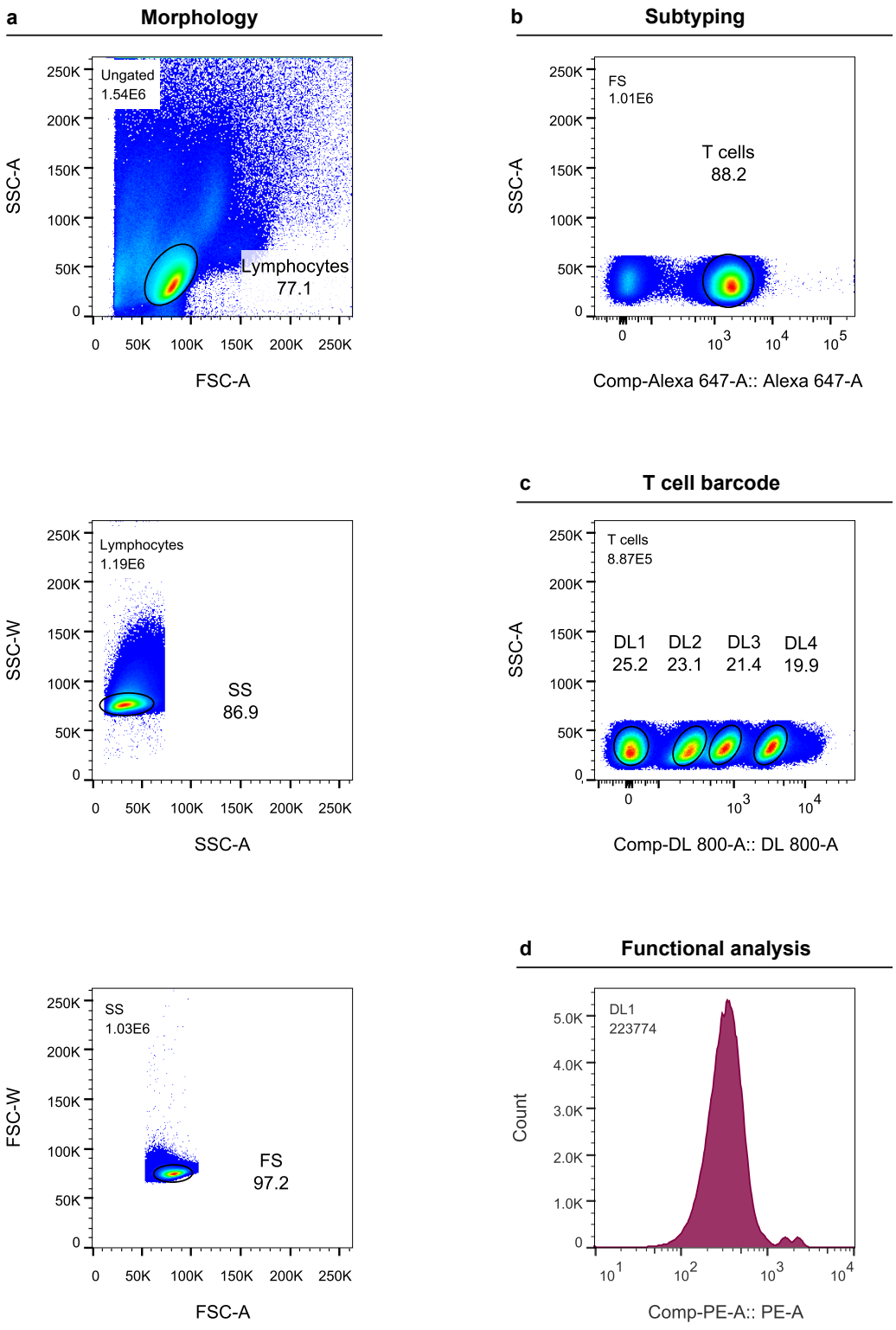

Figure 5.3 Gating strategies for the functional analysis of PLC-γ1 expression in four barcoded T cell populations. (a) Viable cells were gated (FSC-A vs. SSC-A), followed by single cell discrimination (SSC-A vs. SSC-W and FSC-A vs. FSC-W). **(b)** T vs. B lymphocyte cell subtyping using anti-CD3 APC. **(c)** Four populations, each corresponding to a different stimulation condition (TG or vehicle) and compound condition (compound or negative control), were resolved within the T lymphocyte gate following fluorescent cell barcoding using DL 800 (DL 1-4). **(d)** Within each barcoded T cell population functional analysis of intra-cellular signalling epitope PLC–γ1 expression was conducted using anti-human PLC–γ1-PE. Data represents one PBMC sample.

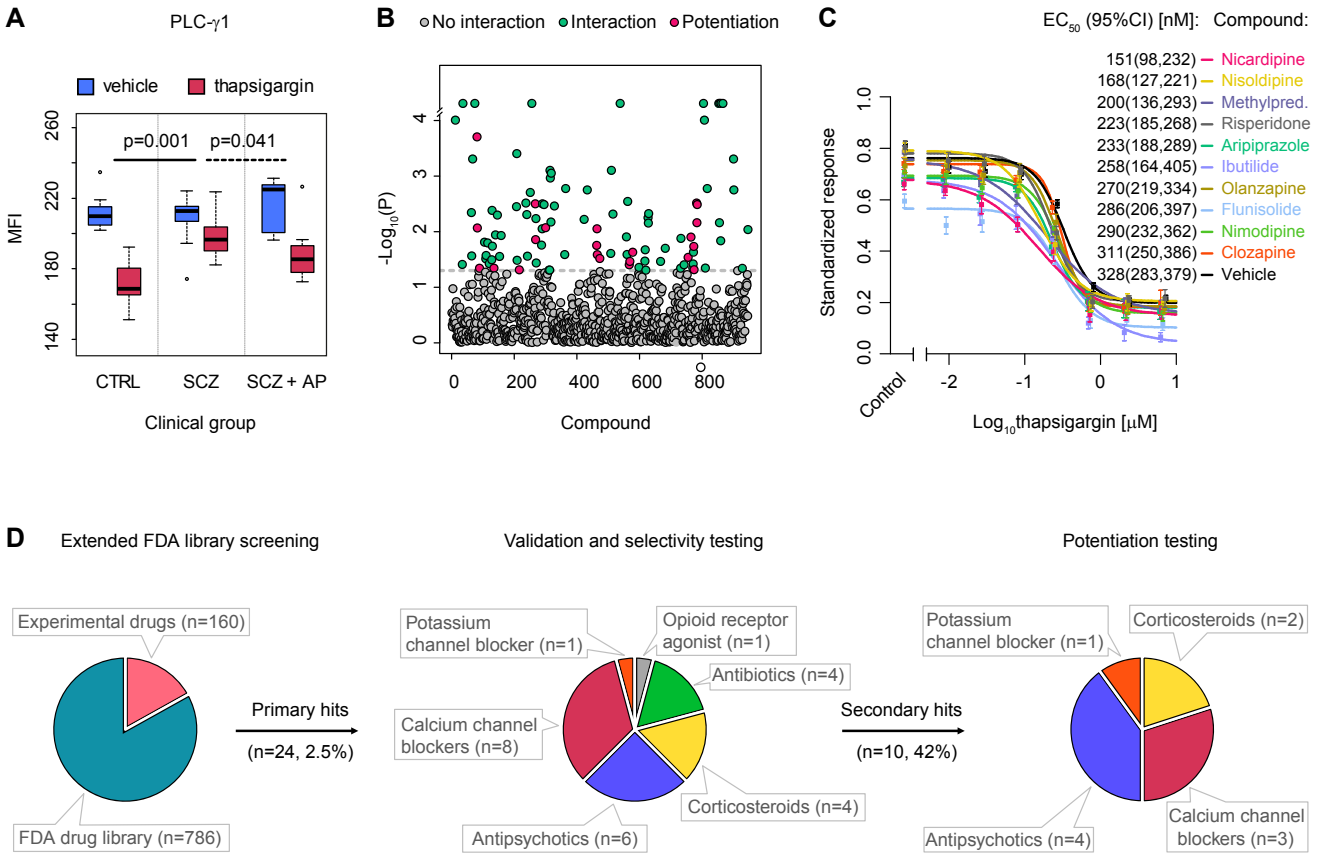

Figure 5.4 Phenotypic drug repurposing based on cellular response. (**A**) Identification of functional cellular drug target. Attenuated response to thapsigargin at phospholipase C (PLC)-γ1 in T cells from drug-naïve schizophrenia (SCZ) patients (p=0.001, two-way ANOVA), relative to healthy controls, was reversed after 6 weeks of clinical treatment with the atypical antipsychotic (AP) drug olanzapine *in vivo* (permuted P=0.041; n=12 healthy controls, n=12 drug-naïve SCZ patients and n=10 SCZ patients after antipsychotic treatment (SCZ+AP)). Box plots show interquartile range with the median (horizontal line) and the minimum and maximum values (whiskers), excluding outliers (dots). MFI - median fluorescence intensity. (**B**) Results of primary drug screen. Permuted P values from thapsigargin-drug interaction testing (two-way ANOVA; n=6-12 healthy PBMC donors) are shown across the combined FDA-approved (n=786) and experimental (n=160) compound libraries. Dashed line represents threshold P value of 0.05. Significant hits are shown in green (n=102) and compounds that additionally showed selective potentiation of the thapsigargin-PLC-γ1 response (post-hoc one-way ANOVA tests; **Fig. 5.1**) are shown in magenta (n=22; **Table 5.1**). (**C**) Ranking of best selective potentiation candidates at 10 μM concentration in terms of EC_{50} shifts in the thapsigargin (TG)-PLC-γ1 dose response curve. Shows mean values from 6 healthy PBMC donors (points) with standard error of the mean (vertical bars) and fitted 4-parameter logistic curves. Y axis represents the MFI standardized as a proportion of minimum and maximum values. Legend shows the EC_{50} values with 95% confidence intervals (CI). Methylprednisolone is abbreviated as Methylpred. (**D**) Distribution of drug classes across repurposing stages. Extended FDA-approved library screening (left) refers to the primary compound screen at a single dose (20 μM unless otherwise specified in **Materials and Methods Table 2.2**) of compound (n=946; panel B). Validation and selectivity testing (centre) refers to dose response titration (24 nM-200 μM) and validation of selective potentiation candidates and structural class relatives (n=24; **Fig. 5.7**; n=6 healthy PBMC donors). Potentiation testing (right) refers to the titration of thapsigargin (12.5 pM-20 μM) in the presence of 10 μM concentration of validated compounds (n=10; panel C). *In vivo* effect of olanzapine (panel A) was reproduced *in vitro* throughout.

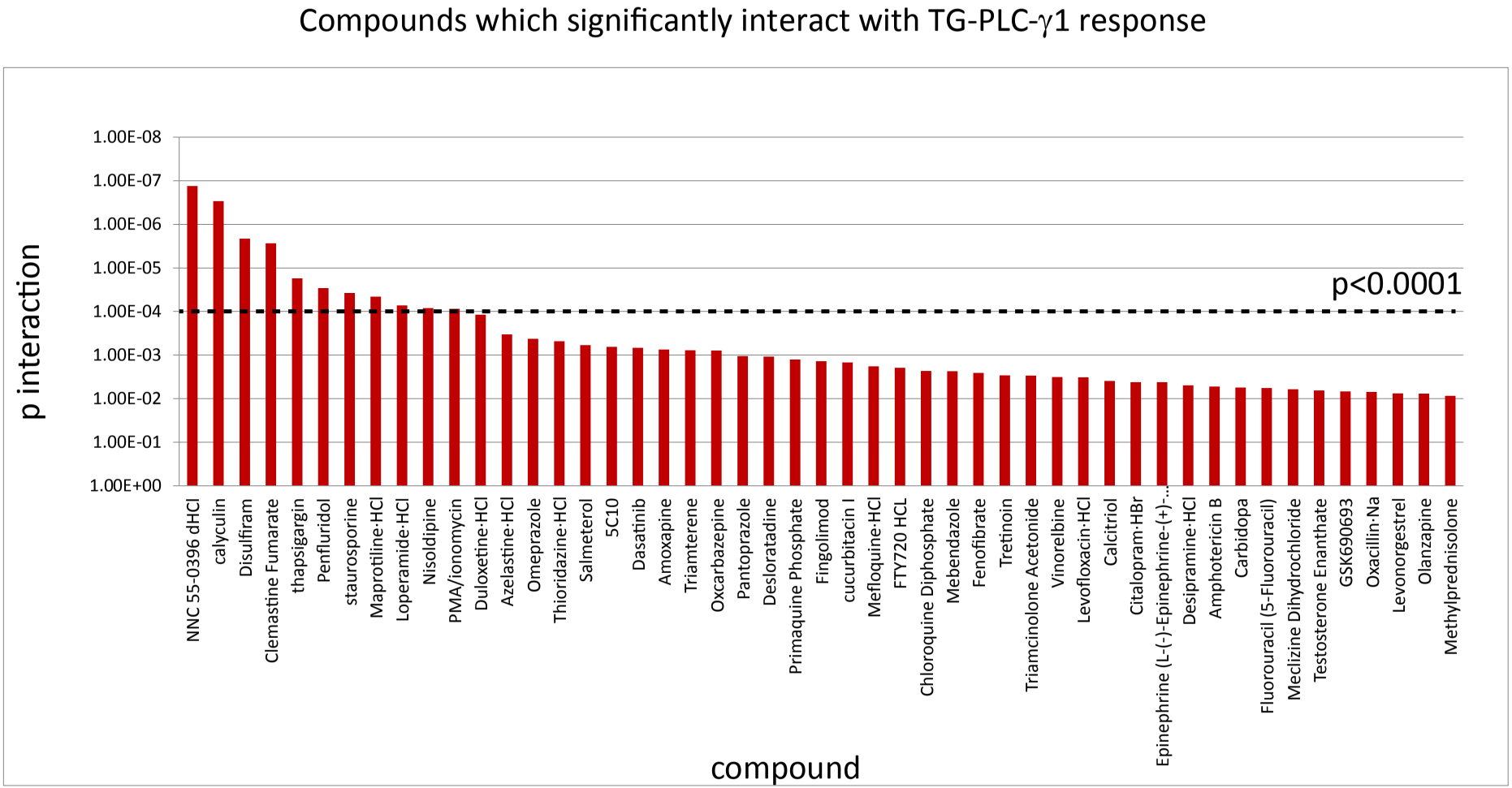

Figure 5.5 Extended FDA-approved library screening compounds which modulate the thapsigargin (TG)-PLC- response. Shows ranked 50 most significant compounds for which a statistical interaction (p interaction<0.05) with the TG-PLC–γ1 response was detected (independent of directionality). Y axis represents interaction p values in inverse order. Hits below p<0.0001 were enriched for positive controls (36% of hits; including calyculin, thapsigargin, staurosporine and PMA/ionomycin) and calcium channel blockers (36% of hits; including NNC 55-0396, penfluridol, loperamide and nisoldipine). Data represents 6-12 PBMC samples per compound.

Compound	n VEH_NC	n VEH_drug	n TG_NC	n TG_drug	p interaction	Potentiation factor	Chemical class
Nisoldipine	12	12	11	11	0.0002	3.1	Dihydropyridine
Tretinoin	6	6	6	6	0.0031	4.1	Retinoid
Fenofibrate	12	12	12	12	0.0032	2.5	Fibrate
Triamterene	6	6	6	6	0.0033	4.1	Thiazide
Triamcinolone Acetonide	6	6	6	6	0.007	4.2	Steroid
Methylprednisolone	12	12	12	12	0.0086	1.5	Steroid
Olanzapine	12	12	11	12	0.0087	2.9	Thienobenzodiazepine
Cefotetan Disodium	6	6	6	6	0.009	2.0	Cephalosporin
Testosterone Enanthate	6	6	6	6	0.0127	2.9	Steroid
Finasteride	12	12	12	12	0.0141	2.5	Steroid
Cefixime	6	6	6	6	0.0179	2.1	Cephalosporin
Tiopronin	6	6	6	6	0.0187	3.6	Thiol
Gemifloxacin	6	6	6	6	0.0238	2.3	Quinolone
Cefoxitin·Na	6	6	6	6	0.0263	2.1	Cephalosporin
Tazarotene	6	6	6	6	0.0294	2.4	Retinoid
Cephalexin Monohydrate	6	6	6	6	0.0308	2.5	Cephalosporin
Fluorometholone	6	6	6	6	0.0348	1.8	Steroid
Flunisolide	6	6	6	6	0.04	1.5	Steroid
Ethacrynic Acid	12	12	12	12	0.046	1.8	Phenoxyacetic acid
Cefepime·HCl Hydrate	12	12	11	12	0.0462	2.6	Cephalosporin
Tirofiban·HCl	6	6	6	6	0.049	3.6	Phenylpropanoic acid
Albendazole	12	12	12	12	0.0493	1.6	Benzimidazole

Table 5.1 Extended (FDA)-approved library screening of compounds which selectively potentiate the PLC-γ1 response in the presence of 0.5 µM thapsigargin (TG). Compounds which significantly interacted with the TG-PLC-γ1 response (*'p interaction'*<0.05, two-way ANOVA; n=102 compounds) were refined to compounds which showed the desired directionality (decrease in PLC-γ1) specifically in the TG condition and were not active in the vehicle (VEH) condition (post-hoc ANOVA tests; n=22 compounds). In other words, these compounds had no intrinsic activity but were capable of potentiating the PLC-γ1 response when co-administered with TG. The compounds are ranked with respect to their p values for interaction. The number ('*n*') of peripheral blood mononuclear cell (PBMC) samples in each comparison group is shown in columns 2-5. *'Potentiation factor'* (calculated as (1 - mean PLC-γ1 MFI in TG-drug condition/mean PLC-γ1 MFI in vehicle-drug condition)/(1 - mean PLC-γ1 MFI in TG-negative control condition/mean PLC-γ1 MFI in vehicle-negative control condition)) represents a factor by which the PLC-γ1 response to TG was enhanced by the drug relative to the untreated condition. Concentration of the compounds is given in Materials and Methods Table 2.2. MFI = median fluorescence intensity.

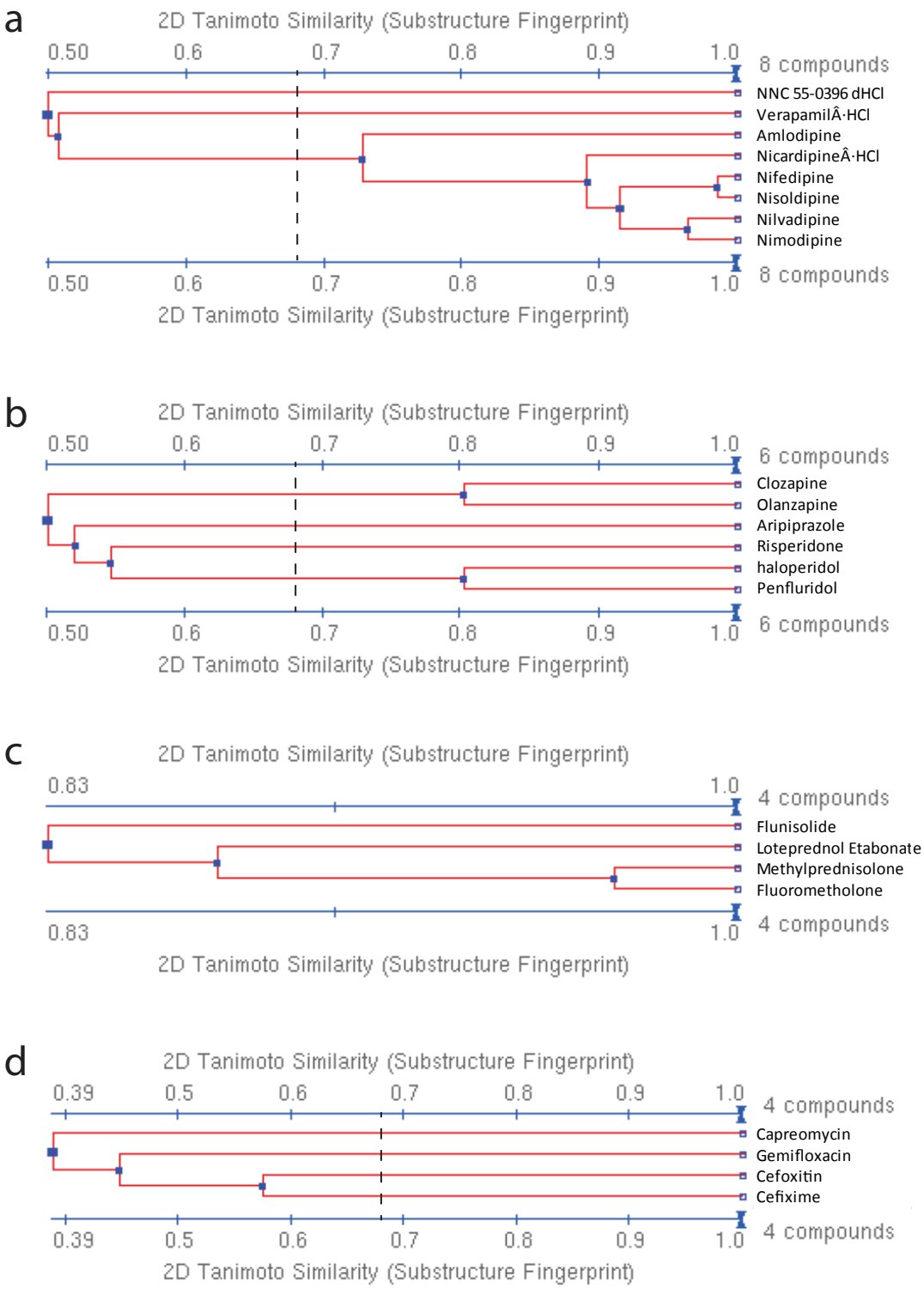

Figure 5.6 Tanimoto structural similarity clustering of (a) calcium channel blocker, (b) antipsychotic, (c) corticosteroid and (d) antibiotic compounds used in dose response validation and selectivity testing at the phospholipase C (PLC)-γ1 target. Compounds are clustered according to 2D structural Tanimoto similarity using the Single Linkage algorithm (PubChem). This grouping hierarchy is used to define the representation order of compounds in each class in **Fig. 5.7**. A 2D similarity score of 0.68 (dashed line) is statistically significant at the 95% confidence interval (Kim et al., 2012).

Nimodipine

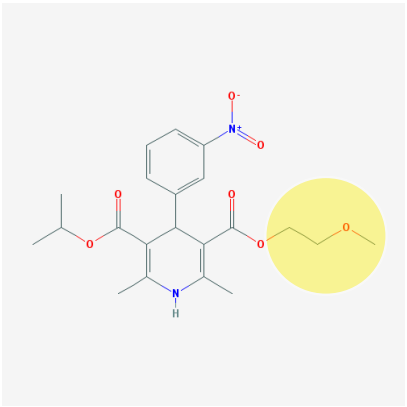

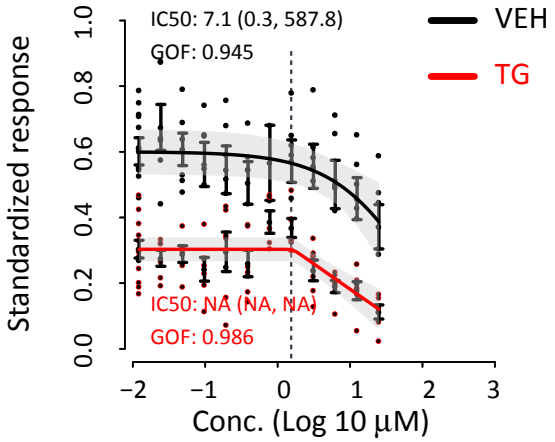

Nilvadipine

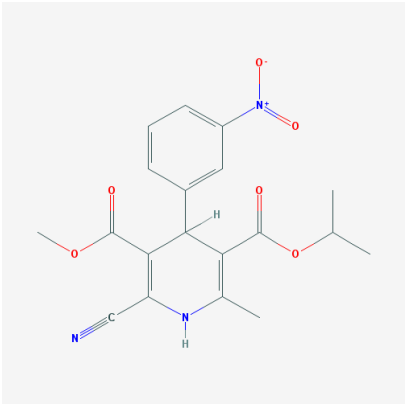

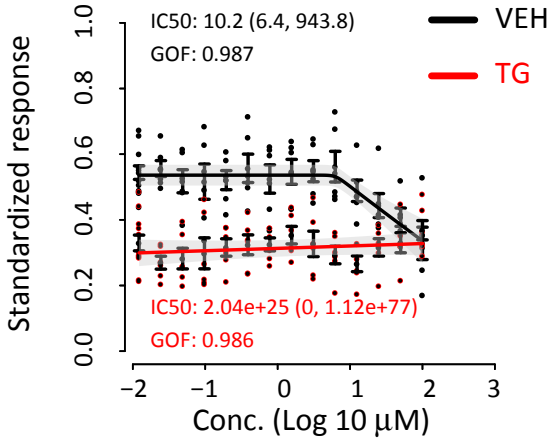

Nisoldipine

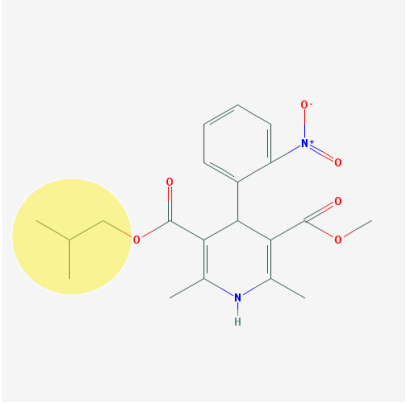

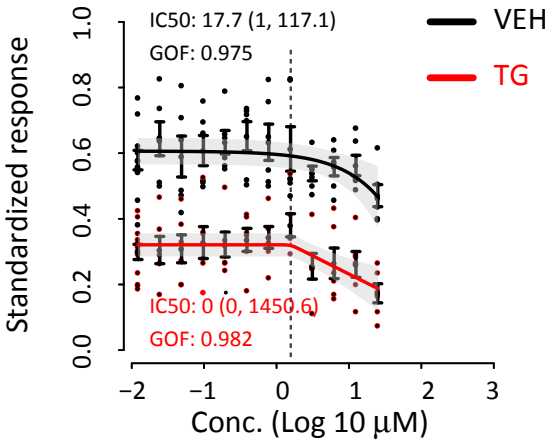

Nifedipine

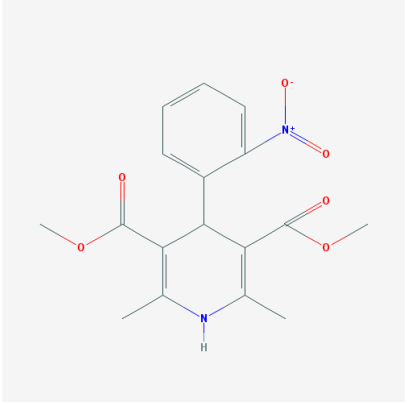

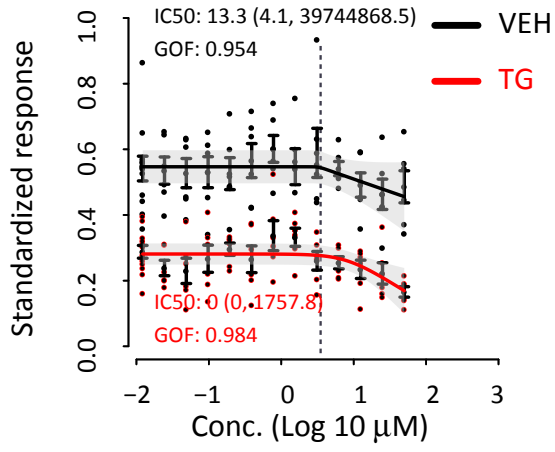

Figure 5.7 Validation and selectivity testing of calcium channel blocker, antipsychotic, corticosteroid, antibiotic and other drug classes at PLC−γ1 continued.

Nicardipine

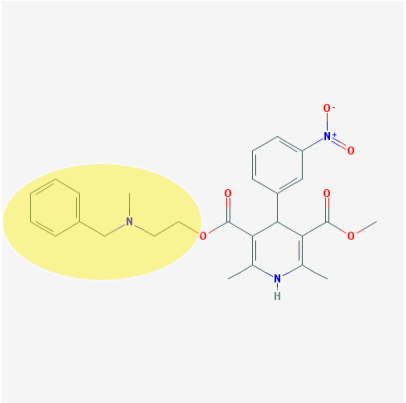

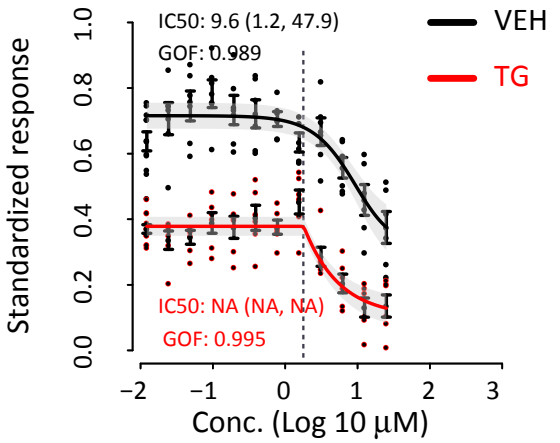

Amlodipine

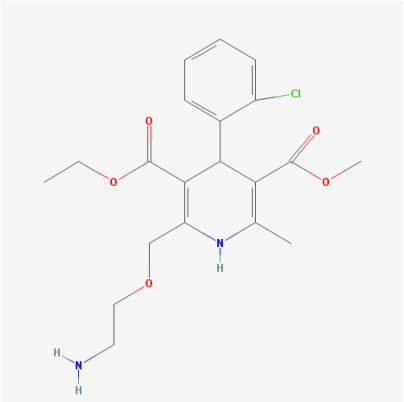

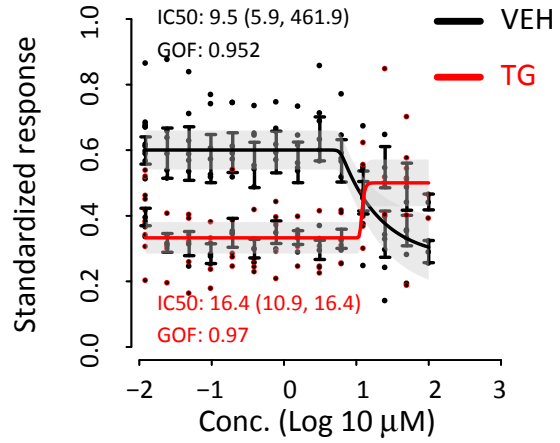

Verapamil

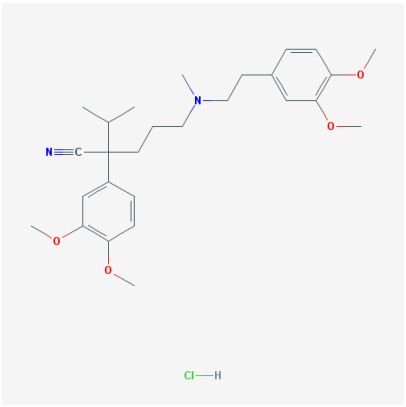

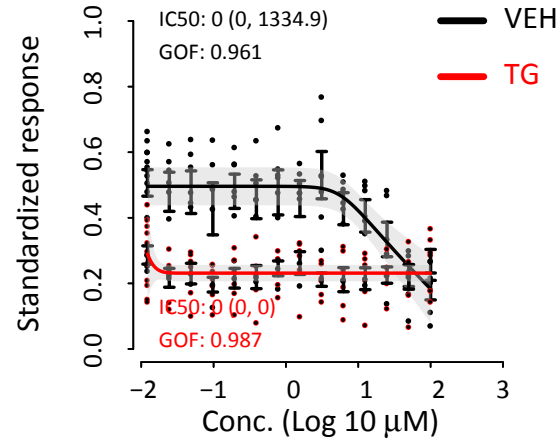

NNC 55−0396

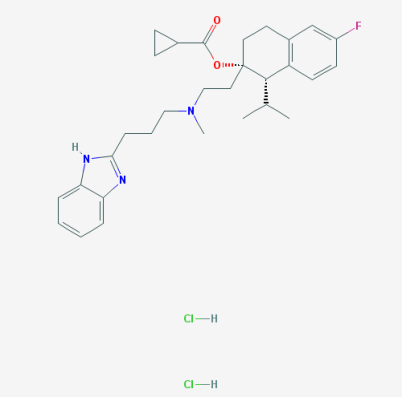

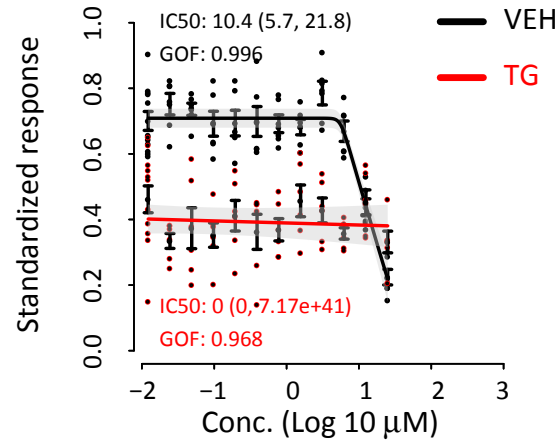

Figure 5.7 Validation and selectivity testing of calcium channel blocker, antipsychotic, corticosteroid, antibiotic and other drug classes at PLC−γ1 continued.

Penfluridol

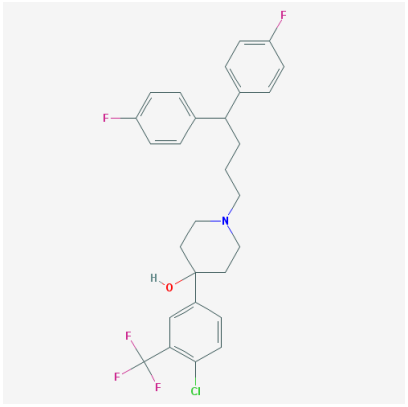

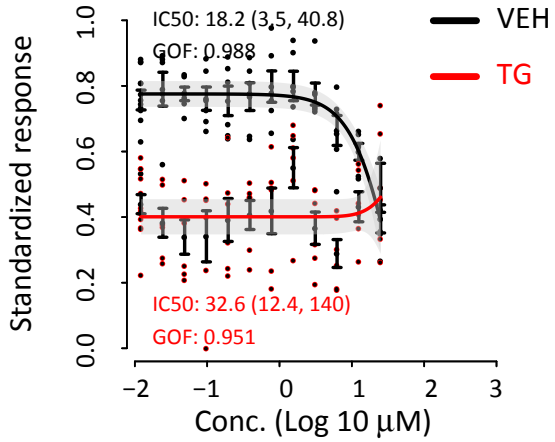

Haloperidol

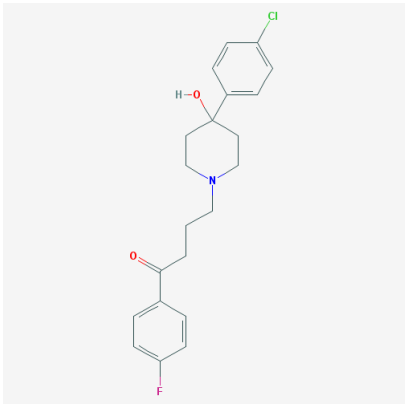

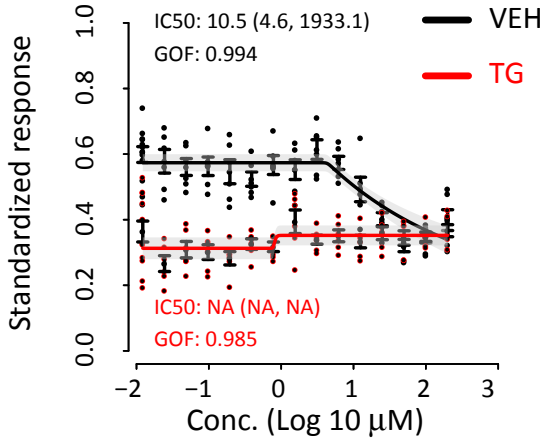

Risperidone

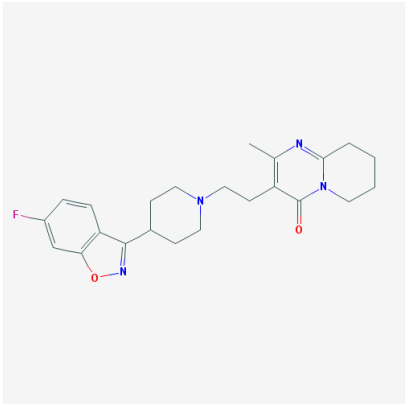

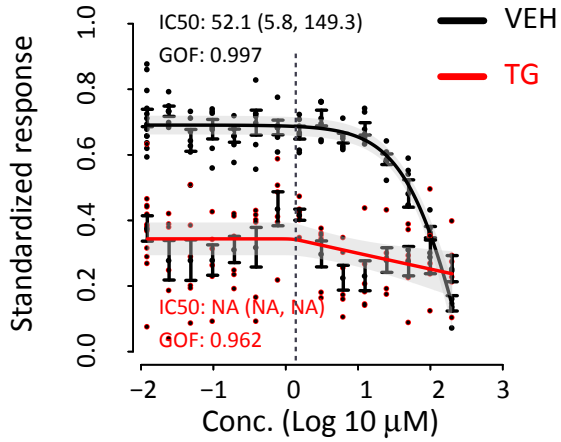

Aripiprazole

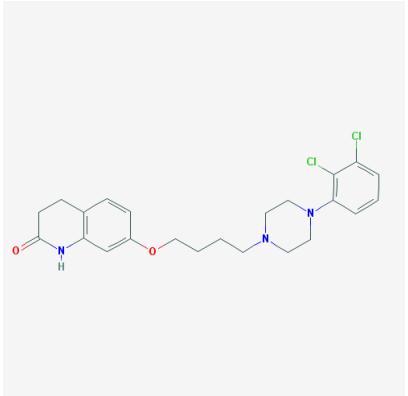

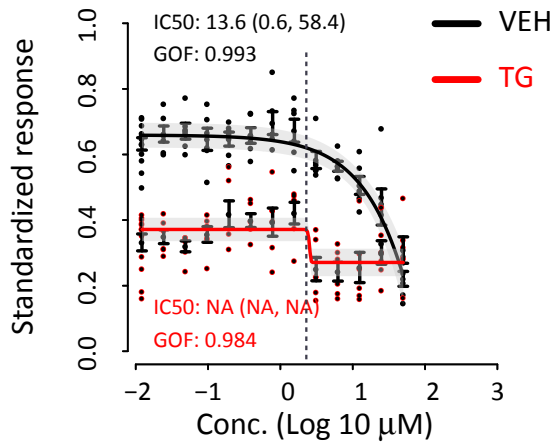

Figure 5.7 Validation and selectivity testing of calcium channel blocker, antipsychotic, corticosteroid, antibiotic and other drug classes at PLC−γ1 continued.

Olanzapine

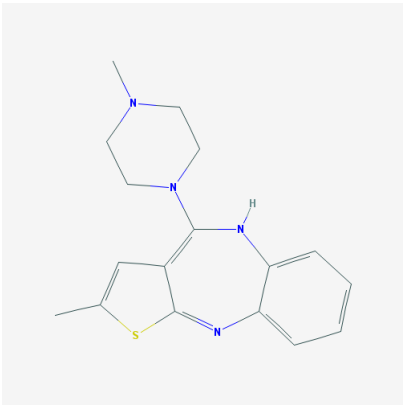

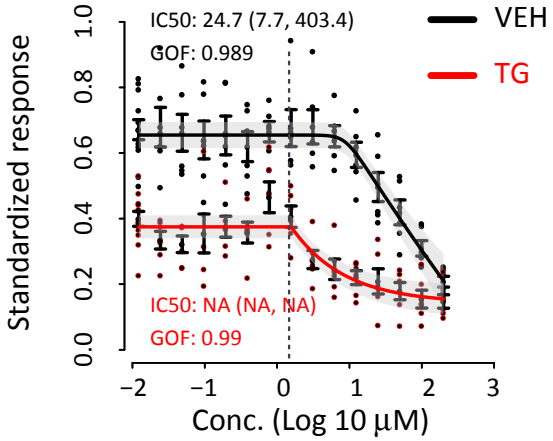

Clozapine

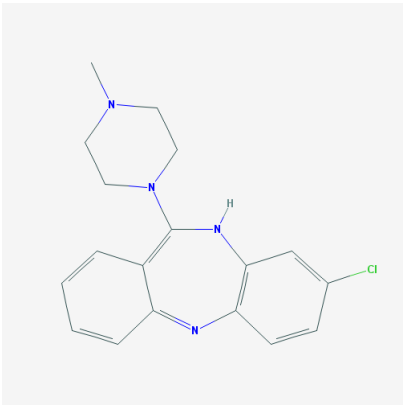

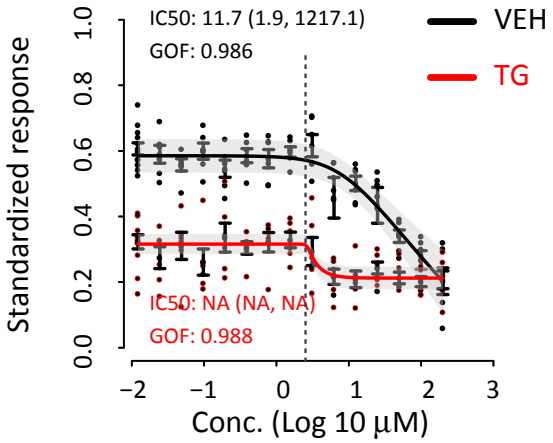

Fluorometholone

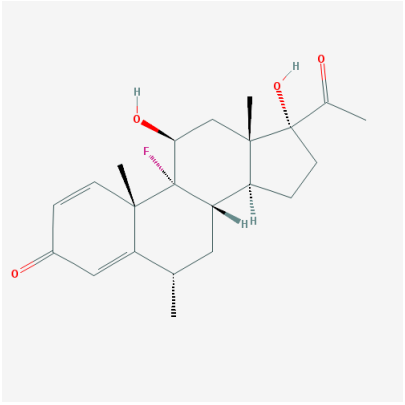

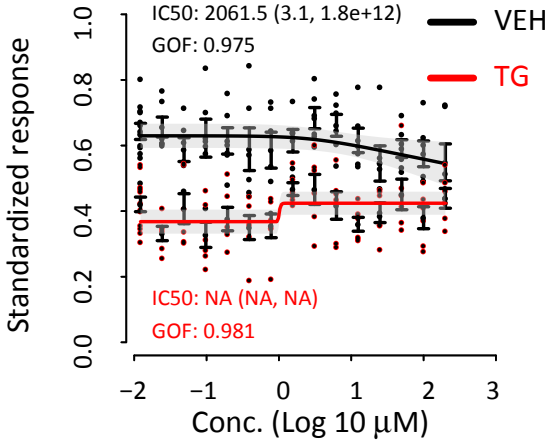

Methylprednisolone

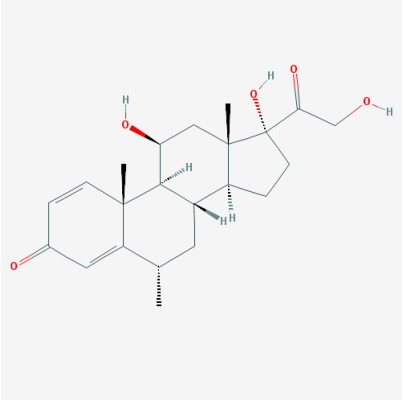

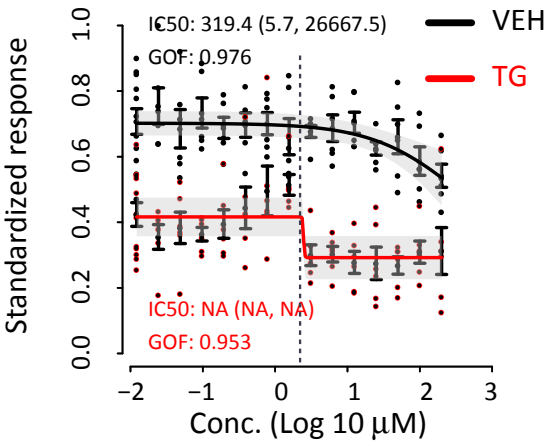

Figure 5.7 Validation and selectivity testing of calcium channel blocker, antipsychotic, corticosteroid, antibiotic and other drug classes at PLC–γ1 continued.

Loteprednol

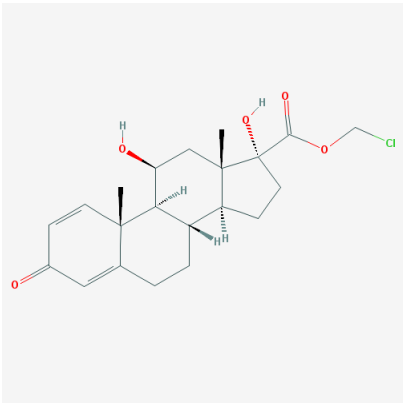

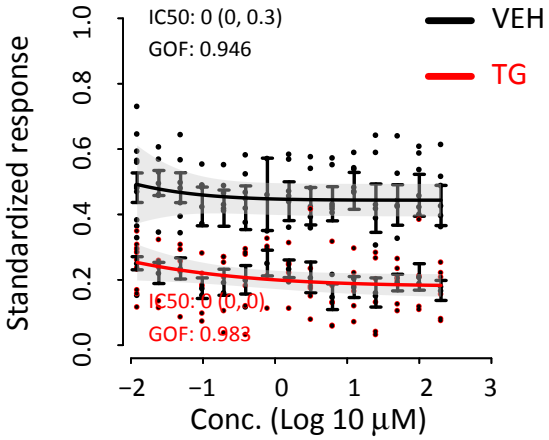

Flunisolide

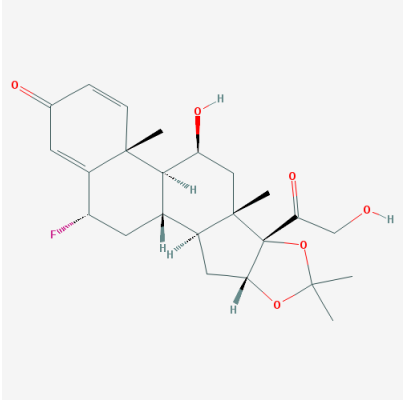

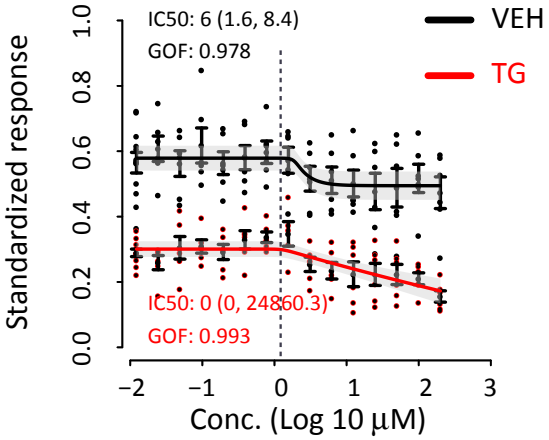

Cefixime

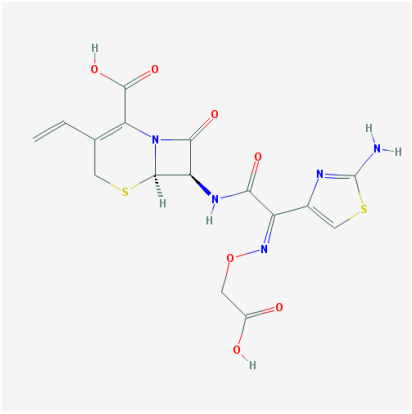

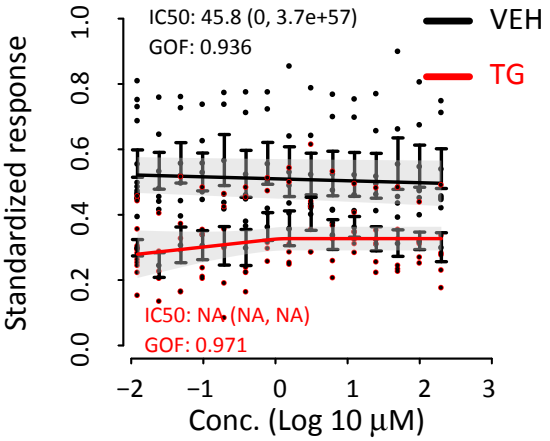

Cefoxitin

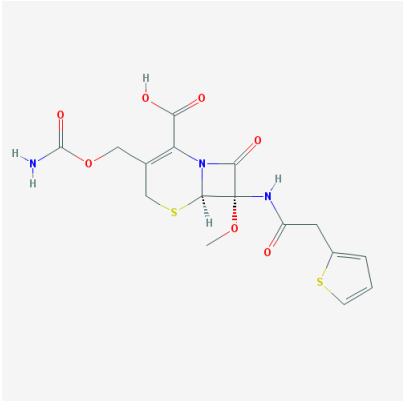

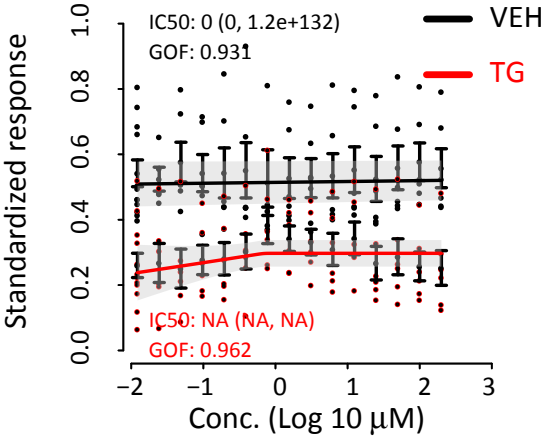

Figure 5.7 Validation and selectivity testing of calcium channel blocker, antipsychotic, corticosteroid, antibiotic and other drug classes at PLC−γ1 continued.

Gemifloxacin

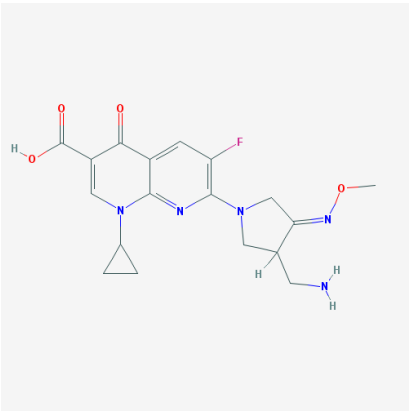

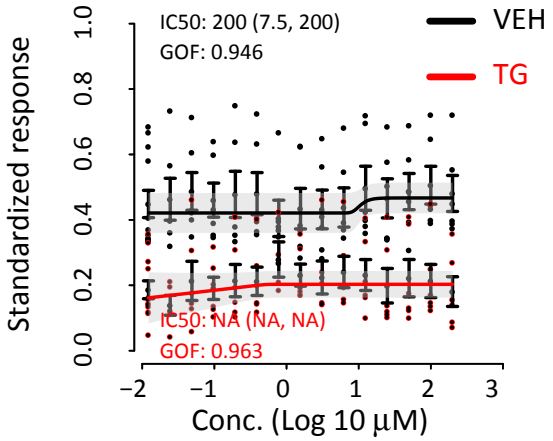

Capreomycin

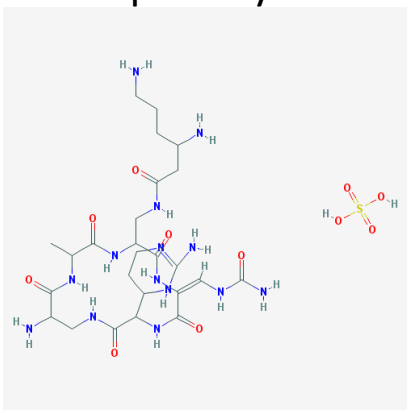

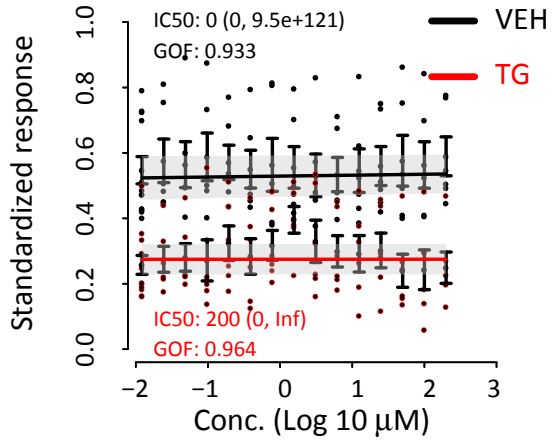

Loperamide

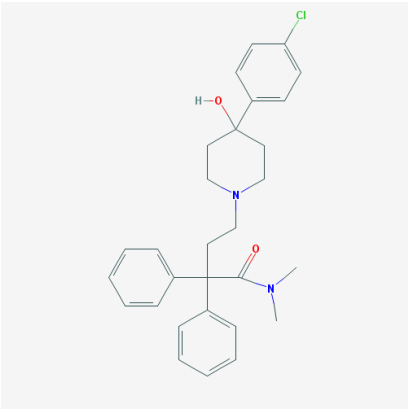

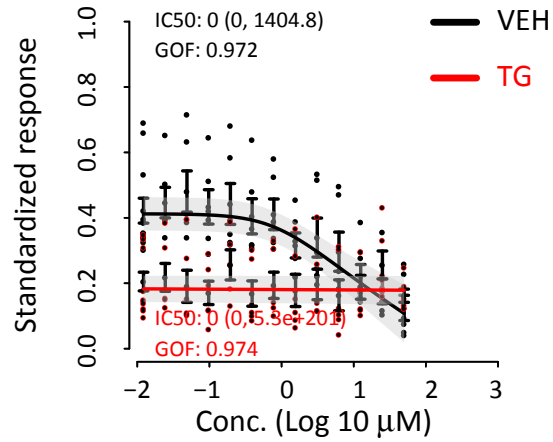

Ibutilide

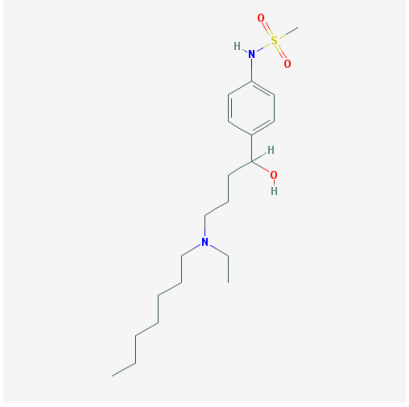

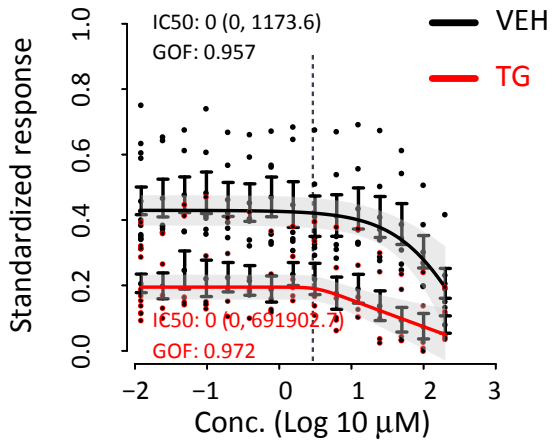

Figure 5.7 Validation and selectivity testing of calcium channel blocker, antipsychotic, corticosteroid, antibiotic and other drug classes at PLC−γ1 continued.

Figure 5.7 Validation and selectivity testing of calcium channel blocker, antipsychotic, corticosteroid, antibiotic and other drug classes at phospholipase C (PLC)–γ1. Compounds for which at least one class member selectively potentiated the PLC-γ1 response in the presence of thapsigargin (TG) in the extended FDA-approved library screen, were explored using a 14-point two-fold dose response of the compound (0.024-200 μM, DMSO 0.2%) in vehicle (VEH; DMSO 0.01%; black colour) and TG (0.5 μM, DMSO 0.01%; red colour) conditions. The lowest plotted concentration represents the negative control condition (DMSO 0.2%). Y axes represent the median fluorescence intensity standardized as a proportion of minimum and maximum values. For compounds which potentiated the PLC-γ1 response in the presence of TG, vertical dashed lines mark the lowest concentration at which potentiation occurred. The difference between the lowest potentiation concentration of the TG curve and the lowest active concentration of the vehicle curve, respectively, represents the putative therapeutic window for selective potentiation in the presence of TG relative to vehicle. Compounds which showed the putative therapeutic window of selective potentiation and were chosen for the final repurposing stage (potentiation testing; **Fig. 5.4c**) are marked with a blue asterisk. Yellow circles indicate structural moieties which differentiate compounds with a selective therapeutic window compared to non-selective or inactive class relatives. Compounds are ordered according to structural similarity within each class using Tanimoto coefficient clustering (**Fig. 5.6**). Data represents 6 peripheral blood mononuclear cell (PBMC) samples (dots), 95% confidence intervals (vertical bars) and fitted 5-parameter logistic curves (lines). GOF = goodness-of-fit; IC50 = half maximal inhibitory concentration. Chemical structures are taken from PubChem.

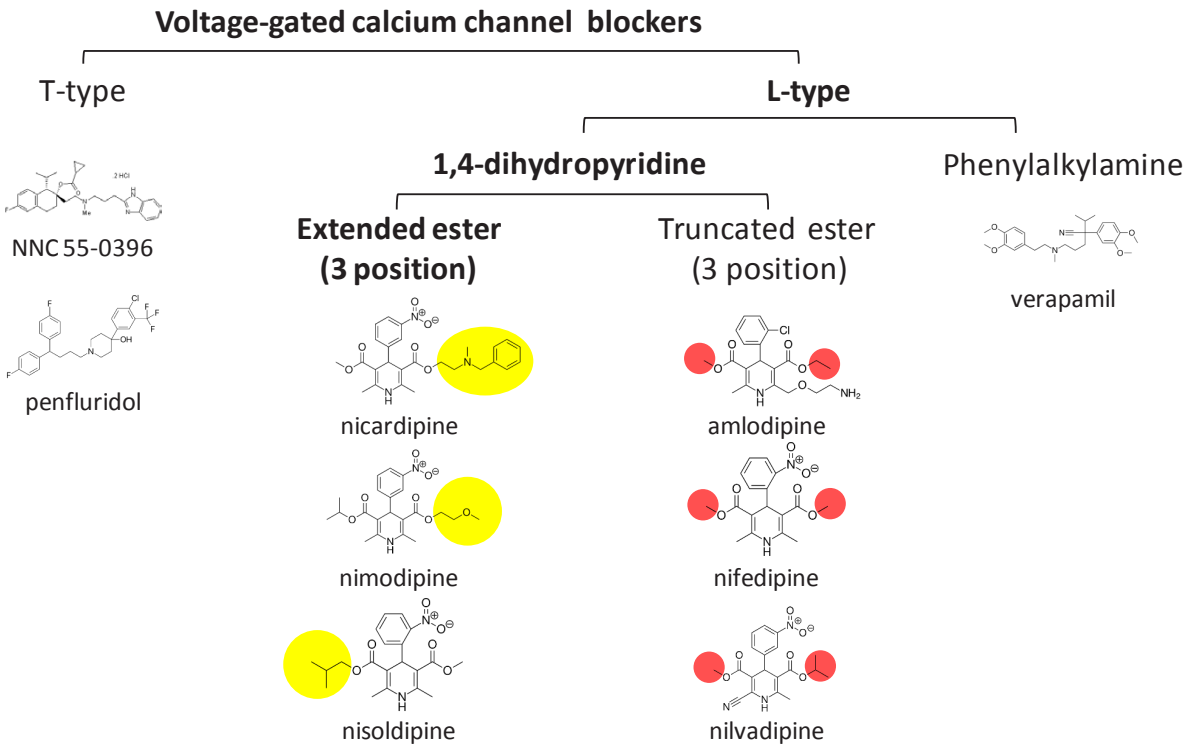

Figure 5.8 Structure-activity classification of voltage-gated calcium channel (Ca_V) blockers with respect to selective potentiation of the TG-PLC-γ1 response. Within the Ca_V blocker compound class, which was tested for selective potentiation of the TG-PLC-γ1 response **(Fig. 5.7)**, a putative therapeutic window of selective potentiation was confined to a subclass of 1,4-dihydropyridine L-type Ca_V blockers with extended (yellow circles), relative to truncated (red circles), ester substitutions at the 3-position of the pyridine ring.

5.3 DISCUSSION

5.3.1 STRUCTURE-ACTIVITY RELATIONSHIPS TO BRIDGE THE KNOWLEDGE GAP BETWEEN GENOMIC SCHIZOPHRENIA RISK LOCI AND CLINICAL EFFICACY

The fact that the initial hits from the extended FDA library screen were reinforced by similar effects across structurally related **(Fig. 5.6)** class members suggests that these compound activities are genuine. Most of the compound classes identified are either currently used to treat schizophrenia (atypical antipsychotics) or have been tested in clinical trials for schizophrenia (calcium channel blockers and corticosteroids)[14,312,313] with the notable exception of ibutilide. Furthermore in the case of the calcium channel blockers these therapeutic compounds interact with drug targets prominently associated with schizophrenia risk loci in GWAS and exome sequencing studies[24,106,107]. This supports the potential of the *ex vivo* functional cytomic pipeline for *de novo* identification of viable therapeutic candidates. However the truly differential feature of this platform is the provision of a tractable cellular model, or 'functional endophenotype', which can predict the relative therapeutic potential of different compound class members based on specific structural moieties. In this way it provides a model for translating generic drug targets implicated by genetic or other molecular profiling methodologies into specific therapeutic pharmacophores. For example L-type calcium channel blockers have been suggested as potential treatments for schizophrenia in light of GWAS and exome sequencing associations of L-type calcium channel subunit genes (e.g. CACNA1C and CACNA1B) with the disease[24,106,107]. However when applied in clinical trials for schizophrenia L-type calcium channel blockers have shown heterogeneous outcomes[312]. For example clinical trials with verampil improved positive symptoms in acute patients but showed no effects in chronic patients. In contrast nilvadipine improved negative symptoms with no change in positive symptoms. Finally nifedipine had no effect in chronic patients but improved cognitive symptoms in patients with tardive dyskinesia[312].

The heterogeneous results obtained from these clinical trials could in part be explained by small sample sizes, difficulties in controlling for clinical variables and divergent brain penetrance of these compounds[312]. However if the model of a selective therapeutic window proposed by the current study **(Fig. 5.7)** is correct it would suggest that these compounds are not the optimal class members for cellular efficacy. Both verampil and nilvadipine lack any potentiation effect on the TG-PLC-γ1 response. Nifedipine does have a potentiation effect but it does not have a therapeutic window for

selective potentiation specifically in the presence of TG. In other words it is equally active in both vehicle and TG conditions. In contrast its close structural relative **(Fig. 5.6)** nisoldipine, which differs only in a longer ester substitution at the 3-position of the pyridine ring **(Fig. 5.8)**, does have a potential selective therapeutic window as observed by the relative gradients of the dose response curves in TG and vehicle conditions and its identification as the most significant compound interaction with the desired profile in the primary compound screen **(Table 5.1)**. Furthermore other DHP class members with extended ester substitutions at the 3-position of the pyridine ring (nimodipine and nicardipine) also showed a selective therapeutic window while DHPs amlodipine and nilvadipine, with truncated ester substitutions at the 3-position, did not (**Fig. 5.8**).

It is notable also that while GWAS data has implicated T-type calcium channels as potential therapeutic targets[24,106], the complete lack of potentiation efficacy observed for highly specific T-type calcium channel blockers NNC 55-0396 and penfluridol would suggest otherwise. Thus it is possible that T-type calcium channels are altered in schizophrenia but that T-type calcium channel blockade is not a viable therapeutic strategy. This is supported by reports of psychotogenic effects and cognitive deficits provoked by clinical administration of T-type calcium channel blocker zonisamide[312]. Taken together these results allow us to refine the generic indications of T- and L-type calcium channel blockade for schizophrenia, suggested by GWAS and exome sequencing analyses, to specifically the DHP class of L-type blockers, by exclusion of verapamil which is a phenylalkylamine, and specifically to those members within the DHP class which have extended ester substitutions at the 3-position of the pyridine ring **(Fig. 5.8)**. Furthermore it provides a testable model of these hypotheses with respect to explaining the variable efficacies of these compounds in clinical trials and ranking the novel drug candidates for enhanced cellular potency relative to established antipsychotic medications **(Fig. 5.4c)**. The potential of lead compounds (nisoldipine and nicardipine) is supported by initial studies of brain penetrance and complete abrogation of aberrant behaviour in phencyclidine animal models of schizophrenia[314,315]. Finally eight out of the ten lead compounds identified in the present study **(Fig. 5.4c)** are consistent with a recent computational analysis of drugs which target the extended protein interactome of schizophrenia genetic risk loci[316]. The remaining two lead compounds (methylprednisolone and flunisolide), which are not mapped to the schizophrenia protein interactome, emphasize the ability of the current approach to access mechanistically diverse potential therapeutic space which is not yet indexed by genomic analyses.

5.3.2 FUNCTIONAL CYTOMIC MODELLING OF COMPOUNDS WHICH TARGET TREATMENT RESISTANT CLINICAL PHENOTYPES

Another important feature of the identification of specific DHP calcium channel blockers in the present study is that previous clinical trials have suggested the potential of this therapeutic class specifically for improvement of negative symptom subtypes, such as cognitive deficits, in schizophrenia. This raises the possibility that the functional cytomics platform might serve the much needed purpose of identifying compounds capable of targeting subtypes of symptoms which are refractory to conventional treatments. In this respect it will be informative to follow the results of the ongoing clinical trial of DHP calcium channel blocker isradipine for cognitive enhancement in schizophrenia and schizoaffective disorder (NCT01658150). Likewise it is possible that the heterogeneous results obtained in previous DHP calcium channel blocker clinical trials were in part due to the lack of stratification of the patient population. The *ex vivo* responses to DHP calcium channel blockers in the present study could constitute companion biomarkers for patient stratification in future clinical trials involving these compounds. This might ultimately increase the chances of successful clinical implementation through targeting of treatment sensitive patient subgroups [312,317].

The corticosteroid drug class, for which a selective therapeutic potentiation window was also observed, have likewise been suggested as a therapeutic option for treating negative symptoms and cognitive deficits. Similarly to the structure activity relationships described for the DHP calcium channel blockers, these results specifically suggest methylprednisolone as the class candidate with the most selective cellular efficacy **(Fig. 5.7).** Clinical trials are currently underway for the parent compound prednisolone in recent-onset schizophrenia patients (University Medical Centre, Utrecht). This will be important for determining the prophylactic properties of this intervention with respect to long-term cognitive decline. In addition to the DHP calcium channel blockers and corticosteroids currently being tested in clinical trials, the functional cytomics platform also identified the structurally unrelated antiarrhythmic compound ibutilide, which has not yet been tested for efficacy in schizophrenia. The provision of a structurally and mechanistically diverse portfolio of novel compounds, at early stages of the drug discovery process, is key to addressing treatment resistance in complex disorders with heterogeneous molecular aetiologies such as schizophrenia.

5.3.3 CLINICAL IMPLICATIONS OF DIVERGENT CELLULAR RESPONSES TO TYPICAL AND ATYPICAL ANTIPSYCHOTIC TREATMENTS

There was a striking dichotomy between the interactions of typical and atypical antipsychotics with the TG-PLC-$\gamma 1$ response. While the typical antipsychotics (haloperidol and penfluridol) did not display any potentiation in the presence of TG, the atypical antipsychotics (risperidone, aripiprazole, olanzapine and clozapine) were all selective potentiators of the response **(Fig 5.7)**. This is consistent with multiple *in vitro* studies using neurons and microglia which indicate a differential effect of typical vs. atypical antipsychotics on TG-induced calcium mobilization from the endoplasmic reticulum[318,319]. Interestingly several of these studies characterized this differential effect in terms of ER stress and neuronal differentiation, suggesting that the current divergence in TG-PLC-$\gamma 1$ modulation between these drug classes may have profound implications on their therapeutic profile in the CNS[318,319]. Furthermore the similarity in the TG-PLC-$\gamma 1$ *ex vivo* profile of the typical antipsychotics to specific T-type calcium channel blocker NNC 55-0396, and that of atypical antipsychotics to the L-type DHP calcium channel blockers, suggests that these differential clinical effects might in part be mediated by the relative specificities of these antipsychotic drug classes to T- and L-type calcium channels respectively[320]. Interestingly, efficacy in rescuing schizophrenia-like behavioural abnormalities (sensorimotor gating deficits) in a PLC-$\beta 1$ knockout animal model has previously been shown to be restricted to the atypical antipsychotic class (clozapine vs. haloperidol)[250]. Thus there is evidence that the mechanism of action of TG and the PLC isotypes used for its detection in the current assay may synergistically contribute to the differential sensitivity of the target response (TG-PLC-$\gamma 1$) to atypical vs. typical antipsychotic drugs. Taken together these findings suggest that, in addition to dissecting the potential effects of novel drug candidates, the functional TG-PLC-$\gamma 1$ *ex vivo* profile could potentially be used for treatment response prediction between different classes of existing antipsychotic therapies in patients with biased calcium channel subtype or PLC isotype functional repertoires. By extension, the rank order of potency for different atypical antipsychotic compounds in shifting the TG EC_{50} at PLC-$\gamma 1$ *ex vivo* **(Fig. 5.4c)** could serve as a means to stratify schizophrenia patients with differential clinical sensitivities to members of this drug class.

5.3.4 DIFFERENTIAL PHARMACOLOGY FOR DISSECTING DISEASE MECHANISMS

In addition to providing clinical insight into potential therapeutic candidates, the differential effects of the library screening compounds on the phenotypic TG-PLC-$\gamma 1$ response could provide insights into the mechanisms of altered cell signalling in the disease state. For example, in **Chapter 4** voltage-

gated L-type calcium channels (especially $Ca_v1.2$) were proposed to be involved in the mechanism of altered TG evoked ER calcium mobilization. However this was based solely on the association of $Ca_v1.2$ subunits to schizophrenia in genomic studies and the relative expression of $Ca_v1.2$ channels in lymphocytes[24,240]. The effects of specific DHP L-type calcium channel blockers in modulating this response in the compound library screen allows further dissection of the functional phenotype and lends support to the mechanistic model proposed. Furthermore the fact that $Ca_v1.2$ channels are implicated in leading hypotheses of schizophrenia pathogenesis supports the validity of the *ex vivo* TG-PLC-$\gamma1$ response as a surrogate drug screening model for CNS efficacy. This is supported by the role of $Ca_v1.2$ in mediating altered excitation-transcription coupling and NMDA receptor hypofunction of GABAergic interneurons in addition to altered microglial activation involving deramification and release of nitric oxide and pro-inflammatory cytokines. However the question still remains as to how the blockade of L-type calcium channels, traditionally associated with calcium influx down the concentration gradient from the extracellular space, is able to rescue the disease-associated phenotype. One possibility is that blockade of L-type calcium channels induces relative cellular starvation of calcium which triggers compensatory release mechanisms from the ER which are synergistic with the elevation of cytosolic calcium induced by TG. An alternative mechanism is that L-type calcium channel blockade inhibits the reuptake of calcium into the ER once the concentration gradient between cytosol and ER has been reversed by TG. Interestingly recent data suggests that L-type calcium channels are constantly being trafficked around the cell and can promiscuously insert themselves into the membranes of different cellular organelles via swapping of membrane micro-domains and lipid rafts[321]. Thus elucidation of the mechanism of altered TG-PLC-$\gamma1$ response in schizophrenia would best be served by measurement of the subcellular localization and trafficking of L-type voltage-gated calcium channels (especially with respect to the mitochondria), their interactions with other proteins involved in calcium homeostasis (e.g. STIM1 and ORAI1) and changes in calcium concentration in subcellular compartments which accompany the kinetic response to TG.

In addition to the mechanistic insight provided by DHP calcium channel blockers, it is notable that other compounds, such as fingolimod and retinoic acid, also interacted with the TG-PLC-$\gamma1$ response **(Fig. 5.5)**. Fingolimod, one of the few compounds to provoke a dose-dependent increase in PLC-$\gamma1$ expression in the TG condition, is a multiple sclerosis medication affecting lymph node T cell sequestration and is currently in clinical trials for schizophrenia (NCT01779700). On the other hand retinoic acid derivatives have known psychotogenic effects[322]. Interactions were also observed for specific inhibitors of key schizophrenia targets described previously in this study and by others, including Akt1 (GSK 690693), GSK-3β (TC-G 24), mTORC1 (Everolimus) and STAT3 (cucurbitacin

I)[143,214]. While these compounds did not fit the desired therapeutic profile in the current study, their interactions nevertheless support the validity of the TG-PLC-γ1 response as a model for detecting functional interactions with schizophrenia-associated targets through differential pharmacology *ex vivo*.

CHAPTER 6

CONCLUSION

To conclude this work we summarize the main findings and their significance to the field of neuropsychiatric drug discovery. Subsequently we discuss limitations of the current study and propose ways in which they might be overcome in future work.

6.1 SUMMARY

We have developed a novel high-content screening platform for the functional characterization of signalling network responses at the single-cell level in PBMCs *ex vivo*. These signalling network responses can be kinetically resolved to reveal regulatory interactions in specific cell subtypes within a heterogeneous primary cell population. The platform has been applied to characterize the effects of common neuropsychiatric medications *ex vivo* in terms of both established (e.g. GSK-3β) and emerging (e.g. CrkL) drug targets with putative CNS efficacy. Furthermore the platform has indicated mechanistic points of convergence between neuropsychiatric drugs with different indications (e.g. antidepressants, mood stabilizers and antipsychotics at 4EBP1 (pT36/pT45)) and also divergent activities of neuropsychiatric drugs within the same indication (e.g. mood stabilizers such as lithium at 4EBP1 (pT36/pT45) and valproic acid at Rb (pS780)). Finally we have used the cell signalling signature of these approved medications as a mechanistic scaffold to identify novel experimental or repurposed drugs (e.g. JB 1121 or rapamycin respectively) and potential treatment response predictors.

Clinical application of the platform demonstrated functional alterations in the T cell signalling repertoire of drug-naive schizophrenia patients relative to controls. Several of these alterations were normalized following a clinical course of antipsychotic olanzapine treatment and subsequently prioritized as putative novel drug targets (thapsigargin-PLC-γ1, forskolin-Src (pY418), Akt1 and

STAT3 (pY705)). These targets were further characterized in terms of their correlation to changes in symptom subscales (e.g. STAT3 (pY705) and negative symptoms) and their specificity for schizophrenia relative to other major neuropsychiatric disorders (bipolar disorder, major depression and autism spectrum disorder). Finally we defined the attenuated response to thapsigargin at PLC-$\gamma 1$ in schizophrenia patients relative to controls as the most significant drug target.

A phenotypic drug library screen using the extended FDA library identified compounds with the potential to normalize the schizophrenia-associated cell signalling alteration in the same manner as achieved by *in vivo* olanzapine treatment. Dose-response validation and structure-activity analysis revealed a selective therapeutic window for corticosteroids (methylprednisolone and flunisolide), 1,4-dihydropyridine (DHP) L-type calcium channel blockers with extended ester substitutions at the 3-position of the pyridine ring (nicardipine, nisoldipine and nimodipine), atypical antipsychotics (risperidone, aripiprazole, olanzapine and clozapine) and an anti-arrhythmic drug (ibutilide). Furthermore these drug candidates allowed the characterization of the schizophrenia-associated cell signalling abnormality in light of prominent schizophrenia GWAS loci including CACNA1C and CACNB2[24].

6.2 SIGNIFICANCE

The elucidation of convergent *ex vivo* cell signalling response phenotypes ('functional endophenotypes') between neuropsychiatric patients with potentially varied genetic risk factors and environmental trajectories is the foremost contribution of this work. It provides a tractable and accessible primary live cell model for *de novo* identification of structurally diverse drug candidates with novel mechanisms of action even before the pathological process is fully understood. Moreover these drug candidates can be compared within the model directly to established treatments to identify structural derivatives with putative enhanced target specificity or cellular potency. This model is amenable to drug repurposing such that candidates with therapeutic potential for treating refractory patients or symptom subtypes are expedited to the clinic. Examples include the 1,4-DHP L-type calcium channel blockers and STAT3 (pY705) phosphorylation modulators for the treatment of cognitive deficits and negative symptoms in schizophrenia respectively. These functional endophenotypes also provide a potential avenue for understanding the functional implications of interactions between multiple common but weak or rare but

penetrant genetic risk loci (e.g. CACNA1C, CACNB2 and PLCB2) at a time when the majority of heritable genetic risk has yet to be indexed (7%)[24].

The second most significant contribution of this work is the identification in PBMCs of differential interactions between neuropsychiatric medications and cell signalling targets plausibly related to CNS efficacy. The differential interactions of lithium at 4EBP1 (pT36/pT45) and valproic acid at Rb (pS780) serve as examples in the case of bipolar disorder. This raises the possibility of treatment response prediction by *ex vivo* testing of the same drugs that are administered clinically. This has the potential to circumvent the challenges of diagnostic uncertainty and identification of treatment resistant individuals early in the disease progression. The highly specific interaction at GSK-3β of ligands CHIR 99021 and JB1121, which have been proposed as alternative therapies for treatment resistant bipolar disorder, suggests that the *ex vivo* methodology might likewise be used to provide alternative treatments in the case of therapeutic resistance.

The work also allows the re-evaluation of the widely accepted theory that neuropsychiatric disorders involve the composite dysregulation of whole cell signalling pathways[32,33,91,323–325]. While this is a useful concept it seems that the reality of the cell signalling environment is more complex. For example many molecular profiling studies synthesise a list of putative disease alterations using *in silico* pathway analysis. This is subsequently presented as a canonical model in which stimulation or inhibition of any one of the components will trigger the dysregulation of the rest[32,33,91,323–325]. In this respect one would expect any ligand which interacts with a protein in a proto-typical schizophrenia associated pathway, such as Akt/GSK-3β, to provoke dysregulation of the whole pathway observable at each of the proteins in the network[91]. The current data suggests that this is not the case. Instead disease-associated cell signalling responses appear sporadically within the network even in the case of broad spectrum cell signalling activators. For example, although thapsigargin was active in the AI and DD studies presented here at over 30% of the epitopes, the only ones which showed abnormal responses to this ligand in schizophrenia were PLC-γ1 and the closely related PLC-γ2. However none of the proteins downstream of PLC-γ1/2 (e.g. PKC-α, PKC-θ or ERK1/2) showed similar dysregulation[236,243,326]. This highlights the fact that there are likely to be extensive regulatory mechanisms across the rest of the network which compensate for pathological responses at individual epitopes. It is more informative to replace the canonical concept of cell signalling with that of a tightly regulated network[114]. By extension the ability of the methodology presented here to identify specific stress points in these networks might ultimately prove more relevant for drug target discovery as these are likely to be the sites which escape regulatory control.

Conversely in the present study the assessment of ligand responses across multiple cell signalling epitopes in parallel has revealed a remarkably promiscuous profile for many of the common neuropsychiatric treatments. While several of these interactions are known, for example at Akt/GSK-3β pathway epitopes, others such as the induction of phosphorylation at CrkL (pY207) in response to antipsychotic administration *ex vivo* and *in vivo* have not been documented[87,90]. Furthermore CrkL has been implicated by several studies as an emergent genetic risk factor[29,215]. This emphasises the importance of high-content cell signalling analysis for characterizing the therapeutic profile of drugs with multi-target interactions such as neuropsychiatric treatments. It is possible that these 'off target' effects may eventually be recognized as key components of therapeutic efficacy or alternatively toxicity. This is poignantly illustrated by the recent publication of the crystal structure of the TREK-2 potassium channel in complex with the active metabolite of fluoxetine (norfluoxetine)[327]. This inhibitory interaction is now recognized as a potentially important contribution to both the antidepressant efficacy and the cardiovascular side effects of this drug, traditionally known as a an inhibitor of the serotonin reuptake transporter (SERT)[327–329]. Finally the ability to resolve these off-target effects discretely at different sites in the cell signalling network raises the possibility of exploiting synergistic interactions between highly specific ligands such CHIR 99021 (GSK-3β inhibitor) and rapamycin (mTORC1 inhibitor) to provide personalized combinatorial therapeutic options for neuropsychiatric disorders[94,108]. This is increasingly recognized as an important therapeutic strategy for overcoming treatment resistance due to molecular heterogeneity in cancer. Treatment resistance in heterogeneous neuropsychiatric disorders might likewise benefit from this novel strategy as opposed to standard monoaminergic augmentation approaches.

6.3 LIMITATIONS AND FUTURE WORK

6.3.1 CLINICAL SAMPLES

Due to the challenges of obtaining well characterized viable PBMCs from neuropsychiatric patients the low sample numbers in this study are a major limitation. Tens of thousands of samples are necessary to resolve risk polymorphisms in major schizophrenia treatment targets such as DRD2[23]. Moreover more prevalent disorders such as major depression are likely to require even larger sample cohorts[30,34]. Comparison to these figures would suggest that the present study is underpowered by several orders of magnitude and that future studies would benefit from

substantially increased sample numbers. In this respect many of the conclusions are best interpreted as speculative models which await further confirmation in larger sample sets. Nevertheless the fact that the most significant schizophrenia associated cellular response (TG-PLC-γ1) was normalized by precisely that same drug class (L-type calcium channel blockers) as indicated by GWAS analysis of schizophrenia risk loci (CACNA1C and CACNB2) in much larger sample cohorts, raises the possibility that functional cytomics is able to summarize genetic risk data and consequently has a lower power requirement. Moreover the data described here is interactive by definition in the sense that it is correlated to active symptomatology, prioritized by reversal over the course of clinical treatment and contrasted across various ligand and epitope classes. Thus it is conceivable that is has different power requirements relative to GWAS data which is mostly confined to additive influences on variance at present[24]. Nevertheless this can only be confirmed by parallel application of the two technologies in the same samples.

While the schizophrenia samples used were all from drug-naive first-onset patients, the sample donors from the other major neuropsychiatric cohorts in the DD study had varying histories of acute or chronic neuropsychiatric pharmacological intervention (particularly the BD and MDD cohorts). While it is very difficult to obtain drug-naive samples, alternative study designs, using PBMCs collected from high risk individuals (e.g. family history of neuropsychiatric disease) prior to disease manifestation or patient groups where the disease often remains undiagnosed (e.g. chronic caregivers with depression), might serve to address these limitations in future work. While the use of samples from prodromal individuals who subsequently convert to a major neuropsychiatric diagnosis has yielded fascinating recent results [54], it might be highly informative also to include prodromal patients which do not subsequently manifest disease. This would allow the identification not only of risk factors but also disease resilience factors.

A final limitation in the clinical design is that, having emphasized the prevalence of diagnostic uncertainty and the limitations of rigid DSM-V and ICD-10 diagnostic categories, these are precisely the diagnostic tools which have been used to classify the current patient cohorts[45,48]. In addition schizophrenia has largely been referred to in the present work as a single disorder. In fact, it is now recognized a heterogeneous clinical syndrome in which a different constellations of symptoms can arise from distinct molecular aetiologies. Unfortunately the treatment of schizophrenia as a single defined disease in the present work is unavoidable given the existing diagnostic framework. However validation of the current methodology and other biomarker discovery efforts using these categories need not be considered as a static paradigm. Future studies would benefit from the redefinition of these diagnostic tools as emergent biomarker strategies become available. Thus iterative cycles of reciprocal redefinition between clinical and biological measures of disease could

potentially optimize the diagnostic efficiency of neuropsychiatric illness which in turn would facilitate novel drug discovery efforts. Likewise the application of this technology to larger sample cohorts is essential to determine which cellular responses are associated to specific subgroups of patients. For example the attenuated response to thapsigargin at PLC-γ1 might only be a feature of a subgroup of patients. This would explain its biased sensitivity to atypical vs. typical antipsychotic drugs known to be differentially efficacious in certain patient subgroups. Finally, future drug target discovery efforts, such as those described in the present work, would benefit from including other major diseases aside from neuropsychiatric disorders in the experimental design. This could serve to define the molecular features which overlap between major human diseases (e.g. 17% pleiotropy of genetic risk loci across disease domains) and also those that segregate (e.g. inverse correlation between schizophrenia and rheumatoid arthritis) to define a more relevant and integrated therapeutic landscape[39,330].

6.3.2 FURTHER CHARACTERIZATION OF CELL SIGNALLING NETWORKS

In the current work we have proposed a heuristic model for phenotypic screening of the most 'druggable' part of the genome. While this has the potential to expedite the identification of therapeutic compounds, the underlying disease mechanisms remain unknown. The disease-associated phenotypes discovered by the current methodology (e.g. attenuated TG-PLC-γ1 response in schizophrenia) require subsequent mechanistic dissection using parallel technologies. For example small interference RNA (siRNA) screens could be used to selectively knock down each of the known signal transduction proteins individually to understand which of these are involved in the TG-PLC-γ1 response. In this respect recently identified sequestration regulators of PLC-γ1, including Sprouty and Cish proteins, warrant further exploration[331,332]. Alternatively clustered regularly-interspaced short palindromic repeat (CRISPR) genome editing of each phosphorylation residue in the signalling network to an inactive amino acid (e.g. serine to alanine mutation) could further resolve these regulatory interactions to the level of individual cell signalling epitopes. This could also be addressed by counter-screening using libraries of specific phosphorylation inhibitors. The influence of L- type calcium channel blockers on the TG-PLC-γ1 response in the FDA screen supports this approach although the residual effects of promiscuous inhibitor profiles and incomplete compound annotation cannot be excluded using pharmacological dissection relative to genome editing or siRNA[108]. A powerful complementary strategy is to use fluorescence activated cell sorting (FACS) to sort cells from the same patient and same cell subtype which differentially express the putative pathological response. This allows characterization of the response using

genomic or proteomic means whereby the molecular variation between sample donors and cell lineages is controlled for. In other words cells which are identical aside from their target response profile are used as an internal control for characterizing single-cell signalling abnormalities.

Validation of the specificity of the antibodies used to detect the changes in cell signalling epitope expression is also an essential subsequent step to this work. Despite the fact that the majority of antibodies used are monoclonal and raised in response to a single recombinant human antigen, it is nevertheless possible that they show varying degrees of cross reactivity. For example the anti-Akt (pS473) antibody, exemplified in both the TC and AI phases of the project, was raised against phosphorylated Akt1 (pS473) peptide. Nevertheless, it cross-reacts with all Akt isoforms (Akt1-3). While members of the Akt kinase family are thought to have largely redundant functions, important variations in the tissue distribution, stimulus specificity, substrate recruitment and subcellular localization of these isoforms have been demonstrated in isoform specific Akt knockout animal models[333]. The question of specificity is particularly poignant with respect to the PLC-γ1 and PLC-γ2 isotypes which share 99.9% sequence homology (UniProt P19174 vs. P16885). As the principal distinction between the two is their relative expression in different tissue types, the specificity of detection within the *ex vivo* assay has critical implications for extrapolation of the cell signalling mechanisms between PBMCs and neurons. In this case the manufacturer explicitly declared no cross-reactivity between PLC-γ1 and PLC-γ2 isotypes.

However in the case of many of the antibodies used, the only evidence presented by the manufacturer is either response to broad spectrum positive controls (e.g. calyculin, PMA/ionomycin, pervanadate, staurosporine) or specific pathway activators/inhibitors (e.g. PDGF-BB, IL-6, IGF-1, LY294002). While these ligands are useful to confirm antibody sensitivity in detection of a given functional response, they do not unequivocally confirm specificity as they can also affect the expression of multiple proteins up- or downstream. Moreover the cell type used for validation is often not of the same lineage as the target cell, thus the scope for cross-reactivity is not adequately modelled. This would be optimally addressed using a combination of the most specific ligand available and siRNA/ CRISPR knockdown of the isoform specific cell signalling epitope in the same cell lineage as used in the analysis[334]. The inclusion of the respective antibody isotype control would also be useful to quantify background fluorescence and confirm whether the knockdown simply reduces or completely ablates the observed staining profile. In addition, in the case of phosphorylation epitopes, parallel staining with a polyclonal antibody or one targeting a different epitope on the same protein, could be used to confirm that the knockdown is site specific. Validation using other methods, for example western blotting, ELISA or immunohistochemistry,

could also provide complimentary indications of abundance, molecular weight and cellular localization with which to interpret antibody specificity.

A final consideration is whether the antibodies which target different sites on the same protein interfere with each other. This is largely controlled by the fact that the cells are paraformaldehyde fixed before staining, negating the possibility of conformational changes induced by antibody binding, and that the antibodies are used separately in small plexes of three. Nevertheless validation of the top screening hits with individual antibody stains would serve to exclude any residual interference. In conclusion, the relative specificity profiles of the ligand responses observed in the present study do not support an excessive promiscuity in the epitope recognition of the antibody array. However it is best to interpret the utility of the platform as an initial screening device which refines the scope of cell signalling alterations for subsequent validation of target phenotype specificity.

The current study would also benefit from spatial resolution of changes in cell signalling protein distribution using super-resolution microscopy approaches[122]. This would help to resolve for example whether the observed decreases in epitope expression represent degradation or sequestration. Combination of this approach with technologies such as fluorescence resonance energy transfer (FRET) has the potential to resolve which proteins are interacting with putative disease targets in a live cell context. Concurrently more precise kinetic resolution of the responses within the spatio-temporal domain would help to define properties such as localized receptor-signalling waves, the dynamics of which are increasingly recognized as important determinants of the ultimate cellular response[242,335]. In this respect the 1-30 min time window for cell signalling responses chosen in the present study could be extended to several hours or days with more intermediate time points to accurately define cell signalling peaks and multiphasic responses[139].

While the nature of the targets identified suggest that lymphocyte subsets can potentially provide relevant surrogate models for mechanisms of CNS drug efficacy this would need to be confirmed in future studies using brain cell lineages. In this respect induced pluripotent stem cells (iPSCs) derived from patient and control donors can be reprogrammed to provide different brain cells lineages including subtypes of neurons, oligodendrocytes, microglia and astrocytes. Two studies have demonstrated the utility of this methodology to explore therapeutic drug response profiles using iPSC-derived neurons from schizophrenia and bipolar patients relative to controls in addition to multiple studies in monogenic disorders[336–339]. While this methodology is limited by difficulties in the selection of the iPSC colonies, monitoring the karyotypic stability across passages and the specificity of end fate differentiation as evidenced by small sample sizes in existing publications, it remains one of the only available technologies to explore the effects of novel drugs in neuronal

tissue with the genomic background of neuropsychiatric patients[336–339]. The recent application of this technology to neuropsychiatric samples with penetrant genetic mutations (e.g. CNVs) is noteworthy in terms of deriving accentuated cellular phenotypes for drug discovery[340]. Cells which share many of the characteristics of brain cell lineages can also be derived directly from primary neuropsychiatric patient tissue without the need for reprogramming. Examples include neuronal-like cells induced from fibroblasts or microglial-like cells induced form peripheral monocytes[27,341]. It is also possible that expansion of the current assay design to other subtypes of blood cells could extend the catchment area for identifying surrogate models of altered CNS signalling (e.g. insulin signalling specific to monocytes). Likewise deeper immunophenotyping of PBMC subsets, for example further dissection of T cells into helper, cytotoxic, memory, regulatory, natural killer and $\gamma\delta$ T cell subsets, could help answer the pending question of whether the altered responses in patient cells derive from differential cell signalling activities intrinsic to each cell or from different relative proportions of cell subtypes within the target lineage. Correlation between disease-associated cellular responses and regional brain activity patterns using fMRI in patients and controls might also be valuable in terms of defining which cellular responses relate to altered brain connectivity[10].

Finally it is vital to emphasise that correlated epitope responses in the current work do not necessarily imply causal relationships in the cell signalling network[342]. Responses at cell signalling epitopes were measured individually or in small multiplexes of three, in succession. Thus all epitopes are not measured in the same cell. Technologies such as mass cytometry which are not constrained by spectral overlap and can simultaneously measure over 50 cell signalling epitopes in parallel provide an excellent opportunity to address this limitation and capitalize on the statistical power of epitope correlations across thousands of single-cells in primary samples[135,136,343]. To date this technology has mainly been applied to acquire depth in terms of lineage or pharmacological intervention due to the relative paucity of cell signalling antibodies conjugated to heavy metal isotopes[135,136,343]. However as the catalogue of available antibodies is extended, this technology in conjunction with bioinformatics platforms developed to interpret the resulting high content data (e.g. SPADE and viSNE), provides an unprecedented opportunity for the definition of cell signalling network abnormalities in neuropsychiatric disorders[136,344–346].

6.3.3 COMPOUND LIBRARIES

Expansion of the current technology using larger compound libraries for target identification and therapeutic drug discovery will provide a significant contribution to the utility of the platform. For example in the present study we have used 14 commonly prescribed neuropsychiatric medications which are representative of the major therapeutic drug classes. However repetition of the same protocol with all the available neuropsychiatric ligands (approximately 100) would allow increased resolution of the structure-activity relationship between these compounds across all cell signalling epitopes. This can further be summarized in high dimensional space as functional lineages of compound efficacy similar to classification of kinase inhibitors in other studies[135]. In the current study the majority of compounds were assayed individually. Recent data suggests that combinatorial drug screening can permit the identification of novel therapeutic strategies which exploit synergistic interactions between compounds, for example targeting specific neuronal subpopulations using GPCR heterodimers and oligomers (e.g. formed of NMDA and CB1 receptors). Compound libraries which could be useful for these combinatorial approaches in neuropsychiatry include the Torrey Pines, Sequoia, Spectrum, Prestwick and NIH Brain Bioactive Chemical libraries. Likewise the majority of compounds were screened at a single dose in both the drug target and drug candidate identification stages of this project. While this represents an attempt to capture as many biologically relevant interactions as possible within the established experimental dimensions, subsequent iterations of both phases using multiple doses of each compound would serve to address the delicate balance between compound efficacy and toxicity.

A final consideration is that despite the premise of identifying neuropsychiatric drug candidates with novel mechanisms of action, we have based our drug target identification on the clinical response to an established monoaminergic drug (olanzapine). The effect of this on the resulting drug candidates is evident as olanzapine, together with other atypical antipsychotic drugs, represented a significant proportion of the final drug selection. While this serves to validate the platform's utility and provides a useful benchmark for the cellular performance of the novel drugs from other drug classes (calcium channel blockers, corticosteroids and the potassium channel blocker), it also suggests that the derivation of drug candidates with radically different mechanisms of action will need to be conducted in iterative cycles, similarly to the redefinition of diagnostic categories described earlier. Nevertheless the identification of compounds which achieve similar cellular effects through different pathways (e.g. methylprednisolone) is a useful therapeutic option for treatment resistance. Finally prioritization of the candidates in the present work is conducted solely on the basis of cellular response as a proof of principle. The application of these compounds to the clinic will require the consideration of their relative pharmacokinetic, biodistribution, toxicity

and side-effect profiles. For example nimodipine is the most likely of the L-type calcium channel blockers identified to achieve therapeutically relevant concentrations in the brain whilst minimizing the cardiovascular side-effects[312,347,348]. Recent improvements in brain targeted formulations and drug delivery systems are likely to further contribute to the ultimate utility of these compounds[349–351].

ACKNOWLEDGEMENTS

There are few, if any, places in the world in which this project could potentially have been executed. The fact that such a research environment exists with the fundamental access to *ex vivo* clinical samples, which are the cornerstone of significance in this study, is due to the work of Prof. Sabine Bahn. The fact that I have been lucky enough, not only to find a place within this unique environment, but also to have been given the freedom to explore a project of these dimensions, is due to the faith Prof. Bahn has afforded me. For this latter contribution in particular, I am profoundly grateful. I am also grateful for her unfailing enthusiasm, which has proved indispensable for navigating the challenges of a novel line of investigation, and her hands-on ability to decisively resolve any obstacles that might jeopardize the success of the endeavour. Finally, and not least, I thank her for the exceptional scientific, clinical and business insight, rarely found in such synergy, which have made this project and my professional development therein possible. Such words do not suffice for an acknowledgement of this magnitude but it is my hope, in the case of Prof. Bahn, that they will serve at least as a start.

Dr. Jakub Tomasik has been the closest experimental collaborator in this project, present from its inception to the last blood cell catapulted through the laser beam. His rigorous approach, relentless effort and acute analytical abilities have been fundamental in the formulation of this endeavour. Not least the vast majority of the statistical analysis and much of the experimental work are attributable to him. His combined prowess in both of these aspects of the project has been essential in welding the pipeline that is described herein. Moreover I have learnt a great deal in his company and consider it a privilege to have been able to share the vision of this project with him. For all these aspects combined and most of all the enjoyment of working with him I am extremely grateful.

This project would not have been possible without the contributions of Geertje van Rees and Hannah Steeb. Their involvement in terms of experimental work and providing the primary cell cultures to satisfy the ever increasing demands of the automated platform has been vital. I am extremely grateful for their enthusiasm and the good company which they have provided. Likewise many other people have contributed to this work. I wish to thank Dr. Frieder Haenisch, Dr. Jantine Broek and Eva Brombacher for preparation of blood samples and Dr. Emiliano Gonzalez Vioque, Marina Fuetterer, Justyna Kucia and Michal Wlodarski for early contributions in the development

of the platform. Statistical analysis has been extensively supported by David Cox, Dr. Jordan Ramsey and Dr. Jason Cooper for which I am very grateful. I wish to thank Dr. Paul Guest and Dr. Hassan Rahmoune for supervision and editing of funding proposals and Pawel Eljasz for IT support. I am also grateful to many other members of the Bahn Lab past and present with whom I have had the privilege of collaborating and the even greater privilege of their company.

I wish to thank all the staff in the Department of Chemical Engineering and Biotechnology not least the administrative and technical teams who have made this work possible and the people who have reviewed my work at different stages in the appraisal process. I am grateful also to many members of Cambridge University and Darwin College for their help. I would like to thank our external collaborators for provision of clinical samples and compounds and the funding bodies which have supported this work including the Engineering and Physical Sciences Research Council, Psynova Neurotech and the Stanley Medical Research Institute.

Last but not least, I would like to thank Dr. Joan Ballesteros. The concept on which this work is based *Combinatorial Cytomic Biomarkers* is one which he taught me during a summer internship in San Diego and over the course of five years working with him at Vivia Biotech in Spain. Likewise the technical knowledge for initiating this project during my PhD was acquired under his supervision and in collaboration with the team at Vivia Biotech. I am extremely grateful for the mentorship and scientific inspiration which he has provided, not to mention fruitful discussions on how best to compose a scientific text.

Briefly, notwithstanding the professional nature of this work, I would like to thank my family and friends. The support which they have provided me is present in every thread from which this fabric is woven.

REFERENCES

1. Conn, P. J. & Roth, B. L. Opportunities and challenges of psychiatric drug discovery: roles for scientists in academic, industry, and government settings. *Neuropsychopharmacology* **33,** 2048–60 (2008).

2. Licinio, J. Translational Psychiatry: leading the transition from the cesspool of devastation to a place where the grass is really greener. *Transl. Psychiatry* **1,** e1 (2011).

3. Wong, M.-L. & Licinio, J. From monoamines to genomic targets: a paradigm shift for drug discovery in depression. *Nat. Rev. Drug Discov.* **3,** 136–151 (2004).

4. Sarter, M. & Tricklebank, M. Revitalizing psychiatric drug discovery. *Nat. Rev. Drug Discov.* **11,** 423–424 (2012).

5. Scannell, J. W., Blanckley, A., Boldon, H. & Warrington, B. Diagnosing the decline in pharmaceutical R&D efficiency. *Nat. Rev. Drug Discov.* **11,** 191–200 (2012).

6. Psychiatric drug discovery on the couch. *Nat. Rev. Drug Discov.* **6,** 171 (2007).

7. Marder, S. R. *et al.* Advancing drug discovery for schizophrenia. *Ann. N. Y. Acad. Sci.* **1236,** 30–43 (2011).

8. Berton, O. & Nestler, E. J. New approaches to antidepressant drug discovery: beyond monoamines. *Nat. Rev. Neurosci.* **7,** 137–151 (2006).

9. Agid, Y. *et al.* How can drug discovery for psychiatric disorders be improved? *Nat. Rev. Drug Discov.* **6,** 189–201 (2007).

10. Kahn, R. S. *et al.* Schizophrenia. *Nat. Rev. Dis. Prim.* **1,** 1-23 (2015).

11. Hyman, S. E. A glimmer of light for neuropsychiatric disorders. *Nature* **455,** 890–893 (2008).

12. Malan-Müller, S. *et al.* A systematic review of genetic variants associated with metabolic syndrome in patients with schizophrenia. *Schizophr. Res.***170,** 1-17 (2015).

13. Mitchell, A. J. *et al.* Prevalence of Metabolic Syndrome and Metabolic Abnormalities in Schizophrenia and Related Disorders--A Systematic Review and Meta-Analysis. *Schizophr. Bull.* **39,** 1–13 (2011).

14. Lally, J. & MacCabe, J. H. Antipsychotic medication in schizophrenia: a review. *Br. Med. Bull.* **114,** 169-79 (2015).

15. Huhn, M. *et al.* Efficacy of pharmacotherapy and psychotherapy for adult psychiatric disorders: a systematic overview of meta-analyses. *JAMA psychiatry* **71,** 706–15 (2014).

16. Schooler, N. R. *et al.* Defining therapeutic benefit for people with schizophrenia: focus on negative symptoms. *Schizophr. Res.* **162,** 169–74 (2015).

17. Leucht, S. *et al.* Comparative efficacy and tolerability of 15 antipsychotic drugs in schizophrenia: A multiple-treatments meta-analysis. *Lancet* **382,** 951–962 (2013).

18. Carpenter, W. T. & Davis, J. M. Another view of the history of antipsychotic drug discovery and development. *Mol. Psychiatry* **17,** 1168–1173 (2012).

19. Zarate, C. A., Singh, J. & Manji, H. K. Cellular plasticity cascades: targets for the development of novel therapeutics for bipolar disorder. *Biol. Psychiatry* **59,** 1006–20 (2006).

20. DiMasi, J. a & Faden, L. B. Competitiveness in follow-on drug R&D: a race or imitation? *Nat. Rev. Drug Discov.* **10,** 23–27 (2011).

21. Asenjo Lobos, C. *et al.* Clozapine versus other atypical antipsychotics for schizophrenia. *Cochrane database Syst. Rev.***11***,* CD006633 (2010).

22. Benes, F. M. Searching for unique endophenotypes for schizophrenia and bipolar disorder within neural circuits and their molecular regulatory mechanisms. *Schizophr. Bull.* **33,** 932–936 (2007).

23. Giusti-Rodríguez, P. & Sullivan, P. F. The genomics of schizophrenia: update and implications. *J. Clin. Invest.* **123,** 4557–63 (2013).

24. Ripke, S. *et al.* Biological insights from 108 schizophrenia-associated genetic loci. *Nature* **511,** 421–427 (2014).

25. Gordon, J. a. Testing the glutamate hypothesis of schizophrenia. *Nat. Neurosci.* **13,** 2–4 (2010).

26. Harrison, P. J. Recent genetic findings in schizophrenia and their therapeutic relevance. *J. Psychopharmacol.* **29,** 85–96 (2015).

27. Heyes, S. *et al.* Genetic disruption of voltage-gated calcium channels in psychiatric and neurological disorders. *Prog. Neurobiol.* **134,** 36–54 (2015).

28. Fromer, M. *et al.* De novo mutations in schizophrenia implicate synaptic networks. *Nature* **506,** 179–184 (2014).

29. Luo, X. *et al.* Systematic prioritization and integrative analysis of copy number variations in schizophrenia reveal key schizophrenia susceptibility genes. *Schizophr. Bull.* **40,** 1285–99 (2014).

30. Lee, S. H. *et al.* Genetic relationship between five psychiatric disorders estimated from genome-wide SNPs. *Nat. Genet.* **45,** 984–994 (2013).

31. Hertzberg, L., Katsel, P., Roussos, P., Haroutunian, V. & Domany, E. Integration of gene expression and GWAS results supports involvement of calcium signaling in Schizophrenia. *Schizophr. Res.* **164,** 92–9 (2015).

32. Ramanan, V. K., Shen, L., Moore, J. H. & Saykin, A. J. Pathway analysis of genomic data: concepts, methods, and prospects for future development. *Trends Genet.* **28,** 323–332 (2012).

33. Sullivan, P. F. Puzzling over schizophrenia: Schizophrenia as a pathway disease. *Nat. Med.* **18,** 210–211 (2012).

34. Identification of risk loci with shared effects on five major psychiatric disorders: a genome-wide analysis. *Lancet* **381,** 1371–9 (2013).

35. Millar, J. K. *et al.* DISC1 and PDE4B are interacting genetic factors in schizophrenia that regulate cAMP signaling. *Science* **310,** 1187–91 (2005).

36. Chubb, J. E., Bradshaw, N. J., Soares, D. C., Porteous, D. J. & Millar, J. K. The DISC locus in psychiatric illness. *Mol. Psychiatry* **13,** 36–64 (2008).

37. Millar, J. K. Disruption of two novel genes by a translocation co-segregating with schizophrenia. *Hum. Mol. Genet.* **9,** 1415–1423 (2000).

38. Stevens, H. E., Smith, K. M., Rash, B. G. & Vaccarino, F. M. Neural stem cell regulation, fibroblast growth factors, and the developmental origins of neuropsychiatric disorders. *Front. Neurosci.* **4,** 1-14

(2010).

39. Sivakumaran, S. *et al.* Abundant Pleiotropy in Human Complex Diseases and Traits. *Am. J. Hum. Genet.* **89,** 607–618 (2011).

40. Loscalzo, J., Kohane, I. & Barabasi, A.-L. Human disease classification in the postgenomic era: A complex systems approach to human pathobiology. *Mol. Syst. Biol.* **3,** (2007).

41. Barabási, A.-L. Network medicine--from obesity to the 'diseasome'. *N. Engl. J. Med.* **357,** 404–7 (2007).

42. Vancampfort, D. *et al.* Risk of metabolic syndrome and its components in people with schizophrenia and related psychotic disorders, bipolar disorder and major depressive disorder: a systematic review and meta-analysis. *World Psychiatry* **14,** 339–347 (2015).

43. Guest, P. C. *et al.* Increased levels of circulating insulin-related peptides in first-onset, antipsychotic naïve schizophrenia patients. *Mol. Psychiatry* **15,** 118–119 (2010).

44. Herberth, M. *et al.* Identification of a molecular profile associated with immune status in first-onset schizophrenia patients. *Clin. Schizophr. Relat. Psychoses* **7,** 207–215 (2014).

45. Adam, D. On the spectrum. *Nature* **496,** 6–8 (2013).

46. Falkai, P. *et al.* Kraepelin revisited: schizophrenia from degeneration to failed regeneration. *Mol. Psychiatry* **20,** 671–6 (2015).

47. Meyer, U., Feldon, J. & Dammann, O. Schizophrenia and autism: both shared and disorder-specific pathogenesis via perinatal inflammation? *Pediatr. Res.* **69,** 26R–33R (2011).

48. Bromet, E. J. *et al.* Diagnostic shifts during the decade following first admission for psychosis. *Am. J. Psychiatry* **168,** 1186–94 (2011).

49. Schwarz, E. & Bahn, S. The utility of biomarker discovery approaches for the detection of disease mechanisms in psychiatric disorders. *Br. J. Pharmacol.* **153 Suppl,** S133–S136 (2008).

50. Schwarz, E. *et al.* Validation of a blood-based laboratory test to aid in the confirmation of a diagnosis of schizophrenia. *Biomark. Insights* **2010,** 39–47 (2010).

51. Chan, M. K. *et al.* Converging evidence of blood-based biomarkers for schizophrenia: an update. *Int. Rev. Neurobiol.* **101,** 95–144 (2011).

52. Haenisch, F. *et al.* Towards a blood-based diagnostic panel for bipolar disorder. *Brain. Behav. Immun.* **52,** 49–57 (2016).

53. Chan, M. K. *et al.* Identification of an Immune-Neuroendocrine Biomarker Panel for Detection of Depression: A Joint Effects Statistical Approach. *Neuroendocrinology **103**,* 693-710 (2015).

54. Chan, M. K. *et al.* Development of a blood-based molecular biomarker test for identification of schizophrenia before disease onset. *Transl. Psychiatry* **5,** 601 (2015).

55. Leucht, S., Helfer, B., Dold, M., Kissling, W. & McGrath, J. J. Lithium for schizophrenia. *Cochrane database Syst. Rev.* **10,** CD003834 (2015).

56. Fillman, S. G. *et al.* Increased inflammatory markers identified in the dorsolateral prefrontal cortex of individuals with schizophrenia. *Mol. Psychiatry* **18,** 206–214 (2013).

57. Fillman, S. G. *et al.* Elevated peripheral cytokines characterize a subgroup of people with schizophrenia displaying poor verbal fluency and reduced Broca's area volume. *Mol. Psychiatry* **21,** 1090-8 (2015).

58. Bot, M. *et al.* Serum proteomic profiling of major depressive disorder. *Transl. Psychiatry* **5,** e599 (2015).

59. Müller, N. *et al.* Impaired monocyte activation in schizophrenia. *Psychiatry Res.* **198,** 341–346 (2012).

60. Steeb, H. *et al.* Serum proteomic analysis identifies sex-specific differences in lipid metabolism and inflammation profiles in adults diagnosed with Asperger syndrome. *Mol. Autism* **5,** 4 (2014).

61. Schwarz, E. *et al.* Sex-specific serum biomarker patterns in adults with Asperger's syndrome. *Mol. Psychiatry* **16,** 1213–1220 (2011).

62. Gottschalk, M. G. *et al.* Discovery of serum biomarkers predicting development of a subsequent depressive episode in social anxiety disorder. *Brain. Behav. Immun.* **48,** 123–31 (2015).

63. Gottschalk, M. G. *et al.* Serum biomarkers predictive of depressive episodes in panic disorder. *J. Psychiatr. Res.* **73,** 53–62 (2015).

64. Haenisch, F. *et al.* Multiplex immunoassay analysis of plasma shows differences in biomarkers related to manic or mixed mood states in bipolar disorder patients. *J. Affect. Disord.* **185,** 12–6 (2015).

65. Schwarz, E. *et al.* Identification of Subgroups of Schizophrenia Patients With Changes in Either Immune or Growth Factor and Hormonal Pathways. *Schizophr. Bull.* **40,** 787–795 (2014).

66. van Beveren, N. J. M. *et al.* Evidence for disturbed insulin and growth hormone signaling as potential risk factors in the development of schizophrenia. *Transl. Psychiatry* **4,** e430 (2014).

67. Schwarz, E., Steiner, J., Guest, P. C., Bogerts, B. & Bahn, S. Investigation of molecular serum profiles associated with predisposition to antipsychotic-induced weight gain. *World J. Biol. Psychiatry* **16,** 22–30 (2015).

68. Tomasik, J. *et al.* Pretreatment levels of the fatty acid handling proteins H-FABP and CD36 predict response to olanzapine in recent-onset schizophrenia patients. *Brain. Behav. Immun.* **in press,** (2015).

69. Drexhage, R. C. *et al.* An activated set point of T-cell and monocyte inflammatory networks in recent-onset schizophrenia patients involves both pro- and anti-inflammatory forces. *Int. J. Neuropsychopharmacol.* **14,** 746–755 (2011).

70. Padmos, R. C. *et al.* Genetic and environmental influences on pro-inflammatory monocytes in bipolar disorder: a twin study. *Arch. Gen. Psychiatry* **66,** 957–965 (2009).

71. Debnath, M. & Berk, M. Th17 pathway-mediated immunopathogenesis of schizophrenia: mechanisms and implications. *Schizophr. Bull.* **40,** 1412–21 (2014).

72. Guo, J., Liu, C., Wang, Y., Feng, B. & Zhang, X. Role of T helper lymphokines in the immune-inflammatory pathophysiology of schizophrenia: Systematic review and meta-analysis. *Nord. J. Psychiatry* **69,** 364–72 (2015).

73. Gladkevich, A., Kauffman, H. F. & Korf, J. Lymphocytes as a neural probe: Potential for studying psychiatric disorders. *Prog. Neuro-Psychopharmacology Biol. Psychiatry* **28,** 559–576 (2004).

74. Roozafzoon, R. *et al.* Expression of NMDA receptor subunits in human peripheral blood lymphocytes in opioid addiction. *Eur. J. Pharmacol.* **638,** 29–32 (2010).

75. Levite, M. Dopamine and T cells: dopamine receptors and potent effects on T cells, dopamine production in T cells, and abnormalities in the dopaminergic system in T cells in autoimmune, neurological and psychiatric diseases. *Acta Physiol.* n/a-n/a (2015).

76. Sarkar, C., Basu, B., Chakroborty, D., Dasgupta, P. S. & Basu, S. The immunoregulatory role of dopamine: an update. *Brain. Behav. Immun.* **24,** 525–8 (2010).

77. Tan, S.-L. & Parker, P. J. Emerging and diverse roles of protein kinase C in immune cell signalling. *Biochem. J.* **376,** 545–52 (2003).

78. Barbosa, I. G. *et al.* Altered intracellular signaling cascades in peripheral blood mononuclear cells from BD patients. *J. Psychiatr. Res.* **47,** 1949–1954 (2013).

79. Kalland, M. E., Oberprieler, N. G., Vang, T., Taskén, K. & Torgersen, K. M. T cell-signaling network analysis reveals distinct differences between CD28 and CD2 costimulation responses in various subsets and in the MAPK pathway between resting and activated regulatory T cells. *J. Immunol.* **187,** 5233–45 (2011).

80. Beaulieu, J.-M., Gainetdinov, R. R. & Caron, M. G. Akt/GSK3 signaling in the action of psychotropic drugs. *Annu. Rev. Pharmacol. Toxicol.* **49,** 327–347 (2009).

81. Emamian, E. S., Hall, D., Birnbaum, M. J., Karayiorgou, M. & Gogos, J. a. Convergent evidence for impaired AKT1-GSK3beta signaling in schizophrenia. *Nat. Genet.* **36,** 131–137 (2004).

82. Li, X., Rosborough, K. M., Friedman, A. B., Zhu, W. & Roth, K. A. Regulation of mouse brain glycogen synthase kinase-3 by atypical antipsychotics. *Int. J. Neuropsychopharmacol.* **10,** 7–19 (2007).

83. Yang, S. *et al.* Deficiency in the Inhibitory Serine-Phosphorylation of Glycogen Synthase Kinase-3 Increases Sensitivity to Mood Disturbances. **3,** 1761–1774 (2010).

84. van Beveren, N. J. M. *et al.* Marked reduction of AKT1 expression and deregulation of AKT1-associated pathways in peripheral blood mononuclear cells of schizophrenia patients. *PLoS One* **7,** 1–12 (2012).

85. Brito-Melo, G. E. a *et al.* Increase in dopaminergic, but not serotoninergic, receptors in T-cells as a marker for schizophrenia severity. *J. Psychiatr. Res.* **46,** 738–742 (2012).

86. Rivera-Baltanas, T. *et al.* Serotonin 2A receptor clustering in peripheral lymphocytes is altered in major depression and may be a biomarker of therapeutic efficacy. *J. Affect. Disord.* **163,** 47–55 (2014).

87. Beaulieu, J.-M. A role for Akt and glycogen synthase kinase-3 as integrators of dopamine and serotonin neurotransmission in mental health. *J. Psychiatry Neurosci.* **37,** 7–16 (2012).

88. Beurel, E., Grieco, S. F. & Jope, R. S. Glycogen synthase kinase-3 (GSK3): Regulation, actions, and diseases. *Pharmacol. Ther.* **148,** 114–131 (2015).

89. Jope, R. S. & Johnson, G. V. . The glamour and gloom of glycogen synthase kinase-3. *Trends Biochem. Sci.* **29,** 95–102 (2004).

90. Li, X. & Jope, R. S. Is glycogen synthase kinase-3 a central modulator in mood regulation? *Neuropsychopharmacology* **35,** 2143–54 (2010).

91. Emamian, E. S. AKT/GSK3 signaling pathway and schizophrenia. *Front. Mol. Neurosci.* **5,** 1–12 (2012).

92. Freyberg, Z., Ferrando, S. J. & Javitch, J. a. Roles of the Akt/GSK-3 and Wnt signaling pathways in schizophrenia and antipsychotic drug action. *Am. J. Psychiatry* **167,** 388–396 (2010).

93. Emamian, E. S., Hall, D., Birnbaum, M. J., Karayiorgou, M. & Gogos, J. A. Convergent evidence for impaired AKT1-GSK3beta signaling in schizophrenia. *Nat. Genet.* **36,** 131–7 (2004).

94. Pan, J. Q. *et al.* AKT kinase activity is required for lithium to modulate mood-related behaviors in mice. *Neuropsychopharmacology* **36,** 1397–411 (2011).

95. Pandey, G. N., Rizavi, H. S., Tripathi, M. & Ren, X. Region-specific dysregulation of glycogen synthase kinase-3β and β-catenin in the postmortem brains of subjects with bipolar disorder and schizophrenia. *Bipolar Disord.* **17,** 160–71 (2015).

96. Kumarasinghe, N. *et al.* Gene expression profiling in treatment-naive schizophrenia patients identifies abnormalities in biological pathways involving AKT1 that are corrected by antipsychotic medication.

Int. J. Neuropsychopharmacol. **16,** 1483–503 (2013).

97. Gonçalves, V. F. *et al.* DRD4 VNTR polymorphism and age at onset of severe mental illnesses. *Neurosci. Lett.* **519,** 9–13 (2012).

98. Siniscalco, D. *et al.* Cannabinoid receptor type 2, but not type 1, is up-regulated in peripheral blood mononuclear cells of children affected by autistic disorders. *J. Autism Dev. Disord.* **43,** 2686–2695 (2013).

99. Kenakin, T. P. Cellular assays as portals to seven-transmembrane receptor-based drug discovery. *Nat. Rev. Drug Discov.* **8,** 617–626 (2009).

100. Danna, E. a & Nolan, G. P. Transcending the biomarker mindset: deciphering disease mechanisms at the single cell level. *Curr. Opin. Chem. Biol.* **10,** 20–7 (2006).

101. Rapaport, M. H. & Bresee, C. Serial mitogen-stimulated cytokine production from continuously ill patients with schizophrenia. *Neuropsychopharmacology* **35,** 428–34 (2010).

102. Carvalho, L. A. *et al.* Clomipramine *in vitro* reduces glucocorticoid receptor function in healthy subjects but not in patients with major depression. *Neuropsychopharmacology* **33,** 3182–3189 (2008).

103. Herberth, M. *et al.* Impaired glycolytic response in peripheral blood mononuclear cells of first-onset antipsychotic-naive schizophrenia patients. *Mol. Psychiatry* **16,** 848–859 (2011).

104. Clutter, M. R., Krutzik, P. O. & Nolan, G. P. Phospho-specific flow cytometry in drug discovery. *Drug Discov. Today. Technol.* **2,** 295–302 (2005).

105. Krutzik, P. O. & Nolan, G. P. Fluorescent cell barcoding in flow cytometry allows high-throughput drug screening and signaling profiling *Nature Methods* **3,** 361-68 (2006).

106. Purcell, S. M. *et al.* A polygenic burden of rare disruptive mutations in schizophrenia. *Nature* **506,** 185–90 (2014).

107. Fromer, M. *et al.* De novo mutations in schizophrenia implicate synaptic networks. *Nature* **506,** 179–84 (2014).

108. Thorne, C. A. *et al.* GSK-3 modulates cellular responses to a broad spectrum of kinase inhibitors. *Nat. Chem. Biol.* **11,** 58–63 (2015).

109. Catapano, L. a & Manji, H. K. G protein-coupled receptors in major psychiatric disorders. *Biochim. Biophys. Acta* **1768,** 976–993 (2007).

110. O'Connor, K. A. & Roth, B. L. Finding New Tricks For Old Drugs: An Efficient Route For Public-Sector Drug Discovery. *Nat. Rev. Drug Discov.* **4,** 1005–1014 (2005).

111. Clutter, M. R., Heffner, G. C., Krutzik, P. O., Sachen, K. L. & Nolan, G. P. Tyramide signal amplification for analysis of kinase activity by intracellular flow cytometry. *Cytometry. A* **77,** 1020–31 (2010).

112. Drews, J. Case histories, magic bullets and the state of drug discovery. *Nat. Rev. Drug Discov.* **5,** 635–640 (2006).

113. Gashaw, I., Ellinghaus, P., Sommer, A. & Asadullah, K. What makes a good drug target? *Drug Discov. Today* **16,** 1037–1043 (2011).

114. Nolan, G. P. What's wrong with drug screening today. *Nat. Chem. Biol.* **3,** 187–91 (2007).

115. Krutzik, P. O., Clutter, M. R., Trejo, A. & Nolan, G. P. Fluorescent cell barcoding for multiplex flow cytometry. *Curr. Protoc. Cytom.* **Chapter 6,** Unit 6.31 (2011).

116. Schulz, K. R., Danna, E. a, Krutzik, P. O. & Nolan, G. P. Single-cell phospho-protein analysis by flow cytometry. *Curr. Protoc. Immunol.* **Chapter 8,** Unit 8.17.1-20 (2012).

117. Irish, J. M. *et al.* Single cell profiling of potentiated phospho-protein networks in cancer cells. *Cell* **118,** 217–28 (2004).

118. Sen, N. *et al.* Single-cell mass cytometry analysis of human tonsil T cell remodeling by varicella zoster virus. *Cell Rep.* **8,** 633–45 (2014).

119. McIlwain, D. R. *et al.* T-cell STAT3 is required for the maintenance of humoral immunity to LCMV. *Eur. J. Immunol.* **45,** 418–27 (2015).

120. O'Gorman, W. E. *et al.* Single-cell systems-level analysis of human Toll-like receptor activation defines a chemokine signature in patients with systemic lupus erythematosus. *J. Allergy Clin. Immunol.* **136,** 1326–36 (2015).

121. Hotson, A. N. *et al.* Coordinate actions of innate immune responses oppose those of the adaptive immune system during Salmonella infection of mice. *Sci. Signal.* **9,** ra4 (2016).

122. Bendall, S. C. & Nolan, G. P. From single cells to deep phenotypes in cancer. *Nat. Biotechnol.* **30,** 639–47 (2012).

123. Mullin R. Tufts Study Finds Big Rise In Cost Of Drug Development *Chemical & Engineering News* (2014)

124. Elphick, G. F. The Human Polyomavirus, JCV, Uses Serotonin Receptors to Infect Cells. *Science* **306,** 1380–1383 (2004).

125. Kong, H. & West, S. Ethical Principles for Medical Research Involving Human Subjects. 1–5 (2008).

126. Bossuyt, P. M. *et al.* Towards Complete and Accurate Reporting of Studies of Diagnostic Accuracy : The STARD Initiative. **6,** (2003).

127. Krutzik, P. O., Crane, J. M., Clutter, M. R. & Nolan, G. P. High-content single-cell drug screening with phosphospecific flow cytometry. *Nat. Chem. Biol.* **4,** 132–142 (2008).

128. Yasgar, A. *et al.* Compound Management for Quantitative High-Throughput Screening *JALA Charlottesv Va*. **13,** 79–89 (2008).

129. Martin, H. L. *et al.* High-Content, High-Throughput Screening for the Identification of Cytotoxic Compounds Based on Cell Morphology and Cell Proliferation Markers. **9,** (2014).

130. Kloverpris, H. *et al.* Dimethyl sulfoxide (DMSO) exposure to human peripheral blood mononuclear cells (PBMCs) abolish T cell responses only in high concentrations and following coincubation for more than two hours. *J. Immunol. Methods* **356,** 70–78 (2010).

131. Timm, M., Saaby, L. & Moesby, L. Considerations regarding use of solvents in *in vitro* cell based assays. *Cytotechnology* **65**, 887–894 (2013).

132. Miller, B. J., Buckley, P., Seabolt, W., Mellor, A. & Kirkpatrick, B. Meta-analysis of cytokine alterations in schizophrenia: Clinical status and antipsychotic effects. *Biol. Psychiatry* **70,** 663–671 (2011).

133. Hale, M. B., Krutzik, P. O., Samra, S. S., Crane, J. M. & Nolan, G. P. Stage dependent aberrant regulation of cytokine-STAT signaling in murine systemic lupus erythematosus. *PLoS One* **4,** e6756 (2009).

134. Zhang, J., Chung, T. & Oldenburg, K. A Simple Statistical Parameter for Use in Evaluation and Validation of High Throughput Screening Assays. *J. Biomol. Screen.* **4,** 67–73 (1999).

135. Bodenmiller, B. *et al.* Multiplexed mass cytometry profiling of cellular states perturbed by small-molecule regulators. *Nat. Biotechnol.* **30,** 858–67 (2012).

136. Bendall, S. C. *et al.* Single-cell mass cytometry of differential immune and drug responses across a human hematopoietic continuum. *Science* **332,** 687–96 (2011).

137. Wolchinsky, R. *et al.* Antigen-dependent integration of opposing proximal TCR-signaling cascades

determines the functional fate of T lymphocytes. *J. Immunol.* **192,** 2109–19 (2014).

138. Mingueneau, M. *et al.* Single-cell mass cytometry of TCR signaling: amplification of small initial differences results in low ERK activation in NOD mice. *Proc. Natl. Acad. Sci. U. S. A.* **111,** 16466–71 (2014).

139. Chalecka-Franaszek, E. & Chuang, D. M. Lithium activates the serine/threonine kinase Akt-1 and suppresses glutamate-induced inhibition of Akt-1 activity in neurons. *Proc. Natl. Acad. Sci. U. S. A.* **96,** 8745–50 (1999).

140. Neuroscience, C. D 2 dopamine receptors induce mitogen-activated protein kinase and cAMP response element-binding protein phosphorylation. **96,** 11607–11612 (1999).

141. Perez, O. D. & Nolan, G. P. Simultaneous measurement of multiple active kinase states using polychromatic flow cytometry. *Nat. Biotechnol.* **20,** 155–62 (2002).

142. Perez, O. D. & Nolan, G. P. Phospho-proteomic immune analysis by flow cytometry: from mechanism to translational medicine at the single-cell level. *Immunol. Rev.* **210,** 208–28 (2006).

143. Lovestone, S., Killick, R., Di Forti, M. & Murray, R. Schizophrenia as a GSK-3 dysregulation disorder. *Trends Neurosci.* **30,** 142–149 (2007).

144. Gould, T. D. & Manji, H. K. Glycogen synthase kinase-3: a putative molecular target for lithium mimetic drugs. *Neuropsychopharmacology* **30,** 1223–1237 (2005).

145. Emamian, E. S. AKT/GSK3 signaling pathway and schizophrenia. *Front. Mol. Neurosci.* **5,** 33 (2012).

146. Duman, R. S. & Aghajanian, G. K. Neurobiology of rapid acting antidepressants: role of BDNF and GSK-3β. *Neuropsychopharmacology* **39,** 233 (2014).

147. Li, X. *et al.* Lithium regulates glycogen synthase kinase-3beta in human peripheral blood mononuclear cells: implication in the treatment of bipolar disorder. *Biol. Psychiatry* **61,** 216–22 (2007).

148. Blasi, G. *et al.* DRD2/AKT1 interaction on D2 c-AMP independent signaling, attentional processing, and response to olanzapine treatment in schizophrenia. *Proc. Natl. Acad. Sci. U. S. A.* **108,** 1158–63 (2011).

149. Strachan, R. T., Ferrara, G. & Roth, B. L. Screening the receptorome: an efficient approach for drug discovery and target validation. *Drug Discov. Today* **11,** 708–716 (2006).

150. Overall, K. L. Natural animal models of human psychiatric conditions: Assessment of mechanism and validity. *Prog. Neuro-Psychopharmacology Biol. Psychiatry* **24,** 727–776 (2000).

151. Machado-Vieira, R., Kapczinski, F. & Soares, J. C. Perspectives for the development of animal models of bipolar disorder. *Prog. Neuro-Psychopharmacology Biol. Psychiatry* **28,** 209–224 (2004).

152. Gould, T. D. & Gottesman, I. I. Psychiatric endophenotypes and the development of valid animal models. *Genes. Brain. Behav.* **5,** 113–9 (2006).

153. Krishnan, V., Berton, O. & Nestler, E. The use of animal models in psychiatric research and treatment. *Am. J. Psychiatry* **165,** 1109 (2008).

154. Joel, D. Current animal models of obsessive compulsive disorder: A critical review. *Prog. Neuro-Psychopharmacology Biol. Psychiatry* **30,** 374–388 (2006).

155. Jin, N., Kovács, A. D., Sui, Z., Dewhurst, S. & Maggirwar, S. B. Opposite effects of lithium and valproic acid on trophic factor deprivation-induced glycogen synthase kinase-3 activation, c-Jun expression and neuronal cell death. *Neuropharmacology* **48,** 576–83 (2005).

156. Park, S. W. *et al.* Differential effects of aripiprazole and haloperidol on BDNF-mediated signal changes in SH-SY5Y cells. *Eur. Neuropsychopharmacol.* **19,** 356–362 (2009).

157. Aubry, J.-M., Schwald, M., Ballmann, E. & Karege, F. Early effects of mood stabilizers on the Akt/GSK-3beta signaling pathway and on cell survival and proliferation. *Psychopharmacology (Berl).* **205,** 419–29 (2009).

158. De Sarno, P., Li, X. & Jope, R. S. Regulation of Akt and glycogen synthase kinase-3β phosphorylation by sodium valproate and lithium. *Neuropharmacology* **43,** 1158–1164 (2002).

159. An, W. *et al.* Discovery of potent and highly selective inhibitors of GSK3b. *Probe Reports from NIH Mol. Libr. Progr.* **1,** 3–8 (2012).

160. Brami-Cherrier, K. *et al.* Epigenetic reprogramming of cortical neurons through alteration of dopaminergic circuits. *Mol. Psychiatry* **19,** 1193–200 (2014).

161. Bodenmiller, B. *et al.* Phosphoproteomic analysis reveals interconnected system-wide responses to perturbations of kinases and phosphatases in yeast. *Sci. Signal.* **3,** rs4 (2010).

162. Maiese, K., Chong, Z. Z., Shang, Y. C. & Wang, S. MTOR: On target for novel therapeutic strategies in the nervous system. *Trends Mol. Med.* **19,** 51–60 (2013).

163. Lyu, D. *et al.* The mTOR signaling pathway regulates pain-related synaptic plasticity in rat entorhinal-hippocampal pathways. *Mol. Pain* **9,** 64 (2013).

164. Giovannini, M. G., Lana, D. & Pepeu, G. The integrated role of ACh, ERK and mTOR in the mechanisms of hippocampal inhibitory avoidance memory. *Neurobiol. Learn. Mem.* **119,** 18–33 (2015).

165. Sarkar, A. *et al.* Hippocampal HDAC4 contributes to postnatal fluoxetine-evoked depression-like behavior. *Neuropsychopharmacology* **39,** 2221–32 (2014).

166. Der-Avakian, A., Mazei-Robison, M. S., Kesby, J. P., Nestler, E. J. & Markou, A. Enduring deficits in brain reward function after chronic social defeat in rats: susceptibility, resilience, and antidepressant response. *Biol. Psychiatry* **76,** 542–9 (2014).

167. Koike, H., Iijima, M. & Chaki, S. Involvement of the mammalian target of rapamycin signaling in the antidepressant-like effect of group II metabotropic glutamate receptor antagonists. *Neuropharmacology* **61,** 1419–23 (2011).

168. Caddy, C., Giaroli, G., White, T. P., Shergill, S. S. & Tracy, D. K. Ketamine as the prototype glutamatergic antidepressant: pharmacodynamic actions, and a systematic review and meta-analysis of efficacy. *Ther. Adv. Psychopharmacol.* **4,** 75–99 (2014).

169. Naughton, M., Clarke, G., O'Leary, O. F., Cryan, J. F. & Dinan, T. G. A review of ketamine in affective disorders: current evidence of clinical efficacy, limitations of use and pre-clinical evidence on proposed mechanisms of action. *J. Affect. Disord.* **156,** 24–35 (2014).

170. Ignácio, Z. M. *et al.* New perspectives on the involvement of mTOR in depression as well as in the action of antidepressant drugs. *Br. J. Clin. Pharmacol.* (2015).

171. Liu, X.-L. *et al.* Fluoxetine regulates mTOR signalling in a region-dependent manner in depression-like mice. *Sci. Rep.* **5,** 16024 (2015).

172. Kenakin, T. Collateral efficacy in drug discovery: taking advantage of the good (allosteric) nature of 7TM receptors. *Trends Pharmacol. Sci.* **28,** 407–415 (2007).

173. Powell, J. J. D., Pollizzi, K. N. K., Heikamp, E. B. & Horton, M. R. Regulation of immune responses by mTOR. *Annu. Rev. …* **30,** 39–68 (2012).

174. Roumestan, C. *et al.* Anti-inflammatory properties of desipramine and fluoxetine. *Respir. Res.* **8,** 35 (2007).

175. Martin, M., Rehani, K., Jope, R. S. & Michalek, S. M. Toll-like receptor-mediated cytokine production is differentially regulated by glycogen synthase kinase 3. *Nat. Immunol.* **6,** 777–84 (2005).

176. Gobin, V. *et al.* Fluoxetine reduces murine graft-versus-host disease by induction of T cell immunosuppression. *J. Neuroimmune Pharmacol.* **8,** 934–43 (2013).

177. Serafeim, A. *et al.* Selective serotonin reuptake inhibitors directly signal for apoptosis in biopsy-like Burkitt lymphoma cells. *Blood* **101,** 3212–9 (2003).

178. Di Rosso, M. E., Palumbo, M. L. & Genaro, A. M. Immunomodulatory effects of fluoxetine. A new potential pharmacological action for a classic antidepressant drug? **109,** 101-7 *Pharmacol Res* (2015).

179. Morag, A., Oved, K. & Gurwitz, D. Sex differences in human lymphoblastoid cells sensitivities to antipsychotic drugs. *J. Mol. Neurosci.* **49,** 554–8 (2013).

180. Felger, J. C. & Lotrich, F. E. Inflammatory cytokines in depression: neurobiological mechanisms and therapeutic implications. *Neuroscience* **246,** 199–229 (2013).

181. Kettenmann, H., Hanisch, U., Noda, M. & Verkhratsky, A. Physiology of Microglia. *Physiol Rev.***91,** 461–553 (2011).

182. Block, M. L., Zecca, L. & Hong, J.-S. Microglia-mediated neurotoxicity: uncovering the molecular mechanisms. *Nat. Rev. Neurosci.* **8,** 57–69 (2007).

183. Miller, A. H. Depression and immunity: A role for T cells? *Brain. Behav. Immun.* **24,** 1–8 (2010).

184. Harris, H. & Rubinsztein, D. C. Control of autophagy as a therapy for neurodegenerative disease. *Nat. Rev. Neurol.* **8,** 108–117 (2011).

185. Rubinsztein, D. C., Codogno, P. & Levine, B. Autophagy modulation as a potential therapeutic target for diverse diseases. *Nat. Rev. Drug Discov.* **11,** 709–730 (2012).

186. Rikiishi, H. Novel Insights into the Interplay between Apoptosis and Autophagy. *Int. J. Cell Biol.* **2012,** 317645 (2012).

187. Maiuri, M. C., Zalckvar, E., Kimchi, A. & Kroemer, G. Self-eating and self-killing: crosstalk between autophagy and apoptosis. *Nat. Rev. Mol. Cell Biol.* **8,** 741–752 (2007).

188. Merenlender-Wagner, A. *et al.* Autophagy has a key role in the pathophysiology of schizophrenia. *Mol. Psychiatry* **20,** 126–132 (2015).

189. Gassen, N. C., Hartmann, J., Schmidt, M. V & Rein, T. FKBP5/FKBP51 enhances autophagy to synergize with antidepressant action. *Autophagy* **11,** 578–80 (2015).

190. Gassen, N. C. *et al.* Association of FKBP51 with Priming of Autophagy Pathways and Mediation of Antidepressant Treatment Response: Evidence in Cells, Mice, and Humans. *PLoS Med.* **11,** e1001755 (2014).

191. Motoi, Y., Shimada, K., Ishiguro, K. & Hattori, N. Lithium and autophagy. *ACS Chem. Neurosci.* **5,** 434–42 (2014).

192. Bové, J., Martínez-Vicente, M. & Vila, M. Fighting neurodegeneration with rapamycin: mechanistic insights. *Nat. Rev. Neurosci.* **12,** 437–452 (2011).

193. Curatolo, P. & Moavero, R. mTOR inhibitors as a new therapeutic option for epilepsy. *Expert Rev. Neurother.* **13,** 627–38 (2013).

194. Chang, P. *et al.* The antiepileptic drug valproic acid and other medium-chain fatty acids acutely reduce phosphoinositide levels independently of inositol in Dictyostelium. *Dis. Model. Mech.* **5,** 115–124 (2012).

195. Curatolo, P., Moavero, R. & de Vries, P. J. Neurological and neuropsychiatric aspects of tuberous sclerosis complex. *Lancet. Neurol.* **14,** 733–45 (2015).

196. Hoerning, A. *et al.* Pharmacodynamic monitoring of mammalian target of rapamycin inhibition by phosphoflow cytometric determination of p70S6 kinase activity. *Transplantation* **99,** 210–9 (2015).

197. Paccalin, M. *et al.* Activated mTOR and PKR kinases in lymphocytes correlate with memory and cognitive decline in Alzheimer's disease. *Dement. Geriatr. Cogn. Disord.* **22,** 320–6 (2006).

198. Andrade-Talavera, Y., Benito, I., Casañas, J. J., Rodríguez-Moreno, A. & Montesinos, M. L. Rapamycin restores BDNF-LTP and the persistence of long-term memory in a model of Down's syndrome. *Neurobiol. Dis.* **82,** 516–25 (2015).

199. Liang, M.-H., Wendland, J. R. & Chuang, D.-M. Lithium inhibits Smad3/4 transactivation via increased CREB activity induced by enhanced PKA and AKT signaling. *Mol. Cell. Neurosci.* **37,** 440–53 (2008).

200. Ganea, K. *et al.* Convergent animal and human evidence suggests the activin/inhibin pathway to be involved in antidepressant response. *Transl. Psychiatry* **2,** e177 (2012).

201. Beech, R. D. *et al.* Gene-expression differences in peripheral blood between lithium responders and non-responders in the Lithium Treatment-Moderate dose Use Study (LiTMUS). *Pharmacogenomics J.* **14,** 182–191 (2014).

202. Beurel, E. & Jope, R. S. Differential regulation of STAT family members by glycogen synthase kinase-3. *J. Biol. Chem.* **283,** 21934–21944 (2008).

203. Zhu, Z. *et al.* Lithium suppresses astrogliogenesis by neural stem and progenitor cells by inhibiting STAT3 pathway independently of glycogen synthase kinase 3 beta. *PLoS One* **6,** e23341 (2011).

204. Machado-Vieira, R., Ibrahim, L. & Zarate, C. A. Histone deacetylases and mood disorders: epigenetic programming in gene-environment interactions. *CNS Neurosci. Ther.* **17,** 699–704 (2011).

205. Göttlicher, M. *et al.* Valproic acid defines a novel class of HDAC inhibitors inducing differentiation of transformed cells. *EMBO J.* **20,** 6969–78 (2001).

206. M. Pritchard, E. Progress in Small Molecule Therapeutics for the Treatment of Retinoblastoma. *Mini-Reviews Med. Chem.* **15,**

207. Brehm, A. & Kouzarides, T. Retinoblastoma protein meets chromatin. *Trends Biochem. Sci.* **24,** 142–145 (1999).

208. McGowan, P. O. *et al.* Epigenetic regulation of the glucocorticoid receptor in human brain associates with childhood abuse. *Nat. Neurosci.* **12,** 342–8 (2009).

209. Hobara, T. *et al.* Altered gene expression of histone deacetylases in mood disorder patients. *J. Psychiatr. Res.* **44,** 263–70 (2010).

210. Otto, M. W. *et al.* Posttraumatic stress disorder in patients with bipolar disorder: a review of prevalence, correlates, and treatment strategies. *Bipolar Disord.* **6,** 470–9 (2004).

211. Gurvich, N. *et al.* Association of valproate-induced teratogenesis with histone deacetylase inhibition in vivo. *FASEB J.* **19,** 1166–8 (2005).

212. Ring, D. B. *et al.* Selective glycogen synthase kinase 3 inhibitors potentiate insulin activation of glucose transport and utilization *in vitro* and in vivo. *Diabetes* **52,** 588–95 (2003).

213. Cohen, P. & Frame, S. The renaissance of GSK3. *Nat. Rev. Mol. Cell Biol.* **2,** 769–776 (2001).

214. Emamian, E. S., Hall, D., Birnbaum, M. J., Karayiorgou, M. & Gogos, J. A. Convergent evidence for impaired AKT1-GSK3beta signaling in schizophrenia. *Nat. Genet.* **36,** 131–7 (2004).

215. Hill, M. J. *et al.* Transcriptional consequences of schizophrenia candidate miR-137 manipulation in human neural progenitor cells. *Schizophr. Res.* **153,** 225–30 (2014).

216. Iossifov, I. *et al.* De novo gene disruptions in children on the autistic spectrum. *Neuron* **74,** 285–99 (2012).

217. Moon, A. M. *et al.* Crkl deficiency disrupts Fgf8 signaling in a mouse model of 22q11 deletion syndromes. *Dev. Cell* **10,** 71–80 (2006).

218. Guris, D. L., Duester, G., Papaioannou, V. E. & Imamoto, A. Dose-dependent interaction of Tbx1 and Crkl and locally aberrant RA signaling in a model of del22q11 syndrome. *Dev. Cell* **10,** 81–92 (2006).

219. D'Arcangelo, G. Reelin in the Years: Controlling Neuronal Migration and Maturation in the Mammalian Brain. *Adv. Neurosci.* **2014,** 1–19 (2014).

220. Li, J. *et al.* Association study between genes in Reelin signaling pathway and autism identifies DAB1 as a susceptibility gene in a Chinese Han population. *Prog. Neuropsychopharmacol. Biol. Psychiatry* **44,** 226–32 (2013).

221. Folsom, T. D. & Fatemi, S. H. The involvement of Reelin in neurodevelopmental disorders. *Neuropharmacology* **68,** 122–35 (2013).

222. Wullschleger, S. *et al.* How moderate changes in Akt T-loop phosphorylation impact on tumorigenesis and insulin resistance. *Dis. Model. Mech.* **4,** 95–103 (2011).

223. Casamayor, A., Morrice, N. A. & Alessi, D. R. Phosphorylation of Ser-241 is essential for the activity of 3-phosphoinositide-dependent protein kinase-1: identification of five sites of phosphorylation in vivo. *Biochem. J.* **342 (Pt 2,** 287–92 (1999).

224. Musil, R., Obermeier, M., Russ, P. & Hamerle, M. Weight gain and antipsychotics: a drug safety review. *Expert Opin. Drug Saf.* **14,** 73–96 (2015).

225. Kroeze, W. K. *et al.* H1-Histamine Receptor Affinity Predicts Short-Term Weight Gain for Typical and Atypical Antipsychotic Drugs. *Neuropsychopharmacology* **28,** 519–526 (2003).

226. Chen, M.-L. *et al.* Risperidone modulates the cytokine and chemokine release of dendritic cells and induces TNF-α-directed cell apoptosis in neutrophils. *Int. Immunopharmacol.* **12,** 197–204 (2012).

227. Kedracka-Krok, S. *et al.* Clozapine influences cytoskeleton structure and calcium homeostasis in rat cerebral cortex and has a different proteomic profile than risperidone. *J. Neurochem.* **132,** 657–76 (2015).

228. Dwivedi, Y. *et al.* Aberrant extracellular signal-regulated kinase (ERK)1/2 signalling in suicide brain: role of ERK kinase 1 (MEK1). *Int. J. Neuropsychopharmacol.* **12,** 1337–54 (2009).

229. Duman, C. H., Schlesinger, L., Kodama, M., Russell, D. S. & Duman, R. S. A role for MAP kinase signaling in behavioral models of depression and antidepressant treatment. *Biol. Psychiatry* **61,** 661–70 (2007).

230. Réus, G. Z. *et al.* MAPK signaling correlates with the antidepressant effects of ketamine. *J. Psychiatr. Res.* **55,** 15–21 (2014).

231. Eriksson, T. M. *et al.* Emotional memory impairments in a genetic rat model of depression: involvement of 5-HT/MEK/Arc signaling in restoration. *Mol. Psychiatry* **17,** 173–84 (2012).

232. Liu, R.-J. *et al.* GSK-3 inhibition potentiates the synaptogenic and antidepressant-like effects of subthreshold doses of ketamine. *Neuropsychopharmacology* **38,** 2268–77 (2013).

233. Bunney, T. D. & Katan, M. PLC regulation: emerging pictures for molecular mechanisms. *Trends Biochem. Sci.* **36,** 88–96 (2011).

234. Yang, Y. R., Follo, M. Y., Cocco, L. & Suh, P.-G. The physiological roles of primary phospholipase C. *Adv. Biol. Regul.* **53,** 232–41 (2013).

235. Jang, H.-J. *et al.* Phospholipase C-γ1 involved in brain disorders. *Adv. Biol. Regul.* **53,** 51–62 (2013).

236. Choi, J. H., Ryu, S. H. & Suh, P. G. On/Off-regulation of phospholipase C-gamma 1-mediated signal transduction. *Adv. Enzyme Regul.* **47,** 104–116 (2007).

237. Ferguson, S. S. G. Receptor tyrosine kinase transactivation: fine-tuning synaptic transmission. *Trends Neurosci.* **26,** 119–22 (2003).

238. Nagahara, A. H. & Tuszynski, M. H. Potential therapeutic uses of BDNF in neurological and psychiatric disorders. *Nat. Rev. Drug Discov.* **10,** 209–219 (2011).

239. Pitcher, G. M. *et al.* Schizophrenia susceptibility pathway neuregulin 1-ErbB4 suppresses Src upregulation of NMDA receptors. *Nat. Med.* **17,** 470–8 (2011).

240. Badou, A., Jha, M. K., Matza, D. & Flavell, R. A. Emerging Roles of L-Type Voltage-Gated and Other Calcium Channels in T Lymphocytes. *Front. Immunol.* **4,** 1–10 (2013).

241. Andersen, T. B., López, C. Q., Manczak, T., Martinez, K. & Simonsen, H. T. Thapsigargin--from Thapsia L. to mipsagargin. *Molecules* **20,** 6113–27 (2015).

242. Kholodenko, B. N. Cell-signalling dynamics in time and space. *Nat. Rev. Mol. Cell Biol.* **7,** 165–176 (2006).

243. Wang, X., Chuang, H.-C., Li, J.-P. & Tan, T.-H. Regulation of PKC-θ function by phosphorylation in T cell receptor signaling. *Front. Immunol.* **3,** 1–8 (2012).

244. Purcell, S. M. *et al.* A polygenic burden of rare disruptive mutations in schizophrenia. *Nature* **506,** 185–190 (2014).

245. Bhat, S. *et al.* CACNA1C (Cav1.2) in the pathophysiology of psychiatric disease. *Prog. Neurobiol.* **99,** 1–14 (2012).

246. Noto, C. *et al.* Effects of risperidone on cytokine profile in drug-naïve first-episode psychosis. *Int. J. Neuropsychopharmacol.* **18,** 1-8 (2015).

247. Yang, Y. R. *et al.* Primary phospholipase C and brain disorders. *Adv. Biol. Regul.***61,** 80-5 (2015).

248. Kim, S.-W., Cho, T. & Lee, S. Phospholipase C-β1 Hypofunction in the Pathogenesis of Schizophrenia. *Front. psychiatry* **6,** 159 (2015).

249. Frégeau, M.-O., Carrier, M. & Guillemette, G. Mechanism of dopamine D2 receptor-induced Ca(2+) release in PC-12 cells. *Cell. Signal.* **25,** 2871–7 (2013).

250. McOmish, C. E. *et al.* Phospholipase C-beta1 knockout mice exhibit endophenotypes modeling schizophrenia which are rescued by environmental enrichment and clozapine administration. *Mol. Psychiatry* **13,** 661–72 (2008).

251. Turecki, G. *et al.* Evidence for a role of phospholipase C-gamma1 in the pathogenesis of bipolar disorder. *Mol. Psychiatry* **3,** 534–8 (1998).

252. Ftouhi-Paquin, N. *et al.* Identification of three polymorphisms in the translated region of PLC-gamma1 and their investigation in lithium responsive bipolar disorder. *Am. J. Med. Genet.* **105,** 301–5 (2001).

253. Rantamäki, T. *et al.* Pharmacologically diverse antidepressants rapidly activate brain-derived neurotrophic factor receptor TrkB and induce phospholipase-Cgamma signaling pathways in mouse brain. *Neuropsychopharmacology* **32,** 2152–62 (2007).

254. Ripke, S. *et al.* Genome-wide association analysis identifies 13 new risk loci for schizophrenia. *Nat.*

Genet. **45,** 1150–9 (2013).

255. Xu, M.-Q. *et al.* Association of AKT1 gene polymorphisms with risk of schizophrenia and with response to antipsychotics in the Chinese population. *J. Clin. Psychiatry* **68,** 1358–67 (2007).

256. Thiselton, D. L. *et al.* AKT1 is associated with schizophrenia across multiple symptom dimensions in the Irish study of high density schizophrenia families. *Biol. Psychiatry* **63,** 449–57 (2008).

257. Schwab, S. G. *et al.* Further evidence for association of variants in the AKT1 gene with schizophrenia in a sample of European sib-pair families. *Biol. Psychiatry* **58,** 446–50 (2005).

258. Ikeda, M. *et al.* Association of AKT1 with schizophrenia confirmed in a Japanese population. *Biol. Psychiatry* **56,** 698–700 (2004).

259. Bajestan, S. N. *et al.* Association of AKT1 haplotype with the risk of schizophrenia in Iranian population. *Am. J. Med. Genet. B. Neuropsychiatr. Genet.* **141B,** 383–6 (2006).

260. Tan, H.-Y. *et al.* Genetic variation in AKT1 is linked to dopamine-associated prefrontal cortical structure and function in humans. *J. Clin. Invest.* **118,** 2200–8 (2008).

261. Horny, H. P. *et al.* Investigation of bone marrow lymphocyte subsets in normal, reactive, and neoplastic states using paraffin-embedded biopsy specimens. *Am. J. Clin. Pathol.* **99,** 142–9 (1993).

262. Chen, M.-L. *et al.* Antipsychotic drugs suppress the AKT/NF-κB pathway and regulate the differentiation of T-cell subsets. *Immunol. Lett.* **140,** 81–91 (2011).

263. Molteni, R., Calabrese, F., Racagni, G., Fumagalli, F. & Riva, M. A. Antipsychotic drug actions on gene modulation and signaling mechanisms. *Pharmacol. Ther.* **124,** 74–85 (2009).

264. Beaulieu, J.-M. & Gainetdinov, R. R. The physiology, signaling, and pharmacology of dopamine receptors. *Pharmacol. Rev.* **63,** 182–217 (2011).

265. Mondelli, V. *et al.* Haloperidol and olanzapine mediate metabolic abnormalities through different molecular pathways. *Transl. Psychiatry* **3,** e208 (2013).

266. Vestri, H. S., Maianu, L., Moellering, D. R. & Garvey, W. T. Atypical Antipsychotic Drugs Directly Impair Insulin Action in Adipocytes: Effects on Glucose Transport, Lipogenesis, and Antilipolysis. *Neuropsychopharmacology* **32,** 765–772 (2007).

267. Miklossy, G., Hilliard, T. S. & Turkson, J. Therapeutic modulators of STAT signalling for human diseases. *Nat. Rev. Drug Discov.* **12,** 611–629 (2013).

268. Schulz, K. R., Danna, E. a, Krutzik, P. O. & Nolan, G. P. Single-cell phospho-protein analysis by flow cytometry. *Curr. Protoc. Immunol.* **Chapter 8,** Unit 8.17 (2007).

269. Murray, P. J. The JAK-STAT Signaling Pathway: Input and Output Integration. *J. Immunol.* **178,** 2623–2629 (2007).

270. Aaronson, D. S. & Horvath, C. M. A road map for those who don't know JAK-STAT. *Science* **296,** 1653–5 (2002).

271. Murase, S. & McKay, R. D. Neuronal activity-dependent STAT3 localization to nucleus is dependent on Tyr-705 and Ser-727 phosphorylation in rat hippocampal neurons. *Eur. J. Neurosci.* **39,** 557–65 (2014).

272. Wakahara, R. *et al.* Phospho-Ser727 of STAT3 regulates STAT3 activity by enhancing dephosphorylation of phospho-Tyr705 largely through TC45. *Genes to Cells* **17,** 132–145 (2012).

273. Abroun, S. *et al.* STATs: An Old Story, Yet Mesmerizing. *Cell J.* **17,** 395–411 (2015).

274. Perkins, D. O. *et al.* Towards a psychosis risk blood diagnostic for persons experiencing high-risk

symptoms: preliminary results from the NAPLS project. *Schizophr. Bull.* **41,** 419–28 (2015).

275. Hu, X. *et al.* Microglial and macrophage polarization—new prospects for brain repair. *Nat. Rev. Neurol.* **11,** 56–64 (2014).

276. Bloomfield, P. S. *et al.* Microglial Activity in People at Ultra High Risk of Psychosis and in Schizophrenia: An [^{11} C]PBR28 PET Brain Imaging Study. *Am. J. Psychiatry* **173,** 44-52 (2015).

277. Nicolas, C. S. *et al.* The role of JAK-STAT signaling within the CNS. *JAK-STAT* **2,** e22925 (2013).

278. Nicolas, C. S. *et al.* The Jak/STAT pathway is involved in synaptic plasticity. *Neuron* **73,** 374–90 (2012).

279. Berridge, M. J. Calcium signalling and psychiatric disease: bipolar disorder and schizophrenia. *Cell Tissue Res.* **357,** 477–92 (2014).

280. Berridge, M. J. Vitamin D cell signalling in health and disease. *Biochem. Biophys. Res. Commun.* **460,** 53–71 (2015).

281. Singh, R. K., Shi, J., Zemaitaitis, B. W. & Muma, N. A. Olanzapine increases RGS7 protein expression via stimulation of the Janus tyrosine kinase-signal transducer and activator of transcription signaling cascade. *J. Pharmacol. Exp. Ther.* **322,** 133–40 (2007).

282. Singh, R. K. *et al.* Activation of the JAK-STAT pathway by olanzapine is necessary for desensitization of serotonin2A receptor-stimulated phospholipase C signaling in rat frontal cortex but not serotonin2A receptor-stimulated hormone release. *J. Psychopharmacol.* **24,** 1079–88 (2010).

283. Dunn, A. J., Swiergiel, A. H. & De Beaurepaire, R. Cytokines as mediators of depression: What can we learn from animal studies? *Neurosci. Biobehav. Rev.* **29,** 891–909 (2005).

284. Song, C. & Wang, H. Cytokines mediated inflammation and decreased neurogenesis in animal models of depression. *Prog. Neuro-Psychopharmacology Biol. Psychiatry* **35,** 760–768 (2011).

285. Flint, J. & Shifman, S. Animal models of psychiatric disease. *Curr. Opin. Genet. Dev.* **18,** 235–240 (2008).

286. Kudielka, B. M. & Kirschbaum, C. Sex differences in HPA axis responses to stress: a review. *Biol. Psychol.* **69,** 113–132 (2005).

287. Girotti, M., Donegan, J. J. & Morilak, D. A. Influence of hypothalamic IL-6/gp130 receptor signaling on the HPA axis response to chronic stress. *Psychoneuroendocrinology* **38,** 1158–69 (2013).

288. Khan, D. *et al.* Long-term effects of maternal immune activation on depression-like behavior in the mouse. *Transl. Psychiatry* **4,** e363 (2014).

289. Kong, E. *et al.* STAT3 controls IL6-dependent regulation of serotonin transporter function and depression-like behavior. *Sci. Rep.* **5,** 9009 (2015).

290. Wong, M.-L., Dong, C., Maestre-Mesa, J. & Licinio, J. Polymorphisms in inflammation-related genes are associated with susceptibility to major depression and antidepressant response. *Mol. Psychiatry* **13,** 800–12 (2008).

291. Bradley, A. J. & Dinan, T. G. Review: A systematic review of hypothalamic-pituitary-adrenal axis function in schizophrenia: implications for mortality. *J. Psychopharmacol.* **24,** 91–118 (2010).

292. Foussias, G., Siddiqui, I., Fervaha, G., Agid, O. & Remington, G. Dissecting negative symptoms in schizophrenia: opportunities for translation into new treatments. *J. Psychopharmacol.* **29,** 116–26 (2015).

293. Tsapakis, E. M., Dimopoulou, T. & Tarazi, F. I. Clinical management of negative symptoms of schizophrenia: An update. *Pharmacol. Ther.* **153,** 135–47 (2015).

294. Gandal, M. J., Edgar, J. C., Klook, K. & Siegel, S. J. Gamma synchrony: Towards a translational biomarker for the treatment-resistant symptoms of schizophrenia. *Neuropharmacology* **62,** 1504–1518 (2012).

295. Scholz, R. *et al.* Minocycline counter-regulates pro-inflammatory microglia responses in the retina and protects from degeneration. *J. Neuroinflammation* **12,** 209 (2015).

296. Levkovitz, Y. *et al.* A double-blind, randomized study of minocycline for the treatment of negative and cognitive symptoms in early-phase schizophrenia. *J. Clin. Psychiatry* **71,** 138–49 (2010).

297. Ataie-Kachoie, P., Morris, D. L. & Pourgholami, M. H. Minocycline suppresses interleukine-6, its receptor system and signaling pathways and impairs migration, invasion and adhesion capacity of ovarian cancer cells: *in vitro* and in vivo studies. *PLoS One* **8,** e60817 (2013).

298. Chaudhry, I. B. *et al.* Minocycline benefits negative symptoms in early schizophrenia: a randomised double-blind placebo-controlled clinical trial in patients on standard treatment. *J. Psychopharmacol.* **26,** 1185–93 (2012).

299. Carbon, M. & Correll, C. U. Thinking and acting beyond the positive: the role of the cognitive and negative symptoms in schizophrenia. *CNS Spectr.* **19 Suppl 1,** 38-52–7, 53 (2014).

300. Mannoury la Cour, C., Salles, M.-J., Pasteau, V. & Millan, M. J. Signaling pathways leading to phosphorylation of Akt and GSK-3β by activation of cloned human and rat cerebral $D_2$and D_3 receptors. *Mol. Pharmacol.* **79,** 91–105 (2011).

301. West, A. E., Griffith, E. C. & Greenberg, M. E. Regulation of transcription factors by neuronal activity. *Nat. Rev. Neurosci.* **3,** 921–31 (2002).

302. Abeyrathna, P. & Su, Y. The critical role of Akt in cardiovascular function. *Vascul. Pharmacol.* **74,** 38–48 (2015).

303. Gu, Z., Jiang, Q., Fu, A. K. Y., Ip, N. Y. & Yan, Z. Regulation of NMDA receptors by neuregulin signaling in prefrontal cortex. *J. Neurosci.* **25,** 4974–84 (2005).

304. Chong, Z. Z. & Maiese, K. The Src homology 2 domain tyrosine phosphatases SHP-1 and SHP-2: diversified control of cell growth, inflammation, and injury. *Histol. Histopathol.* **22,** 1251–67 (2007).

305. Agrawal, V. & Kishan, K. V. R. Promiscuous binding nature of SH3 domains to their target proteins. *Protein Pept. Lett.* **9,** 185–93 (2002).

306. Sephton, C. F. *et al.* The nuclear localization of 3'-phosphoinositide-dependent kinase-1 is dependent on its association with the protein tyrosine phosphatase SHP-1. *Cell. Signal.* **21,** 1634–44 (2009).

307. Xu, J., Wu, R.-C. & O'Malley, B. W. Normal and cancer-related functions of the p160 steroid receptor co-activator (SRC) family. *Nat. Rev. Cancer* **9,** 615–630 (2009).

308. Bates, R. C. *et al.* Activation of Src and release of intracellular calcium by phosphatidic acid during Xenopus laevis fertilization. *Dev. Biol.* **386,** 165–80 (2014).

309. Shu, L. & Shayman, J. A. Src kinase mediates the regulation of phospholipase C-gamma activity by glycosphingolipids. *J. Biol. Chem.* **278,** 31419–25 (2003).

310. Gasparini, F. & Spooren, W. Allosteric modulators for mGlu receptors. *Curr. Neuropharmacol.* **5,** 187–94 (2007).

311. Conn, P. J., Christopoulos, A. & Lindsley, C. W. Allosteric modulators of GPCRs: a novel approach for the treatment of CNS disorders. *Nat. Rev. drug Discov.* **8,** 41–54 (2010).

312. Lencz, T. & Malhotra, A. K. Targeting the schizophrenia genome: a fast track strategy from GWAS to clinic. *Mol. Psychiatry* **20,** 820–826 (2015).

313. Marx, C. E. *et al.* Pregnenolone as a novel therapeutic candidate in schizophrenia: emerging preclinical and clinical evidence. *Neuroscience* **191,** 78–90 (2011).

314. Hori, Y., Takeda, H., Tsuji, M. & Matsumiya, T. Differentiation of the inhibitory effects of calcium antagonists on abnormal behaviors induced by methamphetamine or phencyclidine. *Pharmacology* **56,** 165–74 (1998).

315. Shah, A. B., Poiletman, R. M. & Shah, N. S. The influence of nisoldipine--a 'calcium entry blocker' on drug induced stereotyped behavior in rats. *Prog. Neuropsychopharmacol. Biol. Psychiatry* **7,** 165–73 (1983).

316. Ganapathiraju, M. K. *et al.* Schizophrenia interactome with 504 novel protein–protein interactions. *npj Schizophr.* **2,** 16012 (2016).

317. Trusheim, M. R. *et al.* Quantifying factors for the success of stratified medicine. *Nat. Rev. Drug Discov.* **10,** 817–833 (2011).

318. Mizoguchi, Y., Kato, T. A., Horikawa, H. & Monji, A. Microglial intracellular Ca(2+) signaling as a target of antipsychotic actions for the treatment of schizophrenia. *Front. Cell. Neurosci.* **8,** 370 (2014).

319. Kurosawa, S. *et al.* Olanzapine potentiates neuronal survival and neural stem cell differentiation: regulation of endoplasmic reticulum stress response proteins. *J. Neural Transm.* **114,** 1121–8 (2007).

320. Santi, C. M. *et al.* Differential inhibition of T-type calcium channels by neuroleptics. *J.Neurosci.* **22,** 396–403 (2002).

321. Dolphin, A. C. Calcium channel auxiliary α2δ and β subunits: trafficking and one step beyond. *Nat. Rev. Neurosci.* **13,** 542–55 (2012).

322. Sun, J. *et al.* Schizophrenia gene networks and pathways and their applications for novel candidate gene selection. *PLoS One* **5,** e11351 (2010).

323. Geschwind, D. H. Autism: Many Genes, Common Pathways? *Cell* **135,** 391–395 (2008).

324. Fišar, Z. & Hroudová, J. Intracellular signalling pathways and mood disorders. *Folia Biol. (Praha).* **56,** 135–148 (2010).

325. Rajan, P. BMPs signal alternately through a SMAD or FRAP-STAT pathway to regulate fate choice in CNS stem cells. *J. Cell Biol.* **161,** 911–921 (2003).

326. Mannoury, C., Millan, M. J., Mannoury la Cour, C., Salles, M. J. & Pasteau, V. Signaling Pathways Leading to Phosphorylation of Akt and GSK-3β by Activation of Cloned Human and Rat Cerebral D2 and D3 Receptors. *Mol Pharmacol* **79,** 91–105 (2011).

327. Dong, Y. Y. *et al.* K2P channel gating mechanisms revealed by structures of TREK-2 and a complex with Prozac. *Science* **347,** 1256-9 (2015).

328. Kennard, L. E. *et al.* Inhibition of the human two-pore domain potassium channel, TREK-1, by fluoxetine and its metabolite norfluoxetine. *Br. J. Pharmacol.* **144,** 821–829 (2005).

329. Wawrzynczak, E. ProTREKtion against depression. *Nature.Com* **5,** 2162 (2006).

330. Torrey, E. F. & Yolken, R. H. The Schizophrenia–Rheumatoid Arthritis Connection: Infectious, Immune, or Both? *Brain. Behav. Immun.* **15,** 401–410 (2001).

331. Akbulut, S. *et al.* Sprouty proteins inhibit receptor-mediated activation of phosphatidylinositol-specific phospholipase C. *Mol. Biol. Cell* **21,** 3487–96 (2010).

332. Palmer, D. C. *et al.* Cish actively silences TCR signaling in CD8+ T cells to maintain tumor tolerance. *J.*

Exp. Med. **212,** 1–19 (2015).

333. Manuscript, A. The Akt kinases: isoform specificity in metabolism and cancer. *Gonzalez, Eva McGraw, Timothy E.* **16,** 2502–2508 (2009).

334. Bordeaux, J. *et al.* Antibody validation. *Biotechniques* **48,** 197–209 (2010).

335. Stallforth, P. & Clardy, J. Receptor signals come in waves Tubular worms from the Burgess Shale. *Nature* **495,** 457 (2013).

336. Brennand, K. J. *et al.* Modelling schizophrenia using human induced pluripotent stem cells. *Nature* **473,** 221–225 (2011).

337. Mertens, J. *et al.* Differential responses to lithium in hyperexcitable neurons from patients with bipolar disorder. *Nature* **527,** 95–99 (2015).

338. Cundiff, P. E. & Anderson, S. A. Impact of induced pluripotent stem cells on the study of central nervous system disease. *Curr. Opin. Genet. Dev.* **21,** 354–61 (2011).

339. Marchetto, M. C., Brennand, K. J., Boyer, L. F. & Gage, F. H. Induced pluripotent stem cells (iPSCs) and neurological disease modeling: progress and promises. *Hum. Mol. Genet.* **20,** R109–R115 (2011).

340. Flaherty, E. K. & Brennand, K. J. Using hiPSCs to Model Neuropsychiatric Copy Number Variations (CNVs) has Potential to Reveal Underlying Disease Mechanisms. *Brain Res.* (2016).

341. Etemad, S., Zamin, R. M., Ruitenberg, M. J. & Filgueira, L. A novel *in vitro* human microglia model: Characterization of human monocyte-derived microglia. *J. Neurosci. Methods* **209,** 79–89 (2012).

342. Sachs, K., Perez, O., Pe'er, D., Lauffenburger, D. a & Nolan, G. P. Causal protein-signaling networks derived from multiparameter single-cell data. *Science* **308,** 523–9 (2005).

343. Bendall, S. C., Nolan, G. P., Roederer, M. & Chattopadhyay, P. K. A deep profiler's guide to cytometry. *Trends Immunol.* **33,** 323–32 (2012).

344. Amir, E. D. *et al.* viSNE enables visualization of high dimensional single-cell data and reveals phenotypic heterogeneity of leukemia. *Nat. Biotechnol.* **31,** 545–52 (2013).

345. Sachs, K. *et al.* Learning signaling network structures with sparsely distributed data. *J. Comput. Biol.* **16,** 201–12 (2009).

346. Bruggner, R. V, Bodenmiller, B., Dill, D. L., Tibshirani, R. J. & Nolan, G. P. Automated identification of stratifying signatures in cellular subpopulations. *Proc. Natl. Acad. Sci. U. S. A.* **111,** E2770-7 (2014).

347. Casamassima, F. *et al.* L-type calcium channels and psychiatric disorders: A brief review. *Am. J. Med. Genet. B. Neuropsychiatr. Genet.* **153B,** 1373–90 (2010).

348. Striessnig, J., Pinggera, A., Kaur, G., Bock, G. & Tuluc, P. L-type Ca2+ channels in heart and brain. *Wiley Interdiscip. Rev. Membr. Transp. Signal.* **3,** 15–38 (2014).

349. Liu, J. *et al.* Functionalized nanocarrier combined seizure-specific vector with P-glycoprotein modulation property for antiepileptic drug delivery. *Biomaterials* **74,** 64–76 (2016).

350. Upadhyay, P., Trivedi, J., Pundarikakshudu, K. & Sheth, N. Comparative study between simple and optimized liposomal dispersion of quetiapine fumarate for diffusion through nasal route. *Drug Deliv.***23,** 1214-21 (2015).

351. Bragagni, M., Mennini, N., Ghelardini, C. & Mura, P. Development and characterization of niosomal formulations of doxorubicin aimed at brain targeting. *J. Pharm. Pharm. Sci. a Publ. Can. Soc. Pharm. Sci. Société Can. des Sci. Pharm.* **15,** 184–96 (2012).

GLOSSARY AND ABBREVIATIONS

TERM	ABBREVIATION	DEFINITION
1,4-dihydropyridine	1-4 DHP	Subclass of L-type voltage-gated calcium channel blockers characterized by 1,4-dihydropyridine ring with ester substitutions at the 3,5 positions and a substituted benzene ring at the 4 position.
alexa fluor 488	AF 488	Fluorochrome with peak excitation and peak emission wavelengths of 495 nm and 519 nm respectively, used to labelled antibodies for detection with fluorescence-based technologies.
alexa fluor 647	AF 647	Fluorochrome with peak excitation and peak emission wavelengths of 650 nm and 668 nm respectively, used to labelled antibodies for detection with fluorescence-based technologies.
allophycocyanin	APC	Fluorochrome with peak excitation and peak emission wavelengths of 650 nm and 660 nm respectively, used to labelled antibodies for detection with fluorescence-based technologies.
antidepressant		Drug class used to alleviate the symptoms of low mood associated with major depressive disorder.
antipsychotic		Drug class used to alleviate the symptoms of psychosis associated with schizophrenia.
antipsychotic intervention study	AI	Substudy within the current project in which signalling profiles are compared between peripheral blood mononuclear cells from healthy control donors and antipsychotic drug-naive schizophrenia patients before and after six weeks of clinical treatment with the antipsychotic medication olanzapine.
autism spectrum disorder	ASD	Neuropsychiatric disorder characterized by deficits in social communication and social interaction and repetitive or restrictive patterns of behaviour/ interests.
B cell		Subtype of white blood cell within the lymphocyte class involved in adaptive immune responses including antibody and cytokine secretion and antigen presentation.
B cell receptor	BCR	Transmembrane receptor protein located on the outer surface of B cells responsible for antigen recognition.

basal epitope		Expression level of a cell signalling epitope in the resting unstimulated state. For clinical comparisons, significantly altered basal epitopes were defined as those for which over 30% of nodes displayed a statistical association between clinical group status and epitope expression, which was independent of the ligand activity.
bipolar disorder	BD	Neuropsychiatric disorder, also known as manic-depressive illness, characterized by unusual shifts in mood (including alternating periods of elation and depression), energy, activity levels, and the ability to carry out day-to-day tasks.
cell barcoding dye 450	CBD 450	Fluorochrome excited by 405 nm wavelength laser with peak emission wavelength of 450 nm, used at different concentrations to covalently label cellular amine groups for multiplexing and detection of different cell populations with fluorescence-based technologies.
cell barcoding dye 500	CBD 500	Fluorochrome excited by 405 nm wavelength laser with peak emission wavelength of 500 nm, used at different concentrations to covalently label cellular amine groups for multiplexing and detection of different cell populations with fluorescence-based technologies.
cluster of differentiation	CD	Cell surface molecule providing antigen target for immunophenotyping and lineage distinction of different cell types.
cluster of differentiation 4	CD4	Cell surface molecule providing antigen target for immunophenotyping of T helper lymphocytes.
copy number variation	CNV	Variability between individual organisms of the same species in the number of repeats of a given DNA sequence at a specific genomic locus.
Diagnostic and Statistical Manual of Mental Disorders-IV- Text Review	DSM-IV-TR	Diagnostic manual, produced by the American Psychiatric Association, which provides standard criteria and terminology for the classification of mental disorders. DSM-IV was originally published in 1994 and updated subsequently to DSM-IV-TR (2000) and DSM-V (2013).
differential diagnosis study	DD	Substudy within the current project in which signalling profiles of peripheral blood mononuclear cells are compared across donors from five different clinical groups: healthy controls, schizophrenia, bipolar disorder, major depressive disorder and autism spectrum disorder.
dopamine D2 receptor	DRD2	Subtype of dopamine receptor expressed in the brain and peripheral tissue which is thought to be the principal target of existing antipsychotic medications.
dylight 800	DL800	Fluorochrome with peak excitation and peak emission wavelengths of 770 nm and 794 nm respectively, used at different concentrations to covalently label cellular sulfhydryl groups for multiplexing and detection of different cell

		populations with fluorescence-based technologies.
endoplasmic reticulum	ER	Eukaryotic cellular organelle comprised of a network of membrane-enclosed sacs or tube-like structures, known as cisternae, which are continuous with the outer nuclear membrane.
epitope		Site on an antigen molecule to which an antibody binds.
ex vivo		Removed from a living organism to a viable external environment. Usually refers to viable primary tissue removed from a live organism for functional testing.
expression quantitative trait locus	eQTL	Region of the genome containing DNA sequence variants which influence the expression level of one or more genes.
flow cytometry		Multiparametric bioanalytical methodology in which laminar flow is used to direct single cells in suspension through the narrow focus point of one of more laser beams. The combination of wavelength-specific optical filters and photomultiplier tube sensors then detect either scattering of the laser light (due to cell morphology) or the emission of specific fluorescence wavelengths (due to the fluorescent labelling of molecular targets within the cell).
fluorescein isothiocyanate	FITC	Fluorochrome with peak excitation and peak emission wavelengths of 494 nm and 520 nm respectively, used to labelled antibodies for detection with fluorescence-based technologies.
fluorescent cell barcoding	FCB	Staining of separate cell populations, each with a unique combination of fluorescent dyes at different concentrations, to allow multiplexing of the cell populations for simultaneous antibody staining .
forward scatter-area	FSC-A	Laser light which is diffracted as it passes through the cell and propagates at an angle which is *circa* 0^{o} to the direction of propagation of the incident wave. This is calculated as the area under the signal pulse curve.
functional allosteric modulator		Ligand which enhances or attenuates the activity of another ligand at its target, via an alternative mechanism, and is inactive at that target by itself.
functional endophenotype		Active biological phenotype which represents a point of mechanistic convergence between the potentially disparate and complex molecular pathways from which it arises.
functional magnetic resonance imaging	fMRI	Magnetic resonance imaging that provides three-dimensional images of the brain showing areas of increased blood flow that correlate with specific brain functions.
genetic risk locus		Genomic region in which specific sequence variants are associated with an increased risk of disease. Also known as genetic susceptibility locus.

genome wide association study	GWAS	Study which examines the association between a set of genetic variants, distributed across the genome (usually single-nucleotide polymorphisms), and the manifestation of different behavioural or biological traits across individuals in a population.
glycogen synthase kinase 3-β	GSK-3β	Enzyme, encoded by the GSK3B gene, which is involved in energy metabolism, body pattern formation and neuronal cell development.
G-protein coupled receptor	GPCR	Superfamily of seven-transmembrane domain protein receptors which transduce intracellular signals, following ligand binding to the receptor, via the exchange of guanosine diphosphate to guanosine triphosphate on an adjoining G-protein.
half maximal effective concentration	EC_{50}	Concentration of a ligand which induces a half-maximal response relative to the baseline at a given incubation time, commonly interpreted as a measure of drug potency.
high content screening		Methodology, used in biological research and drug discovery, which involves quantitative and simultaneous analysis of multiple cellular parameters, often in response to treatment with bioactive ligands.
induced pluripotent stem cell	iPSC	Type of pluripotent stem cell which can be generated from the reprogramming of adult cells.
interleukin-1 receptor	IL1R	Receptor which binds the proinflammatory cytokine interleukin-1.
International Classification of Diseases	ICD-10	Internationally recognized manual which describes standard criteria for the diagnostic classification of human diseases. First published in 1992 with updates in 2010, 2014, 2015 and 2016 relevant to this study.
Janus kinase	JAK	Family of intracellular, non-receptor tyrosine kinases which transduce signals from cytokine receptors and activate downstream signal transducer and activator of transcription proteins.
kinase		Enzyme which catalyzes the transfer of phosphate groups from phosphate-donating molecules to specific substrates.
ligand		In pharmacology, an ion or molecule which binds to a receptor.
ligand response		Change in the expression of a given epitope, relative to the vehicle treatment, following incubation of the cells with a ligand. Expressed as a fold change ratio: median MFI of the ligand treatment/ median MFI of the vehicle treatment across PBMC samples. Response ratios which are <1 (i.e. where the stimulant causes a decrease in MFI with respect to the vehicle) are reported as a negative fold changes (-1/ response ratio).

major depressive disorder	MDD	Neuropsychiatric disorder characterized by at least two weeks of low mood, that is present across most situations, and impaires energy and activity levels and the ability to carry out day-to-day tasks.
mammalian target of rapamycin complex 1		Cell signalling protein complex which regulates protein synthesis in response to a range of stimuli. Also known as mechanistic target of rapamycin complex 1.
median fluorescence intensity	MFI	Median value for the area under the fluorescence pulse curve detected at a given wavelength interval across a population of single cells.
mitogen-activated protein kinase	MAPK	Protein kinase which catalyzes the phosphorylation of serine, threonine and tyrosine residues on downstream proteins in response to mitogens and other cell signalling molecules.
mood stabilizer		Drug treatment class used to regulate the abnormal shifts in mood occurring in individuals affected by bipolar disorder.
node		Unique combination of a specific cellular treatment (ligand or vehicle) and the cell signalling epitope used to measure its effect.
olanzapine		Atypical antipsychotic drug used to treat schizophrenia and bipolar disorder.
peridinin chlorophyll	PerCP	Fluorochrome with peak excitation and peak emission wavelengths of 482 nm and 678 nm respectively, used to labelled antibodies for detection with fluorescence-based technologies.
peridinin chlorophyll-eFluor 710	PerCP-eF710	Tandem fluorochrome with peak excitation and peak emission wavelengths of 480 nm and 710 nm respectively, used to labelled antibodies for detection with fluorescence-based technologies.
peripheral blood mononuclear cell	PBMC	Peripheral blood cell with a round nucleus, including lymphocytes (T cells, B cells, NK cells) and monocytes.
phosphatase		Enzyme which catalyzes the removal of a phosphate group from its substrate by the hydrolysis of a phosphoric acid monoester into a molecule with a free hydroxyl group and a phosphate ion.
phospho-flow cytometry		Flow cytometry targeted towards the detection of phosphorylated epitopes on cell signalling proteins.
phospholipase C-γ	PLC-γ	Enzyme class which catalyzes the formation of diacylglycerol and inositol 1,4,5-trisphosphate from phosphatidylinositol 4,5-bisphosphate. Exists as two isoforms, PLC-γ1 and PLC-γ2, which share 99.9% sequence homology (UniProt P19174 vs. P16885) and similar biological activity. PLC-γ1 is expressed in all tissue types while PLC-γ2 is predominantly expressed in the lymphoid system.

phycoerythrin	PE	Fluorochrome with peak excitation and peak emission wavelengths of 496 nm and 578 nm respectively, used to labelled antibodies for detection with fluorescence-based technologies.
phycoerythrin-cyanine 7	PE-Cy7	Tandem fluorochrome with peak excitation and peak emission wavelengths of 496 nm and 785 nm respectively, used to labelled antibodies for detection with fluorescence-based technologies.
Positive and Negative Syndrome Scale	PANSS	Medical rating scale used to measure the symptom severity of patients with schizophrenia. Scores from positive, negative and general psychopathology subscales are added together to provide the total PANSS score.
positron emission tomography	PET	Functional *in vivo* imaging technique which detects pairs of gamma rays emitted indirectly by a positron-emitting radioisotope tracer coupled to a biologically active molecule.
protein kinase A	PKA	Family of protein kinases functionally dependent on the cellular concentration of cyclic AMP.
protein kinase B	AKT	Serine/threonine-specific protein kinase involved in multiple cellular processes including glucose metabolism, cell proliferation, transcription, apoptosis and cell migration.
protein kinase C	PKC	Family of protein kinases which respond to elevated cellular concentrations of calcium and diacylglycerol.
receptor tyrosine kinase	RTK	Transmembrane enzyme receptor for cytokines, hormones and growth factors which undergoes auto-phosphorylation of tyrosine residues following ligand binding.
repurposing		Identification of novel therapeutic indications for drugs which are already approved by regulatory agencies for the treatment of other diseases/disorders.
response node		Unique combination of an active ligand and the cell signalling epitope used to measure its effect. For clinical comparisons, significantly altered response nodes were defined as ligand-epitope combinations in which there was a statistical interaction between clinical group status and the response to the ligand.
reversal node		Cell signalling node in which the direction of alteration in the disease state, relative to healthy controls, is reversed following clinical treatment *in vivo*.
risk profile score	RPS	Measure of disease liability computed from the combined odds ratios of multiple genetic risk loci.
schizophrenia	SCZ	Neuropsychiatric disorder characterized by psychotic symptoms (such as hallucinations, delusions and disorganized thoughts), negative symptoms (such as reduced emotional expression, anhedonia and decreased motivation) and cognitive symptoms (such as poor executive functioning, reduced attention span and problems with working

		memory).
schizophrenia time point zero weeks	SCZ T0	Refers to clinical group within the antipsychotic intervention substudy, comprised of antipsychotic drug-naive schizophrenia patients before initiating the clinical course of treatment with antipsychotic medication olanzpaine (i.e. zero weeks of olanzapine treatment).
schizophrenia time point six weeks	SCZ T6	Refers to clinical group within the antipsychotic intervention substudy, comprised of schizophrenia patients after six weeks of clinical treatment with the antipsychotic medication olanzapine (i.e. six weeks of olanzapine treatment).
selective potentiation		Enhancement of the activity of a primary ligand at its target, by another ligand which alone is not active at that target for a given concentration.
side scatter-area	SSC-A	Laser light which is diffracted as it passes through the cell and propagates at an angle that is *circa* 90^{o} to the direction of propagation of the incident wave. This is calculated as the area under the signal pulse curve.
signal transducer and activator of transcription	STAT	Protein family of transcription factors which are activated by Janus kinases in response to cytokine or growth factor receptor activation.
stain index		Median MFI of the antibody stained sample/ median MFI of the corresponding unstained control, in the vehicle condition, across PBMC samples.
T cell		Subtype of white blood cell within the lymphocyte class involved in adaptive immune responses including cytokine secretion, antigen presentation and destruction of virus-infected or cancerous cells.
T cell receptor	TCR	Transmembrane receptor protein located on the outer surface of T cells responsible for antigen recognition.
thapsigargin	TG	Sesquiterpene lactone compound which is extracted from the *Thapsia garganica* plant. It is a non-competitive inhibitor of the sarco/endoplasmic reticulum calcium ion ATPase and causes an increase in the concetration of intracellular calcium ions.
time course study	TC	Substudy within the current project in which responses to different ligands at a range of cell signalling epitopes are compared across different ligand incubation times.
toll-like receptor	TLR	Transmembrane non-catalytic receptors, expressed primarily on innate immune cells such as monocytes, macrophages and dendritic cells, which recognize structurally conserved molecules derived from microbes.
United States Food and Drug Administration	FDA	Federal executive agency of the United States Department of Health and Human Services responsible for the safety regulation of products for human or animal consumption including food, dietary supplements, pharmaceutical drugs, blood transfusions, vaccines, medical devices and cosmetics.

voltage-gated calcium channel	Ca_V	Membrane calcium channel found primarily in excitable cells which is closed at resting membrane potential and opens in response to membrane depolarization allowing the influx of calcium ions into the cells. Subtypes include long-lasting (L), Purkinje (P/Q), neural (N), residual (R) and transient (T) type channels.
voltage-gated calcium channel auxiliary subunit β2 gene	CACNB2	Gene coding for the auxiliary subunit β2 of L, P/Q, N and R-type voltage-gated calcium channels.
voltage-gated calcium channel subunit α 1C gene	CACNA1C	Gene coding for the pore-forming α 1C subunit of the L-type voltage-gated calcium channel. The α 1C subunit is the binding site for dihydropyridine calcium channel blockers.
voltage-gated calcium channel subunit α 1I gene	CACNA1I	Gene coding for the pore-forming α 1I subunit of the T-type voltage-gated calcium channel.